

ULTRA-NARROW GAP P-GMA WELDING FOR THICK SECTION OF 304LN STAINLESS STEEL TO HSLA STEEL

Ph.D. THESIS

by

RAMKISHOR



**DEPARTMENT OF METALLURGICAL AND MATERIALS ENGINEERING
INDIAN INSTITUTE OF TECHNOLOGY ROORKEE
ROORKEE-247 667, INDIA
JULY, 2017**

ULTRA-NARROW GAP P-GMA WELDING FOR THICK SECTION OF 304LN STAINLESS STEEL TO HSLA STEEL

A THESIS

Submitted in partial fulfilment of the requirements for the award of the degree

of

DOCTOR OF PHILOSOPHY

in

METALLURGICAL AND MATERIALS ENGINEERING

by

RAMKISHOR



**DEPARTMENT OF METALLURGICAL AND MATERIALS ENGINEERING
INDIAN INSTITUTE OF TECHNOLOGY ROORKEE
ROORKEE-247 667, INDIA
JULY, 2017**



INDIAN INSTITUTE OF TECHNOLOGY ROORKEE ROORKEE

CANDIDATE'S DECLARATION

I hereby certify that the work which is being presented in the thesis entitled “**ULTRA-NARROW GAP P-GMA WELDING FOR THICK SECTION OF 304LN STAINLESS STEEL TO HSLA STEEL**” in the partial fulfilment of the requirements for the award of the Degree of Doctor of Philosophy and submitted in the Department of Metallurgical and Materials Engineering of the Indian Institute of Technology Roorkee, Roorkee in an authentic record of my own work carried out during a period from January, 2011 to July, 2017 under the supervision of Dr. P.K. Ghosh, Emeritus Professor, Department of Metallurgical and Materials Engineering, Indian Institute of Technology Roorkee, Roorkee.

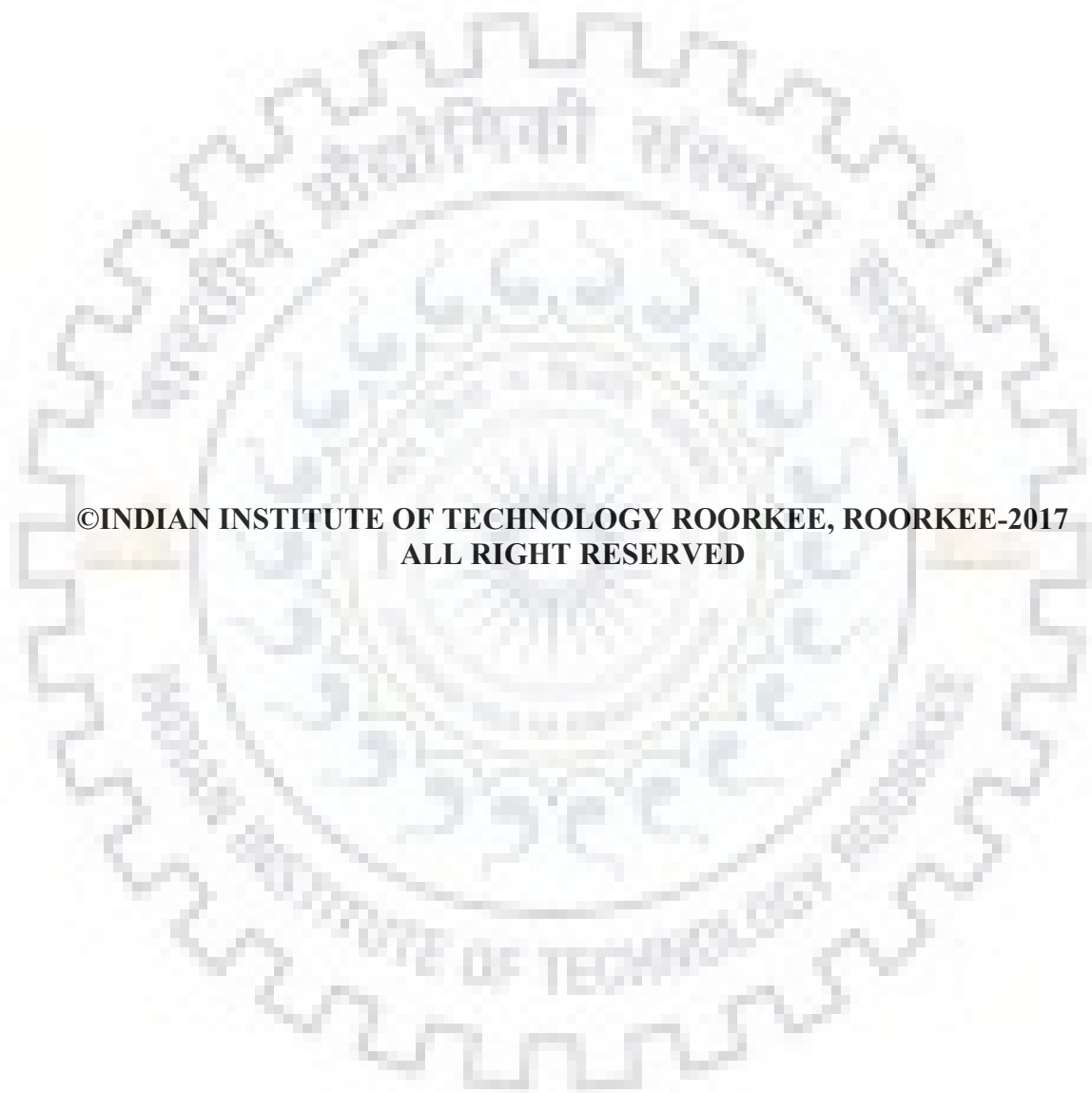
The matter presented in the thesis has not been submitted by me for the award of any other degree of this or any other Institute.

(RAMKISHOR)

This is to certify that the above statement made by the candidate is correct to the best of my knowledge.

(P.K. Ghosh)
Supervisor

Date:



**©INDIAN INSTITUTE OF TECHNOLOGY ROORKEE, ROORKEE-2017
ALL RIGHT RESERVED**





Dissimilar metal welding of thick wall austenitic stainless steel (γ -SS) and high strength low-alloy steel (HSLA) plates are used in defense, power generation, chemical, petrochemical and nuclear industries where the temperature elevates up to a range of the order of 350-450°C. Fusion welding is one of the most commonly used process; it is also largely used for the joining of dissimilar metals.

The success of narrow groove multi-pass welding is primarily governed by manipulation of narrow welding torch inside weld groove by keeping enough room for the minimum required angle of attack to the groove wall to ensure its required fusion and successful inter-pass cleaning of weld bead. But the successful use of GMAW process in a practically narrowest gap butt welding of thick section (≥ 25 mm) largely depends upon manipulation of a narrow torch nozzle relevantly deep inside a narrow weld groove along with a centrally placed single bead per layer of multi-pass weld deposition. Thus, to produce a lowest possible narrow groove GMA weld of thick section it is imperative to design a narrowest torch nozzle that can be successfully accommodated inside a narrowest possible weld groove to produce a sound weld. However, the narrowing down of weld groove may start influencing the flow of shielding gas inside the groove and create turbulence that can adversely affect the weld quality by introducing porosity and oxide inclusion in it.

In this investigation, a model of shielding gas flow dynamics and its flow rate in case of employing newly developed GMAW nozzle has been studied at different projection angle of torch nozzle head inside the narrow groove of butt joint by using ANSYS-CFX (14.5) software. The utility aspect of such a narrow torch nozzle head from the view point of smooth flow of shielding gas inside a close fitted ultra-narrow weld groove has also been studied. The outcome of the analytical studies has been used to produce a defect free ultra-narrow multi-pass weld by employing P-GMAW process with vertically placed electrode depositing centrally placed single bead per layer in weld groove. The effect of various pulse parameters of P-GMAW process to produce ultra-narrow gap weld of thick dissimilar section of austenitic stainless steel to HSLA steel has also been studied. To deal with the complicated critical conditions of controlling the process parameters and thermal behaviour of weld deposit to produce a sound multi pass narrow groove dissimilar weld with centrally located single bead per layer weld deposition, a thermal model has been developed and analysed. In the light of this model analysis appropriate welding parameters have been designed to produce sound multi pass single bead per layer (MPSBPL) welding of thick austenitic stainless steel to HSLA steel plate. The characteristics of ultra-narrow gap dissimilar weld

joint have been studied with respect to weld size, transverse shrinkage and bending stresses, mechanical and metallurgical properties of the weld. The characteristics of the ultra-narrow groove dissimilar weld have been compared with those of conventional groove dissimilar multi pass multi bead per layer (MPMBPL) weld joint of austenitic stainless steel to HSLA steel.

In view of the above an effort has been made to design a narrowest possible torch nozzle head of GMAW that can allow narrowing down the weld groove up to a limit of just accommodating the nozzle head in it during thick section welding. The utility aspect of such a narrow GMAW torch nozzle head from the view point of smooth flow of shielding gas inside a closely fitted narrow weld groove has also been studied. The outcome of these studies has been used to produce a defect free ultra-narrow multi-pass weld of thick dissimilar steel section of an austenitic stainless steel and high strength low alloy (HSLA) structural steel by employing P-GMAW process with vertically placed electrode depositing single bead per layer in weld groove. The welds of same dissimilar steel plates were also prepared by using commonly known technique of MPMBPL of weld deposition in conventional V-groove with the help of P-GMAW process. This is basically planned to study the effectiveness of the newly developed ultra-narrow gap welding procedure over the conventional groove welding with respect to the characteristics of weld joint. The background and prospect of the present work and observations of the above studies are analysed in the light of their objectives are presented in different chapters.

Chapter 1 contains introduction of the area under discussion justifying the necessity to carry out studies on MPSBPL of weld deposition in narrow gap dissimilar welding of thick austenitic stainless steel to HSLA steel plates using P-GMAW process. The importance of P-GMAW and narrow gap welding has been discussed and the problems associated with respect to its practical implications in use are also briefly explained. The methodology which can be followed for practical implementation of MPSBPL of weld deposition in narrow gap P-GMA welding of relatively thick sections has been justified to address in present investigation.

Chapter 2 begins with the survey of existing literature outlining the evolution of arc welding process and procedures used for joining of dissimilar thick section of austenitic stainless steel to HSLA steel. The existing criticality of dissimilar weld joint during welding of thick section of austenitic stainless steel and HSLA steel is also discussed. The state of the art knowledge on thermal influence of welding processes on various weld joint characteristics with respect to its metallurgical and mechanical properties have been critically analysed. Further the understanding on influence of welding procedure on stress distribution across the weld joints has been carefully examined. The deficiency of knowledge regarding the production of sound weld joint of thick steel plate using the technique of multi pass weld deposition in narrowest possible gap has been

consolidated. The support of thermal model to understand the influence of various pulse parameters on characteristics of multi pass weld of thick austenitic stainless steel to HSLA steel plate has been critically identified. In this regard it is realised that the application of P-GMAW process in consideration of thermal and geometrical aspects of weld pool as a function of pulse parameters may play a considerable role to achieve the objective of the present investigation.

Chapter-3 describes designing and development of an advanced nozzle head for narrow gap GMAW torch nozzle to facilitate the application of P-GMAW process in MPSBPL of weld deposition in ultra-narrow gap welding of thick dissimilar plates by considering the thermal influence on torch nozzle through various sources. To facilitate this, a narrowest possible gap system has been arranged. The performance of designed nozzle head system without any damage of burning during its use in MPSBPL of weld deposition in ultra-narrow groove welding has been reported and justified. The simulated characteristics of GMAW for arcing and argon shielding gas flow at a given flow rate inside the ultra-narrow groove of 25 mm thick butt weld are analyzed by 3D CFD modeling using ANSYS-CFX (14.5) software. The effect of variation in intensity of gas flow on the arcing and flow characteristics of shielding gas have been studied at different projection angle of the newly designed nozzle tip to its wall varied from 0° to 60° .

Chapter 4 deals with the thermal model for producing of lack of groove wall fusion free narrow gap weld during multi pass centrally placed single bead per layer of weld deposition in ultra-narrow groove of thick dissimilar plates with no angle of attack to the groove wall. The thermal model has been developed in consideration of thermal and geometrical aspects of the weld pool.

Chapter 5 presents the experimental procedures for bead on plate weld deposition as well as preparation of ultra-narrow groove weld joints, of dissimilar thick (25mm) section of austenitic stainless steel to controlled rolled HSLA steel plate using the P-GMAW process employing solid filler wire. Both the studies of bead on plate weld deposition and preparation of dissimilar weld joint has been carried out by using the welding parameters confirmed by the thermal model applicable to preparation of ultra-narrow gap weld joint by centrally placed MPSBPL weld deposition in narrow weld groove. It also details the experimental procedure of preparation of dissimilar weld joint of austenitic stainless steel using MPMBPL weld deposition in commonly used conventional groove. Various testing of weld bead on plate deposition and weld joints has been described. The welding parameters and procedures used in this investigation with respect to the groove design and welding processes have been thoroughly described so that various aspects of weld characteristics can be suitably realised in the light of it.

The experimental techniques of studying the shrinkage, bending and residual stresses, microstructures of different regions and mechanical properties of dissimilar weld joints prepared at different welding parameters and procedures have also been described. The testing has been planned to study the characteristics of weld joint by correlating them with ϕ and I_m at a given heat input (Ω). This is to establish the basic understanding of superiority of P-GMAW to produce ultra-narrow gap weld joint of 25 mm thick austenitic stainless steel to HSLA steel plate using MPSBPL weld deposition technique. The testing have also been planned to compare the properties of the ultra-narrow groove P-GMA weld to the conventional groove weld joint.

Chapter 6 describes the results of various experiments presented in the preceding chapter and demonstrates the basic analyses of different facets of the investigation having major features explained briefly as stated below. This chapter also present the analysis and validation of proposed thermal model for preparation of sound ultra-narrow gap weld by MPSBPL of weld deposition technique.

Similar to the earlier observations of several investigators here also it is understood that summarized influence of pulse parameters defined by the factor ϕ maintains significant correlation with I_m and Ω to control the P-GMAW process for required characteristics of weld bead deposition. The process control is basically realised through systematic variation of thermal and geometrical aspects of weld pool as well as microstructure of weld deposit and HAZ adjacent to fusion line as a function of ϕ , I_m and Ω . It is observed that comparatively higher values of I_m and ϕ are appropriate for MPSBPL of weld deposition in ultra-narrow gap dissimilar welding of thick sections of austenitic stainless steel to HSLA steel.

Results of simulated model analysis is critically studied to realize the possibility of manipulation of GMA welding torch in a narrowest possible groove of thick section welding and to produce a practically porosity and oxidation free sound weld with no lack of groove wall and inter pass fusion. Accordingly, the attention is basically put forward to study the characteristics of shielding gas flow inside the ultra-narrow groove primarily to avoid turbulence and the arc characteristics promoting a weld pool efficient enough to give required groove wall fusion at different gas flow rate and nozzle tip angle. The arc characteristics are studied mainly with respect to its length and width (spread) especially to realize the thermal distribution in weld pool inside the narrow groove. The gas pressure at outlet of the welding torch as well as the velocity and turbulence kinetic energy of shielding gas flow at different zone has been estimated.

The thermal model based on consideration of thermal and geometrical aspects of weld pool is able to produce a dissimilar weld joint free from lack of fusion by appropriate selection of pulse parameters, whereas a deviation in values from the specified range of the parameters results

a defective weld joint. The adverse situation arises because an unsuitable combination of parameters results in reduction of weld pool temperature than that required for proper groove wall fusion. It also gives unfavourable bead geometry with respect to that requires for required heat transfer to groove wall giving rise to an unsound MPSBPL narrow gap weld joint.

The P-GMAW process has unique capacity to control the amount of heat and its distribution to the weld at a given heat input by appropriate selection of pulse parameters. Thus, it is possible to get a sound weld joint using P-GMAW process in case of MPSBPL narrow gap welding of thick plates. It is observed that MPSBPL narrow gap P-GMA weld joint is having considerably lower shrinkage, bending and residual stresses improved mechanical properties along with refined microstructure than those of conventional groove dissimilar weld joint prepared by using MPMBPL of weld deposition. It has been further observed that the P-GMA welds prepared at higher ϕ and I_m at a given Ω result into comparatively better weld joint characteristics.

Chapter 7 presents conclusion of the investigation by identifying several innovative findings and understandings over the influence of the pulse parameters defined by their summarised influence in the hypothetical factor ϕ and I_m at a given Ω they are decided in consideration of the thermal model, on characteristics of weld joint produced by using P-GMAW process. Superiority of the MPSBPL ultra-narrow gap dissimilar weld joint with respect to several characteristics of conventional groove MPMBPL weld joint of thick austenitic stainless steel and HSLA steel plate is established. Various meritorious aspects with suitable nozzle head of the MPSBPL bound P-GMAW process employed with newly designed GMAW torch nozzle.



ACKNOWLEDGEMENTS

The author has great privilege and gratification to express his heartiest thanks and deep sense of gratitude to his respected supervisor Dr. P.K. Ghosh, Professor, Department of Metallurgical and Materials Engineering, IIT Roorkee, for their valuable guidance and indefatigable efforts throughout the tenure of this work. He has been an inspiring and driving force where targets appeared to be difficult during the course of work. His timely help, constructive criticism, positive attitude, painstaking efforts, humanistic and warm personal approaches made the author capable to compile the thesis in its present form. His painstaking efforts in going through the manuscript, giving good suggestions for its improvement are gratefully acknowledged.

Deep sense of gratitude is acknowledge Dr. Anjan Sil, Professor and Head of Department, Metallurgical and Materials Engineering, for his help and providing the excellent facilities in the department for the research work. Author wishes to record his deep sense of gratitude to Dr. S. K. Nath, Professors, former Heads of Metallurgical and Materials Engineering Department.

Profound sense of appreciation is acknowledged to all the members of Departmental Research Committee (DRC) and Student Research Committee (SRC), Dr. S. K. Nath, Chairman, SRC, Dr. Ujjawal Prakash, Chairman, DRC, Dr. Devendra Singh, Internal Member and Dr. D.B. Karunakar, External Member and Dr. V. Dabhade and Dr. S.R. Meka for their precious assesement throughout.

The author would like to express his sincere thanks to the technical and administrative staff of Department of Metallurgical and Materials Engineering, Mr. H.K. Ahuja, Mr. S.M. Giri, Mr. Shakti Gupta, Mr. R. K. Sharma and Mr. Rajender Sharma, Mr. Ashish Kush who have helped in all possible ways during the Ph.D work.

The author wishes to thank his friends and colleagues for their moral support and camaraderie help to keep things in perspective. Thanks are due to Mr. Nilesh Dorkar, Dr.B.P.Agrawal, Dr. Debesh, Dr. Preeti, Dr. Nidhi, Dr. Rajni, Dr.R.Sunil, Dr.Himanshu, Dr. Tilak, Dr. Kaushal Kumar, Mr. Ravindra Kumar, Mr. Arun Kumar, Mr. Ankit Chauhan, Mr. Rajavel, Mr. Sunthervel, Mr. Sudhir Kumar, Mr. Mrinmoy, Mr. Pankaj, Mr. Nilesh Kumar, Mr. Atul, Mr. Sumit, Mr. Anirudha, Mr. Surendra Chaurasia, Mr. Deepak Sharma all the fellows who helped me directly or indirectly during the entire period of this work.

The author expresses his deepest esteem to his mother, Smt. Kamla Anant and father, Sh. M. R. Anant for keeping their blessing over me and their continued patience, tolrence, understanding, inspiration, encouraging and whole hearted moral support during the entire period

of this work. Last but not least, I am thankful to almighty God who gave me strength and patience throughout the way during my Ph.D Journey.

Roorkee

Dated :

RAMKISHOR



ABSTRACT	i
ACKNOWLEDGEMENTS	vii
CONTENTS	ix
LIST OF FIGURES	xv
LIST OF TABLES	xxv
NOMENCLATURE.....	xxvii
Chapter 1.....	1
INTRODUCTION	1
Chapter 2.....	9
LITERATURE REVIEW	9
2.1. Introduction To Dissimilar Metal Welding.....	9
2.1.1. Physical properties	10
2.1.2. Metallurgical compatibility.....	10
2.1.3. Heat treatment requirements	11
2.1.4. Serviceability	11
2.2. Austenitic Stainless Steel (γ -SS)	12
2.2.1. Classification and its Application	12
2.2.2. Heat Effect on γ -SS.....	13
2.2.3. Stress Effect	14
2.3. Arc Weldability of γ -SS	15
2.4. Conventional Arc Welding of Thick γ -SS Sections.....	18
2.4.1. SMAW Process.....	20
2.4.2. GTAW Process	20
2.4.3. GMAW Process	21
2.4.3.1. Process variables and their control	22
2.4.3.2. Behaviour of metal transfer	25
2.4.3.3. Thermal behaviour of weld.....	26
2.4.4. P-GMAW Process.....	28

2.4.4.1. Process variables and their control.....	29
2.4.4.2. Behaviour of metal transfer.....	32
2.4.4.3. Thermal Behaviour of weld	33
2.4.4.4. Concept of summarised influence of pulse parameters.....	35
2.5. Narrow Gap Arc Welding Of Thick γ -SS Sections	36
2.6. Characteristics Of γ -SS Weld Joint	37
2.6.1. Weld Chemistry	37
2.6.2. Microstructure	38
2.6.2.1. Weld.....	38
2.6.3. Mechanical Properties.....	40
2.6.3.1. Tensile properties	40
2.6.3.2. Hardness	40
2.6.3.3. Residual stresses	41
2.6.3.4. Stress Distribution in thick sections.....	41
2.7. High Strength Low Alloy (HSLA) Steels.....	42
2.8. Properties of HSLA Steels.....	44
2.8.1. Mechanical properties	44
2.8.2. Weldability.....	45
2.9. Factor Affecting the Weldability of HSLA Steels.....	46
2.9.1. Effect of residual Stresses	46
2.9.2. Effect of microstructure	48
2.9.3. Effect of welding processes, procedure and parameters	50
2.10. Conventional Arc Welding of Thick HSLA Steels	53
2.10.1. Gas metal arc welding.....	53
2.10.1.1. Process variables and their control.....	54
2.10.1.2. Thermal behaviour of weld	56
2.10.1.3. Concept Of Summarized Influence Of Pulse Parameters	61
2.11. Narrow Gap Arc Welding of Thick HSLA Steels	61
2.12. Gas metal arc welding	62
2.12.1. Pulsed current gas metal arc welding.....	65

2.13. Characteristics of Weld	65
2.13.1. Weld geometry.....	65
2.14. Modelling of Weld	67
2.15. Formulation Of The Problem	70
2.15.1. Motivation for the Present Study	70
2.15.2. Objectives of the Work.....	72
Chapter 3.....	75
DESIGN OF NARROW GAP GMAW TORCH NOZZLE HEAD	75
3.1. Design Considerations of Narrow Gap Welding Torch Nozzle Head	76
3.2. Simulation by ANSYS 14.5 CFX Software.....	81
Chapter 4.....	87
THERMAL MODELING OF MULTI PASS SINGLE SEAM PER LAYER NARROW GAP WELDING of γ -ss to hsla steel	87
4.1. Requirement for Preparation of a Sound Weld Joint	87
4.2. Spatial Model for Estimation of Geometrical Aspects of Weld Pool	89
4.3. Spatial Model for Estimation of Thermal Behaviour of Weld Pool.....	91
4.4. Summary	97
Chapter 5.....	99
EXPERIMENTATION	99
5.1. Base and Filler Materials.....	99
5.1.1. Used in bead on plate experimentation.....	99
5.1.2. Used in weld joint preparation.....	99
5.2. Welding Power Source	101
5.3. Fixture and Torch Manipulator	102
5.3.1. Welding fixture	102
5.3.2. Torch manipulator.....	102
5.4. Instrumentation and Recording	103
5.4.1. Welding parameters	103
5.4.2. Thermal behaviour	104
5.4.2.1. Measurement of temperature of weld pool	104

5.4.2.2. Estimation of heat input (Ω).....	105
5.4.2.3. Estimation of average weld pool temperature.....	106
5.4.2.4. Estimation of weld isotherm	107
5.5. Weld Bead on Plate Experimentation.....	107
5.5.1. Welding	107
5.5.2. Measurement of thermal behaviour of weld	108
5.5.2.1. Geometrical aspects of weld pool	110
5.6. Preparation of Single Seam Multi Pass Ultra-narrow Gap Weld Joints.....	111
5.6.1. Preparation of weld groove	111
5.6.2. Preparation of weld joints	112
5.6.3. Planning for collection of Specimen for different studies	113
5.6.4. Non-destructive testing of weld joints	113
5.6.4.1. Dye penetrant test.....	113
5.6.4.2. Ultrasonic test.....	113
5.6.5. Characterization of weld joint.....	114
5.6.5.1. Geometrical characteristics of weld joint.....	114
5.6.5.2. Thermal analysis of weld joint.....	114
5.6.5.3. Estimation of transverse shrinkage stress	114
5.6.5.4. Estimation of bending stress	115
5.6.5.5. Metallographic studies	116
5.6.5.6. Porosity/Inclusion content.....	117
5.6.6. Studies on mechanical properties.....	117
5.6.6.1. Tensile testing	117
5.6.6.2. Hardness measurement.....	119
Chapter 6.....	121
RESULTS AND DISCUSSION	121
6.1. Characteristics of Base and Filler Materials.....	121
6.1.1. Chemical Composition.....	121
6.1.2. Microstructure	122
6.1.3. Mechanical properties	123

6.1.3.1. Tensile properties.....	123
6.1.3.2. Hardness.....	125
6.1.4. Summary.....	126
6.2. Studies on Newly Developed Nozzle Head Device.....	126
6.2.1. Performance Analysis of Simulated Gas Shielding.....	126
6.2.2. Shielding Gas Flow Characteristics.....	128
6.2.3. Summary.....	137
6.3. Characteristics of P-GMAW Weld Bead on Plate.....	138
6.3.1. Thermal aspects of weld pool.....	138
6.3.1.1. Summary.....	148
6.4. Analysis and Validity of Proposed Thermal Model for MPSSPL Narrow Gap Weld.....	148
6.4.1. Analyses of the proposed model.....	148
6.4.1.1. Geometry of molten pool inside weld groove.....	148
6.4.1.2. Thermal behaviour of molten pool inside weld groove.....	151
6.4.1.3. Heat transfer in molten pool and critical point of fusion in weld groove.....	155
6.4.1.4. Weld isotherm in molten pool.....	158
6.4.2. Validity of model analysis.....	161
6.4.3. Analyses of weld performance.....	163
6.5. Characteristics of Multi Pass Single Seam per Layer Centrally Laid Ultra-narrow Gap P-GMA Dissimilar Weld.....	169
6.5.1. Commercial benefits.....	198
6.5.1.1. Material consumption.....	198
Chapter 7.....	201
CONCLUSIONS.....	201
REFERENCES.....	203
Annexure A.....	229
SCOPE FOR FUTURE WORK.....	229
Annexure B.....	231



LIST OF FIGURES

Figure 2-1 Pseudo binary section of the Fe–Cr–Ni ternary diagram at 70% Fe, showing solidification modes; A - fully austenitic, AF - austenitic–ferritic, FA - ferritic–austenitic and F -fully ferritic. [Shankar et.al 2003]	14
Figure 2-2 Mean coefficient of thermal expansion plotted on the DeLong diagram as a function of chromium and nickel equivalents [Elmer et al 1982]	15
Figure 2-3 Schaeffler’s constitution diagram giving δ ferrite content in stainless steel. The compositional”ranges of the ferritic, ”martensitic, austenitic, and”duplex alloys have been superimposed”on this diagram. [Shanker et al 2003b]	16
Figure 2-4 DeLong constitution diagram for stainless steel weld metal [DeLong 1974]. .	17
Figure 2-5 The WRC-92 constitution diagram for weld metal ferrite, including solidification mode boundaries [Siewert et al 1988].	17
Figure 2-6 Power supply characteristic curves.	19
Figure 2-7 Thermal conductivity of gases as a function of temperature	24
Figure 2-8 Correlation between super”heat temperature and equivalent”anode melting potential for filler wire and”shielding gas combination of (a) 1.2mm, 100% Ar., (b) 1.6mm, 100% Ar., (c) 1.2mm, 80% Ar+20%CO ₂ and (d) 1.6mm, 100%CO ₂ respectively [Terumi and Kazuo 2002].	27
Figure 2-9 Current waveform for pulsed current”gas metal arc welding.	28
Figure 2-10 Static volt-ampere characteristics of power source.....	55
Figure 2-11 Rotational movement of welding arc produced by twist-arc [Okuda et al 1986].	62
Figure 2-12 Wire waving mechanism (left) and the waved wires (right) [Kwahara et al 1986]	63
Figure 2-13 Corrugated wire and rotating arc [Nakajima et al, 1986].....	63
Figure 2-14 Loop nap method mechanism [Kanbe Y et al, 1986].....	63
Figure 2-15 Bent contact-tip: (a) end view, (b) top view, (c) side view including.....	64
Figure 2-16 High speed rotating arc principle [Nomura H, 1984]	64
Figure 2-17 Electromagnetic arc oscillation [Kang Y H et al, 2003]	64
Figure 3-1 Photograph of commercially available conventional GMAW torch nozzle. ..	76
Figure 3-2 Schematic diagram of (a) Conventional and (b) newly designed narrow GMA torch nozzle. (All dimension in mm)	77

Figure 3-3 Schematic diagram of 7.5 mm narrow groove width for welding of thick section.....	78
Figure 3-4 Photograph of (a) unburnt (b & c) burnt narrow GMAW torch nozzle.	78
Figure 3-5 Isometric drawing of rectangular faced narrow gap GMA welding torch nozzle used in (a) first pass and (b) second pass.	79
Figure 3-6 Photograph of newly developed narrow GMAW torch nozzle.	79
Figure 3-7 GMA torch head with newly developed narrow torch nozzle device.	80
Figure 3-8 Photograph showing closely fitted narrow groove of 25 mm thick dissimilar plates with narrow welding torch nozzle inserted in it.....	81
Figure 3-9 Computational domains of the torch nozzle head placed inside the narrow ..	84
Figure 3-10 Computational domains of the torch nozzle head placed inside the narrow groove at different projection tip angle i.e. 0°-60°.....	84
Figure 4-1 Schematic diagram of metal deposition in a narrow weld groove with the formation of cavity in weld pool. (All dimension in mm)	89
Figure 4-2 Schematic diagram showing effective geometry of weld deposit in contact with groove wall.....	90
Figure 4-3 Schematic profile of molten pool of a weld pass showing distance touching points of its upper and lower most layer with groove wall in reference to the point of heat transfer by droplets in the cavity.....	93
Figure 5-1 Photograph of power source used in this investigation.	101
Figure 5-2 Schematic diagram of welding fixture.	102
Figure 5-3 Typical behaviour of recording of WMS4000 software of (a) arc voltage, 25V (b) welding current, 240A.	103
Figure 5-4 Schematic circuit diagram of welding and recording set up along with cooling system of torch head.....	104
Figure 5-5 (a) Photograph of the strain buster (b) Photograph of the experimental set up used for welding.	105
Figure 5-6 Schematic diagram of double ellipsoidal heat source (volumetric heat source).....	106
Figure 5-7 (a) Schematic diagram showing location of thermocouples in bead on plate deposition (b) Schematic diagram showing the depth of placement of thermocouple (D_T) and typical macrograph showing placement of thermocouple in weld pool.....	109

Figure 5-8 Temperature dependent thermo-physical properties of commercial mild steel.	110
Figure 5-9 Schematic diagram showing geometrical aspects of weld bead.	111
Figure 5-10 Schematic diagram of (a) conventional V-groove (CG) and (b) Ultra-narrow groove (UNG).	111
Figure 5-11 Schematic diagram of (a) multi pass multi seam per layer deposition and (b) multi pass single seam per layer deposition technique.	112
Figure 5-12 Schematic diagram of collection of test specimens from the dissimilar weld joint.	113
Figure 5-13 Photograph of Ultrasonic test on ultra-narrow gap weld joints.	114
Figure 5-14 (a) Schematic diagram showing the technique of measurement of transverse shrinkage (b) Schematic diagram showing the technique of measurement of deflection.....	115
Figure 5-15 Photograph of Equipments used for microstructure recording (a) Electro-etching equipment (b) Leica Optical microscope	117
Figure 5-16 Photograph of the Instron 8802 servohydraulic tensile testing machine. ...	118
Figure 5-17 Schematic diagram of the tensile specimens (a) base metal (b) axial weld and (c) all weld metal (All dimensions are in ‘mm’).....	118
Figure 5-18 Photograph of the Scanning Electron Microscope.....	119
Figure 5-19 Photograph of the Vickers micro hardness tester.....	119
Figure 6-1 Typical microstructure of the γ -SS base metal (a) transverse direction and (b) longitudinal direction.	123
Figure 6-2 Typical microstructure of the HSLA steel base metal (a) transverse direction and (b) longitudinal direction.....	123
Figure 6-3 Typical fractograph of tensile sample at relatively low and high magnifications of HSLA steel base metal and γ -SS base metal.	125
Figure 6-4 Typical indentation observed in (a) HSLA and (b) γ -SS steel base metal....	125
Figure 6-5 Schematic diagram of conventional GMA welding torch with 28mm groove opening.....	127
Figure 6-6 Simulation result of shielding gas flow in conventional groove opening of 28mm in 25mm thick plate.	127
Figure 6-7 Influence of gas flow rate on different flow parameter.(a) Maximum velocity of argon gas at opening (m/sec), (b) Argon gas velocity at outlet (m/sec), (c)	

Average pressure at outlet (Pa) and Turbulence kinetic energy in arc zone (J/kg).....	128
Figure 6-8 At a given gas flow rate effect of projection angle of nozzle tip on the argon shielding gas flow characteristics as (a) maximum velocity at opening and (b) velocity at outlet.....	130
Figure 6-9 At a given gas flow rate the effect of projection angle of nozzle tip on the argon shielding gas flow characteristics as (a) average pressure at the outlet and (b) turbulence kinetic energy in arc zone.....	133
Figure 6-10 At a given argon shielding gas flow rate the effect of projection angle of nozzle tip on the arc characteristics as (a) arc length and (b) arc diameter.....	134
Figure 6-11 Typical flow characteristics of argon gas shielding inside the narrow groove with MHD.....	135
Figure 6-12 Flow characteristics of argon gas shielding inside the narrow groove with MHD for 2 nd pass.....	136
Figure 6-13 Difference in arc characteristics during first and second pass as (a) arc length and (b) arc diameter.....	136
Figure 6-14 Difference in argon gas flow characteristics during first and second pass as (a).....	137
Figure 6-15 Difference in argon gas flow characteristics during first and second pass as (a) average pressure at the outlet and (b) turbulence kinetic energy in arc zone.....	137
Figure 6-16 At a given arc voltage of $25 \pm 1V$ the effect of ϕ on (a) heat content per unit mass of droplet and (b) temperature of droplet at the time of deposition at different I_m of 200, 220 and 240A respectively.....	140
Figure 6-17 At a given arc voltage of $25 \pm 1V$ the effect of ϕ on (a) diameter of droplet and (b) number of droplet transferred per pulse at different I_m of 200, 220 and 240A respectively.....	141
Figure 6-18 At a given arc voltage of $25 \pm 1V$ the effect of ϕ on total heat transfer to weld pool at different I_m of 200, 220 and 240A respectively.....	142
Figure 6-19 At a given arc voltage of $25 \pm 1V$, the effect of ϕ and Ω on weld pool temperature under different mean current of 200, 220 and 240 A respectively.....	143

Figure 6-20 At a given arc voltage of $25\pm 1V$, comparison of measured and estimated weld pool temperature at depths of about 2.5 - 3mm from its weld pool surface at different I_m and ϕ	144
Figure 6-21 Effect of mean current on length of filler wire consumed per unit length of weld deposition at different heat input.....	149
Figure 6-22 Effect of mean current on volume of metal deposited per unit length of weld at different heat input.	150
Figure 6-23 At different mean currents effect of number of weld pass on height of the groove wall covered by weld pool at varied Ω of (a) 7.63 ± 0.4 and (b) 9.81 ± 0.5 kJ/cm.	151
Figure 6-24 At different mean currents, the base metal fusion in dissimilar groove wall at.....	153
Figure 6-25 At different mean currents, the total necessary mass of fusion at each weld pass at Ω of 9.81 ± 0.5	154
Figure 6-26 At different mean currents, the total heat required for desired melting of dissimilar groove wall at each weld pass at Ω of 9.81 ± 0.5 kJ/cm.	155
Figure 6-27 At different mean currents, the average weld pool temperature required at each weld pass for producing dissimilar sound weld joint at Ω of 9.81 ± 0.5 kJ/cm.	155
Figure 6-28 Effect of number of pass and ϕ on estimated depth of cavity formed by impingement of metal droplets at different mean currents.....	156
Figure 6-29 Variation of the distance R_1 and R_2 at each weld pass of a given Ω of $7.63.2\pm 0.4$ kJ/cm under different I_m	157
Figure 6-30 Variation of the distance R_1 and R_2 at each weld pass of a given Ω of 9.81 ± 0.5 kJ/cm under different I_m	158
Figure 6-31 At a given arc voltage the typical isotherm of weld pool at different I_m and same ϕ value respectively of (a) 200A and 0.05, (b) 220A and 0.05 and (c) 240A and 0.05 at Ω of 9.81 ± 0.5	160
Figure 6-32 At a given arc voltage typical isotherm of weld pool at different I_m and ϕ respectively of (a) 200A and 0.25, (b) 220A and 0.25, (c) 240A and 0.25 and at Ω of 9.81 ± 0.5	161
Figure 6-33 Comparison of the estimated and required temperature of the weld pool at different I_m and ϕ respectively of (a) 200A and 0.05, (b) 220A and 0.05 and (c) 240A and 0.05 at Ω of 9.81 ± 0.5 kJ/cm.....	162

Figure 6-34 Comparison of the estimated and required temperature of the weld pool at different I_m and ϕ respectively of (a) 200A and 0.25, (b) 220A and 0.25, (c) 240A and 0.25 at Ω of 9.81 ± 0.5 kJ/cm.	163
Figure 6-35 Typical appearance of interrupted intimate contact of single seam per layer weld deposit with the dissimilar groove wall in ultra-narrow gap welding at (a) 200A and 0.05, (b) 220A and 0.05, (c) 240A and 0.05 at Ω of 7.64 ± 0.5 kJ/cm.	165
Figure 6-36 Typical appearance of uninterrupted intimate contact of single seam per layer weld deposit with the dissimilar groove wall in ultra-narrow gap welding at (a) 200A and 0.05, (b) 220A and 0.05, (c) 240A and 0.05 at Ω of 9.81 ± 0.5 kJ/cm.	165
Figure 6-37 Typical appearance of uninterrupted intimate contact of single seam per layer weld deposit with the dissimilar groove wall in ultra-narrow gap welding at (a) 200A and 0.25, (b) 220A and 0.25, (c) 240A and 0.25 at Ω of 9.81 ± 0.5 kJ/cm.	166
Figure 6-38 Lack of fusion at groove wall typically observed in transverse section of dissimilar weld joint prepared at a given arc voltage and Ω of $25\pm 1V$ and 7.63 ± 0.4 kJ/cm respectively under different I_m and ϕ respectively of (a) 200A and 0.05, (b) 220A and 0.05 and (c) 240A and 0.05.	168
Figure 6-39 Without lack of fusion at groove wall typically observed in transverse section of weld joint prepared at a given arc voltage and Ω of $25\pm 1V$ and 9.81 ± 0.5 kJ/cm respectively under different I_m and ϕ respectively of (a) 200A and 0.05, (b) 220A and 0.05 and (c) 240A and 0.05.	169
Figure 6-40 Typical macrograph of conventional V-groove P-GMA dissimilar weld joint at a given arc voltage and Ω of $25\pm 1V$ and 9.81 ± 0.5 kJ/cm and ϕ , I_m of 0.05, 220A.	171
Figure 6-41 Typical macrographs of ultra-narrow groove P-GMA dissimilar weld joints at a given arc voltage and Ω of $25\pm 1V$ and 9.81 ± 0.5 kJ/cm respectively under different ϕ and I_m	172
Figure 6-42 Effect of weld groove size and I_m and ϕ on weld area of P-GMA dissimilar weld joints prepared at a given arc voltage and Ω of $25\pm 1V$ and 9.81 ± 0.5 kJ/cm respectively.	173

Figure 6-43 Effect of weld groove size and I_m and ϕ on cumulative shrinkage of P-GMA dissimilar weld joints prepared at a given arc voltage and Ω of $25\pm 1V$ and $9.81\pm 0.5kJ/cm$ respectively.	174
Figure 6-44 Effect of weld groove size and I_m and ϕ on transverse shrinkage of P-GMA dissimilar weld joints prepared at a given arc voltage and Ω of $25\pm 1V$ and $9.81\pm 0.5kJ/cm$ respectively.	175
Figure 6-45 At a given arc voltage and Ω of $25\pm 1V$ and $9.81\pm 0.5kJ/cm$ effect of weld groove size and I_m and ϕ of P-GMA weld joints on transverse shrinkage stress.	176
Figure 6-46 At a given arc voltage and Ω of $25\pm 1V$ and $9.81\pm 0.5kJ/cm$ effect of weld groove size and I_m and ϕ of P-GMA weld joints on (a) deflection and (b) bending stress respectively.	178
Figure 6-47 Typical microstructures of CG P-GMA weld deposit from its different portion of the weld joint at a given arc voltage, ϕ , I_m and Ω of $25\pm 1V$, 0.05 and $240A$ and Ω of $9.81\pm 0.4kJ/cm$	179
Figure 6-48 At a given arc voltage and Ω of $25\pm 1V$ and $9.81\pm 0.5kJ/cm$ typical microstructures of intersection part of MPSSPL ultra-narrow gap P-GMA weld joint prepared at different I_m and ϕ	181
Figure 6-49 Effect of weld groove size, I_m and ϕ on percentage of dendritic region of P-GMA weld joints prepared at a given arc voltage and Ω of $25\pm 1V$ and $9.81\pm 0.5kJ/cm$ respectively.	182
Figure 6-50 Effect of weld groove size, I_m and ϕ on percentage of reheat refined region of P-GMA weld joints prepared at a given arc voltage and Ω of $25\pm 1V$ and $9.81\pm 0.5kJ/cm$ respectively.	182
Figure 6-51 Typical dendritic microstructures of MPMSPL conventional groove P-GMA weld joint and MPSSPL ultra-narrow gap P-GMA weld joint at comparatively higher magnification prepared at diverse I_m and ϕ	183
Figure 6-52 Typical reheat refined microstructure of MPMSPL conventional groove P-GMA weld joint and MPSSPL ultra-narrow gap P-GMA weld joint prepared at diverse I_m and ϕ	184
Figure 6-53 Typical microstructures of HAZ (HSLA side) at relatively low and high magnifications of conventional groove and narrow groove weld joints at a given arc voltage Ω of $25\pm 1V$ and $9.81\pm 0.5kJ/cm$ of varied I_m and ϕ	187

Figure 6-54 Effect of weld groove size, I_m and ϕ on HAZ width of P-GMA dissimilar weld joints (HSLA side) prepared at a given arc voltage and Ω of $25\pm 1V$ and $9.81\pm 0.5kJ/cm$ respectively.....	188
Figure 6-55 Effect of weld groove size, I_m and ϕ on coarse grain size adjacent to fusion line of P-GMA dissimilar weld joints (HSLA side) prepared at a given arc voltage and Ω of $25\pm 1V$ and $9.81\pm 0.5kJ/cm$ respectively.	188
Figure 6-56 Typical microstructures of HAZ (γ -SS side) of conventional groove and ultra-narrow groove weld joints at a given arc voltage Ω of $25\pm 1V$ and $9.81\pm 0.5kJ/cm$ of varied I_m and ϕ	189
Figure 6-57 Effect of weld groove size, I_m and ϕ on coarse grain size adjacent to fusion line of P-GMA dissimilar weld joints (γ -SS side) prepared at a given arc voltage and Ω of $25\pm 1V$ and $9.81\pm 0.5kJ/cm$ respectively.	190
Figure 6-58 Typical location of fracture under tensile loading on axial weld test of MPMSPL conventional groove weld joint and MPSSPL narrow gap P-GMA weld joint at different ϕ and I_m of (a) UNG, 0.05 and 200A (b) UNG, 0.25 and 200A, (c) UNG, 0.05 and 220A, (d) UNG, 0.25 and 220A, (e) UNG, 0.05 and 240A (f) UNG, 0.25 and 240A and (g) CG, 0.05 and 220.....	191
Figure 6-59 Effect of I_m and ϕ on yield strength of MPMSPL conventional groove weld joint and MPSSPL ultra-narrow gap P-GMA weld joint prepared at a given Ω of $9.81\pm 0.5kJ/cm$	192
Figure 6-60 Effect of I_m and ϕ on ultimate tensile strength of MPMSPL conventional groove weld joint and MPSSPL ultra-narrow gap P-GMA weld joint prepared at a given Ω of $9.81\pm 0.5kJ/cm$	192
Figure 6-61 Effect of I_m and ϕ on % elongation of MPMSPL conventional groove weld joint and MPSSPL ultra-narrow gap P-GMA weld joint prepared at a given Ω of $9.81\pm 0.5kJ/cm$	193
Figure 6-62 Typical fractured specimen of all weld tensile specimen of MPMSPL conventional groove weld joint and MPSSPL ultra-narrow gap P-GMA weld joint prepared at a given Ω of $9.81\pm 0.5kJ/cm$	194
Figure 6-63 Typical fractographs of all weld tensile specimen of MPMSPL conventional groove weld joint and MPSSPL ultra-narrow gap P-GMA weld joint prepared at a given Ω of $9.81\pm 0.5kJ/cm$	195

Figure 6-64 Typical variation in hardness observed across the MPMSPL conventional groove and MPSSPL ultra-narrow gap P-GMA dissimilar weld joints prepared at a given Ω of $9.81 \pm 0.5 \text{ kJ/cm}$ at different I_m and ϕ 196

Figure 6-65 Typical variation in residual stresses at the top in the weld joint observed across the MPMSPL conventional groove and MPSSPL ultra-narrow gap P-GMA dissimilar weld joints prepared at a given Ω of $9.81 \pm 0.5 \text{ kJ/cm}$ at different I_m and ϕ 197

Figure 6-66 Effect of weld groove size, I_m and ϕ of P-GMA weld joints prepared at a given arc voltage and Ω of $25 \pm 1 \text{ V}$ and $9.81 \pm 0.5 \text{ kJ/cm}$ respectively on filler material consumption per meter length of weld. 199





Table 2-1 The standard compositions of common austenitic stainless steels classified according to the American Iron and Steel Institute (AISI)	13
Table 2-2 Basic physical and chemical characteristics of the gases.	23
Table 2-3 Physical properties of different materials of filler wire [Alum and Quintino 1985b, Colombieer, L. and Hochmann, L 1967, Metals Handbook 1979, Tekriwal and Mazmuder 1988, Waszink and Heuvel 1982].....	27
Table 2-4 Filler Metals for welding austenitic stainless steels From AWS Filler Metal specifications: A5.4,A5.9, A5.22.....	39
Table 5-1 Chemical compositions of base and filler material used in bead on plate as well as weld joint study.	100
Table 5-2 Pulse parameters and corresponding thermal behaviour used in weld bead on plate deposition by P-GMAW process.	108
Table 5-3 Welding parameters used in weld joint studies under P-GMA welding process.....	112
Table 6-1 Chemical compositions of γ -SS and HSLA steel base materials and welding filler metals.	122
Table 6-2 Inclusion content of dissimilar base Materials.	123
Table 6-3 Tensile properties of base materials of different gauge length.....	124
Table 6-4 Flow characteristics of argon gas shielding inside narrow groove without MHD.	131
Table 6-5 Flow characteristics of argon gas shielding inside the narrow groove with MHD.	132
Table 6-6 At a given Ω (7.64 ± 0.4 kJ/cm) and arc voltage (25 ± 1 V) the effect of ϕ and I_m on weld isotherm at γ -SS plate.....	146
Table 6-7 At a given Ω (9.81 ± 0.5 kJ/cm) and arc voltage (25 ± 1 V) the effect of ϕ and I_m on weld isotherm at γ -SS plate.....	147
Table 6-8 Pulse parameters with corresponding thermal behaviour used in preparation of weld joint using P-GMAW process	150



Symbol	Description
γ	Coefficient of surface tension of liquid filler metal, N m^{-1}
ξ	Distance of the point along the x-axis with respect to the origin of moving heat source, m
ψ	Effective melting potential at anode (Al-Mg = 6.66V and Mild steel = 5.8V) or Angle between the tangent to the weld pool boundary and the welding direction, deg
σ_{sbz}	Stefan Boltzmann constant ($\text{Js}^{-1}\text{m}^{-2}\text{K}^{-4}$)(5.68×10^{-8})
δ	Electrode tapering coefficient or Deflection, mm
Ω	Heat input per unit length of weld, kJ cm^{-1}
ϵ_A	Emissivity of argon plasma (0.012)
ϵ_w	Emissivity of weld pool (0.29)
τ	Flight time of droplets, sec.
ν	Kinematic viscosity of ionized shielding gas ($\text{Kg m}^{-1}\text{s}^{-1}$) (0.0044)
ρ	Mass density of the base metal, kg m^{-3}
ρ_c	Density of solid copper as the nozzle material (8954 kg/m^3)
σ	Stefan-boltzman constant, $\text{w m}^{-2} \text{ k}^{-4}$
σ_{tr}	Transverse shrinkage stress, MPa
σ_b	Bending stress, MPa
ϕ	Summarized influence of pulse parameters factor
ζ	Work function of the cathode surface (Al-Mg = 4eV and Mild steel = 4.5eV)
μ_0	Permeability of free space (NA^{-2}) ($4\pi \times 10^{-7}$)
λ_a	Thermal conductivity of argon, $\text{J m}^{-1} \text{ s}^{-1} \text{ K}^{-1}$
μ	Viscosity of ionized argon (0.00029) ($\text{kg m}^{-1} \text{ s}^{-1}$)

η_a	Arc efficiency (%)
η^*	Shape factor
ρ_d	Density of molten filler metal, kg m^{-3}
ρ_g	Mass density of plasma in arc column (kgm^{-3}) (0.06)
α_h	Heat transfer coefficient during flight of the droplets, $\text{j m}^{-2} \text{s}^{-1} \text{k}^{-1}$
ρ_m	Density of molten metal of the weld pool, kg m^{-3}
ΔT_{de}	Degree of superheating of the droplet at the time of deposition
ΔT_i	Degree of superheating of the droplet at the time of detachment
Δ_{tr}	Transverse shrinkage, mm
ρ_w	Density of the solid filler wire, kg.m^{-3}
$1/2\lambda$	Thermal diffusivity of the base plate
a	Thermal diffusivity of the base plate (m^2/sec) (Al-Mg = 8.418×10^{-5} and Mild Steel = 1.172×10^{-5})
a_1	Width of weld metal deposited in current pass, mm
A_1	Cross sectional area covered by molten filler metal during each pass
A_A	Surface area of the arc (m^2)
A_c	Contact area of copper tube with torch nozzle
AC	Alternating current
A_{cc}	Acceleration of the droplet due to plasma aerodynamics drag force, m s^{-2}
a_h, b_h, c_h	Ellipsoidal heat source parameters (m)
$a_h, b_h,$ c_{hf}, c_{hb}	Double ellipsoidal heat source parameters (m)
A_s	Surface area of the droplets transferred per pulse, m^2
A_F	Area of fusion, mm^2
A_R	Area of reinforcement, mm^2
A_T	Cross sectional area of narrow torch nozzle, mm^2
A_t	Area through which heat is transferred to cooling water by convection, m^2

A_w	Cross sectional area of the filler wire, m^2 or Area of weld deposit, m^2
b	Plate width, mm
b_1	Width of weld metal deposited in earlier pass, mm
B_{TA}	Bead toe angle
c	Specific heat of the base plate ($J\ g^{-1}K^{-1}$), (Al-Mg = 1.03 and Mild Steel = 0.486)
CC	Continuous current
C_d	Drag Coefficient
C_{pg}	Specific heat of argon plasma ($10000\ JKg^{-1}K^{-1}$)
$c_{p(l)}$	Specific heat of liquid filler metal, $J\ kg^{-1}\ k^{-1}$
C_{pl}	Specific heat of liquid metal, $J\ kg^{-1}\ k^{-1}$
$c_{p(s)}$	Specific heat of solid filler metal, $J\ kg^{-1}\ k^{-1}$
C_{PC}	Specific heat of copper ($384\ J/kg\ ^0K$)
C_{pw}	Specific heat of water ($4.185\ kJ/kg\ k$)
C_R	Cooling rate, $^0K/sec$
D	Diameter of droplets, m
D_{g0}	Final mean grain diameter
D_{g1}	Initial grain diameter
D_h	Hydraulic diameter
D_L	Dilution %
d	Thickness of the base plate, m
d_w	Diameter of filler wire, mm
D_R	Arc root diameter, mm
D_P	Projected arc diameter, mm
D_L	Dilution of weld deposit, %
D.C	Direct current

E	Young's modulus of base material, $210 \times 10^3 \text{MPa}$
E_w	Electrode extension, m
e	Charge of electron ($1.602 \times 10^{-19} \text{ J}$)
F	Aerodynamic drag force or Force generated due to distortion, N
F_{AT}	Shape factor which dictates the fraction of radiation heat transferred from the arc to the torch nozzle
F_{BMF}	Fraction of base metal fusion per unit mass of bead deposition
FF	Form factor
F_{WT}	Shape factor which considers the fraction of radiation heat transferred from weld pool to the torch nozzle
f	Pulse frequency, Hz
g	Gravitational acceleration, m s^{-2}
H_{AR}	Radiation heat transfer by the arc
H_g	Heat carried away by the argon gas
H_G	Heat transfer to the torch nozzle from argon gas
H_{MR}	Radiation heat transfer by molten weld pool
H_r	Bead height
h	Depth of cavity, m
h_c	Convection heat transfer coefficient
H_T	Total heat gained by the torch nozzle device
H_t	Total heat required to fuse the m_t amount of metal per unit length of weld, kJ
HAZ	Heat affected zone
I	Welding current, A
I_b	Base current, A
I_{eff}	Effective current, A
I_m	Mean current, A
I^m	Moment of inertia, mm^4

I_p	Peak current, A
j_{eff}	Effective current density, $J A^{-2}$
j_g	Current density of plasma in arc column, $A m^{-2}$
k	Thermal conductivity of the base metal ($J m^{-1} s^{-1} K^{-1}$) (Al-Mg = 222 and Mild Steel = 51.6)
K_1	Kinetic constant ($1.26 \times 10^{12} \mu m^2/S$)
k_p	Pulse duty cycle
L	Arc length, mm and Latent heat of fusion, $J kg^{-1}$
l_b	Inclined length of groove wall, mm
l_p	Length of weld pool, mm
L_C	Distance of the measuring point (dial gauge tip) from the central axis of the weld joint, mm
L_w	Length of filler wire consumed per pass of weld deposition, m
m_b	Mass of base material fusion required, kg
m_d	Mass of the droplet, kg
m_f	Amount of filler wire consumed per pass, kg
m_t	Total mass of fusion from the base metal and earlier deposited weld metal, kg
m_{tb}	Mass of filler wire transferred during base current period, kg
m_{tp}	Mass of filler wire transferred during peak current period, kg
m_w	Mass of fusion of weld deposit of earlier pass, kg
M	Bending moment, N-mm
N_D	Number of droplets transfer per pulse
Nu_L	Nusselt number
p	Hydrostatic pressure
Pr	Prandtl number
Q_A	Arc heat transferred to the filler wire, $J s^{-1}$

Q_{app}	Apparent activation energy for grain boundary movement (260kJ/mol)
Q_{arc}	Arc heat generated by the energy input, $J s^{-1}$
Q_{AW}	Arc heat transferred to the weld pool, $J s^{-1}$
Q_{cv}	Heat loss during flight of the droplets due to convection, $J kg^{-1}$
Q_{de}	Heat content per unit mass of the filler wire at the time of deposition, $J kg^{-1}$
Q_f	Heat of the filler metal transferred to the weld pool, $J s^{-1}$
Q_{fp}	Heat content of the droplets transferred per pulse, $J kg^{-1}$
Q_{fpb}	Heat content of the droplets transferred during base current period, $J kg^{-1}$
Q_{fpp}	Heat content of the droplets transferred during peak current period, $J kg^{-1}$
Q_i	Heat content per unit mass of the filler wire at the time of detachment, $J kg^{-1}$
Q_m	Heat required for melting of the filler wire, $J kg^{-1}$
Q_o	Total heat generated at the tip of the filler wire electrode, $J s^{-1}$
Q_p	Heat transferred per unit time by point heat source, $J s^{-1}$
Q_r	Heat generated due to resistive heating of the filler wire, $J s^{-1}$
Q_R	Heat loss during flight of the droplets due to radiation, $J kg^{-1}$
Q_T	Total heat transferred per unit time, $J s^{-1}$
Q_{tl}	Total heat loss during flight of droplet, $J kg^{-1}$
Q_w	Heat required for melting superheating of the droplet, $J s^{-1}$
r	Effective radius of the filler wire, m
r_1	Focal length of paraboloidal cavity, m
r_c	Radius at the projected surface of the cavity, m
Re	Reynold's number
r_f, r_b	Proportion coefficients in front and behind the heat source
R	Distance (mm) of the point with respect to the central axis
Re	Reynold's number
R_G	Growth rate of dendrite, cm/min

R_o	Resistivity of the filler wire, $\Omega.m$
R_s	Electrical resistance of the electrode extension, Ω
R_w	Radius of the filler wire, m
S	Welding speed, cm/min
s_b	Surface area of each side of groove wall in contact with molten weld pool, mm^2
s_w	Surface area of the weld pool in contact with the earlier weld deposit, mm^2
T	Temperature of upper part of the torch surface at location-B, K
t	Thickness of the torch nozzle, mm.
T_A	Temperature of the outer arc chevron, K
T_a	Ambient temperature, K
t_b	Base current duration, s
t_D	Minimum time required for transfer of a droplet, s
T_d	Temperature at any point in the weld due to arc heating, K
T_{de}	Temperature of the droplet at the time of deposition, K
T_g	Temperature of argon gas plasma
T_i	Temperature of droplet at the time of detachment, K
T_{in}	Inlet temperature of cooling water, K
T_m	Melting temperature, K
T_S	Surface temperature of the torch K
T_{rwp}	Required temperature of the weld pool, K
T_{ewp}	Estimated temperature of weld pool, K
T_T	Initial temperature of the torch nozzle, K
T_{ST}	Surface temperature of torch nozzle due to combined heating by convection heat transfer from argon gas plasma and radiation from the arc, K
T_{WP}	Average weld pool temperature, K

T_0	Initial temperature of the base plate, K
ΔT	Rise of temperature of the torch nozzle, K
t_p	Peak current duration, s
t_{pul}	Pulse cycle time, s
t_w	Depth of fusion of earlier weld deposit, mm
V	Arc voltage, V
v	Welding speed, $m.s^{-1}$
V_a	Anode fall voltage, V
V_c	Volume of the cavity, m^3
V_d	Droplet volume, m^3
V_{de}	Velocity of the droplet at the time of detachment in the weld pool, $m s^{-1}$
V_{eff}	Effective velocity of plasma, $m s^{-1}$
V_i	Velocity of the droplet at the time of detachment from the electrode tip, $m s^{-1}$
V_m	Volume of weld deposit respectively, m^3
V_{max}	Maximum axial velocity of the electro-magnetically induced plasma jet, $m s^{-1}$
V_w	Wire feed speed, $m s^{-1}$
$V_{w(pc)}$	Wire burn off rate
V_{wp}	Wire burn off rates during t_p
V_{wb}	Wire burn off rates during t_b
VHN	Vickers hardness number
w	Work done in creating a paraboloidal cavity
W_b	Bead width
W_{rg}	Width of molten pool, mm
x, y, z	Rectangular coordinates w.r.t. to a fixed origin
x_{hw}	Distance between the heat source and the rear of the weld pool, mm

There are many applications of Dissimilar metal welding (DMW) of thick wall austenitic stainless steel (ASS) and high strength low-alloy steel (HSLA) plates such as in power generation, defense, chemical, petrochemical, and nuclear industries where, the temperature elevates up to a range of the order of 350-450°C [Huang 1998, Marshall 1982]. The adoption of this combination has been justified based on both the technical and economical reasons.

The DMW of thick sections of the ASS and HSLA is critical as it requires appropriate care of several difficulties. The difficulties primarily include the problems largely associated with difference in coefficient of thermal expansion (CTE) and thermal conductivity respectively affecting the undesirable development and distribution of residual stresses and development of undesirable weld chemistry due to dilution. It is also extended up to metallurgical incompatibility primarily with respect to the formation of undesirable phases in the weld and HAZ and the segregation of high and low melting phases due to chemical mismatch [Lundin 1982, Faber 1982, Castro 1974, Hearn 1982, Gauzzi 1988].

For versatile application in general weld fabrication of thick sections of γ -SS and HSLA, there may be several choices of fusion welding processes, such as shielded metal arc, gas tungsten arc, gas metal arc and submerged arc welding. Welding of thick sections of γ -SS and HSLA steel are generally carried out by submerged arc welding (SAW), shielded metal arc welding (SMAW), gas tungsten arc welding (GTAW) and gas metal arc welding (GMAW) processes. Every process is having different weld thermal cycle depending upon rate of weld deposition, welding parameters and shielding environment. The amount of weld deposition which also considerably influences the severity of thermal characteristics of a weld can be considerably reduced by using narrow gap welding technique. Amongst all these welding processes the use of gas metal arc welding (GMAW) and gas tungsten arc welding (GTAW) are gaining more attention in fabrication of weld joint. It is especially true in case of dissimilar welding of stainless steel to carbon steel, due to their capability to produce superior quality weld in comparison to that of the commonly used shielded metal arc (SMA) and submerged arc (SA) welds. The superiority of the GMA weld over the SMA weld is primarily understood by its ability to produce inclusion free weld that improve its mechanical properties with better integrity and higher economy. It also facilitates automation in weld fabrication. But the critical control of arc characteristics and behaviour of metal transfer as a function of welding parameters often makes

the application of the GMAW process relatively complicated to achieve desired weld quality especially with respect to defect and metallurgical characteristics of the weld.

The severity of thermal and mechanical effects of welding in case of using conventional weld groove in dissimilar thick sections always remains as a great concern which can be considerably minimized by reducing the amount of weld deposit and its heat content in a joint by using narrow gap welding technique. The SAW can be successfully used for narrow gap welding but under an influence of considerably high heat input. The preparation of narrow groove weld joint by SMAW and GTAW processes usually requires welding at a low angle of attack to groove wall by a skilled welder and the process automation is highly critical. The SMAW has further limitation of slag entrapment resulting in poor mechanical properties, whereas in GTAW process welding speed is significantly lower than SMAW process. These limitations of SMAW and GTAW processes can be suitably addressed by the merits of GMAW process using spray mode of metal transfer which offers better ease of operation with relatively higher rate of weld deposition primarily due to predominating electromagnetic force resulting in projected transfer of droplet. However, depending upon material and size of filler wire and shielding environment the spray transfer in GMAW is achieved at relatively high welding current which also significantly enhances heat input to the weld.

During narrow gap welding with low amount of weld deposition and less thermal severity it is always important to ensure the proper fusion of groove wall particularly in case of dissimilar weld joint of austenitic stainless steel to HSLA steel to produce a sound weld. The difficulties primarily include the problems largely associated with difference in coefficient of thermal expansion (CTE) and thermal conductivity respectively affecting the undesirable development and distribution of residual stresses, development of unwanted weld chemistry due to dilution. It also affects metallurgical incompatibility primarily with respect to the formation of unacceptable phases in the weld and HAZ and the segregation of high and low melting phases due to chemical mismatch. To produce a sound weld it is noted that fusion of groove wall up to a skin depth of the order of 0.5 to 1.0mm is generally considered as a basic requirement. In multipass welding of thick dissimilar section it also includes fusion of earlier deposited weld metal up to a certain extent, which is primarily dictated by the heat content of weld pool and thermal distribution in it in reference to the requirements for desired fusion. These aspects of welding largely depend upon the size and geometry of weld bead. The heat content of weld pool is largely governed by its mass per unit length and temperature. In case of reducing the width of narrow groove to a lowest possible limit it may be required to keep no angle of attack of the electrode to the groove wall. In maximum possible narrowing of groove width, the situation may demand a centrally located

weld deposition in a groove having an efficiency to simultaneously fuse the dissimilar wall of its both sides. For weld deposition with centrally located electrode allowing no angle of attack to the groove wall by the arc, the groove wall fusion may primarily depend upon the thermal behaviour and geometry of molten weld bead intimately touching the dissimilar groove wall for sufficient heat transfer.

In view of the well-known merit of GMAW for preparation of comparatively cleaner sound weld it is successfully tried earlier to prepare narrow gap welding of steel. In this case the control of shape and size of weld pool in order to achieve desired weld isotherm for dissimilar groove wall and temperature of molten metal is largely obtained by the increase of welding current and heat input. The energy input involved in a welding process, causing melting of the filler and base metals also develops certain reactions in a very short period of time which result some dramatic changes in the microstructure of HAZ near to the fusion line. These changes primarily result from the rapid heating and cooling of the base materials during welding. In order to control these changes, it is necessary to regulate thermal behaviour of welding process, especially in reference to critical durations of maximum temperature and the temperature above critical transformation range. In this regard the cooling rate prevailing in the interactive locations of dissimilar material is also quite important with respect to diffusion of active elements, phase transformations and development of residual stress at the joint.

However such derogatory influence of GMAW due to use of comparatively higher heat input during welding, can be successfully addressed by application of relatively low heating pulse current gas metal arc welding (P-GMAW) process. The use of pulsed current gas metal arc welding (P-GMAW) process can be accredited for the possibility of more precisely controlled weld thermal cycle, primarily due to its merit of developing relatively lower heat buildup in weld pool than the conventional GMAW process resulting from interruption in weld metal deposition under pulsed current. Moreover as the P-GMAW is also a low heat input process it may reduce residual stresses and favorably affect the dilution and phase transformation in the weld joint.

The use of P-GMAW process may provide an opportunity to control the size and geometry of weld bead at a relatively low severity of its thermal characteristics. However, the merits and success of pulsed current GMAW process is largely dependent upon right selection of pulse parameters, like mean current (I_m), peak current (I_p), base current (I_b), pulse duration (t_p) and pulse frequency (f). This is because they affect the microstructure of weld and heat affected zone (HAZ) as well as chemistry and porosity content of the weld due to their influence on weld thermal cycle and arc characteristics. Preparation of a superior pulsed current GMA weld needs

thorough understanding of the process due to criticality in selection of pulse parameters, it arises out of simultaneous interaction amongst themselves during welding, which introduces complexity in selection of pulse parameters. This complexity in selection of pulse parameters can be largely solved by using a summarized influence of pulse parameters defined by a

hypothetically derived dimensionless factor $\phi = \frac{I_b}{I_p} \times f \times t_b$, where the pulse off time t_b is

expressed as $t_b = \left[\frac{1}{f} \right] - t_p$, which is amply justified by several investigators in applications of pulsed current GMAW on various materials.

Fusion welding as one of the most commonly used process; it is also largely used for the joining of dissimilar metals. For versatile application in general weld fabrication of thick sections of ASS and HSLA, there may be several choices of fusion welding processes, such as shielded metal arc, gas tungsten arc, gas metal arc and submerged arc welding. Every process is having different weld thermal cycle depending upon rate of weld deposition, welding parameters and shielding environment. The criticality in arc welding of thick dissimilar sections using conventional weld groove primarily arises due to large amount of multi pass metal deposition leading to a cumulative effect of severity of weld thermal cycle [Radaij 1992, Chapman et al 1997]. The amount of weld deposition which also considerably influences the severity of thermal characteristics of a weld can be considerably reduced by using narrow gap welding technique [Malin 1983(a), Malin 1983(b)]. The SAW can be successfully used for narrow gap welding but at fairly higher heat inputs which may adversely affect the mechanical and metallurgical properties of the weld joint. The preparation of narrow groove weld joint by SMAW and GTAW processes generally requires welding at a low angle of attack to groove wall by a skilled welder, which makes the process automation highly critical. The SMAW and SAW has additional limitation of slag entrapment resulting in poor mechanical properties, whereas in case of using GTAW process the welding speed becomes significantly lower. Amongst all these welding processes the use of gas metal arc welding (GMAW) and gas tungsten arc welding (GTAW) are gaining more attention in fabrication of weld joint, especially in case of dissimilar welding of SS to carbon steel, due to their capability to produce superior quality weld in comparison to that of the commonly used shielded metal arc (SMA) and submerged arc (SA) welds. However, as a comparatively low heat input welding process the GTAW is generally preferred for the root pass weld, but not for the filing passes in welding of thick sections [Welding handbook 1972]. The superiority of the GMA weld over the SMA weld is primarily understood by its ability to produce comparatively cleaner weld, improved mechanical properties, better integrity and higher

economy. It also facilitates automation in weld fabrication. But the critical control of arc characteristics and behaviour of metal transfer as a function of welding parameters often makes the application of the GMAW process relatively complicated to achieve desired weld quality especially with respect to defect and metallurgical characteristics of the weld.

However, depending upon material, size of filler wire and shielding environment, the spray transfer in GMAW is achieved at relatively high welding current, which appreciably enhances heat input to the weld. This increase in heat input consequently affects the weld pool size and temperature along with grain coarsening in heat affected zone (HAZ). An increase in weld pool size and temperature adversely influences the residual stresses of weld joint while grain coarsening in HAZ hampers the properties of weld joint. The effective heat input to the weld can be considerably minimised by the use of low heating pulse current gas metal arc welding (P-GMAW) through a control of heat distribution to the weld under pulse current.

The reduction in severity of weld thermal behaviour and stresses of narrow gap weld is primarily governed by narrowness of the groove width due to its ability to significantly reduce the amount of weld metal deposition in producing sound weld joint of a given thickness. However, the reduction in width of narrow groove is largely restricted by the minimum required angle of attack of the electrode to the groove wall which gives rise to desired groove wall fusion during weld metal deposition. In case of GMAW, it is further restricted due to constraint in manipulation of the bulky welding torch nozzle inside weld groove by keeping space for maintaining minimum required angle of attack. Thus, to achieve a narrow gap GMA welding with narrowest possible weld groove, it is required to employ weld deposition through a vertically placed centrally located electrode in the weld groove. Such a procedure using multi pass single seam per layer (MPSSPL) deposition technique with full assurance of groove wall fusion as well as a part of earlier deposited weld is the basic requirement for production of a sound ultra-narrow groove weld joint. The groove wall fusion in MPSSPL ultra narrow gap welding can be ensured by considering the geometrical and thermal aspects of molten weld pool primarily assuring its intimate contact with the groove wall to cause its desired melting. The thermal aspects of weld pool are largely attributed to its heat content and weld isotherm being primarily governed by the deposited mass per unit length and temperature, where the temperature of weld pool is basically dictated by the transfer of heat to it from different sources. In MPSSPL ultra-narrow gap welding using P-GMAW process, two heat sources of different natures act simultaneously on weld pool. One is continuous heat source (arc heat source) considered to be as double ellipsoidal [Goyal et.al 2008(a), Agrawal et.al 2010] acting at the centre over an area, which melts and produces an initial fusion of groove wall due to transfer of heat from it. The other one is an interrupted heat

source in the form of superheated filler metal depositing at the centre of weld, considered as a point heat source creating additional fusion of the groove wall [Goyal et.al. 2008, Ghosh et.al. 2007].

It is desired to have required fusion of dissimilar groove wall as well as a part of earlier deposited weld at an optimum thermal exposure in order to get minimum heat affected zone (HAZ) of undesirable microstructure as well as low residual stresses in the joint. The control of these aspects becomes more critical in case of joining of dissimilar thick wall austenitic stainless steel to micro alloyed HSLA steel using MPSSPL ultra-narrow gap welding. During dissimilar welds of austenitic stainless steel to HSLA steel the carbon migrates from low-alloy steel to the weld interface of the austenitic stainless steels at elevated temperature [Li and Charles 2001]. As a result, a carbon depleted zone forms in the heat-affected zone (HAZ) of low alloy steel adjacent to the stainless steel, and a carbon-enriched zone forms in its close range of austenitic stainless steel weld. The carbon-depleted zone is relatively low in creep strength and also weak in terms of stress rupture [Hyde et.al 2002], whereas the carbon-enriched zone present in matrix adjacent to it gives rise to a significant change in properties with comparatively high hardness and strength across a narrow region of less than 0.25 mm [Rowe et al 1999, Pressouyre et al 1982]. In the carbon enriched zone precipitation of chromium carbides reduces the dissolved Cr concentration in the matrix which causes the stress corrosion cracking in HAZ adjacent to the fusion line [Race et.al 1992, Amuda et.al 2011]. The carbon migration is considered to be a significant factor in determining the life of a weld which changes property across the weld to base metal interface as a function of the diffusion time and temperature. It is the nature of the two interactive zones across the interface that ultimately controls the failure mode.

As far as thermodynamics is concerned, the driving force for the carbon migration is the difference in carbon chemical potential caused by the substitutional variation in solute content in austenitic stainless steel and HSLA steel across the weld interface [Lee et al 2015]. It largely arises due to use of a welding process and procedure introducing large amount of metal deposition and/or severity of weld thermal cycle. Such undesirable conditions may be avoided by selection of a comparatively cleaner welding process, reduction in amount of weld deposition and modification of thermal behaviour of weld deposit through proper selection of welding parameters. The reduction in amount of weld deposition can be made possible by the use of narrow gap welding. However, the thermal behaviour can be manipulated more effectively by using pulse current gas metal arc welding (P-GMAW) process than other welding processes for introducing high heat intensity in desired location at low heat input. It becomes possible due to unique capacity of P-GMAW to maneuver energy distribution in the process with desired weld

isotherm and geometry of weld bead by appropriate control of pulse parameters. Thus, a combination of P-GMAW and MPSSPL ultra-narrow gap welding procedure supported by an appropriate model analysis may be considered as an interesting technique to weld thick dissimilar section of austenitic stainless steel to HSLA steel in order to have improved properties of weld joint than those observed in case of commonly used MPMSPL conventional groove weld. But, hardly any knowledge on welding procedure of MPSSPL ultra-narrow gap welding of thick dissimilar plates is available for GMAW process facilitating the selection of welding parameters for production of a sound weld joint, especially when it involves pulse current.

The use of pulsed current gas metal arc welding (P-GMAW) process can be accredited for the possibility of more precisely controlled weld thermal cycle, primarily due to its merit of developing relatively lower heat buildup in weld pool than the conventional GMAW process resulting from interruption in weld metal deposition under pulsed current [Ghosh et. al. 2006]. The selection of appropriate pulse parameters which can provide desired fusion of groove wall and temperature and geometry of the weld pool through controlled thermal and metal transfer behaviour of depositing droplet becomes relatively complicated due to simultaneous influence of the pulse parameters of peak current (I_p), base current (I_b), pulse time (t_p) and pulse frequency (f) on each other at a given mean current (I_m) of P-GMAW process [Quintino and Allum 1984, Subramaniam et.al. 1998, Randhawa et.al. 2000]. However, the difficulties of selection of the pulse parameters have been well addressed by considering summarized influence of pulse parameters proposed earlier and defined [Ghosh et al 1994, Ghosh 1999, Ghosh et al 2000, Ghosh et al 2001 and Ghosh et al 2007 (a, b)] by a hypothetical dimensionless factor $\left[\phi = \left(\frac{I_b}{I_p} \times f \times t_b \right) \right]$

where, $t_b = \frac{1}{f} - t_p$, derived on the basis of energy balance concept of the system. In addition to the hypothetical factor ϕ , the variation of heat input (Ω) to the system as a function of I_m , arc voltage (V), welding speed (S) and weld isotherm also influences the weld characteristics [Kulkarni 2008, Goyal et.al. 2008]. Moreover as the P-GMAW is also a low heat input process [Ferraresi et.al. 2003, Zhang et.al. 1998] it may reduce residual stresses and favourably affect the dilution [Ghosh et.al. 2004, Kulkarni et. al. 2005] and phase transformation [Goyal et.al. 2006] in the weld joint.

The P-GMAW can also facilitate the application of narrow gap gas metal arc welding [Malin 1983] which may be further effective for lowering of thermal severity and its adverse influences on the dissimilar weld joint of thick sections of ASS and HSLA. However, the narrow gap P-GMAW process often produces lack of fusion in the groove wall due to low angle of attack (arc

strike) to it, along with relatively low heat input and small molten weld pool. Thus, in order to produce minimum residual stresses in a defect free dissimilar weld joint with improved or comparable mechanical, fracture mechanics and corrosion properties in comparison to those either of the dissimilar base materials, the design of appropriate narrow groove and selection of pulse parameters is very much important. This may be achieved by developing a clear understanding over the influence of narrow groove design and pulse parameters on amount of weld deposition, weld thermal cycle and microstructure of the multipass weld. The microstructure is largely influenced by the solidification behaviour [Goyal et.al. 2006] of the P-GMA weld deposit in the joint of dissimilar materials.

In view of the above an effort has been made to design A substantially narrow GMAW torch nozzle has been designed that enables narrowing down of weld groove up to a limit of just accommodating the nozzle in it where the groove wall of thick section virtually acts as a nozzle side wall to produce a narrowest possible butt welding. The utility aspect of such a narrow nozzle from the view point of smooth flow of shielding gas inside a closely fitted narrow weld groove has also been studied. For this purpose a model of shielding gas flow dynamics and its flow rate in case of employing newly developed GMAW nozzle has been studied at different projection angle of torch nozzle inside the narrow groove of butt joint by using ANSYS-CFX (14.5) software. The outcome of these studies has been used to produce a defect free ultra-narrow multi-pass weld of thick dissimilar steel section of an austenitic stainless steel and micro-alloyed high strength low alloy (HSLA) structural steel by employing P-GMAW process with vertically placed electrode depositing single seam per layer deposition in weld groove to significantly reduce the residual stresses as well as improve the metallurgical and mechanical properties.

2.1. Introduction To Dissimilar Metal Welding

Pure metals or alloys that differ metallurgically, or have different intrinsic properties, are considered to be dissimilar. Dissimilar metal fusion welding involves the melting and mixing (alloying) of two or more metals, usually with the addition of a filler metal. The dissimilar metal can be one of the base metals and/or the filler metal. There are two basic types of dissimilar welds [Cox and Kiser 1992].

- 1) Joining different base metals with a filler metal (i.e., A to B with C)
- 2) Joining matching composition base metals with a different filler metal (i.e., A to A with C)

An unlimited number of final properties or alloy can be obtained, depending on the alloys selected, the welding process used, and the welding procedure. The weldability and fitness for purpose of the final product must be considered when selecting the dissimilar welding application. With fusion welding processes, the melted base metals and filler metals all contribute to the final properties of the weld [Cox and Kiser 1992].

When fusion welding dissimilar base metals, the filler metal selected must be one that will alloy metallurgically with the two base metals. However, not only must be the welding consumable is able to accept dilution from all of the elements contained in the base metal alloys, but it must also impart certain characteristics to the final weld. The weld must be as strong as or stronger than the base metal, while retaining metallurgical stability in the intended service [Cox and Kiser 1992]. Weld metal dilution is not the only consideration. One must also consider the melting temperatures, thermal conductivity, thermal expansion and pre-and post-weld heat treatment requirements of each alloy.

The welding engineer must select welding consumables that will closely match the base metal according to the previously mentioned properties (while still obtaining the desired service requirements, such as strength, ductility and corrosion resistance). However, occasionally a filler metal must be selected that will give properties as welded that, as cast, the base metal doesn't have. For instant, some metals have poor properties as cast but can be made acceptable with either working and /or heat treating and it is usually not feasible to work or heat treat welds [Cox and Kiser 1992].

2.1.1. Physical properties

For crack free welding, or satisfactory service, the chosen metals must have closely matching physical properties. If the base metals or filler metal contain elements which have substantially different melting temperatures, then upon weld metal solidification, they will become segregated. The higher melting elements will solidify first, leaving lower-melting constituents segregated [Cox and Kiser 1992]. Low melting eutectics can also form. All of these factors can combine to cause hot cracking, or a loss of weld ability.

If the filler metal or base metals have varying coefficients of thermal expansion (CTE), then this can add an amount of shrinkage stress that can exacerbate a hot cracking problem. Even if the melting temperature closely match, the added stress from different expansions and contractions (during heating and cooling) can still be sufficient to pull the weld apart before it completes solidification. A loss of weldability is compounded with a concern for added stresses during high temperature service [Cox and Kiser 1992]. This added stress can also make the weldment more susceptible to stress corrosion cracking in the as welded conditions.

To minimize stress concentrations, the CTE of the filler metal must be intermediate to the two base metals. If this is not possible, use a welding product whose CTE closely matches the base metal with the lower yield stress value. This will transfer the stress to the base metal with the higher yield strength. Also, if possible, dissimilar welds should be located in low stresses area so that this added stress from CTE differences would be minimized [Cox and Kiser 1992]. The amount of added stress is also dependent upon the metal's modulus of elasticity and yield point. Thermal fatigue is also a consideration if the weldment undergoes temperature cycles. The weld filler metal must be able to resist cracking and crack propagation.

Thermal conductivity differences between two metals should also be considered when welding for higher temperature service. These differences can affect the overall heat input to one of the alloy. The alloy with higher thermal conductivity will undergo a greater heat loss, and the welding procedure must be changed-either with arc manipulation (directing toward the heat loss) or increasing preheat (to the metal with the higher thermal conductivity) to provide for the desired penetration into each material [Cox and Kiser 1992].

2.1.2. Metallurgical compatibility

When arc welding of two dissimilar materials, there are number of aspects need to be addressed, in addition to those associated with welding similar materials. For high temperature services, it is important that whatever filler metal is selected, it must remain stable in relation to the base metals. In the case of heat treatable steels, the induces room-temperature microstructure

will no longer remain above the transformation temperature. Instead, the microstructure will be one of austenite, whose strength depends on nickel and chromium contents [Cox and Kiser 1992]. Thus, these types of welds would not be recommended for high-temperature service. Austenitic stainless steel would be better suited. However, with an austenitic microstructure, some ferrite is needed to avoid hot-cracking. There is the danger of brittle "sigma phases" transforming from the ferrite at the higher temperatures (around 800°C or 1450°F) [Cox and Kiser 1992]. Also secondary carbide formation could lead to embrittlement or a loss in ductility in the weld. A filler metal that would block carbon migration at higher temperature would be an advantage.

Dissimilar liquid weld metal has been shown to cause intergranular attack in the heat affected zones of some base metals, and can cause liquation cracking. The effect depends on the preheat temperature, heat input and joint restraint. A change in welding procedure that minimizes this effect would improve the weldability with metals which have this susceptibility. Magnesium can also be a metallurgical phenomenon that the welding engineer must take under consideration. If one of the base metals is ferromagnetic, it can deflect an arc away from the other nonmagnetic base metal alloy [Cox and Kiser 1992]. Selecting electrode which will maintain good arc characteristics with alternating current will eliminate this type of arc blow.

2.1.3. Heat treatment requirements

Occasionally, two different materials with two different heat treat requirements must be welded together. If this is the case, butter both sides with an alloy that is not affected by the heat treatment, perform the required treatments, and then weld them together. Using a low heat-input welding process, the heat-affected zones of the heat-sensitive alloys will not undergo transformation [Cox and Kiser 1992]. Some welding applications require the selection of a filler metal that produces properties in the cast condition that are similar to those of the base metal in a heat-treated condition, such as 9% nickel steel. In order to attain high notch toughness at low temperatures, this steel must be either double normalized or quenched and tempered. Since the welding process will create a cast structure, a 9% nickel steel welding product will have undesirable mechanical characteristics (as-welded). Therefore a high-nickel or high manganese stainless steel consumable must be selected for the filler metal to obtain acceptable impact strength values [Cox and Kiser 1992].

2.1.4. Serviceability

As stated previously, it is imperative that the weld metal be equal to or stronger than each base metal alloy. This is even more important with high-temperature conditions. Room

temperature yield strength mean very little at elevated temperatures. Since the weld makes up only a small portion of the weldment, it is detrimental if the weld creeps before the base metal does. If creep can be spread over the much greater volume of base metal by choosing stronger weld metal, the welded assembly will usually last longer [Cox and Kiser 1992].

Corrosion resistance also must be better in the weld. This is true for both wet and dry corrosive media. With wet corrosion, a galvanic series may occur when dissimilar metals are joined and in contact with the corrosive media. Therefore, the weld must be more noble so that potential preferential corrosion is transferred to the large area base metal. The weld metal composition can be adjusted so that it is cathodic to the base metals. Micro structural differences in composition due to segregation can also cause selective oxidation of welds at high temperatures in air or oxidizing media [Cox and Kiser 1992]. This phenomenon can cause notch formation, which can give rise to stress oxidation failure with cyclic thermal conditions.

A higher alloyed weld can also compensate for micro segregation of molybdenum-containing alloys [Cox and Kiser 1992]. With molybdenum containing stainless steels, for instance, using a filler metal with a higher molybdenum content will increase the pit-resisting molybdenum content within dendrite to ensure that the weld is as pit-resistant as the base metal.

2.2. Austenitic Stainless Steel (γ -SS)

Austenitic stainless steels were invented in Essen, Germany [Padilha and Rios 2002] in the beginning of the 20th century. These steels primarily contain 16-26% Cr, 8-24% Ni + Mn, normally below 0.15% C and small amounts of a few other elements such as Mo, N, Ti, Nb (Cb) and Ta. The balance between the Cr and Ni + Mn is normally adjusted to suppress austenite/ferrite transition temperature such that a microstructure of 90-100% austenitic grains in the matrix can be obtained at ambient temperature [Covert and Tuthill 2000, Padilha and Rios, 2002, Folkhard 1984].

2.2.1. Classification and its Application

Chemical compositions of austenitic stainless steels as per AISI and UNS method are as given in Table-2.1. In these steels along with iron the main components are Cr to improve corrosion resistance and Ni to stabilize austenite. Chromium contents range from 15 to 26 % and nickel contents from 5 to 37 %. The 200 series have a comparatively lower Ni content than the 300 series. But these steels have a relatively high Mn content up to about 15.5 % and also a high N content that partly replaces Ni as a strong austenite stabilizer. In few compositions 2 to 4 % of Mo is also introduced to promote solid solution hardening and improving the resistance against pitting corrosion [Folkhard 1984].

Table 2-1 The standard compositions of common austenitic stainless steels classified according to the American Iron and Steel Institute (AISI)

Type	UNS No.	Composition, % ^(a)							
		C	Mn	Si	Cr	Ni	P	S	Other
201	S20100	0.15	5.5-7.5	1.00	16.0-18.0	3.5-5.5	0.06	0.03	0.25 N
202	S20200	0.15	7.5-10.0	1.00	17.0-19.0	4.0-6.0	0.06	0.03	0.25 N
205	S20500	0.12-0.25	14.0-15.5	1.00	16.5-18.0	1.0-1.75	0.06	0.03	0.32-0.40 N
301	S30100	0.15	2.0	1.00	16.0-18.0	6.0-8.0	0.045	0.03	...
302	S30200	0.15	2.0	1.00	17.0-19.0	8.0-10.0	0.045	0.03	...
302B	S30215	0.15	2.0	2.0-3.0	17.0-19.0	8.0-10.0	0.045	0.03	...
303	S30300	0.15	2.0	1.00	17.0-19.0	8.0-10.0	0.20	0.15 min	0.6 Mo(b)
303Se	S30323	0.15	2.0	1.00	17.0-19.0	8.0-10.0	0.20	0.06	0.15 min Se
304	S30400	0.08	2.0	1.00	18.0-10.0	8.0-10.5	0.045	0.03	...
304H	S30409	0.04-0.10	2.0	1.00	18.0-20.0	8.0-10.5	0.045	0.03	...
304L	S30403	0.03	2.0	1.00	18.0-20.0	8.0-12.0	0.045	0.03	...
304LN	S30453	0.03	2.0	1.00	18.0-20.0	8.0-12.0	0.045	0.03	0.10-0.16 N
302Cu	S30430	0.08	2.0	1.00	17.0-19.0	8.0-10.0	0.045	0.03	3.0-4.0 Cu
304N	S30451	0.08	2.0	1.00	18.0-20.0	8.0-10.5	0.045	0.03	0.10-0.16 N
305	S30500	0.12	2.0	1.00	17.0-19.0	10.5-13.0	0.045	0.03	...
308	S30800	0.08	2.0	1.00	19.0-21.0	10.0-12.0	0.045	0.03	...
309	S30900	0.20	2.0	1.00	22.0-24.0	12.0-15.0	0.045	0.03	...
309S	S30908	0.08	2.0	1.00	22.0-24.0	12.0-15.0	0.045	0.03	...
310	S31000	0.25	2.0	1.50	24.0-26.0	19.0-22.0	0.045	0.03	...
310S	S31008	0.08	2.0	1.50	24.0-26.0	19.0-22.0	0.045	0.03	...
314	S31400	0.25	2.0	1.5-3.0	23.0-26.0	19.0-22.0	0.045	0.03	...
316	S31600	0.08	2.0	1.00	16.0-18.0	10.0-14.0	0.045	0.03	2.0-3.0 Mo
316F	S31620	0.08	2.0	1.00	16.0-18.0	10.0-14.0	0.20	0.10 min	1.75-2.5 Mo
316H	S31609	0.04-0.10	2.0	1.00	16.0-18.0	10.0-14.0	0.045	0.03	2.0-3.0 Mo
316L	S31603	0.03	2.0	1.00	16.0-18.0	10.0-14.0	0.045	0.03	2.0-3.0 Mo
316LN	S31653	0.03	2.0	1.00	16.0-18.0	10.0-14.0	0.045	0.03	2.0-3.0 Mo; 0.10-0.16 N
316N	S31651	0.08	2.0	1.00	16.0-18.0	10.0-14.0	0.045	0.03	2.0-3.0 Mo; 0.10-0.16 N
317	S31700	0.08	2.0	1.00	18.0-20.0	11.0-15.0	0.045	0.03	3.0-4.0 Mo
317L	S31703	0.03	2.0	1.00	18.0-20.0	11.0-15.0	0.045	0.03	3.0-4.0 Mo
321	S32100	0.08	2.0	1.00	17.0-19.0	9.0-12.0	0.045	0.03	5 × %C min Ti
321H	S32109	0.04-0.10	2.0	1.00	17.0-19.0	9.0-12.0	0.045	0.03	5 × %C min Ti
330	N08330	0.08	2.0	0.75-1.5	17.0-20.0	34.0-37.0	0.04	0.03	...
347	S34700	0.08	2.0	1.00	17.0-19.0	9.0-13.0	0.045	0.03	10 × %C min Nb
347H	S34709	0.04-0.10	2.0	1.00	17.0-19.0	9.0-13.0	0.045	0.03	8 × %C min - 1.0 max Nb
348	S34800	0.08	2.0	1.00	17.0-19.0	9.0-13.0	0.045	0.03	0.2 Co; 10 × %C min Nb; 0.10 Ta
348H	S34809	0.04-0.10	2.0	1.00	17.0-19.0	9.0-13.0	0.045	0.03	0.2 Co; 10 × %C min - 1.0 max Nb; 0.10 Ta
384	S38400	0.08	2.0	1.00	15.0-17.0	17.0-19.0	0.045	0.03	...

(a) Single values are maximum values unless otherwise indicated. (b) Optional

2.2.2. Heat Effect on γ -SS

Austenitic stainless steels are generally put to service in the solution-annealed condition as they are quenched in water or other fast cooling media depending on the section size and distortion considerations from the annealing temperature (1040⁰C-1130⁰C). The purpose of the annealing in ASS is either to eliminate and effect of prior work or to dissolve any carbide that may be present or both. However specific time-temperature combinations required represents a compromise between achieving the primary purpose and avoiding excessive grain growth.

However as most of the stainless steel compositions in wide use occur on the iron-rich side of the ternary around 70wt. % iron, the ternary phase diagram as shown in Fig. 2.1 is commonly used to identify the primary solidifying phases or solidification modes for various compositions.

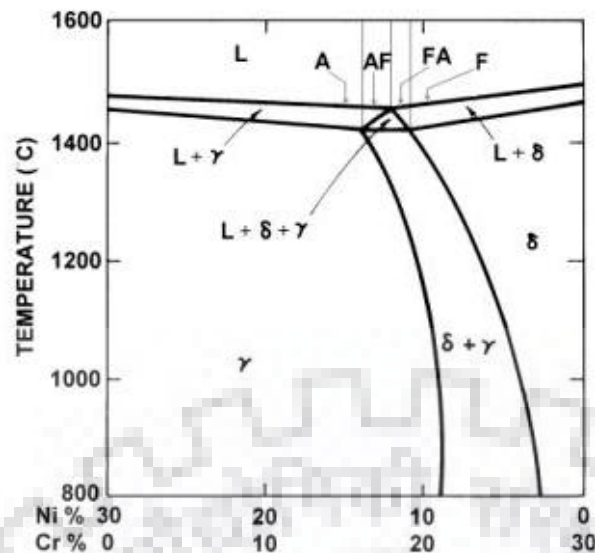


Figure 2-1 Pseudo binary section of the Fe–Cr–Ni ternary diagram at 70% Fe, showing solidification modes; A - fully austenitic, AF - austenitic–ferritic, FA - ferritic–austenitic and F -fully ferritic. [Shankar et.al 2003]

2.2.3. Stress Effect

Stresses in any material can be introduced by an external loading, arising out of service conditions or mechanical working and fabrication process. Out of mechanical working or forming process, rolling and forging are largely known as the means to introduce significant amount of stresses during the process that may affect the phase transformation behaviour in the material [Parvathavarthini and Dayal 2002]. Similarly during the fabrication process like arc welding or fusion welding, the differential of expansion and contraction behaviour of material also introduces stresses in the area of joining influencing the phase transformation behaviour in this region [Elmer et al 1982]. In all the above cases of mechanical working, hot forming as well as fabrication, the material may also have some locked in stresses in the matrix that may influence the properties of material subsequently under the service condition. However in contrast to hot rolling and forging wherein temperature of base metal does not cross its melting point, weld metal solidifies from the temperature much above its melting point at a comparatively higher solidification rate. This results in significant amount of thermal stress distribution depending on both the difference in coefficient of thermal expansion (CTE) between the weld and base metals and the temperature change from the stress free temperature [Elmer et al 1982]. When the tensile strained metal is welded, the cracks form in the heat affected zone because of a sufficiently high level of residual surface stresses and precipitation of brittle secondary phases [Erve et al 1997].

In γ -SS based on DeLong diagram the mean CTE plotted as a function of Cr and Ni equivalents have been shown in Fig. 2.2. The figure shows three different regions of interest: single phase austenite field (A), two phase austenite and ferrite field (A + F) and the three phase

austenite, ferrite and martensite field (A+F+M). The CTE is influenced by the presence of these phases, wherein highest CTE of around $19\mu\text{m}/\text{m}/^{\circ}\text{C}$ has been marked in the austenite phase field at a composition of 14 Ni_{eq} and 18 Cr_{eq}. The presence of ferrite in a stainless steel at room temperature will reduce its CTE due to reduction in its transformation to denser austenite phase at elevated temperatures. A contractive strain of 4.5×10^{-5} has been measured and shown to accompany each percent ferrite that transforms to austenite. This strain is directly associated with this phase transformation and can have the effect of loading the weld joint in tension [Elmer et al 1982].

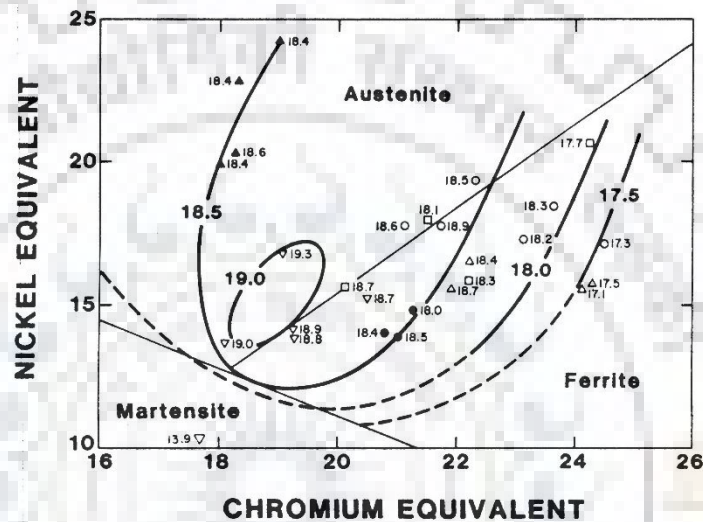


Figure 2-2 Mean coefficient of thermal expansion plotted on the Delong diagram as a function of chromium and nickel equivalents [Elmer et al 1982]

In stabilized ASS inspite of sufficient addition of niobium, micro stress leading to tensile strain exists in the austenite matrix around the undissolved NbC particles. It primarily occurs due to the mismatch of thermal contraction between NbC and austenite leading to $M_{23}C_6$ nucleation at the interface between undissolved NbC particles and the austenite matrix. It has been further observed that the morphologies of $M_{23}C_6$ grown around undissolved NbC particles are different from those of $M_{23}C_6$ grown at other sites. Hence the basic intention of addition of Nb to bind C and avoid harmful $M_{23}C_6$ precipitation could not be fulfilled due to micro stress generation [Sarafianos 1992, Sasmal 1997].

2.3. Arc Weldability of γ -SS

Many metallurgical reactions take place during welding which influence the crystallization structure, segregations, phase transformations, precipitation and embrittlement [Folkhard 1984] depending primarily upon alloy composition. In case of welding of austenitic stainless steel the equilibrium phase diagrams are often found insufficient to precisely predict the resulting

microstructure of solidification. However the best known method in this regard is followed by consideration of the Schaeffler and Delong diagrams.

Schaeffler and Delong divided the alloying elements in two groups according to their basic characteristics as ferrite and austenite stabilizers. Depending upon the degree of influence of an element on ferrite or austenite formation and to retain their stability at room temperature the expressions in terms of equivalent to chromium content and as equivalent to nickel content was developed [Folkhard 1984]. Schaeffler's diagram as shown in Fig. 2.3, therefore allowed an estimation of the microstructure primarily in terms of δ ferrite and austenite formation as a function of the steel composition in weld metal. In many applications, the ability to control the δ ferrite content of stainless steel weld metal becomes important in order to negotiate its hot cracking resistance, corrosion resistance, mechanical properties and fracture toughness.

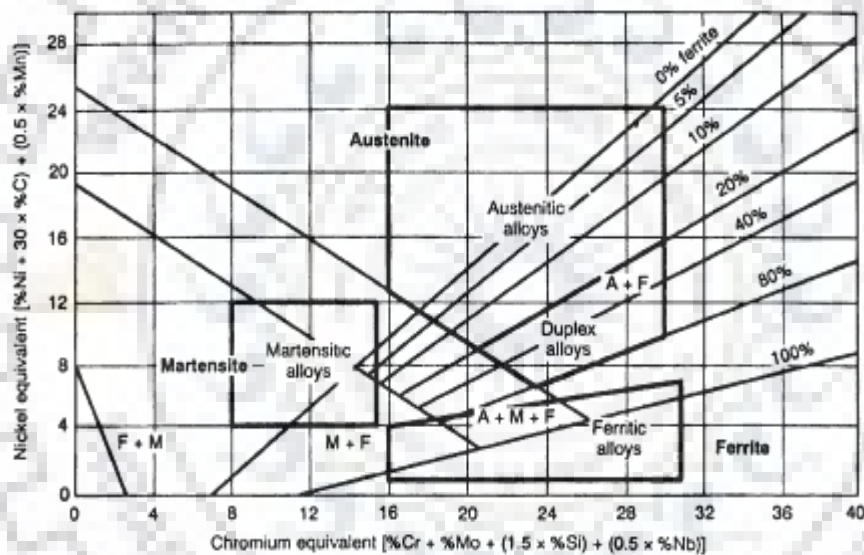


Figure 2-3 Schaeffler's constitution diagram giving δ ferrite content in stainless steel. The compositional ranges of the ferritic, martensitic, austenitic, and duplex alloys have been superimposed on this diagram. [Shanker et al 2003b]

However, the De Long diagram (Fig.2.4) developed for low nitrogen containing austenitic stainless steels are not suitable for the higher manganese, higher nitrogen grades [Delong 1974].. For example, manganese content beyond 4 % is not potent as an austenite stabilizer, and may in fact act as a ferrite former [Shankar 2003b].

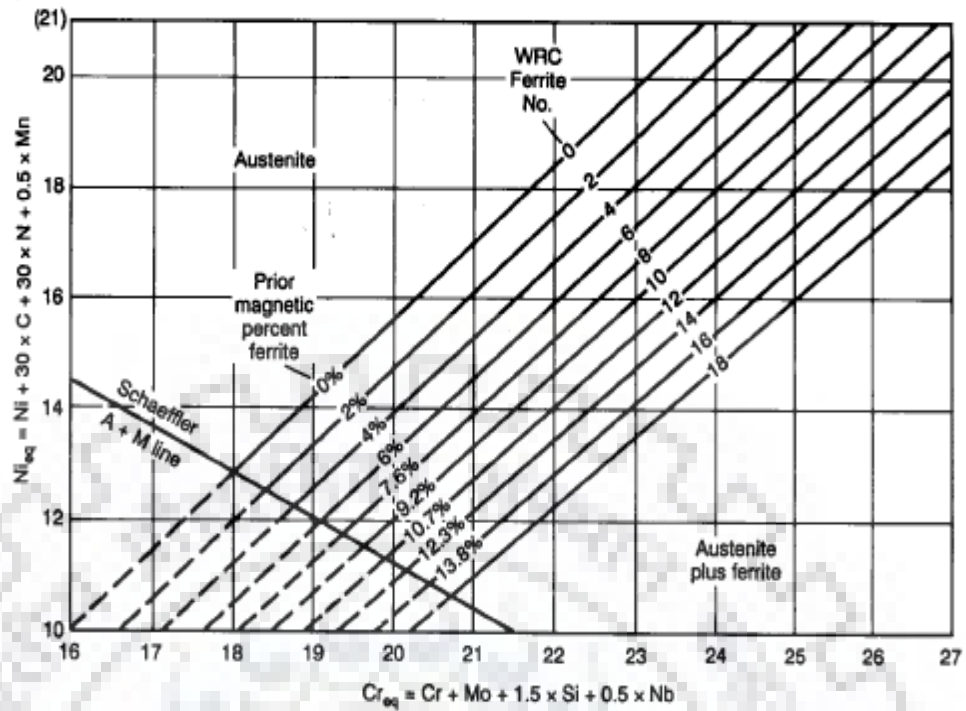


Figure 2-4 DeLong constitution diagram for stainless steel weld metal [Delong 1974].

Siewert proposed a new ferrite diagram (Fig. 2.5) that predicted [Delong 1974]. ferrite up to 100FN and thus covered the complete range of austenitic and duplex stainless steels. The accuracy of this diagram is superior to that of the DeLong diagram, since the bias due to a higher coefficient for N has been removed. More importantly from the point of view of cracking, the solidification mode boundaries have been included [Siewert et al 1988, Shankar et al 2003b].

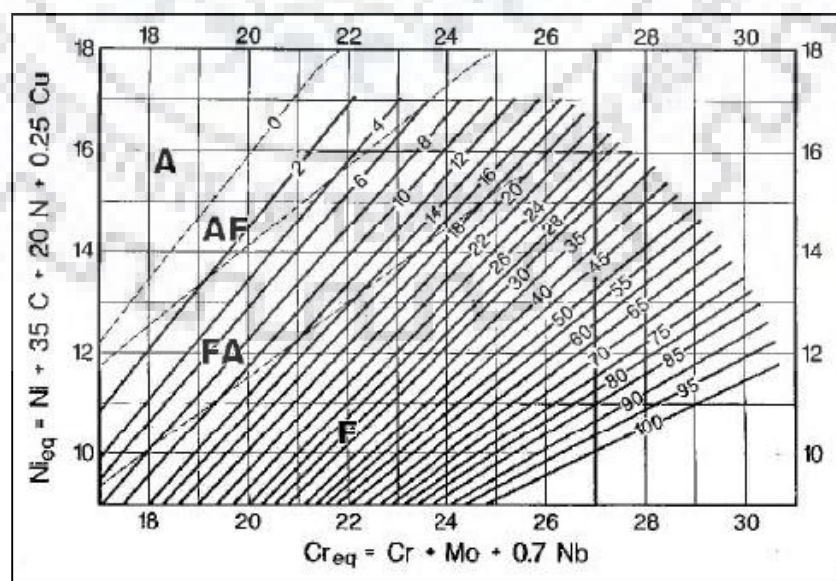


Figure 2-5 The WRC-92 constitution diagram for weld metal ferrite, including solidification mode boundaries [Siewert et al 1988].

2.4. Conventional Arc Welding of Thick γ -SS Sections

In last 30 years the most important contributions to welding technology have been through changes in the design of welding power sources [Ghosh et.al. 2001,] from generator set to inverter based digitally transistorized power source. It has achieved a significant improvement in volt-ampere characteristics, duty cycle, efficiency along with reduction in weight [Johnson et.al. 1995, Shanmugam 1997]. Performance of power source is of vital importance to the welding process with respect to arc ignition, stability of transfer of the melted electrode material and amount of spatter that is generated [Shanmugam 1997]. For this purpose, it is important that the two terms which are commonly used to define the V-A characteristics of a power source, static output and dynamic response are optimised to maintain a stable arc during the welding process [Johnson et.al. 1995].

Static output

Static output characteristics primarily indicates the achievable envelope of output limits, including the highest voltage the machine will support at a given current and the highest current that can be drawn at a given voltage [Johnson et.al. 1995]. It can be obtained by statically loading pure resistive load from minimum or no load condition to the maximum or short circuit condition. These characteristics as shown in Fig. 2.6 are classified as steeply drooping, gradually drooping, flat, which are used for manual metal arc welding (MMAW), submerged arc welding (SAW) and gas metal arc welding (GMAW) processes respectively. Power sources with drooping and flat characteristics are known as constant current (CC) and constant voltage (CV) power source respectively.

(a) Steeply drooping

The welding power source with steeply drooping V-I characteristics has a high open circuit voltage (OCV) and low short circuit current. In these power sources change in arc length does not affect welding current appreciably as depicted by Fig. 2.6. With the change in arc length between $(l - \Delta l)$ and $(l + \Delta l)$, the change in welding current is small. This is best suited for SMAW process because a slight change in arc length due to intrinsic movement of human hand during welding does not affect the melting rate of the electrode significantly. Also high OCV ensures easy initiation and maintenance of welding arc.

(b) Gradually drooping

The welding power source with gradually drooping V-I characteristics has comparatively lower OCV than steeply drooping characteristic power source. In this as the arc length changes from l to $(l \pm \Delta l)$, change in welding current is comparatively more and hence provides some sort of self-regulation of the arc length. This is best suited for SAW process.

(c) Flat

In these power sources, for a small change in arc length, change in welding current is very high which makes it quite sensitive and helps in maintaining the constant arc length. This is generally referred to as self-regulation of the arc length and is essential requirement for GMAW process. However, flat characteristic is not truly flat but normally droops at 1-3V per 100 A. All welding power sources with flat V-I characteristics are almost invariably of the transformer cum rectifier type and electrode positive polarity is normally employed.

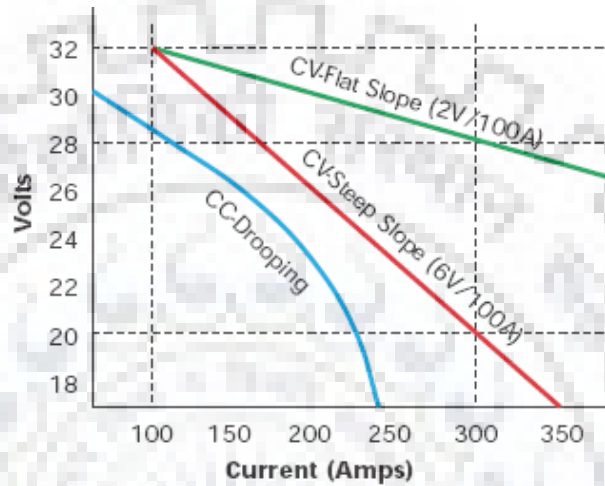


Figure 2-6 Power supply characteristic curves.

Dynamic response

The dynamic characteristics of an arc welding power source is determined by recording the transient variations occurring over a short interval in welding current and the arc voltage [Johnson et.al. 1995]. In short, the dynamic characteristics is instantaneous response of power source to step changes in load voltage primarily associated with striking of arc, metal transfer from the electrode to the weld pool, and arc extinction and re-ignition during each half cycle of AC welding. The influence of these factors on the process stability is reflected in the current and voltage waveform of the welding arc [Shanmugam 1997]. These are obtained by recording the volt-ampere transients during actual welding operation. From dynamic characteristics it is possible to know the mode of metal transfer for a given set of welding parameters.

Depending upon power source characteristics, welding of thick pipelines is generally carried out by following processes, which are preferably used according to their specific process characteristics primarily in respect to working range of parameters and resulting weld quality.

- (i) Shielded metal arc welding (SMAW)
- (ii) Gas tungsten arc welding (GTAW)
- (iii) Gas metal arc welding (GMAW)

(iv) Pulsed current gas metal arc welding (P-GMAW)

2.4.1. SMAW Process

The shielded metal arc welding has maximum flexibility and can weld many metals in all positions. There is definite relationship amongst the welding current, size of welding electrode and welding position. The molten weld metal can be retained in position by lowering the heat input to reduce the fluidity of molten weld metal and to give a small size of weld pool which solidifies before it has time to spill out of the joint. The heat input can be reduced by using a smaller diameter electrode (2.5-4mm) at about 90-140A of welding current [Kearns 1978]. The arc length can be varied to control the heat input and amount of molten metal in position [ASM handbook 1994]. The heat input can also be distributed and side wall fusion can be achieved by adapting an appropriate weaving technique. The sagging and spilling of weld metal can also be prevented by reducing the welding current and increasing the number of passes. However SMAW process has following disadvantages.

1. Lower heat transfer efficiency of 0.55-0.70 [Radaij 1992] as comparable amount of energy is lost in resistance heating and flux melting resulting in comparatively lower metal deposition rate [Lancaster 1984].
2. Interruption in metal deposition due to limitation of electrode length enhances probability of defect formation.
3. Entrapment of slag occurs if it does not have 30-40% higher coefficient of thermal expansion (CTE) than that of parent metal.
4. Process automation is practically not viable.

Life of a weldment gets considerably affected by entrapment of slag primarily due to poor tensile and fracture mechanics properties [S´anchez-Cabrera 2007]. Thus SMAW process even though largely used in joining of thick sections, its use in welding especially in critical applications such as pressure vessels, piping etc. is on the verge of extension.

2.4.2. GTAW Process

In this process, an arc is established in between a tungsten electrode (non-consumable) and base metal. The arc gap is kept constant and current is controlled by the power source. The heat of the arc thus produced is utilized to achieve coalescence of metals with and without use of filler metal. Filler metal, usually available in 1 meter length of wire, is added to the leading edge of the pool as required. The arcing electrode and molten weld pool are generally shielded by inert gas or gas mixture of argon and/or helium. The current and heat input range of the process are followed of the order of 10-300A and 0.2 to 8 kJ/s respectively [ASM handbook 1994]. The most

popular variation of this process is known as pulsed current GTAW. Both low frequency pulsation typically (0.1-20Hz) and high frequency pulsation (>100Hz) are often used in this process [Tujsek 2000]. The heat input depends on the mean current which is a function of the pulse height, pulse frequency and pulse duration. The pulsed current mode of this process offers a better control over the size of weld pool and its fluidity to manage the pool in position as well as over the penetration behaviour of the weld. The process has all positional welding capacity and lends itself to produce high quality welds of metals such as aluminium, stainless steel, nimonic alloy and copper in chemical plants, sheet work in aircraft engines and structures. However GTAW process has following limitations.

1. Low process economy due to its considerably poor heat transfer efficiency of 0.20-0.50 [Radaij 1992].
2. Contamination due to both the transfer of molten tungsten from the electrode to the weld pool and exposure of the hot filler rod to air occurs during welding with comparable welding currents used in other processes.
3. Higher cost of operation due to relatively expensive shielding gases required during its comparatively slow deposition rate [Lowke et.al. 1997, Lucus 1992].

In addition to above limitations, a major disadvantage of GTAW process is very low metal deposition rate at comparatively lower welding speeds resulting in considerably severe weld thermal cycle. This problem of especially lower metal deposition rates has been largely solved with the invention of hot wire GTAW process. In this process consumable filler wire provided to the arc region is heated to a temperature just below its melting point by a different power source. Thus the major arc energy is utilized in melting of groove wall for proper fusion at considerably higher weld metal deposition rates. However the considerably large amount of heat generated by the welding arc and hot filler metal results in significant increase in weld pool temperature due to heat accumulation especially in metals having comparatively lower thermal conductivity such as austenitic stainless steel. Hence hot wire GTAW even though found suitable for joining ASS must be critically considered before its practical application. For these limitations, GTAW is generally not commercially competitive with other welding processes such as SMAW, submerged arc welding (SAW) and GMAW processes.

2.4.3. GMAW Process

The growing need of quality, economy and automation in welding has been found, in number of cases, to replace the versatile SMAW by GMAW process. The process is also popular as it provides to a weld a high resistance to hydrogen induced cracking due to its low diffusible hydrogen level (1-2ml/100gm) achieved by using bare solid filler wires, less chances of slag

entrapment and low creation of smoke levels [Redding 2002]. In GMAW process a low voltage electric arc is established between a consumable filler wire and base metal, which melts both of them by arc heating. The wire is fed at a preset speed, which governs the magnitude of welding current, through a welding torch wherein it provides electrical connections and the shielding gas.

2.4.3.1. Process variables and their control

In GMAW process, the term “Process stability” primarily depending upon welding current, arc voltage and electrode extension employed [Shanmurgam 1997] refers to the dynamic behaviour of the welding arc. Thus the characteristics of the weld pool [ASM handbook 1994, Kearns 1978] including the penetration, solidification mechanism, heat flow and rate of metal deposition are significantly influenced by arc stability [Shanmurgam 1997].

Welding current

Welding current plays an important role in deciding the mode of metal transfer and subsequently the weld quality. At low current, the globular transfer occurs if the arc length is sufficient. The drops grow at the tip of the electrode with a classic pendant drop shape, due to the competition between gravity and surface tension in the presence of relatively small electromagnetic forces [Kim and Eagar 1993a, Liu and Siewert 1989]. At a very high value of current, asymmetric force becomes significant compared to the initial force in the streaming of metal and the column spirals about the electrode axis [Lancaster 1984].

Arc voltage

Arc voltage primarily governs the arc length and affects size and shape of the fusion zone. When the arc length is too short, electrode may touch or short weld pool resulting in low base metal melting, narrow weld deposit and lower heat input and hence enhances the possibility of forming flat and shallow deposit, allowing the arc to wander, increases spattering and may also cause porosity in weld deposit due to air aspiration in the shielding gas jacket [Johnson et.al. 1995]

Electrode Extension

Electrode extension governs the arc length [Quinnet et.al. 1994]. Longer extension results in enhanced resistive heating and consequently reduces the balance of energy available to melt the filler wire and base metal, which may result in lack of fusion [Ralph and Yeo 1983, Stenbacka and Person 1989]. It may also reduce the stability of metal and may increase the risk of porosity in weld metal [Stenbacka and Person 1989].

It has been established that in the operating range of process variables (5mm arc length, 10-20mm electrode extension, 5-20% CO₂ mixture in any shielding) the specific burn off rate of 1-1.2 mm diameter filler wire and V-I relationship is linear. Consequently, the generalized burn

off relationship in the range of parameters may be represented by linear control equations and can be applied for synergic control. Burn off rate is directly proportional to the electrode extension and resistivity of filler wire [Amin and Ahmed 1987].

Shielding Gas

The role of shielding gas in arc welding process is to protect the electrode and the work piece from harmful atmospheric contaminants and act as a medium in which current can flow to sustain the arc [Kearns 1978]. In welding area where molten droplets are transferred across the arc into the weld pool, protection from atmospheric contaminants can be provided successfully by suitable shielding gas or gases [Suban and Tusek 2001, Jonsson et.al. 1995]. The selection of a gas or a mixture of gases is also primarily guided by the physical and chemical properties of the gas, the operating characteristics that each gas imparts to a particular process and the kind of metal or alloy that the gas is suppose to protect. The basic properties of a shielding gas that governs its right selection to improve weld quality at reduced overall cost of the welding operation are listed in Table 2.2. Argon and carbon dioxide due to their relatively higher gas density than air (Table-2.2) requires lower flow rates in use than do the lighter gases as they can easily displace air from the electrode region to ensure adequate protection of the weld puddle [ASM handbook 1994]. Whereas gases such as hydrogen and helium which are 7 and 14 times less dense than air are prone to turbulent flow at the exit from the blowpipe nozzle due to thermal buoyancy [Suban and Tusek 2001]. Ionization potential [ASM handbook 1994] is the amount of energy required to remove an electron from a gas atom and make it an ion or an electrically charged gas atom. The importance of ionization potential of a gas in welding process is from the welding arc, arc power and energy distribution point of view [Jonsson et.al. 1995].

Table 2-2 Basic physical and chemical characteristics of the gases.

Gas	Atomic weight (Kg/ kmol)	Relative gas density with regard to air at 273K and 1.013 bar	Ionization potential (eV)	Reaction in arc
Argon (Ar)	39.948	1.380	15.7	Inert
Helium (He)	4.002	0.138	24.5	Inert
Carbon Dioxide (CO ₂)	44.011	1.529	14.4	Oxidizing
Oxygen (O ₂)	31.998	1.105	13.2	Oxidizing
Nitrogen (N ₂)	28.013	0.968	14.5	Reactive
Hydrogen (H ₂)	2.016	0.070	13.5	Reducing

Energy distribution in axial and radial direction in an arc is also affected by the thermal conductivity of a gas [ASM handbook 1994] which varies with temperature as shown in Fig. 2.7

[Tusek and Suban 2000]. But for welding, the radial energy distribution is much more important because the radial energy distribution affects the axial one. Energy flow in radial direction has lower path length than the axial one i.e. path of least resistance, hence gas with higher thermal conductivity will have energy distribution across the arc in radial direction resulting in comparatively lower energy availability in axial direction [ASM handbook 1994, Liao and Chen 1999, Tusek and Suban 2000]. Inert gas helium which has higher thermal conductivity than argon (Fig.2.7) will produce lenticular shape of penetration in comparison with wine glass shaped penetration in steel material. Fig. 2.7 further shows that thermal conductivity of multi atom gases such as carbon dioxide, hydrogen and oxygen in the temperature range between 3000 and 4500 K is much higher than that of argon and helium [Tusek and Suban 2000]. When heated to high temperatures within the arc plasma, these gases break down or dissociate into their component atoms which get partially ionized, producing free electrons and current flow. As the dissociated gas comes in contact with relatively cool work surface, the atoms recombine and release heat at that point. This heat of recombination causes multi atomic gases to behave as if they have a higher thermal conductivity [ASM handbook 1994].

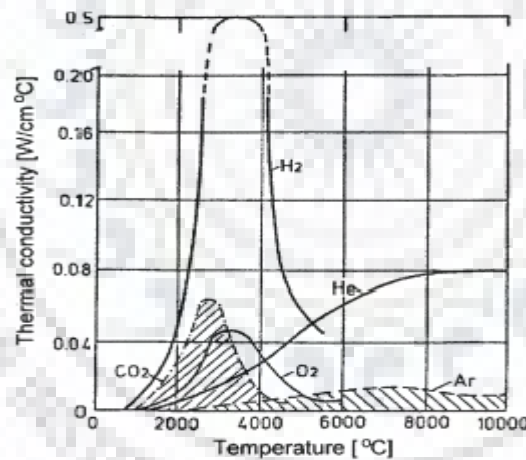


Figure 2-7 Thermal conductivity of gases as a function of temperature

By far the gas blends developed can be roughly divided into three categories: pure gases, two gas blends and three part gas blends composed of argon, helium, oxygen, carbon dioxide, or hydrogen [ASM handbook 1994]. However there are number of other factors which influence the desirability of a gas for arc shielding. Some of these are the influence of the shielding gas on the arcing and metal transfer characteristics during welding, weld penetration, width of fusion and surface shape patterns, speed of welding and undercut tendency. Hence selection of pure or combination of gases will depend upon the function it has to perform in the desired application.

2.4.3.2. Behaviour of metal transfer

Metal transfer in gas metal arc welding (GMAW) refers to the process of transferring material of the welding wire in the form of molten liquid droplets to the workpiece. Metal transfer behaviour primarily depending upon the process parameters such as welding current, arc voltage, electrode extension, size and composition of filler wire and shielding atmosphere [Collard 1988, Kim and Eagar 1993a] are further influenced by a number of physical variables such as temperature, velocity, current density, electric potential, magnetic field, electromagnetic force, and pressure [Wang et.al. 2003]. Thus depending on the welding conditions, metal transfer can take place in three principally suitable modes: short-circuiting, globular and spray modes. Each of the modes have own characteristic arc length, weld penetration and weld pool shape [Heald et.al. 1994, Johnson et.al. 1995, Kim and Eagar 1993a].

Spray transfer

Spray transfer mode is a highly stable and efficient process widely used in welding of thick sections of ferrous and non-ferrous materials. This mode occurs generally under argon shielding at medium and high current above a transition level when the series of droplets much smaller than the filler wire diameter are propelled axially from its tapered end at a considerably higher drop frequency [Wang et.al. 2003, Choi et.al. 1998a, Johnson et.al. 1995]. The tapering of wire at a given speed (WFS) occurs due to influence of distributions of temperature, velocity and electromagnetic force in the droplet as typically shown in Fig. 2.9 [Wang et.al. 2003]. The condensation of electrons on the side of the electrode [Jonsson et.al. 1995] generates heat on the unmelted portion of the wire resulting in preheating of the wire surface to an elevated temperature such that it tends to melt faster than the interior metal. When the current increases, the height of the convex melting interface also increases. The increased electromagnetic force pinches the molten fluid and drives it to move along the sloped surface to the bottom of the wire tip. Because of the liquid flow along the sloped surface, a thin liquid layer is formed on the surface. This thin liquid layer allows the arc heat to penetrate such that the melting proceeds in the direction perpendicular to the sloped wire surface. For the necking of a liquid column, the diameter of the liquid shrinks due to external forces. But for taper formation, a solid wire first becomes tapered and the liquid moves along the tapered conical region and moves out of it in the form of small droplets. This conical region remains in quasi-stationary condition during the metal transfer process [Wang et.al. 2003].

2.4.3.3. Thermal behaviour of weld

Wire melting characteristics

For successful arc operation of GMAW process, the burn off rate must be equal to the wire feed rate to maintain constant arc length. Therefore, the following energy balance per unit time has been proposed [Lancaster 1984, Smati 1986].

$$A_w V_{w(cc)} \rho_w Q_m = \left[V_a + \xi + \frac{3kT}{2e} \right] I + \frac{R_0 E_w I^2}{A_w} \quad (2.5)$$

Where A_w is the cross sectional area of the filler wire (m^2), $V_{w(cc)}$ is the wire feed rate (m/s^2) for continuous current welding, ρ_w is the density (kg/m^3) of the filler wire, Q_m is heat per unit mass (J/kg) required for melting the filler wire, V_a is anode fall voltage (V), ξ is work function of metal surface (V), $\frac{3kT}{2e}$ is thermal energy of electrons (V), R_0 is resistivity (Ωm) of the filler wire, E_w is electrode extension (m) and I is welding current (A). Eq.(2.5) may be rewritten as,

$$V_{w(cc)} = \frac{\psi I}{A_w V_w Q_m} + \frac{R_0 E_w I^2}{A_w^2 \rho_w Q_m} \quad (2.6)$$

Where, $\psi = \left[V_a + \xi + \frac{3kT}{2e} \right]$ is the equivalent melting potential at anode (Work function + anode voltage fall + thermal energy of electrons) which can be estimated based on the expressions mentioned in the Fig.2.10 [Terumi and Kazuo 2002] depending upon filler wire size and shielding gas used for welding.

Eq. 2.6 may also be expressed as,

$$V_{w(cc)} = AI + BE_w I^2 \quad (2.7)$$

Where, A and B are constants representing wire melting due to arc heating and resistive heating respectively expressed as

$$A = \frac{\psi I}{A_w V_w Q_m} \quad (2.8)$$

$$B = \frac{R_0 E_w I^2}{A_w^2 \rho_w Q_m} \quad (2.9)$$

The reported values of physical constants for materials of the filler wire [Alum and Quintino 1985b, Colombeer, L. and Hochmann, L 1967, Metals Handbook 1979, Tekriwal and Mazmuder 1988, Waszink and Heuvel 1982] are given in Table-2.3.

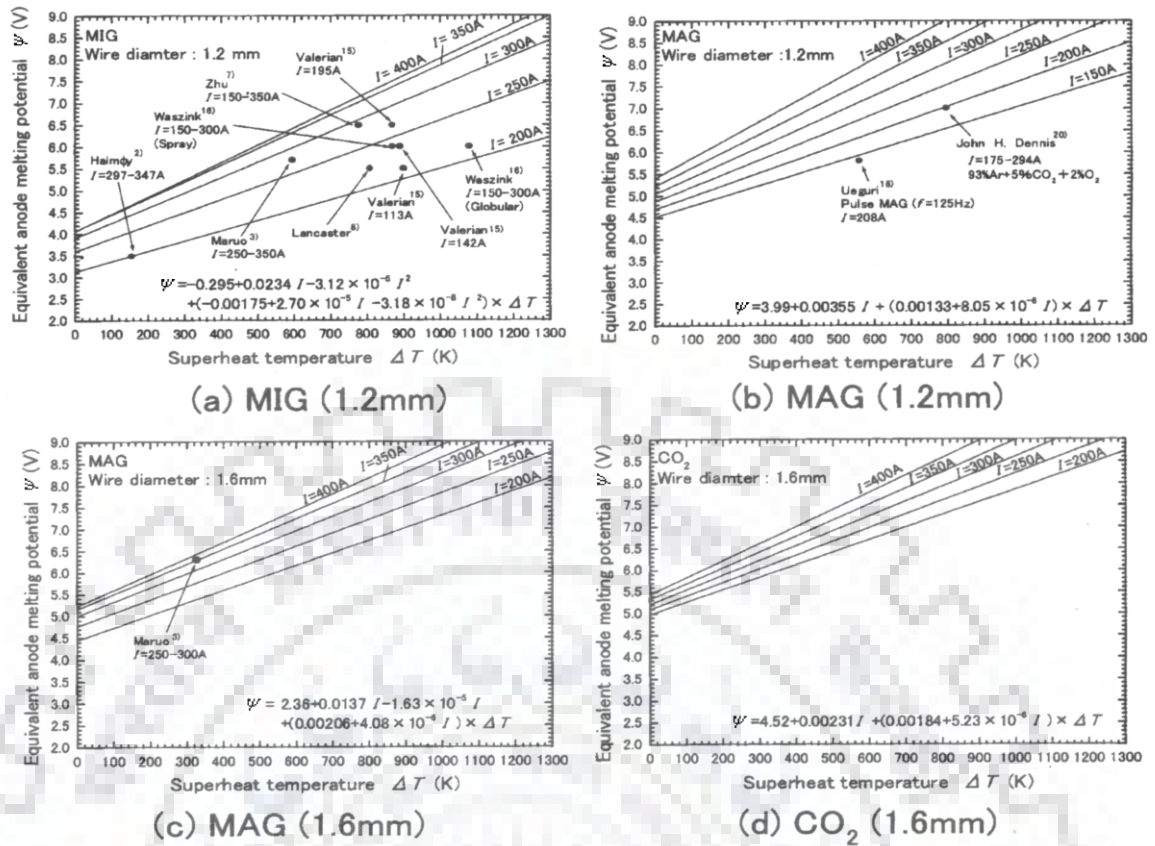


Figure 2-8 Correlation between super heat temperature and equivalent anode melting potential for filler wire and shielding gas combination of (a) 1.2mm, 100% Ar., (b) 1.6mm, 100% Ar., (c) 1.2mm, 80% Ar+20% CO₂ and (d) 1.6mm, 100%CO₂ respectively [Terumi and Kazuo 2002].

Table 2-3 Physical properties of different materials of filler wire [Alum and Quintino 1985b, Colombier, L. and Hochmann, L 1967, Metals Handbook 1979, Tekriwal and Mazmuder 1988, Waszink and Heuvel 1982]

Property	Mild steel	Stainless steel
Melting Point, T _m , (K)	1750	1728
Specific heat, C _{p(s)} , (J/kg/K)	686	500
Specific heat, C _{p(l)} , (J/kg/K)	855	760
Latent heat of fusion, L, (J/kg)	2.76e5	2.84e5
Density of the solid metal, ρ _w , (kg/m ³)	7870	7750
Density of the molten metal, ρ _w , (kg/m ³)	6500	7507
Coefficient of surface tension, γ, (N/m)	1.03	1.35
Resistivity at melting point, R ₀ , (Ωm)	8.2E-7	1.3E-6
Emissivity of molten droplet, ε	0.25	0.25

2.4.4. P-GMAW Process

In spray mode of metal transfer in gas metal arc welding (GMAW) rate of droplet detachment considerably increases and droplet size decreases sharply giving a stiff arc and better control over metal transfer. However the major disadvantage of this mode is that it demands considerably higher welding current and therefore increases the heating of the work piece. During the 1960s an intermediate pulsed mode [Allum and Quintino 1985(b)] was invented and its use became widespread. In this mode, the current is well below the threshold current of the spray mode most of the time [Amin1983, Craig 1987(b), Ghosh and Gupta 1996], so the heat dissipated in the work piece is relatively small [Ghosh and Dorn 1993]. These low-current periods are interrupted by high-current pulses above the threshold. During this pulse the arc transfers into spray mode. Since the pulse is short enough, it does not heat the work piece significantly. In other words in the pulsed regime arc current is maintained at a value high enough to permit spray transfer and long enough to initiate detachment of molten droplets [Jacobsen 1992]. Once the droplets are transferred, the current is reduced to a relatively low value, efficiently a pilot arc [Kim and Eagar 1993b]. These periods of low current allows the average arc current to be reduced into the range suitable for positional welding [Randhawa et.al. 1998], while periodic injection of high current pulses allows metal to be transferred in the spray mode [Ghosh and Rai 1998]. Thus, by repeated applications of current pulses as shown schematically in Fig. 2.11, synthetic spray transfer is produced at lower heat input. The process offers greater ease of operation for welding in any position for root passes without backing [Randhawa et.al. 1998] and the welding of heat sensitive materials and thin sheets [Trindade and Allum 1984, Ghosh et.al. 2007b].

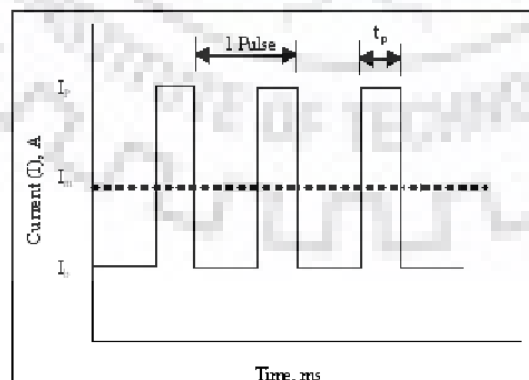


Figure 2-9 Current waveform for pulsed current gas metal arc welding.

2.4.4.1. Process variables and their control

In the recent past the pulsed current GMAW has gathered considerable attention of welding technologists due to its number of unique merits in better control over metal transfer and heat input, resulting in improved weld quality and properties as compared to those observed in case of conventional continuous current GMAW process [Praveen et.al. 2005, Collard 1988, Craig 1987a and b]. However, the exploitation of the merits of pulsed current GMAW process is largely dependent upon right selection of pulse parameters, like mean current (I_m), peak current (I_p), base current (I_b), pulse duration (t_p) and pulse frequency (f) as they affect the microstructure of weld and heat affected zone (HAZ) as well as chemistry and porosity content of the weld due to their influence on weld thermal cycle and arc characteristics [Ghosh and Dorn 1993, Ghosh and Rai 1998, Ghosh and Sharma 1991, Lambentt 1989].

Peak current (I_p)

The peak current which must be maintained in spray transfer mode but/ not be too high, as it may lead to variation in arc pressure causing an air aspiration into the inert jacket resulting in instability of arc. Higher peak currents will result in greater axial force due to magnetic field generated by the current carried through the electrode and if numerous drops of relatively smaller diameter develop, the arc forces may cause them to be fragmented or propelled laterally [Palani and Murugan 2006, Praveen et.al. 2005, Quintino and Allum 1984, Trindade and Allum 1984]. Hence in order to ensure appropriate amplitude and duration of peak current many researchers [Quintino and Allum 1984, Trindade and Allum 1984, Wang et. al 2004] have used power law relations ($I_p^n t_p = \text{constant}$, $n=2$), for determining the amplitude of peak current and duration. Minimum pulse amplitude has also been found out by using following expression for mild steel filler wire [Jacobsen 1992]

$$I_{p,\min} = \frac{2.85 \times 10^4 \sigma^{0.5} d_e f^{0.245}}{I_{\text{eff}}^{0.465} t_p^{0.6}} \quad (2.10)$$

Here σ is the surface coefficient, in N/m, d_e is electrode diameter, in mm, f is pulse recurrence frequency, in pulses/sec, I_{eff} is effective current given as $I_{\text{eff}}^2 = \{k_p I_p^2 + (1 - k_p) I_b^2\}^{1/2}$ wherein k_p is pulse duty cycle defined as t_p/t_{pul} , in A, t_p is pulse time, in sec. It has been further observed that depending upon filler wire size, the combination of the highest I_p and lowest t_p was found to be capable of providing both uniform arc length and uniform droplet detachment when compared to the combination of lowest I_p and highest t_p . In stainless steels slightly higher peaks and lower background currents are generally used in comparison with mild steel because of surface tension characteristics [Palani and Murugan 2006].

Base current (I_b)

The main function of the base current is to maintain the welding arc between pulses. By setting the base current to minimum value, heat flow in weld pool can be controlled and hence bead shape can get greatly influenced [Palani and Murugan 2006, Praveen et.al. 2005, Lenivkin1981]. Very low base current will produce a high crowned weld bead which may cause poor sidewall fusion. Hence base current levels can vary substantially depending upon material; for mild steel this will range from 30-50A, around 50A and 20A for austenitic stainless steel and aluminium alloys respectively. However base current level and its duration are primarily decided based on mean current employed [Palani and Murugan 2006].

Pulse frequency (f)

The pulse frequency is having significant effect on both the minimum base current and minimum electrode melting rate [Quintino and Allum 1984, Smati 1986, Subramaniam et.al. 1998] to obtain a constant arc length. At a given base current the increase in frequency of sinusoidal pulse enhances the mean and effective currents and electrode melting rate. However in case of variation in pulse frequency by keeping the mean current constant the base current should remain free to vary by following the energy balance criteria to achieve constant arc length. It is in general reported that [Trindade and Allum 1984, Palani and Murugan 2006] at a low pulse frequency the metal transfers as large drops or lumps where the weld pool appears viscous and the arc becomes erratic. Whereas with the increase in pulse frequency the metal transfer takes place as small axial droplets with size corresponding to the balance between detaching forces at the peak current and retaining surface tension force. Hence the appropriate frequency, which is primarily a function of average current, can be pre-selected at a given condition based on a theoretically calculated frequency obtained by dividing the electrode melting rate by the mass of one drop as given in Eq. 2.11 [Praveen et.al. 2005].

$$\text{Theoretical frequency} = \frac{m_{\text{pulse}}}{V_{\text{drop}}(I_p) \rho_d} \quad (2.11)$$

Where m_{pulse} is the electrode melting rate with current pulsing, $V_{\text{drop}}(I_p)$ the volume of the drop at the peak current and ρ_d is the density of the drop. The average melting rate for the square wave current may be estimated as the weighed sum of the melting rate at the peak current and at the base current, as given in Eq. 2.12.

$$m_{\text{pulse}} = Dm(I_p) + (1-D)m(I_b) \quad (2.12)$$

Where D is the load duty cycle, $m(I_p)$ and $m(I_b)$ are the melting rate at peak and base current respectively. At a high pulse frequency of the order of 100 Hz the metal transfer takes place as small axial droplets where, the arc remains stable due to higher arc pressure and the weld pool

widens. A low pulse frequency of the order of 25 Hz enables to use a low mean current, when it is convenient for welding thin sheets [Praveen et.al. 2005, Palani and Murugan 2006]. However the mechanism of the influence of pulse frequency on welding process and weld characteristics is yet not fully understood.

Pulse duration (t_p)

Pulse duration is variable which would be altered to achieve the ultimate reduction in power to the GMAW arc, while sustaining spray transfer mode of metal transfer. Power input to the arc is affected by changing the shape of pulse. A square wave, for example, has greater effective width than that of sine wave or triangular wave [Palani and Murugan 2006, Lenivkin 1981]. The pulse duration is regarded as an important operating parameter as neck formation and elongation of the pendent drop occurs mostly during this period. If the pulse duration is kept too short, the elongated drop would recoil back to a spherical shape after the pulse and if the duration is too long, several drops might get detached during the period. As given by eq. 2.13, where value of t_p and t_b should be given in milliseconds. This threshold decreases slightly as the peak current is increased.

$$t_p = \left[\left(496.1 \times \left(1 - e^{-0.003 \times I_b t_b} \right) \right) + \frac{270.1}{\left(\frac{I_b t_b - 188.2}{8423.5} \right)^2} \right] / I_p \quad (2.13)$$

$$T = \frac{240V_{drop}}{\pi d_e^2 W_f} \quad (2.14)$$

Where $T = t_p + t_b$, V_{drop} is the droplet volume, $(\pi D_d^3) / 6$ (mm^3), D_d the droplet diameter (mm) and W_f is the wire feed speed (m/min)

Ratio of peak current to base current (I_p / I_b)

During continuous current GMA welding the increase in welding current reduces the duration of presence of molten droplet in arc cavern. Thus, it reduces the absorption of gases and consequently the porosity content of weld deposit. Whereas in case of pulsed current welding, the variation in arc pressure, which is primarily governed by the ratio of peak current to base current, leads to formation of vortex in inert jacket resulting air aspiration into shielding atmosphere causing enhancement of porosity content in weld metal. However it is also observed that a combination of highest I_p and the lowest t_p provides more uniform arc length (stable arc) and droplet detachment when compared to the combination of the lowest I_p and the highest t_p . Thus the ratio of peak current to base current (I_p / I_b) should preferably be kept less than 10 in case of pulse current MIG welding [Ghosh 1996] by suitable adjustment of pulse frequency,

pulse duration and wire feed speed to avoid difficulties such as rotating arc, heavy tapering of the liquid tip and disturbance in the shielding caused by the fluctuation in arc pressure. Earlier investigation [Ghosh and Sharma 1991, Ghosh and Gupta 1996] carried out on single pass pulsed current MIG of Al-Zn-Mg alloy have shown the influence of the ratio of I_p/I_b on the porosity content of weld deposit and suggested that the I_p/I_b ratio should be maintained in the range of 7.5 at a mean current of 150 A and around 4 at a mean current of 220 A to achieve a significant reduction in porosity content of the weld deposit. It has also been observed that by keeping the mean current in P-GMAW process similar to the welding current of continuous current deposition, the porosity content of weld metal becomes comparatively lower than that observed in case of later one.

Superiority of P-GMAW however depends upon critical selection of pulse parameters by considering interaction amongst them during welding. This complicity in selection of pulse parameters for desired weld characteristics has been largely solved by using a hypothetical factor $\phi = [(I_b/I_p)ft_b]$ where, the t_b is expressed as $[(1/f) - t_p]$ which is having potentiality to analyse various basic characteristics of the weld and pulsed current GMAW process in reference to the pulse parameters [Ghosh 1999]. Utility of the factor ϕ has been amply justified by several investigators in various applications of pulsed current GMAW, such as welding of steel using solid and flux cored filler wires, positional welding of steel, stainless steel cladding of structural steel, single and multipass welding of high strength aluminium alloy [Ghosh and Dorn 1993, Ghosh et.al. 1998, Ghosh et.al. 1999].

2.4.4.2. Behaviour of metal transfer

Mechanism of drop detachment

Total time for the detachment of a droplet in P-GMAW can be divided into four stages as time required for heating, drop growth, necking and detachment, while the current amplitude may be different during each stage [Jilong and Apps 1982]. Under the influence of peak current, a continuous spray of drops may transfer if the pulse duration is prolonged. Time required to form and detach a droplet is inversely proportional to the amplitude of peak current but is independent of its duration. Once the necking starts, it requires a certain period to detach the droplet, which primarily depends upon peak current and wire diameter, irrespective of the current level at the time of its detachment. Necking, a plastic deformation of the heated electrode is due to the Lorentz force and melting of filler wire occurs under the neck. The detachment of the drop is induced by the vaporisation of molten metal at the neck due to resistance heating. The speed of droplet detachment is determined by the rate at which the fused metal is compressed into

droplet [Cornu 1988]. Hence, it has been well established that in P-GMAW, the metal transfer characteristics and thermal behaviour of weld deposit are governed by the pulse parameters, which interact amongst themselves during welding and dictate the characteristics of weld deposit [Ghosh and Rai 1996, Ghosh 1996, Ghosh et.al.1991].

2.4.4.3. Thermal Behaviour of weld

Wire melting characteristics

The wire burn off rate/melting rate for P-GMAW is expressed [Craig 1987, Smati 1986] as

$$V_{w(pc)} = \int_0^{t_{pul}} V_w t_{pul} dt_{pul} \quad (2.15)$$

For a square pulsed current waveform it gives

$$V_{w(pc)} = (V_{wp} t_p + V_{wb} t_b) t_{pul}^{-1} \quad (2.16)$$

Where, $V_{w(pc)}$ is wire burn off rate and V_{wp} and V_{wb} are wire burn off rates during t_p and t_b respectively.

The V_{wp} and V_{wb} may be expressed as

$$V_{wp} = A.I_p + B.E_w.I_p^2 \quad (2.17)$$

$$V_{wb} = A.I_b + B.E_w.I_b^2 \quad (2.18)$$

Therefore,

$$V_{w(pc)} = \left[\frac{(A.I_p + B.E_w.I_p^2)t_p + (A.I_b + B.E_w.I_b^2)t_b}{t_{pul}} \right] \quad (2.19)$$

Eq.(2.19) may be rewritten as

$$V_{w(pc)} = \left[\frac{A(I_p t_p + I_b t_b) + BE_w (I_p^2 t_p + I_b^2 t_b)}{t_{pul}} \right] \quad (2.20)$$

Using $I_m = [(I_p t_p + I_b t_b)/t]$ in eq. (2.20)

$$V_{w(pc)} = AI_m + BE_w (I_p^2 t_p + I_b^2 t_b) t_{pul}^{-1} \quad (2.21)$$

As $I_p^2 t_p \gg I_b^2 t_b$ neglecting ohmic heating during base current period, Eq. (2.21) reduces to

$$V_{w(pc)} = AI_m + BE_w I_p^2 t_p t_{pul}^{-1} \quad (2.22)$$

Considering $f = 1/t_{pul}$ and $I_p^2 t_p = D_n$ Eq.(2.22) gives

$$V_{w(pc)} = AI_m + BE_w D_n f \quad (2.23)$$

By considering $V_d = A_w V_w / f$ in Eq.(2.23) a linear relationship has been obtained [Lambentt 1989] as follows,

$$\frac{f}{I_m} = \frac{AA_w}{V_d - BDA_w E_w} \quad (2.24)$$

Solving eq.(2.24) for droplet volume V_d ,

$$V_d = AA_w \left(\frac{I_m}{f} \right) + A_w E_w BD \quad (2.25)$$

Eq.(2.25) shows that for any wire feed rate, by fixing (I_m/f) , the droplet size can be held constant for a given wire diameter, electrode extension and detachment parameter.

It has been observed that for 1.2 mm diameter steel filler wire [Quintino and Alum 1984] for a desired combination of peak current and its duration, giving one drop per pulse, the base current and its duration may be evaluated using frequency value of 50Hz for 100A mean current. It gives satisfactory droplet transfer as well as volume of droplet remains insensitive to I_m . It can be expressed as

$$I_m/f = 2 \quad (2.26)$$

By combining Eqs.(2.23) and (2.26)

$$V_{w(pc)} = AI_m + \frac{BE_w DI_m}{2} = I_m \left(A + \frac{BE_w D}{2} \right) = \bar{A} I_m \quad (2.27)$$

Where, $\bar{A} = \left(A + \frac{BE_w D}{2} \right)$ is modified burn off factor

In P-GMAW process, by considering ohmic heating during base current duration, Eq. (2.27) reduces to

$$V_{w(pc)} = AI_m + BE_w I_{eff}^2 \quad (2.28)$$

Where, $I_{eff}^2 = \left\{ k_p I_p^2 + (1-k_p) I_b^2 \right\}^{1/2}$ and k_p is pulse duty cycle defined as t_p/t_{pul}

I_{eff} may also be expressed as,

$$I_{eff}^2 = I_m^2 + k_p (1-k_p) I_e^2 \quad (2.29)$$

By combining Eqs. (2.28) and (2.29),

$$V_{w(pc)} = AI_m + BE_w (I_m^2 + k_p (1-k_p) I_e^2) \quad (2.30)$$

In consideration of Eq.(2.7), Eq. (2.33) may be expressed as

$$V_{w(pc)} = V_{w(cc)equiv.} + BE_w k_p (1-k_p) I_e^2 \quad (2.31)$$

Eq. (2.32) reveals the following aspects of P-GMAW [Alum 1983].

1. The burn off rate of pulsed current welding is higher than continuous current welding under the same equivalent welding current.

2. Pulsed structure influences burn off rate for a given mean current and maximum burn off rate can be achieved when $k_p=1/2$ i.e., equal peak and base current time and at largest peak current in excess over the base current.

It has also been observed that melting rate under P-GMAW is practically greater than melting rate estimated using weighted sum of the melting rate (for DC currents) at the peak and base current [Kim and Eagar 1993b]. It is also pointed out that under certain circumstances, the power source dynamics i.e. rate of rise and fall of current pulse, may have a significant influence on the wire melting rate at given mean current [Joseph et.al. 2003].

Thermal behaviour of droplet

Recent developments in P-GMAW have led to a number of potential applications, where low heat input along with directional capability of metal transfer is required. Thermal analysis of metal transfer indicates that droplet temperature is comparatively lower [Waszink and Piena 1986] which is favourable to better control of weld pool. It is observed that the characteristics of metal transfer and thermal behaviour of weld deposit in the process are largely governed by pulse parameters [Ghosh and Dorn 1983] which simultaneously interact among themselves during welding and dictate the characteristics of weld deposit. It has been reported [Ghosh and Dorn 1983] that at a given mean current and pulse duration, heat content of the droplet at the time of detachment enhances significantly with the increase in pulse frequency. It has been identified [Ghosh et.al. 2006] that the variation in pulse parameters significantly affects the thermal and transferring nature of depositing metal, the control of which is imperative for desired weld characteristics. The heat content and temperature of the droplets at the time of deposition in the weld pool reduces with the increase of I_m significantly.

2.4.4.4. Concept of summarised influence of pulse parameters

The benefits of P-GMAW over GMAW in improving the weld characteristics and properties of various ferrous and non-ferrous metals, under different conditions of pulsation have been reported by many investigators [Weber1982, Allum and Quintino 1985(a), Amin 1983, Craig 1987b]. However, the wide acceptance of the process in fabrication is largely handicapped due to the criticality in the selection of pulse parameters. It is well established [Ghosh and Dorn 1983, Praveen et.al. 2005, Palani and Murugan 2006] that the variations in pulse parameters identified as I_m , I_p , I_b , t_p and f influence the weld characteristics to a great extent. It has been realized that a change in any one parameter affects the others also under the concept of energy balance. The variation in pulse parameter significantly influences the thermal behaviour and nature of metal transfer affecting the characteristics of weldment. Under these circumstances, the control of weld characteristics within a desired range is possible only by establishing a correlation amongst pulse

parameters. It was also suggested that consideration of summarised influence of pulse parameters instead of individual one may be useful to study the different characteristics of the weldment.

A summarised influence of pulse parameters has been proposed by Ghosh [Ghosh 1999, Ghosh

and Dorn 1983,], defined by a factor, $\left[\phi = \left(\frac{I_b}{I_p} f t_b \right) \right]$, where t_b is defined by $t_b = \frac{1}{f} - t_p$ and a good

potentiality of the factor ϕ to analyse various basic characteristics of weld deposit has been reported.

Many investigators [Praveen et.al. 2005, Hussain et.al 1996] have justified the applicability of ϕ in different conditions of pulsation by studying its effect on different weld characteristics using ferrous and non-ferrous materials.

2.5. Narrow Gap Arc Welding Of Thick γ -SS Sections

Narrow gap welding has generated great interest in the welding industry and has been the subject of much investigation in the last twenty years. But till to date there is some controversy around a proper definition for the technique. Most authors agree that narrow gap welding is applied to any welding process used for joining of heavy section (>25 mm) using an essentially square butt joint preparation with small gaps which will yield a weld with low volume weld metal [Shtrikman and Grinin 1977, Swada et al 1979, Vornovitskii et al 1977]. In broad terms narrow gap welding is a property –oriented bead-deposition technique associated with an arc welding process characterized by a constant number of beads per layer that are deposited one on top of the other in a deep, narrow square groove. Some of the advantages attributed to narrow gap welding processes, when compared with other welding processes for thick joints is listed below:

- Reduction in welding time due to less weld deposition with least number of beads
- Reduction in severity of weld thermal cycle producing less axial and radial shrinkage which may favourably affect the stresses at the root area compared to those observed in conventional groove welding
- A low dwell time in the critical sensitising temperature range due to less number of bead deposition and a favourable residual stress profile in the weld and heat affected zone which may improve the properties of the weld joint [Murugan et al 2001, Vornovitskii, L.V. et al 1977]

However in order to produce high-quality multipass narrow gap welds one of the most important parameters namely the width of the gap must be maintained constant during the welding of each pass. With the reduction in gap width the access to the welding zone becomes more and more difficult and the welding process may be disrupted as a result of short-circuiting

of the electrode with the edge. In addition to this a reduction in gap width increases the thickness of the layer of liquid metal (weld pool) underneath the arc and this may lead to lack of fusion between layers. The experimental results indicate that after welding 8-10 layers the gap may decrease by 25-40% [Shtrikman and Grinin 1979]. Hence this aspect should be considered while designing the narrow groove.

2.6. Characteristics Of γ -SS Weld Joint

2.6.1. Weld Chemistry

Chemistry of weld metal primarily depends upon proper selection of filler metal. The filler metal should not only provide good weldability, but also produce weldments having mechanical and corrosion properties equivalent to those of the base metal [Han and Sun 1999]. Two principles are normally applied while selecting filler metals for producing corrosion-resistant weldments of stainless steels:

- 1) Use of additional alloying elements to obtain desirable corrosion properties, and
- 2) High level of purity in the steel should be maintained by reducing impurity contents (*i.e.*, carbon, sulphur and phosphorus) to achieve the enhanced corrosion properties.

To produce sound weld joints, microfissuring tendency should also be controlled by maintaining purity of consumable composition such that amounts of ferrite in the weld metal vary from 3 FN to 8 FN [Cui, 2004]. A higher nominal ferrite content does not ensure uniform distribution throughout the weld metal [Brooks et al 1983]. To achieve this filler metals for welding stainless steels are produced as coated electrodes (AWS A5.4), solid and metal core wire (AWS A5.9) and flux core wire (AWS A5.22). Mostly popular electrodes such as E308-16, E308L-16, E309-16, E310-16, E316-16, E316L-16 and E347-16 are used for welding of this class of steel. The electrodes are available with a lime coating (-15) (for use with DC only), a titania coating (-16) (for use with AC or DC) or a silica-titania coating (-17) (for use with AC or DC mainly in the downhand or horizontal positions) and in the standard or low carbon variety. These alloys which are mainly used in coated electrodes are also available as either solid wire, metal cored wire or flux cored wire. A few are available only as coated electrodes. These are 310H, 310Cb, 310Mo and 330H. Filler metals in general for austenitic stainless steels should either match or exceed the alloy content of the base metal. If a filler material of the correct match is not available, filler with higher alloy content normally should be used. There are several austenitic stainless types for which no exact matching fillers are made. Examples are 201, 202, 205, 216, 301, 302, 304 and 305. The filler materials recommended for these base alloys are somewhat higher in Cr and Ni content. For example, 308 is used for 301, 302, 304 and 305 and

may be used for 201, 202, 205 and 216 if 209, 219 or 240 are not available. The major recommended filler materials in the form of coated electrodes, solid and metal core wire and flux core wire are as listed in Table-2.4.

2.6.2. Microstructure

2.6.2.1. Weld

The solidification mechanism of weld metal during P-GMAW differs from that of GMAW and SMAW processes. In GMAW and SMAW process the solidification of weld metal takes place under a continuous supply of heat coming from the direction of heat source giving a coaxial dendritic structure [ASM handbook, 1994]. Whereas, heat transferred to the solidification front is of intermittent nature in P-GMAW process. During P-GMA welding the molten pool solidifies during the pulse off time being initiated from its front part and the same remelts during the subsequent pulsation wherein, the back part of the molten pool continues to solidify. Thus the solidification takes place primarily into two steps, one during the off time period and other during development of weld spot resulting from the next pulse. The peculiar form of heat balance caused by this phenomena has been [Hussain et al 1996] found to affect the micro structural characteristics of the weld pool. During the pulse off time the solidification of droplets starts from its circumference as a coaxial growth of dendrite under a condition of practically no heat gain from outside because of the existence of a low arc current at the off time where no metal transfer is available. This process is called the off time solidification process. The extent of solidification of the droplet primarily depends upon the super heating, size of the droplet and the extent of off-time [Ghosh 1996, Hussain et al 1996]. However when the subsequent pulsation sets in the deposition of later droplet on the earlier one, it causes a localized melting and produces a thermal shock to the adjacent regions below it. The local melting may cause necking and pinching off the dendrite arms, and the crystallites may be removed from the liquid caused by agitation resulting from a thermal gradient. Many of these crystallites remelt at the upper part of the bead due to high temperature while the others retain in some part of the bead at a comparatively low temperature. These crystallites grow to new randomly oriented crystals resulting into a fine grain cast structure of the weld by a grain multiplication process [Hussain et al 1996].

Pulsed current GMAW can refine the microstructure by controlling the inward growing columnar grains into smaller equiaxed grains. A detailed micrographic study of the welds has suggested that suitable nuclei for equiaxed solidification would be stable only at or shortly after the pulse duration because of considerable superheat in the weld pool. Thus, high frequency

pulsing is supposed to be more effective but, this would be limited by thermal inertia effects at higher pulse frequencies. It is also observed that at a given comparatively higher mean current (200 A) and pulse frequency, the increase in pulse duration also found to coarsen the microstructure due to enhancement in superheating of a droplet at higher peak current for a longer duration. In aluminium weld [Ghosh and Sharma 1991, Ghosh and Dorn 1993] the refinement of microstructure improves with the increase in pulse frequency up to 50 Hz where the mean current is kept of the order of 210 A. However with the further increase in pulse frequency up to 100 Hz, the droplet transferred to the weld pool does not get sufficient period to solidify enough at the low pulse off period before receiving the successive one and consequently it re-melts to a greater extent. Thus the process of solidification tends to be similar to that of continuous current weld deposit and the microstructure shows considerable growth of dendrite [Ghosh and Gupta 1996].

Table 2-4 Filler Metals for welding austenitic stainless steels From AWS Filler Metal specifications: A5.4,A5.9, A5.22.

Base Stainless Steel		Recommended Filler Metal		
Wrought	Cast	Coated Electrode	Solid, Metal Core Wire	Flux Core Wire
201		E209, E219, E308	ER209, ER219, ER308, ER308Si	E308TX-X
202		E209, E219, E308	ER209, ER219, ER308, ER308Si	E308TX-X
205		E240	ER240	
216		E209	ER209	E316TX-X
301		E308	ER308, ER308Si	E308TX-X
302	CF-20	E308	ER308, ER308Si	E308TX-X
304	CF-8	E308, E309	ER308, ER308Si, ER309, ER309Si	E308TX-X, E309TX-X
304H		E308H	ER308H	
304L	CF-3	E308L, E347	ER308L, ER308LSi, ER347	E308LTX-X, E347TX-X
304LN		E308L, E347	ER308L, ER308LSi, ER347	E308LTX-X, E347TX-X
304N		E308, E309	ER308, ER308Si, ER309, ER309Si	E308TX-X, E309TX-X
304HN		E308H	ER308H	
305		E308, E309	ER308, ER308Si, ER309, ER309Si	E308TX-X, E309TX-X
308		E308, E309	ER308, ER308Si, ER309, ER309Si	E308TX-X, E309TX-X
308L		E308L, E347	ER308L, ER308LSi, ER347	E308LTX-X, E347TX-X
309	CH-20	E309, E310	ER309, ER309Si, ER310	E309TX-X, ER310TX-X
309S	CH-10	E309L, E309Cb	ER309L, ER309LSi	E309LTX-X, E309CbLTX-X
309SCb		E309Cb		E309CbLTX-X
309CbTa		E309Cb		E309CbLTX-X
310	CK-20	E310	ER310	E310TX-X
310S		E310Cb, E310	ER310	E310TX-X
312	CE-30	E312	ER312	E312T-3
314		E310	ER310	E310TX-X
316	CF-8M	E316, E308Mo	ER316, ER308Mo	E316TX-X, E308MoTX-X
316H	CF-12M	E316H, E16-8-2	ER316H, ER16-8-2	E316TX-X, E308MoTX-X
316L	CF-3M	E316L, E308MoL	ER316L, ER316LSi, ER308MoL	E316LTX-X, E308MoLTX-X
316LN		E316L	ER316L, ER316LSi	E316LTX-X
316N		E316	ER316	E316TX-X
317	OG-8M	E317, E317L	ER317	E317LTX-X
317L		E317L, E316L	ER317L	E317LTX-X
321		E308L, E347	ER321	E308LTX-X, E347TX-X
321H		E347	ER321	E347TX-X
329		E312	ER312	E312T-3
330	HT	E330	ER330	
330HC		E330H	ER330	
332		E330	ER330	
347	CF-8C	E347, E308L	ER347, ER347Si	E347TX-X, E308LTX-X
347H		E347	ER347, ER347Si	E347TX-X
348		E347	ER347, ER347Si	E347TX-X
348H		E347	ER347, ER347Si	E347TX-X
Nitronic 33		E240	ER240	
Nitronic 40		E219	ER219	
Nitronic 50		E209	ER209	
Nitronic 60			ER218	
254SMo		ENiCrMo-3	ERNiCrMo-3	
AL-6XN		ENiCrMo-10	ERNiCrMo-10	

2.6.3. Mechanical Properties

The design, prediction of performance, and safety analysis of austenitic stainless steel welded components generally require a complete knowledge of their physical and mechanical properties. In particular, it would be useful to have at one's disposal more information on the mechanical properties of the weld deposited metal as influenced by its material variability. This is characterized by microstructural variations between the parent metal (usually fully austenitic) and the weld metal (containing various amounts of δ -ferrite retained at room temperature). The presence of δ -ferrite in the austenite matrix is necessary to prevent cracking during welding according to a well-established practice [Piatti and Vedani 1990].

2.6.3.1. Tensile properties

Austenitic stainless steel welds generally contain delta ferrite content to avoid hot cracking. The weld thus obtained in comparison to base metal has relatively higher yield strength and ultimate tensile strength accompanied by reduction in elongation [Shaikh et al 1995]. During welding, the severe plastic deformation may occur in heat affected zone very near to the fusion line. Thus it has been observed the tensile properties depending upon crystallographic anisotropy may show considerable deviation in direction parallel and perpendicular to the direction of welding. The yield strength, and to a lesser extent the tensile strength are the properties most affected [Dieter 2001]. The yield strength in the direction perpendicular to the main direction of welding may be greater or less than the yield strength in the longitudinal direction, depending on the type of preferred orientation which exists. Such a anisotropy may play an important role in designing of thick wall tubes like pressure vessels which are subjected to high internal pressures [Dieter 2001]. Tensile properties are also greatly impaired by the presence of inclusion and porosity content in the matrix of weld metal. The typical ductile fracture behaviour showing cup and cone appearance on the macroscopic scale enlarges the cup or flat portion of the fracture surface and a strong diminution of the cone or shear portion depending upon presence of dimples associated with impurity particles which are generally round and have various different sizes [Piatti and Vedani 1990, Çam et al 1999]. Thus void nucleation occurs at such impurity particle/matrix interface separation giving inferior tensile properties.

2.6.3.2. Hardness

In welds metallurgical transformations takes place over very small areas. Thus mostly micro hardness measurements are carried to determine the formation of phases [Dieter,2001]. In austenitic stainless steel welds, ferrite content and the influence of weld thermal cycle on it

causes precipitation of number of phases. Thus the increase in scattering magnitude primarily indicates that hard phases such as carbides and sigma are formed in the matrix.

2.6.3.3. Residual stresses

Residual stresses are those stresses remaining in a solid body under zero external force. During welding, the deposited metal fuses groove area and heats it up sharply relative to the adjoining cooler area of base metal [Sarkani et al 2001]. As a result thermal expansion of the fused area is restrained by the surrounding colder area, giving rise to elastic thermal stresses. These thermal stresses which partly exceed the yield limit of weld metal at elevated temperature consequently plastically hot compress the weld area. Subsequently during cooling and solidification, the plastically hot compressed molten material will tend to shrink and pull adjoining parent material which will either follow the shrinking movement resulting in distortion or shrinkage or it will fully or partially resist distortion resulting in residual stresses. It thus displays tensile residual stresses and the surrounding area compressive residual stresses [Webster et al 2002, Basavaraju 2000]. These thermo mechanical treatments caused by complex multipass welding operations result in strain induced deformation which accelerates transformation reaction rates in materials through its effects on

- 1) increasing the vacancy concentration leading to an increased diffusivity
- 2) lowering the activation barrier to diffusion
- 3) decreasing the free energy barrier to nucleation and
- 4) increasing the effective driving force for nucleation .

The formation of residual stresses can be effectively controlled if the highest temperature reached at the weld centreline is just below the melting point of the material and that only elastic strains occur and no phase transformations whatsoever take place. However this practically impossible task can be optimized by reducing thermal strains accompanied by plastic upsetting to a lowest possible extent [Teng et al 2003, Lin and Chen, 2001]. This objective can be achieved by first understanding the stress distribution in thick sections and then with proper control of welding process and procedure.

2.6.3.4. Stress Distribution in thick sections

In a multipass welding operation, the number of thermal cycles that the material undergoes during welding is same as the number of passes, and with each pass, the residual stress pattern changes [Teng et al 2003]. The complex metallurgical process due to thermal cycles in welding, such as shrinkage, phase transformations produce both tensile or compressive residual stress in different zones of the welded structure. Residual stress, particularly tensile residual stress in the

weldment, can be a very important factor in affecting the reliability and integrity of the weld [Yaghi 2005]. The formation of tensile residual stress may result in initiation of fatigue cracks, stress corrosion cracking, or other types of fracture. The development and distribution of such harmful residual stress in thick sections primarily depends on

1. Thermal expansion and contraction characteristics of weld metal resulting in plastic upsetting.
2. Welding direction as residual stresses near the weld interface on thick multi-pass weldments are more tensile in the direction normal to the weld than in the direction parallel to the weld [Brickstad and Josefson 1998].
3. Weld shrinkage which primarily depends on weld thermal cycle and groove design, affects the level and the distribution of residual stresses in the root area resulting in strain hardening in this area [Teng et al 2002].
4. Thicker pipes with lower diameter have less tensile or compressive residual stresses on the inside surface of the pipe [Brickstad and Josefson 1998].
5. In pipe structures, axial stress distribution is not rotationally symmetric, whilst the hoop stress may show a rotational symmetry [Chang and Teng 2004, Brickstad and Josefson 1998].
6. The heat deposited during circumferential butt welding is high enough to result in a uniform temperature increase through the pipe thickness at the weld. The only deformation that will create thermal stresses is the circumferential strain due to the radial expansion and subsequent contraction. This radial decrease during cooling after welding together with symmetry condition at the centre section results in a almost linear through thickness axial stress variation with tensile axial stresses at the inner surface (sometimes of yield stress magnitude) and compressive axial stresses on the outer surface. The compressive hoop stresses are normally tensile all through the thickness and have about the same magnitude as the maximum axial stresses if the yield properties of the weld and base material are about the same [Brickstad and Josefson 1998]

2.7. High Strength Low Alloy (HSLA) Steels

HSLA steels are intended to provide better mechanical properties and/or greater resistance to atmospheric corrosion than conventional carbon steels [AWS handbook 1978, Metals handbook 1979(a), (b), Rothwell and Malcolm Gray 1976]. They are considered as low alloy steel owing to small content (3-5 Wt. %) of alloying element including some selective elements in order to meet high strength along with other properties [Suzuki et al 2001, AWS handbook 1978]. The chemical composition of HSLA steel plate may also vary in production

of different types of steel for diverse thicknesses to meet specific requirements in mechanical properties [ASM handbook 1992, Kearns AWS handbook 1978, Metals handbook 1979 (a), (b)]. HSLA steels keep low carbon content (0.05 - 0.25 Wt. %) with varying manganese content up to 2.0 Wt %, in order to exhibit adequate formability and weldability. As a selective minor addition small quantity of chromium, nickel, molybdenum, copper, nitrogen, vanadium, niobium, titanium, and zirconium are used in various combinations. HSLA steels have yield strength (YS) and ultimate tensile strength (UTS) greater than 275 and 500MPa respectively [ASM handbook 1992, Kearns AWS handbook 1978, Metals handbook 1979 (a), (b), Rothwell and Malcolm Gray 1976]. The addition of micro-alloying (e.g., niobium (Nb), vanadium (V), or titanium (Ti)) with controlled processing has been successfully implemented to HSLA steels mainly to increase the strength by maintaining fine grained ferrite/pearlite structure and to maintain cost effectiveness [Craven et al 2000(a, b), Fernandez et al 2007, Hong et al 2003, Hou et al]. The main advantages of the micro-alloyed HSLA steels are good combination of strength and toughness and weldability. Usually depending on the micro-alloying elements, the desired mechanical and metallurgical properties were achieved by austenite grain size conditioning and precipitation strengthening [ASM handbook 1992, Metals handbook 1979(a), Rothwell and Malcolm Gray 1976].

The new grade of HSLA steels has been produced with as hot-rolled yield strengths exceeding 480 MPa in 20mm thick plate in combination with low temperature toughness [ASM Handbook 1992, Gunduz and Cochrane 2005 and Hou et al 2003]. These properties have been obtained by appropriate alloying and controlled rolling. The higher strength steels generally contain lower carbon but higher manganese and molybdenum (Mo) in combination with one or two micro alloying elements (e.g., Nb, V, or Ti). HSLA -100 is easily weldable high-strength steel for naval applications [Das et al 2006, Dhua et al 2002, Laing et al 1985 and Narayanasamy et al 2007].

2.8 Properties of HSLA Steels

HSLA steels must have certain characteristics and properties to use in construction of various advanced welded structures such as strength, toughness, ductility, formability and weldability so that it can be fabricated successfully by customary methods depending upon applications. In addition to this, improved corrosion resistance is generally required [Pickering 1978]. All of the HSLA steels have higher strength than the majority of as rolled or normalized structural carbon steels and have fairly good formability commensurate with their strength level. Their corrosion resistance and notch toughness depends upon composition and processing.

2.8. Properties of HSLA Steels

HSLA steels must have certain characteristics and properties to use in construction of various advanced welded structures such as strength, toughness, ductility, formability and weldability so that it can be fabricated successfully by customary methods depending upon applications. In addition to this, improved corrosion resistance is generally required [Pickering 1978]. All of the HSLA steels have higher strength than the majority of as rolled or normalized structural carbon steels and have fairly good formability commensurate with their strength level. Their corrosion resistance and notch toughness depends upon composition and processing.

2.8.1. Mechanical properties

The mechanical properties of HSLA steels are primarily dictated by their microstructure. These have generally ferrite - pearlite microstructures, and their properties are affected by changes in the microstructure. Strength can be increased by increasing the amount of pearlite, the fineness of the microstructure, and the amount of dispersed phases. As the strength is increased by these micro structural changes, notch toughness is usually impaired in proportion to the increase of strength, but a finer microstructure is accompanied by an increase in notch toughness [Pickering 1978]. Higher strength is often obtained by the addition of small amounts of niobium or vanadium, or titanium [ASM Handbook 1994, Tamura et al 1988]. These elements provide strengthening by precipitation hardening [ASM Handbook 1994, Tamura et al 1988 and Pickering 1978]. The minimum mechanical properties of HSLA steels of different thickness has been given in table -2.5.

Table - 2.5 Minimum mechanical properties of HSLA Steels [Tamura et al 1988].

Property	Minimum value
Thickness, up to 20mm	
Tensile strength	485 MPa
Yield strength	345 MPa
Elongation in 200 mm	18 %
Thickness, 20 to 38 mm	
Tensile strength	460 MPa
Yield strength	325 MPa
Elongation in 200 mm	19 %

The notch toughness of high strength low alloy steel, as evaluated by Charpy-impact tests, is superior to that of structural carbon steels [Tamura et al 1988] whereas, the transition

temperature of the HSLA steels is lower [Tamura et al 1988, Pickering 1978]. Notch toughness of both precipitations hardened and quenched & tempered steels is primarily function of microstructure. HSLA steels are designed to have adequate notch toughness for their intended application, but generally are not supplied to a minimum notch-toughness criterion [Tamura et al 1988, Pickering 1978]. The suitability of the notch toughness of specific HSLA grades may be based on established service performance alone or in combination with the results of impact tests on notched specimen. Some HSLA steels are produced with exceptionally good notch toughness to meet the stringent requirements of certain applications. For example, controlled hot-rolling practices are now commonly used in the production of HSLA plate to be fabricated into welded line pipe; [Kearns AWS handbook 1978]. Such pipes are required to meet notch-toughness specifications established by the American Petroleum Institute (API). The ASTM A572 and A588 grades must meet impact requirements at -12 to 21⁰C when used for main tension members in highway bridges [Kearns AWS handbook 1978, Metals Handbook 1979(a)].

2.8.2. Weldability

In view of the fact that welding is generally utilized in fabrication of structural steel, it is important that HSLA steels must be readily weldable for these applications by commonly used arc welding processes. It is also desired that the welds in fabricated structures should have the required strength and ductility to withstand the adverse conditions expected in the desired service. The development of the HSLA steels has paralleled the growth of the various welding processes, and particular care was exercised to ensure that these steels possess suitable welding characteristics. Most of these steels are considered to be readily weldable by conventional processes when good shop or field practices are used [Babu et al 2002 and Tamura et al 1988]. For shielded-metal-arc welding of HSLA steels having minimum yield stress up to about 345 MPa, E-60 or E-70 grade electrodes are generally used. E-70 grade electrodes are suggested for steel grades having somewhat higher minimum yield points [Das et al 2008 (a, b), Das et al 2006, Davies 1983, Dhooge et al 1978, Sierdzinski and Ferree 1999]. For heavier sections and for grades that have higher carbon and manganese contents, preheating and/or low-hydrogen practices should be used for all thicknesses. Low-alloy-steel electrodes are generally required for steels with minimum yield points higher than about 415MPa or when specific characteristics [Tamura et al 1988], such as enhanced corrosion resistance is required in the weld metal. Electrodes or electrode flux combinations that provide filler metal similar to that of the suggested electrodes for shielded metal arc welding are recommended for submerged arc, gas metal arc and flux cored arc welding [Cerjak et al 1999, Yongyuth et al 1992]. In the automotive HSLA sheet

steels, good spot weldability is achieved through the use of low carbon contents which are generally restricted to about 0.13 percent or less [Tamura et al 1988]. HSLA steels are welded with SAW consumables covered by ANSI/AWS A5.23 include ASTM specifications A-242, A 537 class 1 and 2, A-572 grades 42-65, A 588, and A-633 grades A-E [Kearns AWS handbook 1978, Metals Handbook 1979(a, b)]. It must be noted that some of these steels can also be welded with consumables specified in ANSI/AWS A-5.17; the choice depends on the mechanical property requirements. ASTM A-242 and A-588 steels are resistant to rusting [Kearns AWS handbook 1978, Tamura et al 1988]. Some applications require welding these materials with electrode/flux combinations that will result in the same appearance and oxidation resistance as the base material [Chen et al 2006].

2.9. Factor Affecting the Weldability of HSLA Steels

Weldability of HSLA steels is comparable to plain carbon steel that have similar carbon equivalent [Metals Handbook 1979 (a)]. It is therefore HSLA steels have been widely used in the construction of buildings, pipelines and ships. However, it is very difficult to monitor and estimate the local property distribution of welded joints due to low alloying addition [Davies 1983, Metals Handbook 1979 (a)]. Welded structure e.g. submarine hulls (or other naval vessels), may be subjected to dynamic loading from impact or explosion. Such a critical condition causing failure initiation is frequently found in the heat-affected zones and weld [Davies 1983, Tamura et al 1988], and is principally caused by tensile stresses [Chapman et al 1997]. The expression for finding carbon equivalent (CE) to determine the pre-heating temperature of HSLA steel proposed by international institute of welding (IIW) is as follows [ASM handbook 1994, Davies 1983, Rothwell and Malcolm Gray 1976, Radaj 1992].

$$CE = \%C + \% \frac{Mn}{6} + \frac{(\%Cr + \%Mo + \%V)}{5} + \frac{(\%Ni + \%Cu)}{15} \quad (2.38)$$

If the CE exceeds 0.45, the welding situation changes due to the possibility of cracking in HAZ [Sindo Kou 1987].

2.9.1. Effect of residual Stresses

The welded joint may be susceptible to structural failure due to development of residual stress resulting from the welding process [Teng et al 2003, Henderson and Steffens 1976]. The complex metallurgical processes in welding, such as shrinkage, quenching, or phase transformations is producing both tensile and compressive residual stress in different zones of the welded structure. Residual stress of tensile in nature in the weldment, can be a very important factor dictating the reliability and integrity of the weld joint. The formation of tensile residual

stress may develop initiation of fatigue cracks, stress corrosion cracking, or other types of fracture [Chang et al 2004, Clark et al 2002, Dong 2001, Fricke et al 2001, Roos et al 2005, Radaij 1992, Teng et al 2002].

Residual stresses may be sufficient to cause a metal part to fail suddenly and split into two or more pieces without applying any external load [Davies 1983]. Residual stresses are stresses that are inside or locked up into a component or assembly of parts. The internal state of stress is generally caused by thermal and /or mechanical processing of the parts [Dieter 1988, Tamura et al 1988] e.g. bending, rolling or forging. Another situation is the thermal stresses induced by welding. In other extreme in certain cases residual stresses can play a significant role in preventing failure of a component. One example of residual stresses preventing failure is the shot peening of component to induce surface compressive stresses that improve the fatigue life. Unfortunately, there are also processes or processing errors that can induce excessive tensile residual stresses in locations that might promote failure of a component. The internal stresses are balanced in a component. Tensile residual stresses are counter balanced by compressive residual stresses. To better visualize residual stresses, it is sometimes helpful to use tension and compression springs to represent tensile and compressive residual stresses. Residual stresses are three-dimensional [Dieter 1988]. Residual stresses can result in visible distortion of a component. The distortion may be useful in estimating the magnitude or direction of the residual stresses. Thermal residual stresses are primarily due to differential expansion and contraction when a metal is successively heated or cooled. The factors that control this are thermal treatment (heating or cooling) and restraint. Both the thermal treatment and restraint of the component must be present to generate residual stresses.

Gao et al [1997] has found residual stress by X-ray diffraction in HSLA-100 steel weldment prepared by using GMAW process under different welding heat input and restraint condition [Gao et al 1997]. They observed that transverse residual stress is always compressive on the surface near the weld and gradually become tensile as the distance from the weld increases. However, longitudinal residual stresses are usually tensile on the surface near the weld and slowly decrease as the distance from the weld increases. Higher welding heat input generates smaller residual stresses at slower cooling rate of the weldments due to inhibition of shrinkage and phase transformation. Restraint of the weldment has a significant effect on residual stress. Additional tensile stress will be generated because the shrinkage of the weldment is impeded by rapid restraint. However restraint stress can also lead to an induced martensite/bainite transformation, resulting in an additional compressive stress. There exist tensile longitudinal

residual stress and a compressive transverse residual stress on the subsurface near weld under restrained and non-restrained condition respectively.

2.9.2. Effect of microstructure

Higher strength and toughness along with low carbon steel plate with improved weldability can be achieved by the combination of micro-alloying and controlled rolling. The improvements in mechanical properties result mainly from the refinement of the ferrite grain size together with a controlled amount of dispersion strengthening. One of the beneficial effects of Ti additions in Nb high strength low alloy (HSLA) steels is an improvement in the toughness of the heat affected zone (HAZ) resulting from welding, especially after high heat inputs [Gery et al 2005, Sundaram et al 1987]. This is because of forming of stable Ti rich carbonitride particles and these can restrict austenite grain growth in the HAZ at high temperature and hence improve HAZ toughness [Varughese et al 1993].

When the quenched and tempered low carbon low alloy steels are welded, it is necessary to control the microstructures of both the heat affected zone and the weld deposit [Tamura et al 1988]. Adequate toughness in a ferritic weld deposit can be obtained by minimizing the percentage of Widmanstatten side plate ferrite and maximizing the acicular ferrite content [Zhao et al 2003]. Widmanstatten side plate ferrite nucleates from the prior austenite grain boundaries, while acicular ferrite is nucleated intra-granularly on oxide inclusions. Research has also focused on the heterogeneous nature of the oxide inclusions and especially on the crystalline compounds present in the oxide inclusions [Babu et al 2002, Tamura et al 1988]. Two methods have been adopted to identify these crystalline compounds. One is to electrolytically extract the oxide inclusions and determine the presence of crystalline compounds by X-ray diffraction. The other is to identify the crystalline compounds in individual inclusions by electron diffraction. Widmanstatten side plate ferrite grows as parallel laths of similar crystallographic orientation and hence offers little resistance to crack propagation. Acicular ferrite grows in many directions and a crack is required to change directions repeatedly, thus providing better toughness.

Shome et al [2004, 2007] developed the analytical model for predicting the grain size in the heat affected zone (HAZ) near to fusion line by considering with and without grain boundary pinning precipitates in the micro alloyed HSLA matrix as follows.

$$D_{g0}^{1/n} - D_{g1}^{1/n} = K_1 \left(\int_{t_1}^{t_3} \exp\left(-\frac{Q_{app}}{RT_p}\right) dt - \int_{t_1}^{t_2} \exp\left(-\frac{Q_{app}}{RT_p}\right) dt \right) \quad (2.2)$$

Where, D_{g0} is the final mean grain diameter, D_{g1} is the initial grain diameter, n is the time exponent (0.5), K_1 is a kinetic constant ($1.26 \times 10^{12} \mu\text{m}^2/\text{s}$), Q_{app} is the apparent activation energy

for grain boundary movement (260kJ/mol), R is universal gas constant, T_p is peak temperature in fusion line, t_1 , t_2 and t_3 are temperature cycle in austenite. It has been reported that the predicted grain size are within 10% of the mean experimental values of the grain size, and more accurate than predictions using earlier model proposed by Anderson's [Shome et al 2004].

The effect of heat-input on austenite grain size in the different locations of heat affected zone of HSLA-100 steel has been reported [Shome et al 2007]. The single pass weld deposition was made by using GMAW and SAW process at relatively low and high heat input of 10 and 40kJ/cm respectively. The grain size at different locations of HAZ was related to the peak temperature and determined with the help of existing Ashby–Easterling [Dieter, 1988] analytical model based on Gaussian heat source distribution for two different heat-input conditions. It has been concluded that at a same peak temperature and relatively higher heat input of 40kJ/cm, the grain size increases considerably than those of lower heat input of 10kJ/cm which significantly influences the microstructure and properties of the heat affected zone.

In general it is observed that acicular ferritic microstructure is becoming an optimal microstructure because of its excellent combination of strength and toughness than ferrite–pearlite microstructures [Xiao et al 2005, Yongyuth et al 1992, Zarandi et al 2005, Zhao et al 2003, Zrilica et al 2007] and also the carbon contents of these acicular ferrite steels are lower than that of conventional micro-alloyed ferritic-pearlitic steels. The major constituents in the acicular ferrite microstructure are transformation products at quite low temperature during the controlled cooling process [Tamura et al 1988]. Although, acicular microstructure contains non-equiaxial ferrite with dense dislocations and second-phase islands dispersed in the matrix [Zhao et al 2003]. In this regard, Xiao F et al [2005] designed the acicular ferrite microstructure for low carbon Mn-Mo-Nb micro-alloyed pipeline steel through hot deformation of continuous cooling and isothermal transformation processes. This investigation showed that the lowest cooling rate of $0.1^\circ\text{C}/\text{sec}$ revealed the microstructure as polygonal ferrite + acicular ferrite and relatively higher cooling rate in wide range of 0.2 to $7.5^\circ\text{C}/\text{sec}$ revealed that acicular ferrite and also increases the starting transformation temperature from 620 to 740°C and, the polygonal ferrite disappears when the cooling rate was beyond $7.5^\circ\text{C}/\text{sec}$.

During welding at high heat input significant austenite grain growth may occur in the heat affected zone of welded joints, leading to bainitic microstructures after completion of the weld. These microstructures are known to be sometimes sensitive to cleavage cracking, especially when some austenite is retained after the bainite transformation, leading to martensite–austenite (M–A) constituents [Tamura et al 1988]. These M–A constituents may be located between bainitic laths as well as at prior austenite grain boundaries [Tamura et al 1988]. In this regard,

Lambert- Perlade et al [2004] investigated austenite to bainite phase transformation in the heat-affected zone of a high strength low alloy steel by means of light microscopy, electron backscatter diffraction and transmission electron microscopy. It is observed that the bainite phase transformation appears to occur in two stages. In the first stage, discrete, non-parallel, highly intricate, straight groups of laths form. The second stage is thickening of these groups, leading to coarse crystallographic packets containing both elongated and equiaxed M–A constituents. Upper bainite packets of the fully transformed microstructures consist of highly intricate, non-parallel sets of plate-shaped groups of laths. These groups have a low angle misorientation relationship but highly misoriented habit planes.

Shvachko et al [2000] investigated Hydrogen induced cold cracking (HICC) of HSLA steel weldments. These cracks can appear few minutes after welding or sometimes few hours or even days. If a great deal of elastic energy is stored in a joint then the cold crack propagate through a full section of a joint at very significant sound and mechanical effects. The hydrogen cracking problem both in welding and in other metallurgical fields has been studied for many years. In spite of that, the practical recommendations of how to avoid hydrogen cracking up until now are based on empirical knowledge [Sierdzinski et al 1999]. It is still not possible to explain exactly how the presence of hydrogen within the metal structure leads to the formation of cracks in certain circumstances. So the new model of hydrogen embrittlement (HE) has been described. The new model of HE suggests that the micro crack occurs in dislocation cluster by a micro cleavage mechanism during straining and propagates at the initial period analogous to the Griffith classic scheme; hydrogen, adsorbed in the form of negative ions on the new surfaces in a crack, promotes cracking [Sierdzinski et al 1999].

2.9.3. Effect of welding processes, procedure and parameters

The multi-pass welds of quenched and tempered 50-mm-thick steel plate have been carried out by depositing with a single wire narrow gap process using gas metal arc welding (GMAW) and submerged arc welding (SAW) processes [Powell and Herfurth 1998, Kanjilal et al 2007]. C_v impact toughness at -20°C and microstructure including oxide inclusion size and ferrite morphologies had been studied and correlated to the Al to Ti ratio of both the oxide inclusions and the weld deposits. It has been observed that the combination of more oxide inclusions greater than 1 mm and less acicular ferrite lowers the C_v impact toughness.

The effect of alloying element powder additions on the microstructure and toughness of weld metals in HSLA- 70 line-pipe steel produced by submerged arc welding technique was investigated [Linnert 1994]. It was observed that the addition of Mo in the range 0.817 – 0.881 wt. % resulted in a decrease of fracture appearance transition temperature (FATT) and an increase

of impact toughness. The beneficial effect of Mo is due to the formation of predominant acicular ferrite (AF) and granular bainite (GB), at the expense of ferrite with second phase (FS (A)) and grain boundary ferrite (GBF) in weld metal. The combined presence of Ni (2.03–2.91 wt.%) and Mo (0.7–0.995 wt.%) in the weld metal, leads to a high volume fraction of fine AF with good toughness, because the amount of both FS(A) and GBF are reduced. When Ni is added alone in the range of 2.03–3.75 Wt %, the weld metal shows a lower toughness and an increased FATT, due to a lower amount of AF and a high volume fraction of (FS (A)). The weld metal with a mixed microstructure comprising around 77% AF and 20% GB shows the optimum impact toughness at -45°C [Tamura et al 1988].

Tso-Liang et al [2002] proposed a mathematical model to predict the effects of important butt weld geometry parameters (such as weld toe radius, weld bead flank angle, preparation angle, and plate thickness), and residual stresses on the fatigue crack initiation (FCI) life of butt-welded joints. In addition, this investigation develops theoretical explanations for the improvement of fatigue life from reductions in tensile weld residual stress introduced by varying the preheating temperature. An effective procedure is also developed by combining the thermal elasto-plastic theory, finite element and strain-life methods. It was observed that localized heating caused by welding and subsequent rapid cooling can cause tensile residual stresses at the weld toe of butt-welded joints. These tensile residual stresses were considered to be one of the major factors influencing fatigue strength. Longitudinal weld residual stress was found to be insensitive to changes in flank angle and weld toe radius. Modifying the weld geometry parameters such as increasing the radius of the weld toes and decreasing the value of the flank angle can improve FCI life of butt-welded joints. Preheating temperature thus affects the residual stress near the weld toe of the butt-welded joints in the following three ways 1) Preheating reduces the maximum cooling rate (temperature gradients) in HAZ during welding and thus reduces residual stress. (2) Preheating reduces the temperature variation and thus alters the shrinkage through the weldment thickness during cool down, thus decreasing residual stress. (3) Preheating maintains temperatures in HAZ after welding, so the yield stress and Young's modulus are lower than at room temperature for the same time, thus reducing the residual stress. It is also observed that the peak transverse residual stresses in the central region decrease with an increasing specimen length. The tensile residual stresses in the region near the fusion zone increase with a decreasing specimen thickness. A higher welding speed reduces the amount of adjacent material affected by the heat of the arc and progressively decreases the residual stresses. The magnitude of the residual stresses with a restrained joint is larger than that estimated with an unrestrained joint. The preheating treatment, the weldment significantly reduces the residual

stresses. In line of the above, Peng-Hsiang Chang et al [2004] performed numerical and experimental investigations on the residual stresses of the butt-welded joints. It was reported that a very large tensile longitudinal and transverse residual stress occurs near the weld toe, and a compressive stress appears away from the weld bead. Meanwhile, the stress approaches zero as the distance from the weld toe increases.

Murugan et al [2001] investigated temperature distribution and residual stresses due to multi-pass welding in 304 -L type stainless steel and low carbon steel with 6, 8 and 12mm thicknesses using SMAW process. X-ray diffraction method was used for residual stress measurements. The peak temperature attained at different points during deposition of weld beads in stainless steel and low carbon steel weld pads are compared. Changes in the tensile stress with the deposition of weld beads, and the relation between the peak temperatures and residual stresses in the weld pads has been discussed. It is observed that peak temperatures in stainless steel weld pads (closer to weld fusion line) are higher than those in low carbon steel weld pads at lower heat input due to the lower thermal conductivity of stainless steel. With the number of passes, the peak tensile residual stress gradually reduces in magnitude on the root side, and gradually increases in magnitude on the top side of the weld pads. The distribution of residual stress increases with the increase in the plate thickness of the weld pad. This increase is more pronounced in low carbon steel weld pads. For any specified peak temperature at the middle plane of the weld pad, the residual stress in the low carbon steel weld pad has been found to be higher than the residual stress in the stainless steel weld pad of the same thickness.

Jang et al [2001] studied the effects of root opening on mechanical properties, deformation and residual stress of weldments. Tensile, bend, impact and hardness tests were carried out on weld specimens having 0, 6 and 30 mm root openings. It was reported that the tensile strength is approximately 534–540 MPa for the 0-mm root opening, 528–537 MPa for the 6-mm root opening and 536–547 MPa for the 30-mm root opening. There is little difference in the results, but in the case of the 30-mm root opening weld, the scatter in the tensile strength data is higher than for the other welds because of the extensive weld fusion zone and weld pool. There was no crack propagation for each specimen. The results of the bend tests were satisfactory. According to the impact tests, there was little difference in the 0 and 6mm root opening welds, but the scatter of impact values for the 30mm root opening weld was higher and non uniform. In terms of microstructure, refined regions resulting from weld heat and solidification that were not dissolved by the heat but were retained, appeared as a non uniform structure. With regard to mechanical properties, it appears there are problems in attaining toughness. The static strength such as tensile and bend strength in the 24-mm build up weld should have no problems in

manufacturing structures, such as the steel bridges. However, there may be problems in reliability of the weldment as a result of reductions in toughness because of non uniformity in the deteriorated regions of the weldment. The residual stress is distributed symmetrically, and maximum value is the same for the 0 and 6mm root opening welds. In case of the 30mm root opening weld, the equilibrium temperature is lower than the within-tolerance specimens and the distribution of the residual stress extends over a wide range asymmetrically because of the build up weld. It might be a problem in dynamic strength because most of the residual stress is biased toward the built up weld part.

2.10. Conventional Arc Welding of Thick HSLA Steels

Large amount of work has been carried out to study the welding of HSLA steels [Basak et al 1995, Cerjak et al 1999, Hafele 1994, Kanjilal et al 2007, Kanjilal et al 2006, Megudeeswaran et al 2009, Madhusudan Reddy et al 1996, Murugan et al 1994, 1995, Bhadeshia H. K. D. H. et. al 1985, Bhadeshia H. K. D. H. et. al 1993, Ghosh P. K. et. al. 1989] by using different welding processes, procedures and parameters. The studies show that HSLA steels are generally have good weldability with respect to producing weld joint free from any discontinuity defects. However, in so many of cases, the integrity and safety of the weld joints in reference to their long term fatigue and corrosion properties are questioned. Moreover, in certain cases, the post weld formability of the component has been found to be impaired [Sindo Kou 1987]. These problems to a large extent are successfully addressed by several workers [Das et al 2008(a, b), Das et al 2006, Dhooge et al 1978] on case to case basis but the solutions are yet to be found for their general applications.

2.10.1. Gas metal arc welding

In gas metal arc welding (GMAW) process a low voltage electric arc is created between a consumable filler wire and base metal, which melts both of them by arc heating as major part and resistance heating as minor part. The wire is fed at a preset speed, which governs the magnitude of welding current, through a welding torch wherein it provides electrical connections and the shielding gas. The process has two basic requirements for successful open arc operation.

1. The wire feed speed must be balanced with its melting rate to maintain constant arc length.
2. Transfer of metal from the electrode tip to weld pool should be stable.

The arc length is self-adjusted because of the constant potential (CP) characteristics of the power source. The weld metal is protected with suitable shielding gas and metal is transferred to the weld pool by desired mode of metal transfer. Welding current and heat input commonly used are of the order of 60-500A and 1-25kJ/s respectively. It is broadly used in welding of steels,

aluminium, magnesium, nickel, copper, titanium and their alloys. However, functioning of process primarily depends upon proper control of process variables, behaviour of metal transfer and thermal behaviour of weld.

2.10.1.1. Process variables and their control

Filler metal is transferred in the form of superheated molten metal droplets. The mode of metal transfer defined by size and rate of droplet transfer, primarily determine the stability of the process [Liu and Siewert 1989] which is dependent upon the process variables [Choi et al 1998, Kim and Eagar 1993(a)]. These have considerable influence on the behaviour of the weld pool [Johnson et al 1989], which in turn affects the properties of weld through influence on penetration, solidification mechanism, heat flow and rate of metal deposition.

Welding current

Welding current plays primary role in deciding the mode of metal transfer. At a comparatively lower value of it, drops are relatively larger than the filler wire diameter and assume classic pendent drop shapes, determined by surface tension and gravitational forces. With the increase in welding current, size of droplets reduces but frequency of transfer increases and a situation comes when the end of the wire electrode becomes tapered and drop becomes relatively smaller than the diameter of the filler wire. At still higher value of current, a short column of molten metal streams off at the end of the electrode tip and small drops are formed as a result of breaking of this column and at a very high value of current, asymmetric magnetic force becomes significant compared to the inertial force in the streaming column of the metal and the column spirals about the electrode axis [Lancaster 1984].

Arc voltage

Arc voltage primarily governs the arc length and affects the size and shape of the fusion zone. When the arc length is too short, electrode may touch or short circuit the weld pool resulting in low base metal melting, narrow weld deposit and variation in heat input and hence enhances the possibility of forming the weld defects. Long arc length causes a flat and shallow deposit, allows the arc to wander, increases spattering and may also cause porosity in weld deposit due to air aspiration in the shielding gas [jacket et al 1995]. Hence, it is important to select the proper arc voltage / arc length to obtain control of weld pool resulting in governing of properties of the weld. The use of long arc length increases the arc plasma perimeter resulting in a wider weld pool, reduces the heat concentration directly below the welding electrode and makes the weld pool response to weave very sluggish [Matthews et al 1992]. Shorter arc length improves wetting characteristics and weld pool control.

Electrode Extension

It has been observed that an increase of electrode extension reduces transition current i.e. it dominates the transition current region of the filler wire [Lancaster 1984]. It depends on the contact tube to work distance (CTWD), and affects the mode of metal transfer by changing the extent of ohmic heating. It has been revealed that at a given arc voltage, wire feed rate should be increased with the increase in CTWD [Heald et al 1994]. Electrode extension governs the arc length [Quinn et al 1994]. Longer extension results in enhanced resistive heating and consequently reduces the balance of energy available to melt the filler wire and base metal, which may result in lack of fusion [Quintino and Allum 1984, Stenbacka and Person 1989]. It may also reduce the stability of metal and may increase the risk of porosity in weld metal [Stenbacka and Person 1989].

It has been established that in the operating range of process variables (5-10 mm arc length, 10-20 mm electrode extension, 5-20% CO₂ mixture in argon shielding) the specific burn off rate of 1-1.2 mm diameter filler wire and V-I relationship (Fig. 2.15) is linear. Consequently, the generalized burn off relationship in that range of parameters may be represented by linear control equations and can be applied for synergic control [Amin and Ahmed 1987]. Burn off rate is directly proportional to the electrode extension and resistivity of filler wire [Amin and Ahmed 1987].

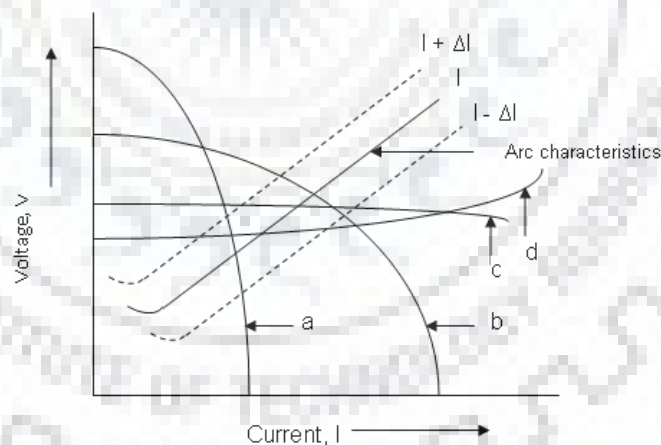


Figure 2-10 Static volt-ampere characteristics of power source.

Shielding gas govern the stability of arc, mode of metal transfer, bead appearance, spatters generation and transition current of filler wire [Ghosh et al 2009 (b)]. Shielding gases commonly used in the process are argon (Ar), helium (He), carbon dioxide (CO₂) and their mixtures. Selection of proper shielding gas to be used primarily depends on the filler wire material and required mode of metal transfer. Gas flow rate plays an important role in deciding the properties of the weld and therefore, flow measurement techniques [Stenbacka and Person 1989] may be

employed to know the actual flow rate of the shielding gas. For obtaining the spray transfer, argon based shielding gases such as argon with 1 – 5 % of O₂ or with 5 – 25 % of CO₂ is generally required. It is a common practice in welding of steels to add CO₂ or O₂ to an inert gas, such as, Ar, for use as shielding gas because oxygen atoms promote the electron emission level in ferrous alloys, which stabilize the arc and regulate metal transfer, even on electrode negative polarity [Shinoda et al 1987]. However, such a oxygen bearing shielding gases cannot be used for welding of aluminium, as the production of refractory oxides inhibit proper metal transfer and deposition. However, chlorine may be used as an oxidising gas as an addition to the argon shielding for welding of aluminium by this process [Lucas 1992 (a, b), Suban and Tusek 2001, Subramaniam et al 1998]. For aluminium welding shielding gas serves three functions.

- It provides plasma for commutation of current.
- Protects the weld pool and filler wire tip from reacting with the air environment.
- Provides the cleaning action, which partially removes the oxide layer from the aluminium plate.

Studies were carried out to select the shielding gas for welding of aluminium using different gases and their mixtures and found that desirable weld geometry with maximum penetration can be obtained with pure argon shielding [Lucas 1992 (a, b), Suban and Tusek 2001, Subramaniam et al 1998].

2.10.1.2. Thermal behaviour of weld

Wire melting characteristics

The wire burn off rate/melting rate for P-GMAW is expressed [Craig 1987, Smati 1986] as

$$V_{w(pc)} = \int_0^{t_{pul}} V_w t_{pul} dt_{pul} \quad (2.19)$$

For a square pulsed current waveform it gives

$$V_{w(pc)} = (V_{wp} t_p + V_{wb} t_b) t_{pul}^{-1} \quad (2.20)$$

Where, $V_{w(pc)}$ is wire burn off rate and V_{wp} and V_{wb} are wire burn off rates during t_p and t_b respectively.

The V_{wp} and V_{wb} may be expressed as

$$V_{wp} = A.I_p + B.E_w.I_p^2 \quad (2.21)$$

$$V_{wb} = A.I_b + B.E_w.I_b^2 \quad (2.22)$$

Therefore, Eq.(2.20) may be rewritten as

$$V_{w(pc)} = \left[\frac{(A.I_p + B.E_w.I_p^2)t_p + (A.I_b + B.E_w.I_b^2)t_b}{t_{pul}} \right] \quad (2.23)$$

Eq.(2.23) may be rewritten as

$$V_{w(pc)} = \left[\frac{A(I_p t_p + I_b t_b) + BE_w (I_p^2 t_p + I_b^2 t_b)}{t_{pul}} \right] \quad (2.24)$$

Using $I_m = [(I_p t_p + I_b t_b)/t]$ in eq. (2.24)

$$V_{w(pc)} = AI_m + BE_w (I_p^2 t_p + I_b^2 t_b) t_{pul}^{-1} \quad (2.25)$$

As $I_p^2 t_p \ll I_b^2 t_b$ neglecting ohmic heating during base current period, Eq. (2.25) reduces to

$$V_{w(pc)} = AI_m + BE_w I_p^2 t_p t_{pul}^{-1} \quad (2.26)$$

Considering $f = 1/t_{pul}$ and $I_p^2 t_p = D_n$ Eq.(2.26) gives

$$V_{w(pc)} = AI_m + BE_w D_n f \quad (2.27)$$

By considering $V_d = A_w V_w / f$ in Eq.(2.27) a linear relationship has been obtained as follows,

$$\frac{f}{I_m} = \frac{AA_w}{V_d - BDA_w E_w} \quad (2.28)$$

Solving eq.(2.28) for droplet volume V_d ,

$$V_d = AA_w \left(\frac{I_m}{f} \right) + A_w E_w BD \quad (2.29)$$

Eq.(2.29) shows that for any wire feed rate, by fixing (I_m/f) , the droplet size can be held constant for a given wire diameter, electrode extension and detachment parameter.

It has been observed that for 1.2 mm diameter steel filler wire [Quintino and Alum 1984] for a desired combination of peak current and its duration, giving one drop per pulse, the base current and its duration may be evaluated using frequency value of 50Hz for 100A mean current. It gives satisfactory droplet transfer as well as volume of droplet remains insensitive to I_m . It can be expressed as

$$I_m/f = 2 \quad (2.30)$$

By combining Eqs.(2.27) and (2.30)

$$V_{w(pc)} = AI_m + \frac{BE_w D I_m}{2} = I_m \left(A + \frac{BE_w D}{2} \right) = \bar{A} I_m \quad (2.31)$$

Where, $\bar{A} = \left(A + \frac{BE_w D}{2} \right)$ is modified burn off factor

In P-GMAW process, by considering ohmic heating during base current duration, Eq. (2.29) reduces to

$$V_{w(pc)} = AI_m + BE_w I_{eff}^2 \quad (2.32)$$

Where, $I_{eff}^2 = \{k_p I_p^2 + (1-k_p)I_b^2\}^{1/2}$ and k_p is pulse duty cycle defined as t_p/t_{pul}

I_{eff} may also be expressed as,

$$I_{eff}^2 = I_m^2 + k_p(1-k_p)I_e^2 \quad (2.33)$$

By combining Eqs. (2.32) and (2.33),

$$V_{w(pc)} = AI_m + BE_w(I_m^2 + k_p(1-k_p)I_e^2) \quad (2.34)$$

In consideration of Eq.(2.5), Eq. (2.37) may be expressed as

$$V_{w(pc)} = V_{w(cc)equiv.} + BE_w k_p(1-k_p)I_e^2 \quad (2.35)$$

Eq. (2.37) reveals the following aspects of P-GMAW [Alum 1983].

Total heat transferred to weld pool

The heat transferred to weld pool (Q_T) of GMAW was estimated in consideration of the total heat, Q_T , transferred to the weld pool as a function of arc heat transferred to the weld pool (Q_{AW} , Js^{-1}), heat of the filler metal transferred to the weld pool (Q_f , Js^{-1}) and welding speed (S) as follows [Ghosh et al 2006, Goyal et al 2008 (b)].

$$Q_T = Q/S \quad (2.36)$$

$$\text{Where, } Q = Q_{AW} + Q_f \quad (2.37)$$

Q_{AW} may be estimated as (Js^{-1})

$$Q_{AW} = (V I_{eff} - \psi I_{eff}) \eta_a \quad (2.38)$$

Where, V and I_{eff} are the arc voltage and effective current (root mean square value of the pulsed current wave form) respectively and ψ is the effective melting potential [Lancaster 1984] at anode. The I_{eff} is estimated by the following expression [Praveen et al 2005].

$$I_{eff} = \sqrt{[k_p \cdot I_p^2 + (1 - k_p) \cdot I_b^2]} \quad (2.39)$$

$$\text{Where, the pulse duty cycle, } k_p = \frac{t_p}{t_{pul}} \quad (2.40)$$

Q_f may be estimated as

$$Q_f = Q_{de} m_t f \quad (2.41)$$

Where, m_t is mass of filler wire transferred per pulse (kg), Q_{de} is heat content per unit mass of the filler wire (Jkg^{-1}) at the time of deposition, f is pulse frequency (Hz) and m_t is estimated as

$$m_t = \frac{A_w \cdot V_w \cdot \rho_w}{f} \quad (2.42)$$

Where, A_w is the cross sectional area of the filler wire, V_w is wire feed rate (ms^{-1}) and ρ_w is density of the solid filler wire (kgm^{-3}). The Q_{de} is estimated as follows.

$$Q_{de} = Q_i - Q_{tl} \quad (2.43)$$

Where, Q_i is heat content per unit mass of the filler wire (Jkg^{-1}) at the time of detachment and Q_{tl} is total heat loss (Jkg^{-1}) during flight of droplet. They may be estimated as follows

$$Q_i = [c_{p(s)}(T_m - T_a) + L + c_{p(l)}(T_i - T_m)] \quad (2.44)$$

$$Q_{tl} = Q_{cv} + Q_R \quad (2.45)$$

Where, $c_{p(s)}$ is specific heat of solid filler metal ($\text{Jkg}^{-1}\text{k}^{-1}$), $c_{p(l)}$ is specific heat of liquid filler metal ($\text{Jkg}^{-1}\text{k}^{-1}$), T_m is melting temperature (K), T_a is ambient temperature (K), T_i is temperature of droplet at the time of detachment (K) and L is latent heat of fusion (Jkg^{-1}).

The Q_{cv} is heat loss during flight of the droplets due to convection (Jkg^{-1}) and Q_R as heat loss during flight of the droplets due to radiation (Jkg^{-1}) are expressed as follows.

$$Q_{cv} = \frac{[\alpha_h \cdot (T_i - T_a) \cdot A_s \cdot \tau]}{m_t} \quad (2.46)$$

$$Q_R = \frac{\varepsilon \cdot \sigma \cdot T_i^4 \cdot A_s \cdot \tau}{m_t} \quad (2.47)$$

Here, α_h is heat transfer coefficient of droplets in flight, ε is emissivity, σ is the Stefan-Boltzmann constant, τ is flight time of the droplet and A_s and m_t are total surface area of the droplets and mass of the filler wire transferred per pulse respectively. The A_s can be estimated as

$$A_s = \pi D^2 N_d \quad (2.48)$$

Where, D and N_d are diameter of the droplet and number of droplets transferred per pulse respectively. The D can be estimated by considering the electrode tapering coefficient under the concept of energy balance in detachment dynamics [Ghosh et al 2006, Goyal et al 2008 (b)].

Accordingly the molten metal transferred per pulse in number of droplets, N_d , can be derived as

$$D = 4r / (1 + 3\theta / 16) \quad (2.49)$$

$$\theta = \mu_o I_p^2 / (\gamma \pi^2 r) \quad (2.50)$$

$$N_d = 6m_t / (\pi D^3 \rho_d) \quad (2.51)$$

Where, the effective radius (r) of tapering of electrode is considered [Ghosh et al 2009 (a)] as 0.8 ± 0.2 mm. The coefficient of surface tension (γ), density of molten filler metal and the permeability of free space (μ_o) are considered as 1.2 Nm^{-1} , 7.85 g cm^{-3} and $4\pi \times 10^{-7} \text{ NA}^{-2}$ respectively.

Estimation of weld pool temperature

It is assumed that during pulsed current GMA welding (P-GMAW) process, the metal transfer primarily takes place at peak current (I_p) so the heat content of filler metal is largely governed by it. During welding the heat transfer to the weld pool is primarily attributed to the initial arc heating (Q_{AW}) followed by the deposition of superheated filler metal (Q_f). Accordingly two heat sources of different nature act simultaneously in the P-GMAW process. One is continuous heat source (arc heat source) of double ellipsoidal [Robert W. Messler, Jr., 1999, ASM Handbook 1994] nature acting at the surface of the base plate, which melts the base plate and produces an initial weld pool in the base metal. The other one is an interrupted heat source supplying superheated filler metal, as considered in the nature of a point heat source which dictates the size and geometry of the initial weld pool developed by the arc heating. Due to impact of the transferring droplets a cavity is formed in the weld pool, where droplets transfer their heat in the weld pool. Therefore, it may be assumed that point heat source of the superheated filler metal is acting at depth, h , of the cavity. Thus the temperature at any point in the weld fusion zone may be estimated by superimposing the analytical solution of the distributed heat source on that of the point heat source. The expressions for the temperature, T , at any point ($x(\xi)$, y , z) in the weld fusion zone at a distance R with respect to central axis of the welding arc using combined heat source technique can be expressed as

$$T = \frac{Q_f}{2\pi.k} e^{-\lambda.v.\xi} \left[\frac{e^{-\lambda.v.R}}{R} + \sum_{n=1}^{\infty} \left(\frac{e^{-\lambda.v.R_n}}{R_n} + \frac{e^{-\lambda.v.R'_n}}{R'_n} \right) \right] + T_d \quad (2.52)$$

$$\text{Where } R, R_n \text{ and } R'_n \text{ are } R = \sqrt{\xi^2 + y^2 + (z-h)^2} \quad (2.53)$$

$$R_n = \sqrt{(2.n.d - (z-h))^2 + \xi^2 + y^2} \quad (2.54)$$

$$R'_n = \sqrt{(2.n.d + (z-h))^2 + \xi^2 + y^2} \quad (2.55)$$

Q_f is the heat transferred to the weld pool by the droplets of super heated filler metal and T_d is the temperature of the point ($x(\xi)$, y , z) due to arc heating using the distributed heat source expressed as follows:

$$T_d = \frac{3\sqrt{3}.Q_{AW}}{\rho.c.\pi\sqrt{\pi}} \int_0^t \left[\frac{\frac{dt'}{\sqrt{(12a(t-t') + a_h^2)} \cdot \sqrt{(12a(t-t') + b_h^2)}}}{\left(\frac{A'}{\sqrt{(12a(t-t') + c_{hf}^2)}} + \frac{B'}{\sqrt{(12a(t-t') + c_{hb}^2)}} \right)} \right] + T_0 \quad (2.56)$$

Where, Q_{AW} is the arc heat transferred to the weld pool.

2.10.1.3. Concept Of Summarized Influence Of Pulse Parameters

The advantages of P-GMAW over GMAW in improving the characteristics of weld and properties of various ferrous and non-ferrous metals, under different conditions of pulsation have been reported by many investigators [Ghosh et al 1994, Ghosh 1999, Ghosh et al 2000, Ghosh et al 2001 and Ghosh et al 2007 (a, b), Kulkarni 2008, Devakumaran 2009]. However, the wide acceptance of the process in fabrication is largely handicapped due to the criticality in the selection of pulse parameters. It is well established [Ghosh et al 1994, Ghosh 1999, Ghosh et al 2000, Ghosh et al 2001 and Ghosh et al 2007 (a, b)] that the variations in pulse parameters identified as I_m , I_p , I_b , t_p , and f influence the weld characteristics to a great extent. It has been realized that a change in any one parameter affects the others also under the concept of energy balance. The variation in pulse parameter significantly influences the thermal behaviour and nature of metal transfer affecting the characteristics of weldment. Under these circumstances, the control of weld characteristics within a desired range is possible only by establishing a correlation amongst pulse parameters. It was also suggested [Ghosh et al 1994, Ghosh 1999, Ghosh et al 2000, Ghosh et al 2001 and Ghosh et al 2007 (a, b)] that consideration of summarized influence of pulse parameters instead of individual one may be useful to study the different characteristics of the weldment. A summarized influence of pulse parameters has been proposed by Ghosh [Ghosh et al 1994, Ghosh 1999, Ghosh et al 2000, Ghosh et al 2001 and Ghosh et al 2007 (a, b)],

defined by a factor, $\left[\phi = \left(\frac{I_b f t_b}{I_p} \right) \right]$, where t_b is defined by $t_b = \frac{1}{f} - t_p$ and a good potentiality of

the factor ϕ to analyse various basic characteristics of weld deposit. Many investigators have justified the applicability of ϕ in different conditions of pulsation by studying its effect on different weld characteristics using ferrous and non-ferrous materials.

2.11. Narrow Gap Arc Welding of Thick HSLA Steels

The developments of narrow gap welding (NGW) is aimed to reduce required amount of weld metal in thick section welding, thereby reducing cost of welding, time and residual stresses. The main welding process associated with NGW are shielded metal arc welding, gas tungsten arc welding, submerged arc welding and gas metal arc welding. The major problems in NGW technique are formation of defects such as lack of side wall fusion, undercutting and centre line cracking as a result of minor variation in welding conditions. NGW can be separated into two group based on electrode feeding technique used to ensure side wall penetration. The first group achieve side wall penetration through electrode/arc manipulation, including directing fixed electrode towards the side wall, oscillating or rotating the arc. The second group attempt to

control sidewall penetration through manipulation of welding parameters. Some advantages attributed to narrow gap welding processes when compared with conventional welding processes in thick sections are

- Reduction in welding time
- Lower consumable costs
- Reduction in slag removal time
- Reduction in preparation cost
- Improved toughness
- Reduction in residual stresses

2.12. Gas metal arc welding

GMAW is one of the commonly used processes with narrow gap welding technique due to the easily observable arc, relatively narrow groove, high welding quality, productivity and cost effectiveness. However, NGW with GMAW are relatively prone to defects formation of lack of fusion in side walls, spattering and shielding gas deficiencies. Pores formation due to improper gas shielding and magnetic arc blow is frequent problems associated with NGW using GMAW. These problems which are associated with difficulty in feeding the electrodes and supplying a proper shielding gas coverage into a very narrow and deep groove and in obtaining well balanced arc heating between the side wall and the bottom of the joint has been major hindrance to greater acceptance of NGW using GMAW process. In order to overcome these limitations, several wire deposition approaches have been tried out such as pre casting the wire and depositing alternating stringer beads, oscillating wire inside groove, rotating alternately a bent contact tip about its axis inside the groove, plastically deforming wire into some wavy shape before its entrance in the contact tube in order to oscillate the arc across the groove, rotating the arc by feeding the wire through an eccentric contact tube that rotates and rotating the arc by using special twist electrode wire. Some of wire deposition approaches used in industrial applications have been shown in Fig. (2.16-2.22).

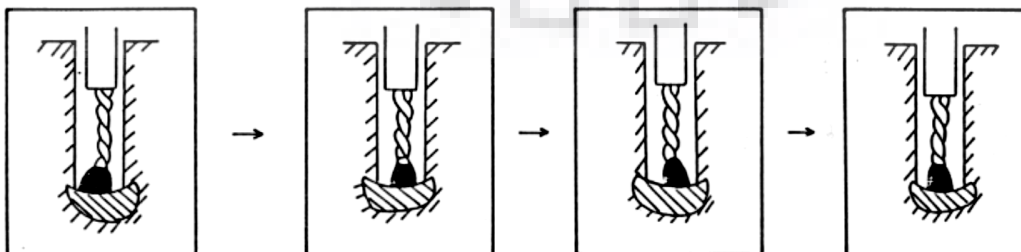


Figure 2-11 Rotational movement of welding arc produced by twist-arc [Okuda et al 1986].

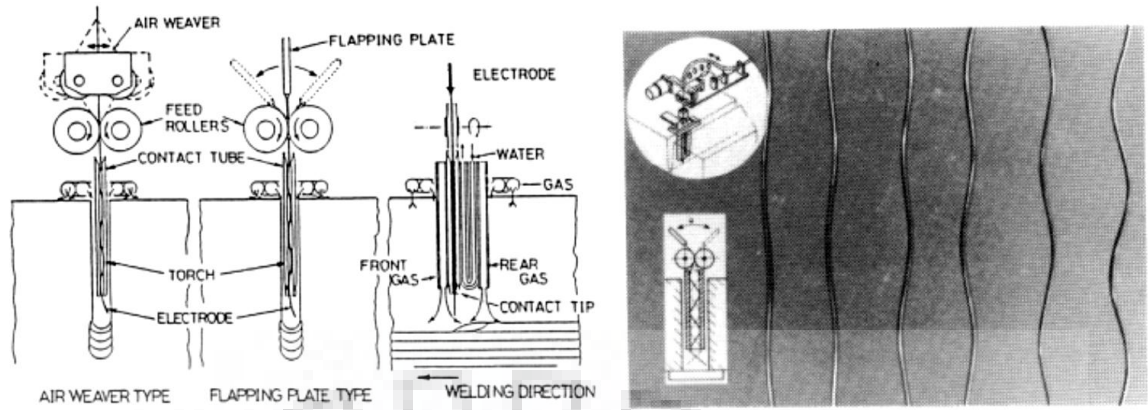


Figure 2-12 Wire waving mechanism (left) and the waved wires (right) [Kwahara et al 1986]

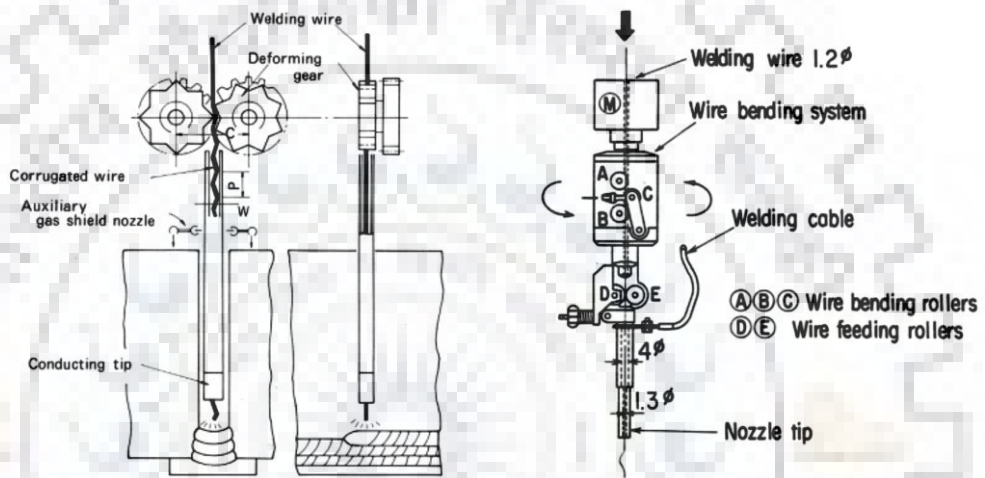


Figure 2-13 Corrugated wire and rotating arc [Nakajima et al, 1986]

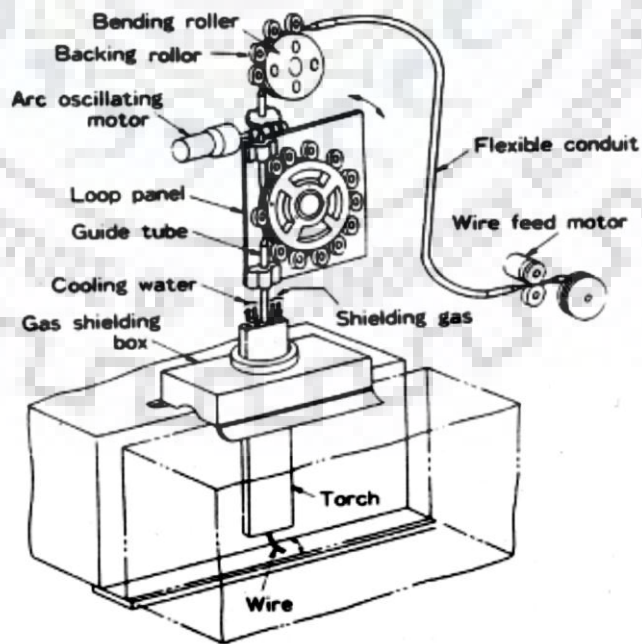


Figure 2-14 Loop nap method mechanism [Kanbe Y et al, 1986]

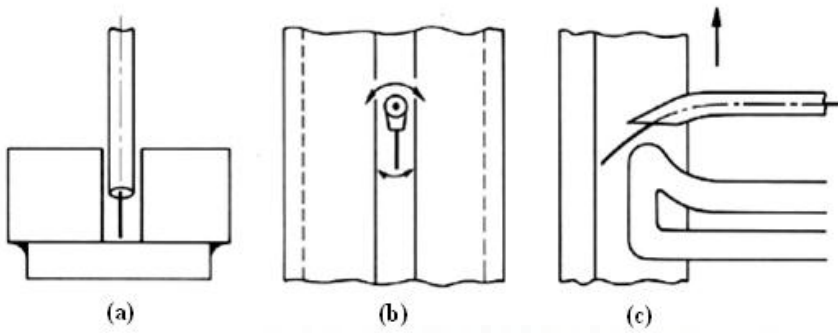


Figure 2-15 Bent contact-tip: (a) end view, (b) top view, (c) side view including copper bend weld pool support [Halmoy E, 1983]

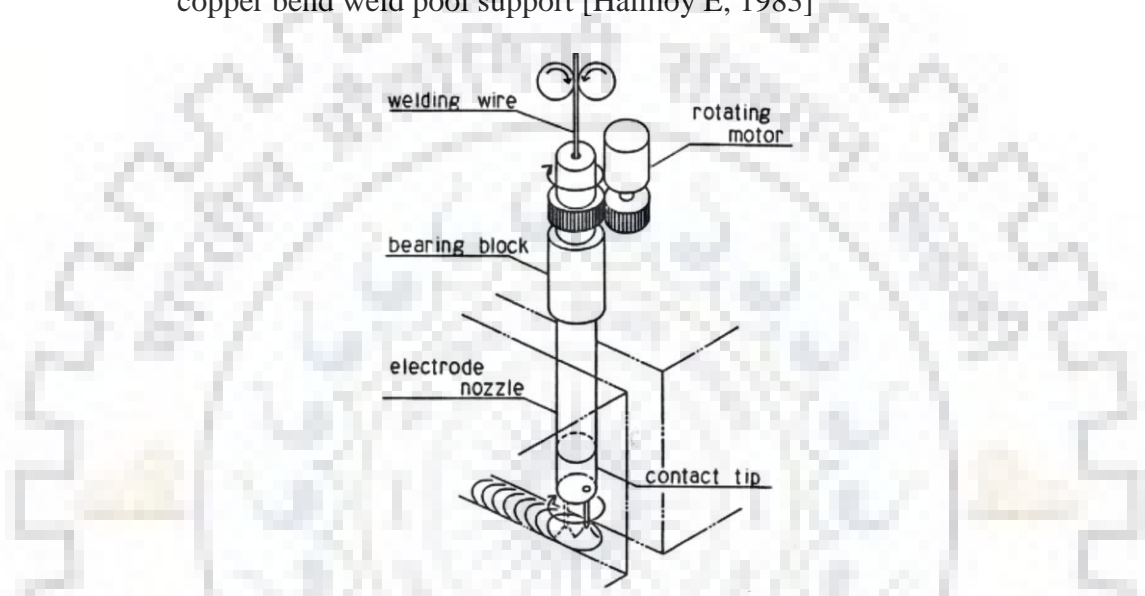


Figure 2-16 High speed rotating arc principle [Nomura H, 1984]

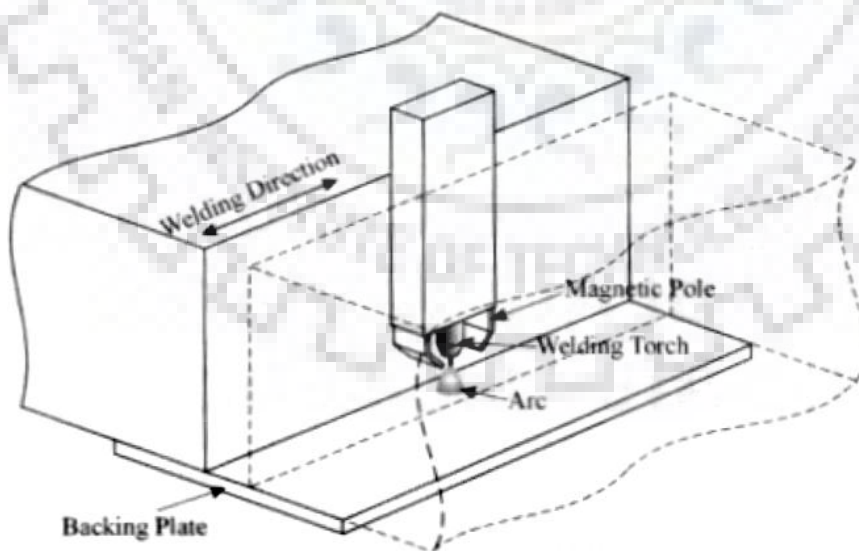


Figure 2-17 Electromagnetic arc oscillation [Kang Y H et al, 2003]

Basic disadvantage of GMAW process is its comparatively larger torch nozzle which does not provide the required manipulation in the weld groove. Another major difficulty in GMAW-NG is to ensure effective shielding gas coverage for the arc and weld pool inside the gap. The geometric configuration of the joint can promote air being entrained by the shielding gas column inside the groove while the relatively long distance that sometimes separates the gas nozzles from the arc, renders the process very sensitive to draughts. As a result, porosity can be formed. Narrow gap welding by using GMAW process is generally carried out in spray transfer mode as explained earlier in the section 2.3. Thus the considerably higher heat input employed further deteriorates the properties of the weld joint.

2.12.1. Pulsed current gas metal arc welding

The problem of side wall fusion in thick section through careful control of selection of welding parameters has been tried out by using MPMSPL pulsed current GMAW welding process (Lebedev, 1977, Kulkarni, 2008, Devkumar, 2009). However, the use of pulse current generates the complexity in selection of welding parameters due to simultaneously interaction among them. But, the required angle of attack which should be provided to get the side wall fusion restricts the side wall to come closer. This problem has not been addressed by the researcher which can be overcome by depositing the superheated molten filler metal deep inside narrow weld groove centrally without providing any angle of attack with the side wall. With proper control of pulse parameters, P-GMAW has numerous advantages over the conventional GMAW process [Praveen et al 2005, Collard 1988, Craig 1987a and b]. Hence from the literature it appears that, if a suitable cooling system for narrow torch nozzle is developed with proper control of P-GMAW process parameters, the characteristics of the weld joint can be suitably improved by employing MPSSPL narrow gap welding procedure.

2.13. Characteristics of Weld

2.13.1. Weld geometry

Bead geometry is influenced by pulse parameters of P-GMA welding.

(a) Penetration

Influence of pulse parameters on bead geometry during GMA welding of Al-alloys has revealed that increase in mean current and pulse duration enhances the super heating of the molten filler metal and consequently its fluidity, which results in an increased penetration [Ghosh et al 1989, Ghosh and Rai 1996, Ghosh et al 1998]. At given welding parameter, in general, the penetration is inversely proportional to the welding speed and the electrode diameter. The reduced time of arc force acting on the metal surface results in less penetration with increase of

speed. A finger type penetration observed during spray transfer is directly related to the momentum of individual droplet impinging on the base metal. The weld penetration decreases non-linearly with an increase in electrode diameter, due to reduction in current density [Davies 1983].

(b) Bead height and width

Weld bead height is directly proportional to the welding current and inversely proportional to the arc voltage and electrode diameter. At a given mean current, an increase in pulse duration reduces the bead height due to increase in fluidity [Ghosh et al 1998]. Bead width is directly proportional to the arc voltage and electrode diameter, which affects the area of distribution of arc force and is indirectly proportional to the welding speed [Robert W. Messler, Jr., 1999].

(c) Bead area

The area of the weld bead is directly proportional to the welding current and arc voltage [Robert W. Messler, Jr., 1999] because of their significant influence on wire melting. It increases with the voltage and is inversely proportional to the welding speed and electrode diameter due to reduction in deposition per unit area [Davies 1983]. Qualitative approach to understand the effect of welding variables on bead geometry does not lead to prediction of bead dimensions effectively [Davies 1983]. Even for GTAW, where filler metal is not used, pool size and shape are found to be dependent on convection driven by arc forces [Lancaster 1984].

(d) Porosity

In case of GMAW, an increase in welding current reduces the flight time of molten droplet in the arc cavern which reduces the absorption of gases and consequently the porosity contents of weld deposit [Ghosh et al 2000, Ghosh et al 2007 (a), Ghosh et al 2008], whereas, in case of P-GMAW, variation in arc pressure, which is primarily governed by the ratio of peak current to base current, leads to formation of vortex in inert jacket resulting in the air aspiration into shielding atmosphere causing enhancement of porosity content in the weld metal [Ghosh et al 1991(b)]. In this process variation in pulse parameters affects the porosity content of the weld [Ghosh et al 1990 (a)].

In P-GMAW of aluminium alloy it was observed [Ghosh et al 1990 (b)] that, at any given mean current and pulse frequency; increase in pulse duration reduces the porosity content of weld metal. During deposition at a given pulse frequency and duration, the increase in mean current tends to lower the porosity content of weld metal and similarly at any given mean current and pulse duration, the increase in pulse frequency also reduces the porosity content of weld metal. During pulse current deposition, by keeping the mean current similar to the welding current of

continuous current deposition, the porosity content of weld metal has been found to be comparatively lower in pulsed current deposition [Ghosh et al 1990 (b)].

2.13.2 Microstructure

During P-GMA welding of Al alloy, microstructure of weld metal has been found to be refined under the influence of characteristics of metal transfer and thermal behaviour of weld metal at the time of deposition, governed by pulse parameters [Ghosh et al 1999]. It has been observed that it refines the microstructure by controlling the inward growing columnar grains into smaller equiaxed grains. A detailed microscopic study of the welds has suggested that suitable nuclei for equiaxed solidification would be stable only after the pulse duration because of considerable superheat in the weld pool. Thus, high frequency pulsing is supposed to be more effective, but this may limit the thermal inertia effect at higher pulse frequencies [Praveen et al 2005]. During stainless steel cladding [Ghosh et al 1998], it has been revealed that, at a given f and t_p , increase in I_m comparatively coarsen the microstructure of the overlay. It has also been observed that, at comparatively higher I_m of 200A and given f , increase in t_p also coarsen the microstructure due to enhancement of superheating of the droplet [Ghosh et al 1999]. During welding of aluminium alloy, at high frequency of the order of 100 Hz, microstructure tends to be coarsened as heat flow characteristics approaches to GMAW [Robert W. Messler, Jr., 1999]. An analytical model of thermal behaviour of P-GMAW [Goyal et al 2008 (b), Goyal 2007] by considering the heat losses of the droplet during flight and pulse off period temperature gradient of weld metal at the time of deposition and at the end of the pulse off period has been estimated which may affect the microstructure of weld and HAZ [Goyal et al 2008 (a)].

It has been reported [Goyal et al 2007] that microstructure of the HAZ of pulsed current GMA weld of aluminium alloy has finer grains than those of continuous current GMA weld primarily due to intermittent heat flow leading to lowering of peak temperature of HAZ. In the pulse current welding of Al-Zn-Mg alloy the extent of re-crystallization of HAZ was found to be significantly lower than that of continuous current welding at same welding current, which may be considered as a beneficial effect of P-GMAW.

2.14. Modelling of Weld

Rosenthal et al, 1946 has used the Fourier partial differential equation of heat conduction and introduced the moving coordinate system to develop solutions for the point and line heat sources and applied it successfully to address a wide range of welding problems. In his solutions, quasi steady state condition (an observer stationed at the point heat source fails to notice any change in the temperature around him as the source moves on) was assumed which can also be

justified experimentally for a long weld. Starting from the partial differential equation of heat conduction, expressed in rectangular coordinates (x,y,z) w.r.t. a fixed origin in the solid, he applied it successfully for welding by considering a moving coordinate system. It is well known that Rosenthal's solutions are valid at locations away from the heat source but are subjected to considerable error at or near the heat source due to assumption of a point or line heat source.

Wells et al, 1952, considered a two-dimensional moving rectangular heat source with a uniform distribution of heat intensity. He proposed the estimation of heat input and welding speed by examining the finished weld. Paley et al, 1975, investigated the heat flow in welding thick steel plates by considering the effects of boundary surfaces (bottom or edge of the plate) assuming them adiabatic based on the Rosenthal's solution for point heat source. Christensen et al, [1965], developed generalized plots of temperature distribution in dimensionless form at surface as well as at different depths of any substrate, which was found useful for estimation of HAZ, cooling rate and residence time between two temperatures. Pavelic et al [1969] developed a finite difference method to determine the temperature distribution in a 2-D plate using line heat source. By using melting temperature isotherms as a boundary condition, the shape of the weld pool was correlated with the welding variables. In this method experimental work is required to determine the boundary conditions. The details of the weld pool shape could not be correlated using line source theory therefore distributed heat source with Gaussian distribution of heat flux (W/m^2) was suggested. Friedman [1975] developed a thermo mechanical analysis of welding process using FEM. The model enables calculation of temperatures, stresses, and distortions resulting from the welding process. Friedman and Glickstein [1976] developed FEM analysis for transient heat conduction to investigate the effect of various welding parameters such as heat input and its duration from the arc and its distribution at the surface of the weldments on the thermal response characteristics, in particular the weld bead shape and the depth of penetration. Tsai et al [1992] developed a semi empirical 2-D finite element heat transfer model that treats the melting interface as an inner boundary to calculate the quasi steady state temperature field and cooling rate in HAZ. Eager and Tsai [1983] modified the Rosenthal's model considering a 2-D Gaussian distributed heat source after assuming (i) no convective or radiative heat flow, (ii) constant average thermal properties, and (iii) a quasi steady state semi-infinite medium. They also developed its solution for the temperature of a semi-infinite body using a constant distribution parameter and obtained results were compared with their experimental values on various metals. Goldak et al [1984] developed a mathematical model based on a Gaussian distribution of the power density and proposed a three-dimensional double ellipsoidal moving heat source. Finite element modelling was used to calculate the temperature field for bead on

plate study and found that the use of 3-D heat source can predict the temperature of the weld joints with much deeper penetration compared to the 2-D model. The computed results of temperature distributions for submerged arc welds in thick work pieces were compared with the experimental values of Christensen et al [1965]. Tekriwal and Mazumder [1988,1986] developed a 3-D transient heat conduction model for arc welding using FEM analysis and compared the predicted size of the weld pool and HAZ with the experimental results and found good agreement. Na and Lee [1987] conducted 3-D finite element analysis of the transient temperature distribution in GTA welding by introduced a solution domain which moves along with the welding heat source and it was verified with the experiments on medium carbon steel under various welding conditions. Boo and Cho [1990] developed an analytical solution of 3-D heat conduction equation with convective boundary conditions at welding surface to predict the transient temperature distribution in a finite thick plate. The results were compared with the experimental values of GTA bead on plate weld on medium carbon steel. Vishnu Ravi et al [1991] developed an analytical model of heat flow during pulsed current GTAW considering Gaussian distributed heat source and the results were compared with mild steel weld. The investigation shows that pulsed current welding refines the grain structure of the weld metal. Kumar Subodh et. al, [1992] developed three dimensional finite element modelling of gas metal arc welding. He has considered volumetric distribution of heat content of transferring droplets. The model is validated by predicting weld bead dimensions and comparing them with experimental data. Ghosh et al [1993, 2006, 1999] developed a model to predict the thermal and metal transfer behaviour during P-GMAW process and validated the model considering a summarized influence of pulse parameter factor ϕ . Prasad Silva and Sankara Narayanan [1996] developed a technique involving finite element analysis of temperature distribution during arc welding by using a transient adaptive grid technique. It gives a finer mesh around the arc source, where the temperature gradients are high, and a coarser mesh in other places to increase computational efficiency of the analysis. Nguyen et al [1999], Nguyen et al [2004] developed the analytical solutions for transient temperature field of a semi-infinite body subjected to a double ellipsoidal power density moving heat source with conduction only. The results were compared with the bead on plate deposition on HT-780 plates using GMA welding. The model failed to predict the shape of the weld pool in the transversal cross section. Pathak and Datta [2000] presented a three-dimensional transient finite element analysis of heat flow in arc welding using Gaussian distributed heat source and the results were compared with the published values. It was found that arc length significantly affects the temperature of weld pool and adjacent base metal. Komanduri and Hou [2000] developed an analytical solution for the temperature rise distribution in short work pieces in arc welding

considering the arc beam as a moving plane (disc) heat source with a pseudo-Gaussian distribution of heat intensity. Christensen et al has proposed a neural network approach [2003] for GMA butt joint welding. Fanous Ishab F. Z. et. al. [2003] have done 3D finite element modelling of welding process using element birth and element movement techniques. Mahaptra M. M. et. al., [2006] developed 3D finite element analysis to predict the effect of shielded metal arc welding process parameters on temperature distribution, angular distortion and weldment zones in but and one sided fillet welds. The predicted temperature distributions in butt bead on plate and one sided fillet weld under various conditions of welding are compared with experimental results and found to be in good agreement. Bag S. and De A. [2008] have developed a finite element based 3 dimensional quasi steady heat transfer model to compute temperature field in gas tungsten arc welding process. The welding heat has been considered as volumetric heat source. The model is validated with experimentally measured weld dimensions. Goyal V. K. et. al [2008] has developed analytical solution to find the temperature distribution in weld pool for pulse current gas metal arc welding considering two types of heat source acting simultaneously. Arc heat source has been considered as double ellipsoidal while transfer of heat by super heated metal droplets as point heat source. The results are validated by comparing the results of bead on plate study. The equation is unable to determine the temperature within a radius of 2mm from arc centre. Bag S. and De A. [2009] have developed efficient numerical heat transfer model coupled with genetic algorithm based optimization for prediction of process variables in GTA spot welding. Genetic algorithm identifies suitable value of process variable for a target weld dimensions.

2.15. Formulation Of The Problem

2.15.1. Motivation for the Present Study

A fairly large number of publications are available on the joining of dissimilar metals such as austenitic stainless steel (ASS) to low alloy steel by arc welding process. But, a review of literatures shows that majority of the studies are primarily focused on microstructure and tensile properties of the joints. However, there is not much data available in open literature regarding other critical aspects of joint properties including the residual stresses, stress distributions and fracture sensitivity/behaviour of various regions of arc weld. A systematic study from a scientific angle is therefore desirable in these areas for effective usage of such dissimilar joint. The objectives of the project are precisely formulated in this regard.

The energy input involved in a welding process, causing melting of the filler and base metals, also develops certain reactions in a very short period of time which result some dramatic changes

in the microstructure of HAZ near to the fusion line. These changes primarily result from the relatively rapid heating and cooling of the base materials during welding. In order to control these changes, it is necessary to regulate the thermal behaviour of the welding process. This is especially important in reference to the critical durations of maximum temperature and the temperature above some critical range as well as cooling rate prevailing in the interactive locations of the materials involved with respect to diffusion of active elements, phase transformations and development of residual stress at the joint.

The use of pulsed current gas metal arc welding (P-GMAW) process can be accredited for the possibility of more precisely controlled weld isotherm and weld thermal cycle, primarily due to its merit of developing relatively lower heat build up in weld pool than the conventional GMAW process resulting from interruption in weld metal deposition under pulsed current. Moreover as the P-GMAW is also a low heat input process [Ferraresi et.al. 2003, Zhang et.al. 1998] it may reduce residual stresses and favourably affect the dilution [Ghosh et.al. 2004, Kulkarni et. al. 2005] and phase transformation [Goyal et.al. 2006] in weld joint.

Due to its several merits of lowering of thermal severity and its adverse influences the P-GMAW can also facilitate the application of narrow gap gas metal arc welding [Malin 1983] in dissimilar welding of thick sections of ASS and HSLA. However, an ultra-narrow gap P-GMAW process often produces lack of fusion in the groove wall due to low angle of attack (arc strike), low heat input and small molten weld pool. Thus, in order to produce minimum residual stresses in a defect free dissimilar weld joint with improved or comparable mechanical properties with respect to those of the base materials having widely different physical properties the design of appropriate ultra-narrow groove and selection of pulse parameters is very much important. This may be achieved by developing a clear understanding over the influence of ultra-narrow groove design and pulse parameters on amount of weld deposition, weld isotherm, weld thermal cycle and microstructure of the multipass weld being largely influenced by the solidification behaviour [Goyal et.al. 2006] of the P-GMA of dissimilar weld deposit in the joint.

It is also well established that the use of narrow groove in welding of thick sections of 25 mm may significantly reduces number of adverse influence of welding including the severity of thermal cycle and residual stresses in weld joint. Thus, a combination of P-GMAW and ultra-narrow gap welding procedure can be considered as an interesting technique to weld thick dissimilar sections of stainless steel to HSLA steel, having improved properties of weld joint than those observed in case of conventional weld joint.

In this context it is also realised that the effective use of P-GMAW in ultra-narrow groove of at least 25 mm thick section becomes practically impossible due to difficulties in manipulation

of relatively large conventional torch head of the order of 24 mm O.D. in weld groove. In order to successfully implement this technique, development of a narrow torch head which can produce narrowest possible weld joint for thick section by allowing desired protection to weld deposition, effective torch manipulation to achieve sufficient groove wall fusion and satisfactory arc stability is very much essential. Here it should also be noted that the critical selection of simultaneously interactive pulse parameters can only be made by developing a clear understanding of the influence of the hypothetical factor f (Summarised influence of pulse parameters), total heat transferred to the weld pool (QT) and the variation of heat input (Ω) on characteristics of the weld bead.

2.15.2. Objectives of the Work

In view of the above the present investigation on welding of thick dissimilar section of 304LN stainless steel to HSLA steel has been carried out using pulse current gas metal arc welding (P-GMAW) in ultra-narrow weld groove. The studies have been systematically planned as stated below in order to gain sufficient knowledge to establish a welding technique superior to some conventionally used welding process and weld groove design.

The various aspects and objectives of the studies primarily consist of following.

1. To design an advanced nozzle head system for narrow gap GMAW torch nozzle to facilitate the application of P-GMAW process in multi pass ultra-narrow gap welding of thick plates.
2. Study of shielding gas flow behaviour inside the ultra-narrow groove and optimization of its flow rate by simulation in ANSYS-CFX software.
3. To develop a thermal model for preparation of multi pass ultra-narrow gap weld joint of thick dissimilar plates, free from lack of groove wall fusion, using single seam centrally located weld deposition per layer technique inside the weld groove.
4. To study the effect of the mean current (I_m), heat input (Ω) and factor η of P-GMAW process by analysing their influence on thermal behaviour and geometry of weld pool in bead on plate weld deposition. This is in order to develop an understanding of efficient use of them to produce ultra-narrow gap thick dissimilar steel weld free from lack of groove wall fusion by single bead per layer of weld deposition technique.
5. To analyse and validate the proposed thermal model for development of an ultra-narrow gap welding procedure for preparation of sound P-GMA weld joint using the MPSBPL of weld deposition technique.
6. To study the effect of variation in pulse parameters, considered by their summarized influence known in terms of the factor f , on metallurgical and mechanical properties as well as shrinkage stress and bending stress of dissimilar weld joints.

7. To establish suitability of the MPSBPL narrow gap P-GMA weld for its use to improve the properties of dissimilar weld joint with respect to those prepared by commonly used MPMBPL weld deposition in conventional weld groove.





There are a numerous advantages in gas metal arc welding (GMAW) process such as the ability to produce cleaner weld with finer microstructure and better weld properties over commonly used gas tungsten arc welding (GTAW), submerged arc welding (SAW) and shielded metal arc welding (SMAW) processes. In spite of that GMAW process is not preferred in narrow gap welding of thick section of the order of 25mm and above due to its comparatively bulky (large diameter) torch nozzle head which is generally supplied with commercially available GMAW process that poses difficulties in its deep manipulation inside the weld groove.

The major problems like formation of inclusion and porosity in weld deposit due to inadequate shielding gas coverage of the arc and weld pool, lack of fusion of the groove wall and spatter generation are generally create because of inappropriate or faulty manipulation and positioning of torch nozzle inside weld groove. Thus, there is a worldwide demand for research to develop GMAW torch nozzle head with effective shielding of weld pool from air contamination [Tyagi 2000, Nosse 2001, Jones 2004] and preparation of narrowest gap weld joint of thick section ($\geq 25\text{mm}$). It also reduces stresses in weld joint and cost of production. Due to large diameter of its torch nozzle head which is biggest limitation to produce narrowest gap GMA weld joint of thick section, several weld deposition procedures and torch designs have been proposed by several investigators such as electromagnetic arc oscillation [Kang et al 2003], wire oscillation inside the groove through swinging of contact tube across or along the groove [Nakayama et al 1976, Futamura et al 1978], alternate rotation of a bent contact tip about its axis inside the groove [Innyi et al 1975], plastic deformation of filler wire into some wavy shape before its entrance in the contact tube that produces oscillating arc across the groove [Sawada et al 1979, Kawahara et al 1986], rotating the arc by feeding the wire through an eccentric contact tube that rotates [Nomura and Sugitani 1984] and rotating the arc by using a special “twist” electrode wire [Okuda et al 1986].

However, any appropriate torch head is not commercially available which can be used for producing narrowest possible GMA weld of thick section along with proper consideration of maintaining the necessary characteristics of shielding jacket at the outlet of torch head protecting the weld deposit from any types of contamination. It requires special attention while welding in narrow weld groove primarily due to significant constraints to dynamics of gas flow imposed by the groove wall. The constraints on gas flow due to boundary conditions applied by groove design may induce turbulence in the shielding jacket resulting in porosity due to air aspiration in it at a

given gas flow rate while using narrow torch head. Hence in the present study a narrow torch head addressing the above aspects has been designed and employed in maximum possible narrow gap welding of thick plates (25mm).

3.1. Design Considerations of Narrow Gap Welding Torch Nozzle Head

The commercially available torch nozzle for gas metal arc welding has been shown in Fig. 3.1 which is having an integrally formed copper tube with relatively large outlet diameter (Fig. 3.2). This is primarily suitable for shielding gas discharge in conventional V-groove butt welding of 10-12 mm thick sections when fitted to the forward end portion of a welding torch during use. Such large outlet diameter torch nozzle can seldom be used in conventional or narrow groove GMA welding of thick sections beyond about 15-20mm.



Figure 3-1 Photograph of commercially available conventional GMAW torch nozzle.

The schematic diagram of modified torch head has been shown in Fig. 3.2(b). A narrow rectangular faced torch nozzle, suitable for appropriate manipulation inside a practically narrowest possible weld groove, has been designed by removing both of its lengthwise side walls as shown in Fig. 3.3. This is done to avoid burning of the side wall (Fig3.4 b and c) of the nozzle being close to the electrode tip. As such the general approach of increase in wall thickness of the copper nozzle to avoid its burning could be ignored as it consequently enhances the nozzle width. Increase of nozzle width is not compatible to the objective of exploring GMAW with narrowest possible groove width in case of thick section butt welding.

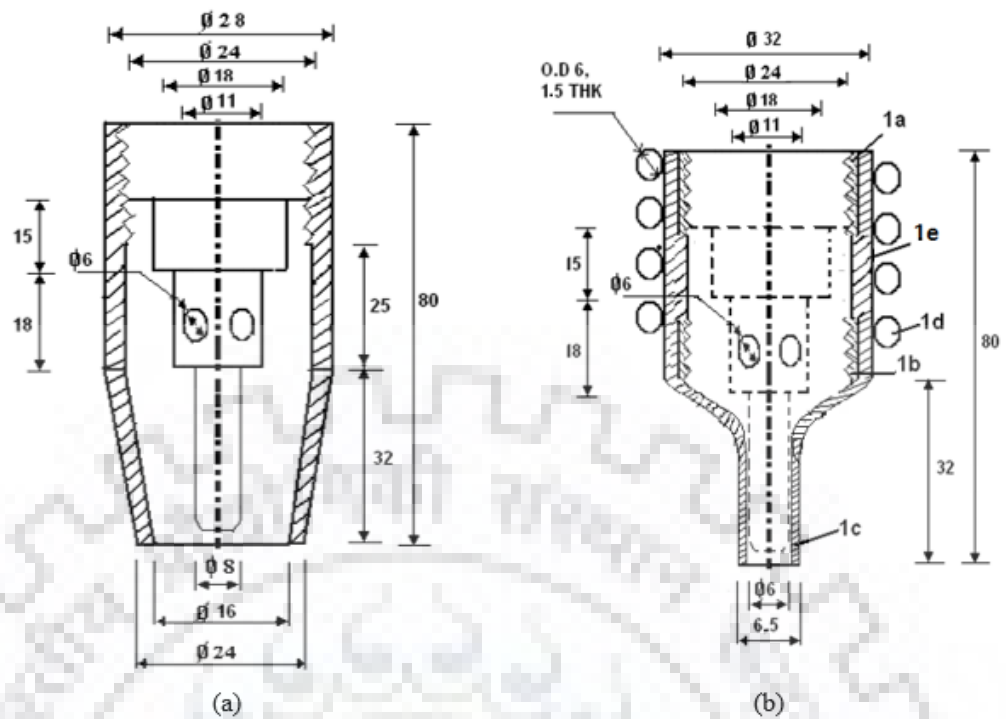


Figure 3-2 Schematic diagram of (a) Conventional and (b) newly designed narrow GMA torch nozzle. (All dimension in mm)

The use of such torch nozzle in narrow groove welding is considered by lengthwise placing of the rectangular faced nozzle in the direction of welding, where the walls of the narrow groove may virtually act as lengthwise side wall of the nozzle as schematically shown in Fig. 3.5(a). However, the success of such nozzle in producing sound weld having no discontinuity defect of lack of fusion primarily depends upon providing an appropriate oxidation protective inert gas shielding and enough thermal intensity to the weld pool required for necessary groove wall fusion and inter-pass fusion in single pass per layer of weld deposition. After each weld pass the deposited weld metal fill the weld groove and to maintain the contact tip to weld distance (15-17 mm) one has to uplift the welding nozzle. Such movement of welding torch or nozzle introduces an open exposure between the nozzle and groove wall of the plate. Thus, there is a requirement of shortening of the nozzle head as shown in Fig. 3.5(b) for effective shielding of arc zone by covering the opening between the nozzle and groove wall, which otherwise may introduce turbulence in shielding of the arc zone and degrade the weld quality.

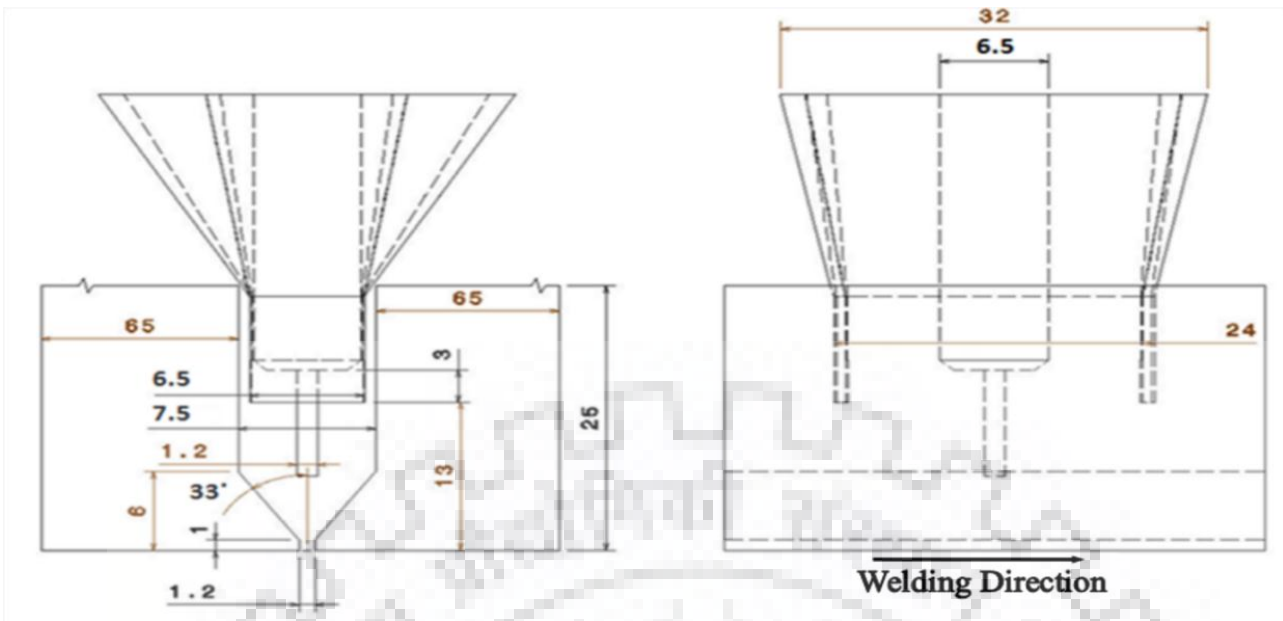


Figure 3-3 Schematic diagram of 7.5 mm narrow groove width for welding of thick section.

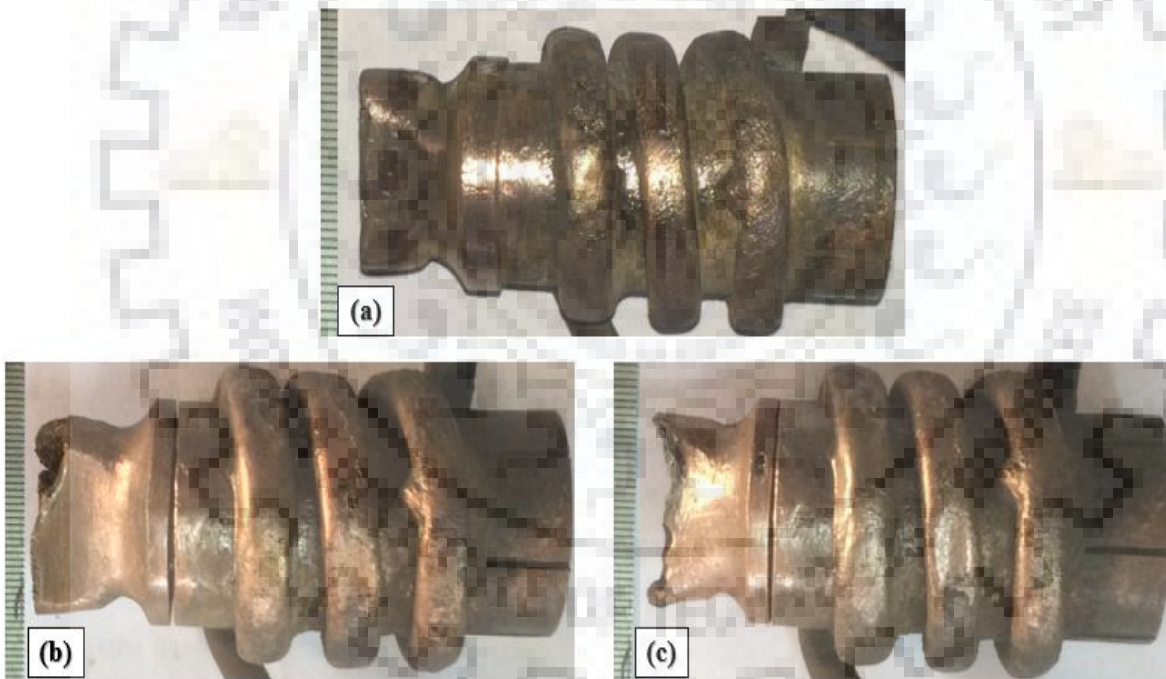


Figure 3-4 Photograph of (a) unburnt (b & c) burnt narrow GMAW torch nozzle.

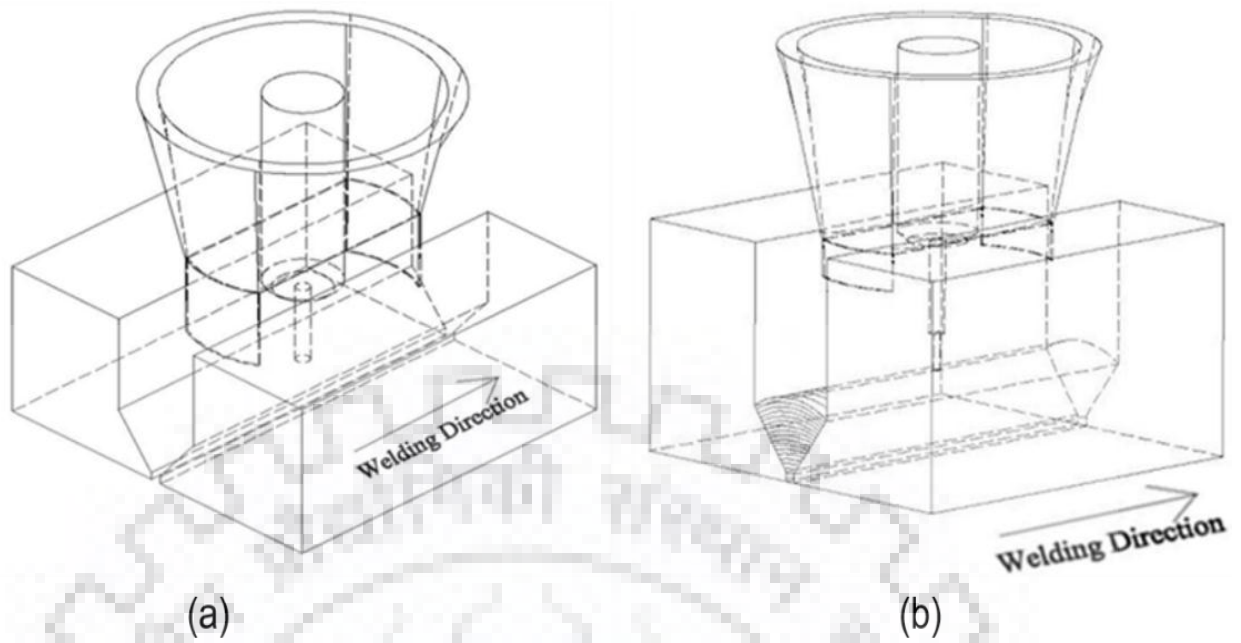


Figure 3-5 Isometric drawing of rectangular faced narrow gap GMA welding torch nozzle used in (a) first pass and (b) second pass.

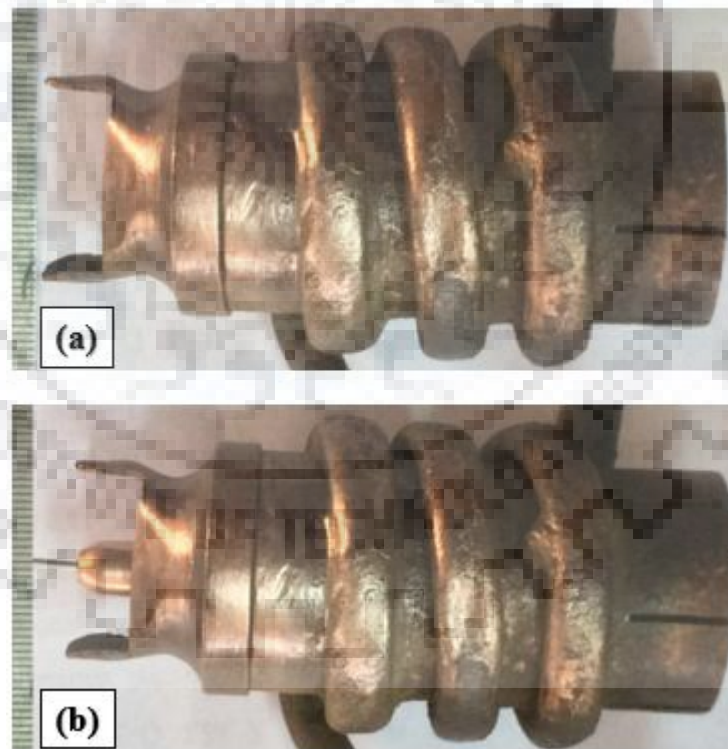


Figure 3-6 Photograph of newly developed narrow GMAW torch nozzle.

In this work a relatively easily attachable narrow torch nozzle head device as shown schematically in Fig. 3.2(b) and Fig.3.3 has been prepared to introduce GMAW and especially P-GMAW process to produce narrowest possible gap welding of thick sections. The isometric

drawing and photograph of the narrow torch nozzle head device are also shown in Fig.3.5 and 3.6 respectively. The device could be easily attached to the commercially available GMA welding torch in such a manner that the wire holder, contact tip adaptor and contact tip are totally hidden within the welding nozzle. The newly developed narrow torch nozzle head (Fig. 3.3) with respect to its use as a cost effective easily attachable part to the conventional GMAW torch nozzle consist of three members. The first one is the torch nozzle device having a tubular internally threaded member (1a) which is removable from the welding torch (2), usually through the use of a screw threading method. The second one is the round tubular body (1e) with a drawn rectangular end portion which is nozzle head (1c) of suitable length, which is fitted on the internally threaded member (1b) and the third one is the coiled copper tubular section (1d) brazed on the round tubular body (1e) to carry cooling fluid. This newly designed nozzle head (1c) provides the desired torch manipulation in narrow weld groove of thick section. An adequate cooling is provided by the high conductive water cooled copper tubes (1d) spirally braided on the cylindrical portion of the torch nozzle to prevent excessive heating and burning thereof. As a result the durability of the narrow torch nozzle is extended up to that of a conventional one.

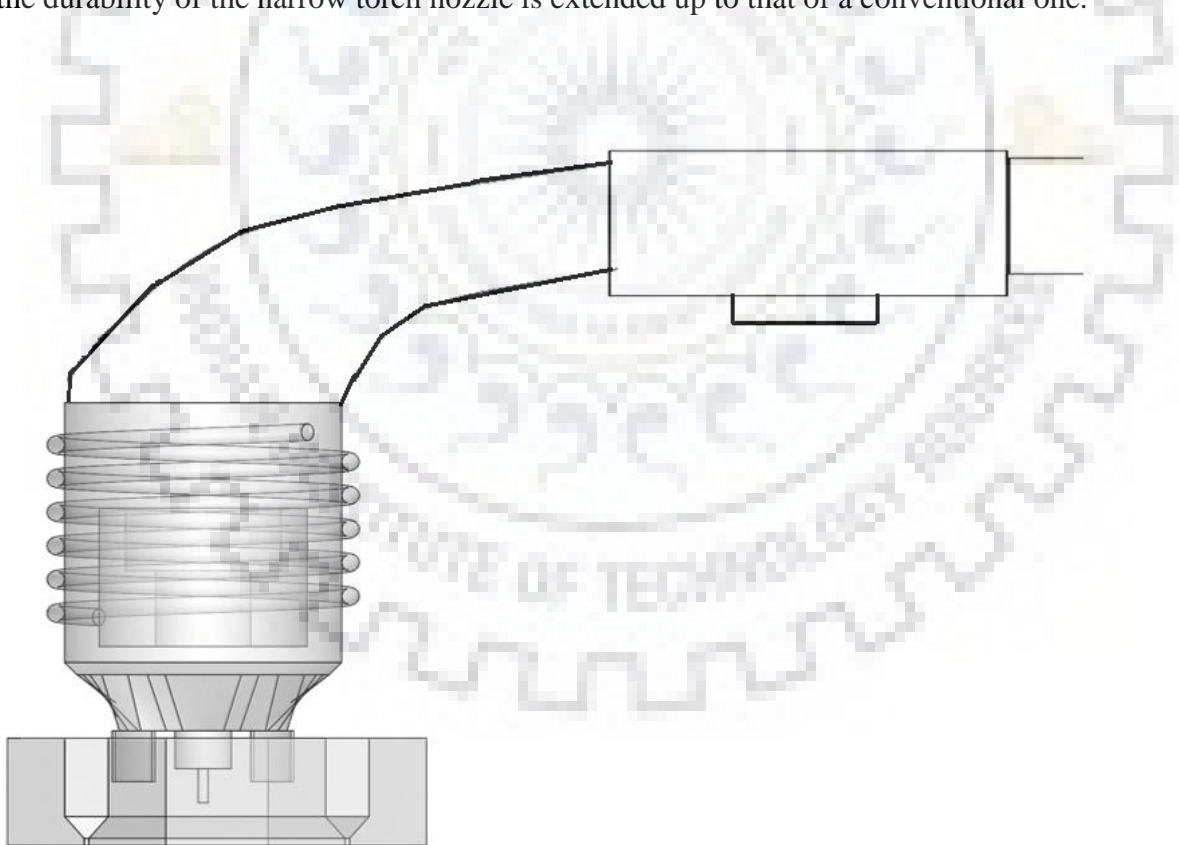


Figure 3-7 GMA torch head with newly developed narrow torch nozzle device.



Figure 3-8 Photograph showing closely fitted narrow groove of 25 mm thick dissimilar plates with narrow welding torch nozzle inserted in it.

3.2. Simulation by ANSYS 14.5 CFX Software

A model of shielding gas flow dynamics and its flow rate in case of employing newly developed GMAW nozzle has been studied at different projection angle of torch nozzle inside the narrow groove of butt joint by using ANSYS-CFX (14.5) software. The simulated characteristics of GMAW for arcing and argon shielding gas flow at a given flow rate inside the narrow groove of 25 mm thick butt weld are analyzed by 3D CFD modeling using ANSYS-CFX(14.5) software. The model geometry was constructed in 3D CAD design software CATIA in which newly designed welding torch is vertically positioned 12 mm above the surface inside the narrow weld groove with groove width of 7.5mm as shown in Fig.3.3. Both the stick out of the 1.2 mm diameter filler wire electrode and the distance between electrode tip and the work piece is kept as 6 mm. Fig.3.9 depicts all relevant zones and parts of the welding torch nozzle head with respect to gas flow behavior in it while studied inside the 7.5mm narrow groove width. The simulation studies were carried out at the welding current and arc voltage of 220A and 25V respectively. The effect of variation in intensity of gas flow on the arcing and flow characteristics of shielding gas have been studied at different projection angle of the newly designed nozzle tip varied from 0 to 60° (Fig.3.10). The density, specific heat capacity, dynamic viscosity and thermal conductivity of argon as considered are given in Table-1.

Table 3.1: Physical properties of argon gas.

Density	1.784 g/L
Specific heat capacity	20.786 J·mol ⁻¹ ·K
Dynamic Viscosity	2.1017E-04 Poise
Thermal Conductivity	16.483 mW/(m.K)

In addition to the equation for conservation of mass, the equations of momentum and energy are also applied in order to establish a mathematical model of the combined plasma arc. To simplify its calculation, the following assumptions have been made:

1. Pure argon plasma arc is in local thermodynamic equilibrium (LTE), which is considered to mean that the temperature of electron and heavy particle are not significantly different.
2. The flow of plasma arc is laminar and radially in three dimensional approach, which is appropriate for the operating conditions.
3. The heating effects of viscous dissipation and compressibility effects are negligible.
4. The governing equations are not time dependent because plasma arc is steady and optically thin for radiation.

With the above-mentioned assumptions, a group of magneto hydrodynamics (MHD) equations are expressed in terms of all coordinates as follows:

Equation of Mass Continuity

$$\frac{\partial \rho}{\partial t} + \frac{1}{r} \frac{\partial(\rho r u)}{\partial r} + \frac{\partial(\rho w)}{\partial z} = 0 \quad (3.1)$$

Where ρ = mass density in kg/m³, r = radial distance in m, z = axial distance in m, u = radial velocity in m/s, w = axial velocity in m/s

Conservation of Radial Momentum

$$\frac{\partial \rho u}{\partial t} + \frac{1}{r} \frac{\partial(\rho r u u)}{\partial r} + \frac{\partial(\rho u w)}{\partial z} = -\frac{\partial P}{\partial r} + \left[\frac{2}{r} \frac{\partial}{\partial r} \left(\mu r \frac{\partial u}{\partial r} \right) - \mu \frac{2u}{r^2} + \frac{\partial}{\partial z} \left(\mu \left\{ \frac{\partial u}{\partial z} + \frac{\partial w}{\partial r} \right\} \right) \right] - J_z B_\theta \quad (3.2)$$

Conservation of Axial Momentum

$$\frac{\partial \rho w}{\partial t} + \frac{1}{r} \frac{\partial(\rho r u w)}{\partial r} + \frac{\partial(\rho w w)}{\partial z} = -\frac{\partial P}{\partial z} + \left[\frac{1}{r} \frac{\partial}{\partial r} \left(\mu r \frac{\partial u}{\partial r} + \frac{\partial w}{\partial r} \right) - 2 \frac{\partial}{\partial z} \left(\mu \left\{ \frac{\partial w}{\partial z} \right\} \right) \right] - J_r B_\theta \quad (3.3)$$

Where J_r = radial current density in A/m², J_z = Axial current density in A/m², P = Pressure in N/m², μ = Viscosity in N-s/m², B_θ = Azimuthal magnetic field in Tesla in equations (3.2) and (3.3)

Conservation of Energy

$$\frac{\partial \rho h}{\partial t} + \frac{1}{r} \frac{\partial(\rho r u h)}{\partial r} + \frac{\partial(\rho w h)}{\partial z} = \frac{1}{r} \frac{\partial}{\partial r} \left(\frac{k r}{c_p} \frac{\partial h}{\partial r} \right) + \frac{\partial}{\partial z} \left(\frac{k}{c_p} \frac{\partial h}{\partial z} \right) + \frac{J_z^2 + J_r^2}{\sigma_e} - S_R + \frac{5K_b}{2e} \left(\frac{J_r}{c_p} \frac{\partial h}{\partial r} + \frac{J_z}{c_p} \frac{\partial h}{\partial z} \right) \quad (3.4)$$

Where h = Enthalpy in joule, k = Thermal conductivity in w/m-k, C_p = Specific heat at constant pressure, σ_e = Electrical conductivity in 1/Ω-m, S_R = Radiation heat loss, K_b = Boltzmann constant (8.617332×10^{-5} eV/k), Elementary charge (1.602176×10^{-19} C)

Current Continuity Equation

$$\frac{1}{r} \frac{\partial}{\partial r} \left[\sigma_e r \frac{\partial \phi}{\partial r} \right] + \frac{\partial}{\partial z} \left[\sigma_e \frac{\partial \phi}{\partial z} \right] = 0 \quad (3.5)$$

Where ϕ = Electric potential in V. The current density can be obtained from Ohm's law which is given by,

Ohm's Law

$$J_r = \sigma_e \frac{\partial \phi}{\partial r} J_z = \sigma_e \frac{\partial \phi}{\partial z} \quad (3.6)$$

Ampere's Law

$$\frac{1}{r} \frac{\partial}{\partial r} [r B_\theta] = J_z \mu_0 \quad (3.7)$$

Where, μ_0 is the vacuum permeability ($4\pi \times 10^{-7} \text{H/m}$).

The above equations are based on the magneto-hydrodynamic approximation (MHD) which combines the fluid mechanics equations with the Maxwell's equations of the electro-magnetics.

The boundary conditions used in solving the equations are shown in table 3.2.

Table 3.2: Used boundary conditions for the equation system.

Boundary	Mass and Momentum	Energy	Current	Magnetic Potential
Wire Top		1800K	220A	Zero Flux
Wire Surface		1800K	Conservative flux	Conservative flux
Nozzle Top		900K		Zero Flux
Nozzle Surface		900K		Conservative flux
Plasma Top	P=1bar	300K	Zero Flux	Zero Flux
Plasma Side	P=1bar	300K	Zero Flux	0 T/m
Plasma Back	P=1bar	300K	Zero Flux	0 T/m
Shielding Gas Inlet	V=10 l/min	300K	Zero Flux	Zero Flux
Wire Surface	No Slip	1800K	Conservative flux	Conservative flux
Nozzle Surface	No Slip	900K	Zero Flux	Conservative flux
Work piece Surface		q_{plasma}	Conservative flux	Conservative flux

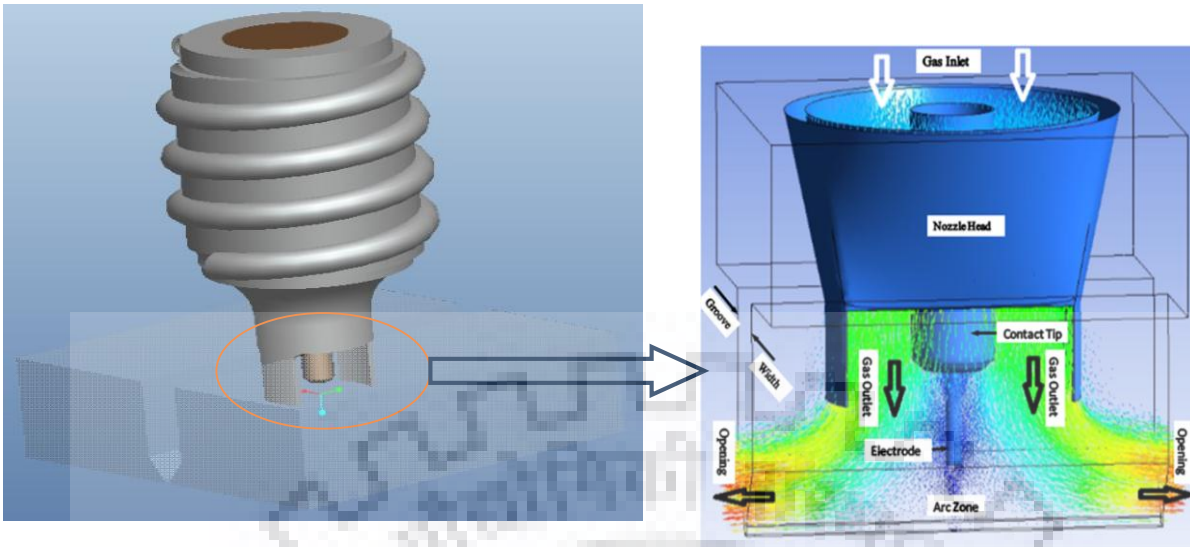


Figure 3-9 Computational domains of the torch nozzle head placed inside the narrow groove.

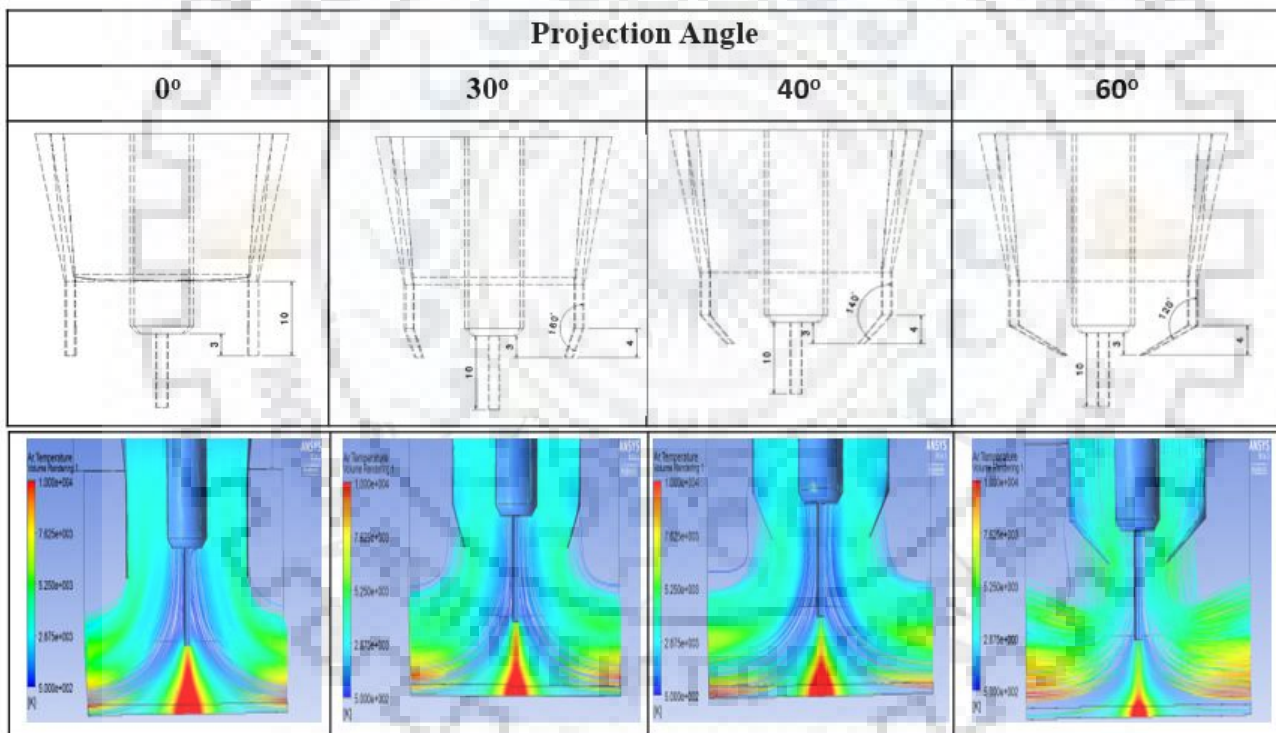


Figure 3-10 Computational domains of the torch nozzle head placed inside the narrow groove at different projection tip angle i.e. 0°-60°.

The geometric model analysis of shielding gas flow in narrow groove assembly was carried out in the region starting from inside the welding torch to free region between the gas nozzle and the work piece. The model was meshed using hexahedral element consisting of 281695 nodes for shielding gas and was refined further in relevant regions according to the computational gradients. In this simulation Shear-Stress-Transport (SST) turbulence-model was also applied.

The equations of this turbulence model are applied in the domain of ANSYS 14.5 database. The arc was modeled with the help of Magneto-hydro dynamics (MHD) model applied in the arc column and an assumption of Local Thermodynamic Equilibrium (LTE) in the near electrode region. The MHD model combines the equations of the fluid mechanics (Navier-Stokes equations) with the maxwell's equation of the electro-magnetic field.





THERMAL MODELING OF MULTI PASS SINGLE SEAM PER LAYER NARROW GAP WELDING OF γ -SS TO HSLA STEEL

In this chapter a thermal model has been developed for production of a multi-pass single seam per layer deposition (MPSSPL) ultra- narrow gap pulse current GMA weld joint of dissimilar sections free from lack of groove wall fusion under partially zero angle of attack to dissimilar groove wall. To produce a weld joint free from lack of fusion, the weld pool inside the narrow groove must have enough heat which is required to fuse both sides of the groove wall as well as apart of earlier deposited weld. The heat content of the weld pool is primarily dictated by the amount of weld deposit and the temperature of the weld pool. which primarily arises out of initial arc heating and heating by superheated droplets of filler metal transferred to the weld pool. For production of a sound weld joint, the favourable role of pulse current gas metal arc welding (P-GMAW) has been also justified.

4.1. Requirement for Preparation of a Sound Weld Joint

The basic requirement of preparation of sound weld joint by using MPSSPL deposition technique and specially in case of dissimilar plate weld joint the fusion of groove wall up to a skin depth of 0.5 to 1.0mm [Radaij D., 1992] is generally considered. During MPSSPL deposition technique for thick section the fusion of earlier deposited weld metal up to a certain extent is also very much required. This is primarily dictated by the heat content of weld pool and bead geometry affecting the thermal distribution as it is necessary for desired fusion. The heat content of weld pool is largely governed by its mass per unit length and temperature.

In case of conventional gas metal arc welding (GMAW) the weld bead geometry to touch the wall of thick section and sufficient heat transfer wall for fusion is basically governed by the welding parameters and heat input. It becomes difficult during a low angle of attack or approach of the conventional GMAW arc to the narrow groove wall. This is required fusion can be controlled by the geometry of molten weld bead intimately touching the groove wall for quick for sufficient heat transfer, Control of this condition becomes highly critical especially when a comparatively low heat input GMAW than high heat input submerged arc welding (SAW) is used. Thus, during the use of GMAW process in narrow gap welding, it is imperative to have a clear understanding primary on the control of heat and geometry of weld pool as a function of welding parameters [Goyal V. K. et. al., 2008(a), Goyal V. K. et. al., 2008(b)] so as to apply it appropriately in narrow groove.

The use of pulse current in GMAW process, often known as P-GMAW process, has considerably widen the scope of welding with more precise control of heat and geometry of weld pool as a function of welding parameters [Ghosh P. K. et. al. 2006, Ghosh P. K. et. al. 2010]. It has significantly broadened the range of application of this process in comparison to that of the conventional GMAW process. It may further provide an opportunity to appropriate positioning of heat transfer in weld pool through control of cavity formation on it, regulated by the transfer of superheated droplets from the filler electrode, which can facilitate required fusion at desired location. Such an advantage of this process can be properly used in laying weld deposit of required geometry and thermal characteristics in appropriate location with respect to the groove wall in order to ensure its required fusion, especially in case of centrally laid MPSSPL narrow gap welding process. Thus, in this regard the application of right pulse parameters of P-GMAW process with necessary knowledge of their selection for required geometry and thermal behaviour of weld pool in each pass may play a vital role in preparation of a sound MPSSPL narrow gap weld free from lack of groove wall fusion. Further, the selection of pulse parameters of P-GMAW process is quite complex due to their relatively large number with simultaneously interactive nature [Ghosh P. K. et. al. 2007].

In consideration of the above, an effort has been made to develop an experimentally verified spatial model to analyse the geometry and thermal behaviour of weld pool in order to prepare ultra-narrow gap dissimilar weld of thick section of austenitic stainless steel to HSLA steel using centrally laid MPSSPL weld deposition, which is free from lack of dissimilar groove wall fusion, especially in case of a dissimilar weld.

On the basis of model analysis, the selected parameter can be used to get a ultra-narrow groove dissimilar weld joint of thick section of austenitic stainless steel to HSLA steel without any lack of groove wall fusion in thick section using MPSSPL welding by employing P-GMAW process in narrowest possible weld groove. The use of pulsed current GMA welding process has been found to improve the conventional mechanical properties as well as metallurgical properties of the weld, over those observed in case of the conventional continuous current GMA weld, primarily due to its favorable influence on microstructure of the weld and HAZ [Gupta P.C. et.al. 1998]. The advantage of using such a welding parameter, process and procedure may be realised in production of weld joint with introduction of higher integrity in fabrication. The production of a weld joint using narrowest possible weld groove results into consumption of less filler material and energy, leading to reduction of the cost of production of faster welding. The selection of parameter with the help of model, which is able to produce a narrow groove dissimilar weld joint without any lack of fusion on both side of dissimilar wall, prior to carrying

out welding may facilitate accomplishment of the highly critical ultra-narrow gap welding more conveniently. Such an advanced narrowest groove butt weld of thick section may be advantageous especially to attain maximum reduction of residual stresses and elimination of adverse metallurgical transformation as well as severity of thermal characteristics of weld joint.

In order to produce a dissimilar weld joint free from lack of groove wall fusion by using MPSSPL ultra-narrow gap welding, the weld pool temperature should be able to fuse it apart from melting a part of weld deposit of earlier pass. It may be achieved by having a weld pool of required geometry and temperature primarily depending upon the design of weld groove (Fig. 4.1) accommodating and allowing the weld metal to come in contact with the dissimilar groove wall of austenitic stainless steel and HSLA steel. The critical geometry and the temperature of the weld pool necessary to produce MPSSPL ultra-narrow groove weld free from lack of dissimilar groove wall fusion can be estimated as follows.

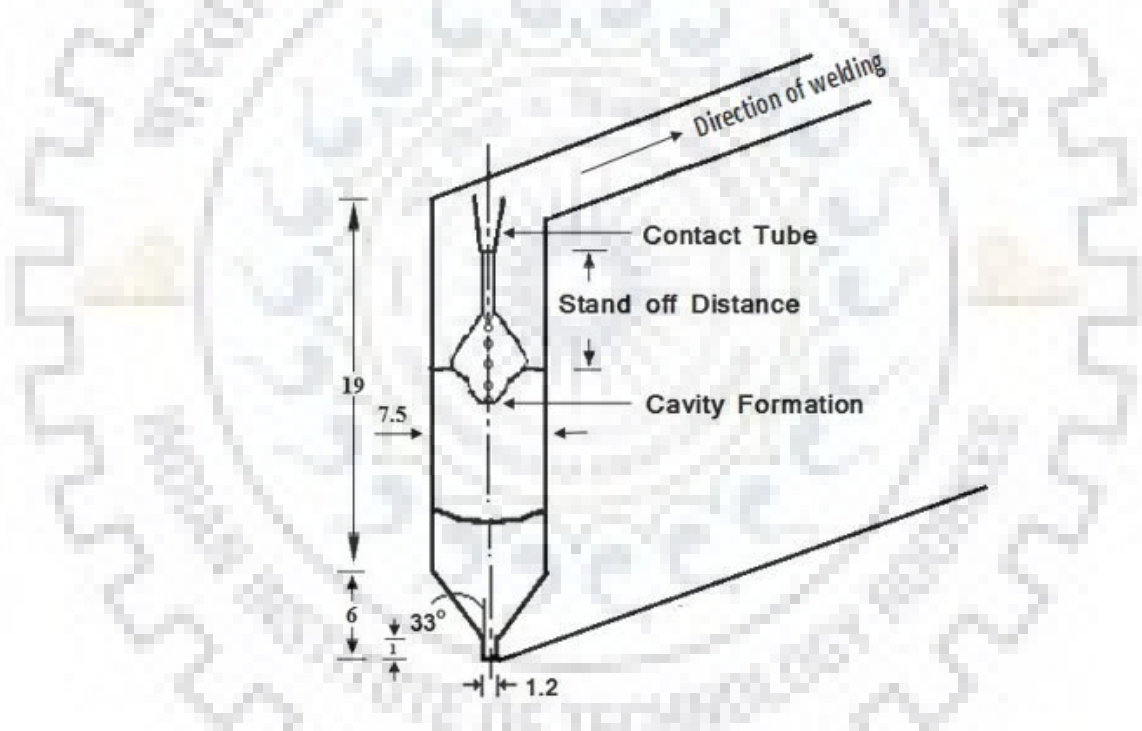


Figure 4-1 Schematic diagram of metal deposition in a narrow weld groove with the formation of cavity in weld pool. (All dimension in mm)

4.2. Spatial Model for Estimation of Geometrical Aspects of Weld Pool

The geometrical aspects of weld pool in MPSSPL narrow gap welding primarily concern its ability to intimately contact the dissimilar groove wall of austenitic stainless steel and HSLA steel in order to result its desired fusion on both side and filling the fraction of weld groove as estimated by their proportionate cross sectional area. In multi-pass welding of thick section, each weld pass fills a portion of the cross sectional area of weld groove. The cross

sectional area (A_1) covered by molten filler metal during each pass of weld deposition in MPSSPL ultra-narrow gap welding can be estimated as

$$A_1 = \frac{V_m}{L} \quad (4.1)$$

Where, L and V_m are the length and volume of weld deposit respectively. The V_m can be estimated by the following expression as a function of the length of filler wire (L_w) of a given diameter (d_w) consumed per pass of weld deposition.

$$V_m = L_w \cdot \frac{\pi}{4} \cdot d_w^2 \quad (4.2)$$

The L_w , as a function of welding speed (S) and wire feed rate (w) is expressed as follows,

$$L_w = \frac{L}{S} \cdot w \quad (4.3)$$

In order to find out dissimilar base metal fusion within the entire zone of its contact with the weld pool of each pass, height of weld metal deposited per pass is necessary to be estimated by considering the geometry of weld groove. The cross sectional geometry of weld deposit of a given weld pass can be considered as rectangular as schematically shown in Fig. 4.2. Thus the cross-sectional area of weld deposit may also be obtained as

$$A_1 = a \times h \quad (4.4)$$

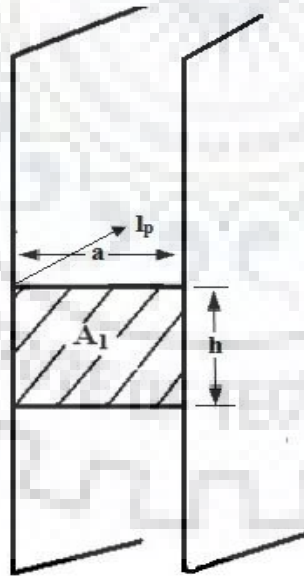


Figure 4-2 Schematic diagram showing effective geometry of weld deposit in contact with groove wall.

where, h is the height covered by the deposit of a given weld pass and a is the width of weld metal deposited in earlier pass or current pass. Solving the equations (1) and (4) the height covered by a weld pass within a weld groove can be estimated as

$$h = \frac{V_m}{L \times a} \quad (4.5)$$

4.3. Spatial Model for Estimation of Thermal Behaviour of Weld Pool

In order to find out the amount of heat required for necessary fusion of both the sides of a dissimilar groove wall and a part of earlier deposited weld, it is necessary to evaluate the mass of material to be fused per pass of weld deposition. By assuming certain depth (t_b) of groove wall fusion is necessary to produce a weld free from lack of groove wall fusion, the mass (m_{bHS}) and (m_{bSS}) of dissimilar base material fusion required upto this depth along the entire surface area (s_b) of each side of groove wall in contact with molten weld pool, can be estimated as follows.

$$m_{bHS} = s_b \cdot t_b \cdot \rho_{bHS}, \quad m_{bSS} = s_b \cdot t_b \cdot \rho_{bSS} \quad (4.6)$$

Where

$$s_b = h \cdot l_p \quad (4.7)$$

Where, h and l_p are the vertical length of groove wall and run on length of weld pool respectively in contact (Fig. 4.2) with the molten weld pool and ρ_{bHS} and ρ_{bSS} is the density of solid dissimilar base metal. To avoid lack of fusion with the weld deposit of earlier pass, the mass of it (m_w) required to be fused, can also be similarly estimated as follows by assuming a requirement of its certain (t_w) depth of fusion along the entire surface area (s_w) of the weld pool in contact with the earlier weld deposit.

$$m_w = s_w \cdot t_w \cdot \rho_w \quad (4.8)$$

$$s_w = a \cdot l_p \quad (4.9)$$

Thus, the total mass of fusion involved from the base metal (m_t) and earlier deposited weld metal in preparation of a sound weld joint can be expressed as follows.

$$m_t = (m_{bHS} + m_{bSS}) + m_w \quad (4.10)$$

Heat required to fuse m_{bHS} amount of metal per unit length of HSLA side base metal for weld preparation can be estimated as :

$$H_{(HS)} = m_{(bHS)} [C_{PH(s)}(T_{mHS} - T_{iHS}) + L_{HS} + C_{PH(l)}(T - T_m)] \quad (4.11)$$

Heat required to fuse m_{bSS} amount of metal per unit length of γ -SS side base metal for weld preparation can be estimated as :

$$H_{(SS)} = m_{(bSS)} [C_{PS(s)}(T_{mSS} - T_{iSS}) + L_{SS} + C_{PS(l)}(T - T_m)] \quad (4.12)$$

Heat required to fuse m_W amount of metal per unit length of earlier deposited weld metal for weld preparation can be estimated as :

$$H_{(W)} = m_{(W)} [C_{PW(s)}(T_{mW} - T_{iW}) + L_W + C_{PW(l)}(T - T_m)] \quad (4.13)$$

where, $C_{PH(s)}, C_{PS(s)}, C_{PW(s)}, T_{mHS}, T_{mSS}, T_{mW}, T_{iHS}, T_{iSS}, T_{iW}, L_{HS}, L_{SS}, L_W, C_{PH(l)}, C_{PS(l)}, C_{PW(l)}$, and T are the specific heat of solid HSLA, γ -SS steel and earlier weld deposit respectively, melting temperature of the HSLA, γ -SS steel and earlier weld deposit respectively, initial temperature of the HSLA, γ -SS steel and earlier weld deposit respectively with preheating, are the latent heat of fusion of the HSLA, γ -SS steel and earlier weld deposit respectively, are the specific heat of liquid metal of γ -SS steel and earlier weld deposit respectively and T is the temperature of the liquid metal respectively.

So, the total heat required of fusion involved from the base metal (m_t) and earlier deposited weld metal in preparation of a sound weld joint can be expressed as follows.

$$H_t = (H_{HS} + H_{SS}) + H_W \quad (4.14)$$

Considering the efficiency of welding process dictating the melting efficiency (η_m) of the system, gross amount of heat (H_G) required to fuse both sides of the groove wall as well as a part of earlier deposited weld metal can be evaluated by using the following expression

$$H_G = \frac{H_t}{\eta_m} \quad (4.15)$$

Thus, to produce sound single seam per layer narrow gap weld without lack of fusion, at least H_G amount of heat has to be introduced to a given pass of weld pool. The H_G can also be expressed as

$$H_G = m_f [C_{pf}(T_{mf} - T_{af}) + L_f + C_{pl}(T_{rWP} - T_m)] \quad (4.16)$$

Where, T_{rwp} is the required temperature of the weld pool and m_f is the amount of filler wire of density ρ_f consumed per pass. The m_f can be estimated as follows.

$$m_f = V_m \cdot \rho_f \quad (4.17)$$

Solving the equations (4.16) and (4.17), the required temperature of the weld pool T_{rwp} for producing a weld joint without lack of fusion can be found out as

$$T_{rwp} = \frac{1}{C_{pl}} \left[\frac{H_t}{\eta_m \cdot m_f} - \{C_{pf}(T_{mf} - T_{af})\} - L_f \right] + T_m \quad (4.18)$$

In order to produce sound dissimilar weld joint having no lack of fusion to the both side of the dissimilar groove wall in contact with the weld pool, it is imperative to identify the predominantly effective location of the molten pool in this regard in single seam per layer multi-pass welding. In view of this, the factor which may primarily dictate the effective fusion of dissimilar groove wall can be primarily considered by the distance of its contact points with the molten metal in reference to the location of heat transfer by the droplets in the cavity formed in the weld pool. Considering the farthest contact points of groove wall with the upper and lower surface of the molten pool of each weld pass on both dissimilar side of groove wall as P_1, P_1' and P_2, P_2' respectively (Fig.4.3), the distances of these two points from the center of the arc, P , denoted as R_1 and R_2 respectively can be estimated as

$$R_1^2 = \left(\frac{a}{2}\right)^2 + d^2 \quad (4.20)$$

$$R_2^2 = \left(\frac{a}{2}\right)^2 + (h-d)^2 \quad (4.21)$$

A solution from Eqs. (4.20) and (4.21) for the square of ratio of R_1 and R_2 , by considering $d/h \ll 1$, may be written as

$$\left(\frac{R_1}{R_2}\right)^2 = \frac{1}{\left(\frac{2h}{a}\right)^2 + 1} \quad (4.22)$$

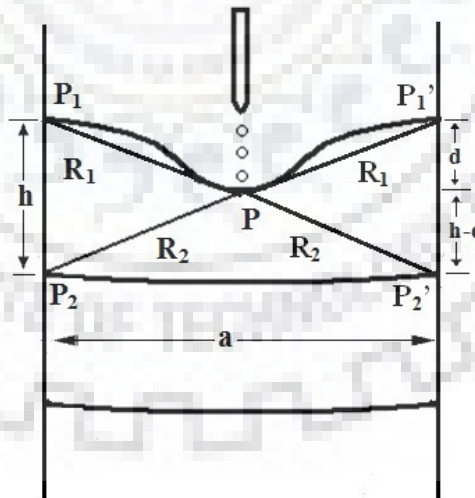


Figure 4-3 Schematic profile of molten pool of a weld pass showing distance touching points of its upper and lower most layer with groove wall in reference to the point of heat transfer by droplets in the cavity.

As the values of the ratio of (h/a) are less than one, the values of (R_1/R_2) will be less than one, which shows that R_2 shall always be higher than R_1 . Thus, the point P_2 at a distance R_2 from

the arc center shall predominantly play the critical role to assure required fusion of the groove wall.

The heating of weld pool under P-GMAW is primarily attributed to arc heat and heat transfer by the superheated filler metal under pulsed current. The arc heat acting continuously on the system as double ellipsoidal heat source is defined by three-dimensional ellipsoidal heat source [Goldak J. et. al., 1984] parameters (Fig.4.4). The arc may cover a part of the weld pool (Fig. 4.1) from where the heat is transferred to rest of the weld pool primarily by conduction and convection of liquid metal. The arc heat transferred to the point P₂ of the weld pool is contributing to raise the temperature of groove wall from initial preheating temperature upto a temperature of T_{arc}, which may cause an initial fusion to it. The heat transferred by the superheated filler metal as point heat source, acting at the depth of cavity formed on the weld pool contributes additional heat to the point P₂ to raise its temperature further to T_{filler}. Accordingly, the final temperature of weld pool at location P₂ denoted as T_{ewp} in each pass may be considered to be arising out of the contributions of arc heat and heat transfer by the superheated filler metal. Thus, minimum thermal condition of welding necessary to establish required fusion at a point P₂ of the groove wall may be expressed as follows:

$$\text{Weld pool temperature } (T_{rwp}) \leq T_{arc} + T_{filler} \quad (4.23)$$

Where (T_{arc}) is the temperature required for initiation of base metal fusion at a point P₂ out of arc heating, and (T_{filler}) is the additional temperature required to produce desired extent of base metal fusion at the point P₂ out of superheated filler metal. The temperature (T_{arc}) at the point P₂ arising out of arc heating can be expressed as follows [Nguyen N. T. et. al., 1999, Nguyen N. T. et. al., 2003].

$$T_{arc} = \frac{3\sqrt{3} \cdot Q_{AW}}{\rho \cdot c \cdot \pi \cdot \sqrt{\pi}} \times \int_0^1 \left[\frac{dt'}{\sqrt{(12a(t-t') + a_h^2)} \cdot \sqrt{(12a(t-t') + b_h^2)}} \right] + T_0 \quad (4.24)$$

where Q_{AW}, ρ, c, a, T₀ and a_h, b_h, c_{hf}, c_{hb} are the arc heat transferred to the weld pool, mass density of the base metal, specific heat of the base metal, thermal diffusivity of the base metal, initial preheated temperature of groove wall, and rests are ellipsoidal heat source parameters (Fig. 4.4) respectively:

$$A' = r_f \cdot \exp \left(- \frac{3(x - v \cdot t')^2}{12a(t-t') + c_{hf}^2} - \frac{3(a/2)^2}{12a(t-t') + a_h^2} - \frac{3d^2}{12a(t-t') + b_h^2} \right) \quad (4.25)$$

$$B' = r_b \cdot \exp\left(-\frac{3(x - v \cdot t')^2}{12a(t - t') + c_{hb}^2} - \frac{3(a/2)^2}{12a(t - t') + a_h^2} - \frac{3d^2}{12a(t - t') + b_h^2}\right) \quad (4.26)$$

Where, r_f and r_b are the proportion coefficients in front and behind the heat source, estimated as

$$r_f = \frac{2 \cdot c_{hf}}{c_{hf} + c_{hb}} \quad (4.27)$$

$$r_b = \frac{2 \cdot c_{hb}}{c_{hf} + c_{hb}} \quad (4.28)$$

The heat source parameter c_{hf} (in front of the heat source) and c_{hb} (behind the arc) may be considered [Nguyen N. T. et. al., 1999] as $c_{hf} = a_h$ and $c_{hb} = 2 c_{hf}$.

The arc heat transferred to the weld pool, Q_{AW} , can be estimated as

$$Q_{AW} = (V \cdot I_{eff} - \psi \cdot I_{eff}) \cdot \eta_a \quad (4.29)$$

where, ψ is the effective melting potential at anode and η_a is the arc heat transfer efficiency [Christensen, N., 1965]. The effective current, I_{eff} , is estimated by considering the root mean square of the pulsed current wave form as

$$I_{eff} = \sqrt{[k_p \cdot I_p^2 + (1 - k_p) \cdot I_b^2]} \quad (4.30)$$

where, k_p is the pulse duty cycle defined as

$$k_p = \frac{t_p}{t_{pul}} \quad (4.31)$$

Where, t_{pul} is the pulse cycle time estimated as

$$t_{pul} = t_p + t_b \quad (4.32)$$

Similarly the contribution to the temperature rise of weld pool (T_{filler}) from superheated filler metal at point P_2 [Roshanthal, D. et. al., 1946] can be estimated by using the expressions as follows

$$T_{filler} = \frac{Q_f}{2 \cdot \pi \cdot k} e^{-\lambda \cdot v \cdot \xi} \cdot \left[\frac{e^{-\lambda \cdot v \cdot R}}{R_1} + \sum_{n=1}^{n=\infty} \left(\frac{e^{-\lambda \cdot v \cdot R_n}}{R_{1n}} + \frac{e^{-\lambda \cdot v \cdot R'_n}}{R'_{1n}} \right) \right] \quad (4.33)$$

where, R_1 , R_{1n} and R'_{1n} are estimated as stated below.

$$R_1 = \sqrt{\xi^2 + (a/2)^2 + d^2} \quad (4.34)$$

$$R_{1n} = \sqrt{(2 \cdot n \cdot d - d)^2 + \xi^2 + (a/2)^2} \quad (4.35)$$

$$R'_{1n} = \sqrt{(2 \cdot n \cdot d + d)^2 + \xi^2 + (a/2)^2} \quad (4.36)$$

The heat transfers to the weld pool by superheated filler metal per pulse (H_{fp}) and per unit time (Q_f) are expressed as follows

$$H_{fp} = H_{de} \cdot m_{tp} \quad (4.37)$$

$$Q_f = H_{de} \cdot m_{tp} \cdot f \quad (4.38)$$

where, m_{tp} and f are the mass of the filler wire transferred per pulse [Goyal, V.K. et. al., 2008] and pulse frequency respectively. The eq.4.24 and eq.4.33 show that the temperature of weld pool is dependent on location of point of interest. Accordingly surface tension of the weld pool may vary because of changes in temperature leading primarily to convective fluid motion (weld pool stirring).

The heat distribution in weld pool is largely dictated by fluidity of weld pool and location of heat transfer by the droplets at certain depth (d) inside the weld pool. The depth of penetration of the transferring droplets is largely determined by their impact [Kumar Subodh et. al., 1994] on the weld pool imparting kinetic energy to a region adjacent to the pool surface resulting in a cavity formation in it as shown in Fig. 4.3. In this context it is assumed for simplicity that the cavity formation in molten weld pool is primarily dictated by the force exerted by the momentum of the droplets [Goyal V. K. et. al., 2008(a)] rather than the magnetic forces of arc zone. In consideration of work done, W_D , in creating paraboloidal cavity formed on the weld pool as a function of creation of new surface to the cavity and imparted kinetic energy of the droplet [Goyal V. K. et. al., 2008(a)], the depth d of the cavity can be estimated as follows.

$$d = \left[\sqrt{\frac{\gamma^2}{r_1 \cdot \rho_m^2 \cdot g^2} + \frac{3 \cdot m_d \cdot V_{de}^2}{8 \cdot \pi \cdot r_1 \cdot \rho_m}} - \frac{\gamma}{\rho_m \cdot g \cdot \sqrt{r_1}} \right]^{\frac{2}{3}} \quad (4.39)$$

Where, γ , r_1 , ρ_m , g , m_d and V_{de} are the coefficient of surface tension of liquid molten weld pool, focal length of paraboloidal cavity, density of molten metal of the weld pool, acceleration due to gravity, mass of droplet and velocity of droplet at the time of striking the weld pool respectively. The mass of the droplet, m_d , may be estimated as mass of the molten metal transferred per pulse, m_{tp} , divided by the number of droplets transferred per pulse, N_D . The velocity of droplet at the time of striking the weld pool, V_{de} , as a function of velocity of the droplet at the time of its detachment from the electrode, V_i , acceleration due to arc plasma, a_{cc} , acceleration due to gravity, g , and flight time of the droplet, τ , can be estimated as

$$V_{de} = V_i + (a_{cc} + g) \cdot \tau \quad (4.40)$$

where, the values of V_i , a_{cc} and τ are estimated by using the expressions as follows reported earlier [Ghosh P. K. et. al. 2006]. The depth of the cavity, d , formed by the impact of droplets on the weld pool can be determined by considering that the focal length of the paraboloidal cavity r_1 is equal to radius of the droplet.

The analysis of model expressions as stated above reveals that a higher depth of cavity on weld pool can bring the point P_2 closer to the point of heat transfer by the superheated filler metal allowing the presence of groove wall within the range of a relatively stronger weld isotherm necessary for its required fusion. In this context, it may be interesting to note the favourable role of P-GMAW where, a higher value of I_p may increase the d and amount of weld deposition per pulse but, enhances heat transfer to the weld pool by relatively larger superheated droplets reducing their heat loss during deposition through the arc chevron [Ghosh P. K. et. al. 2006]. In view of all these relevant aspects of welding conditions dictating the groove wall fusion, it is imperative to assure the required geometry and thermal characteristics of weld pool by appropriate selection of pulse parameters. It gives rise to intimate contact of weld pool to the groove wall with sufficient heat for its required melting. However, in this context the influence of arc length on the width of weld pool has not been considered due to its insignificant effect expected on it under the constraint of narrow groove wall.

4.4. Summary

The proposed thermal model is able to help in proper selection of pulse parameters to produce ultra-narrow gap dissimilar weld joint prior to carrying out welding based on geometrical and thermal aspects of weld pool with appropriate dissimilar groove wall fusion.



This chapter describes the experimental procedures used in present investigation on bead on plate as well as dissimilar weld joint study of thick section of austenitic stainless steel (γ -SS 304LN) and controlled rolled high strength low alloy (HSLA) steel plates have been stated in detail. The weld joints are prepared by P-GMAW welding process using multi pass single seam per layer deposition technique having no angle of attack with the dissimilar groove wall in ultra-narrow weld groove and multi pass multi seam per layer deposition in conventional dissimilar weld groove of the thick plates of γ -SS and HSLA steel using solid filler wires.

5.1. Base and Filler Materials

5.1.1. Used in bead on plate experimentation

The bead on plate weld deposition has been carried out on 20 mm thick plate of austenitic stainless steel of grade AISI 304LN as base material using direct current electrode positive (DCEP) pulsed current gas metal arc welding (P-GMAW) processes using 1.2 mm diameter filler wire of specification SFA-5.9 ER308L grade. Chemical composition as per ASTM of the base plates as per test certificates given by the supplier as well as obtained through spark emission optical spectroscopy have been shown in Table - 5.1. Similarly the chemical composition of the filler wire as per test certificate given by the supplier is also mentioned in Table-5.1. The results of chemical analysis obtained by using spark emission spectroscopy are found to be in good agreement with the results of the test certificates given by the supplier. The bead on plate weld deposition was performed with DCEP polarity under commercial pure argon (99.98%) gas shielding at a flow rate of 18 l/min.

5.1.2. Used in weld joint preparation

The weld joint studies have been carried out on 25 mm thick austenitic stainless steel (γ -SS) and controlled rolled high strength low alloy (HSLA) steel plates of specification AISI-304LN and SAILMA-410HI/SA543 grade respectively as base material. The chemical composition, confirming the specification, ASTM obtained by using spark emission optical spectroscopy and test certificate given by the supplier has also been given in Table - 5.1. Similar to the earlier observation of chemical analysis of 20mm thick base metal, here also it is observed that the results of spark emission spectroscopy are in good agreement to the test certificate given by the supplier. The dissimilar weld joints were prepared using 1.2 mm diameter filler wire of specification SFA-5.9 ER308L grade. The welding was performed with the polarity of DCEP

under commercial pure argon (99.98%) gas shielding at a flow rate of 10-12 l/min for ultra-narrow gap dissimilar weld joint and 18 l/min for conventional gap dissimilar weld joint. During welding the plates were rigidly fixed in a fixture to minimize distortion. The weld deposition was carried out in flat position by a vertically placed centrally located welding torch in ultra-narrow groove, which was moving on an automated trolley. Welding was performed by keeping the distance between the nozzle to work piece as 16-17 mm. A relatively higher electrode extension has been used to facilitate torch manipulation in the ultra-narrow weld groove for weld deposition with satisfactory root and dissimilar groove wall fusion. Before welding the 25mm thick control rolled micro alloyed high strength low alloy (HSLA) steel plate of specification SAILMA - 410HI/SA543 grade was preheated at about 125 - 130°C for 60 seconds. The flow rate of gas was controlled with the help of a flow meter and a pressure regulator fitted to the gas cylinder. The weld joints were prepared by using pulse current gas metal arc welding (P-GMAW) process. The size, chemical composition and specification of filler wire used in welding processes are also shown in Table - 5.1.

Table 5-1 Chemical compositions of base and filler material used in bead on plate as well as weld joint study.

Material	Source	Chemical analysis (Wt.%)									
		C	Cr	Ni	Mn	N	Mo	Si	Cu	S	P
γ -SS (304LN)	ASTM	0.035	18-20	8-11	2.0	0.1- 0.16	-	0.75	-	0.03	0.04
Base metal 20mm and 25mm	Supplier test certificate	0.024	18.8	9.3	1.7	0.15	-	0.55	-	0.001	0.022
	*	0.022	19.0	9.1	1.8	0.16	0.19	0.57	0.30	0.002	0.021
HSLA SAILMA - 410HI/ SA543	Supplier Test certificate	0.14	0.023	0.04 (v)	1.46	0.02 (Ti)	0.04 (Nb)	0.28	0.02	0.008	0.02
Base metal 25mm thick	*	0.154	0.014	0.08 (v)	0.50	0.02 (Ti)	0.04 (Nb)	0.31	0.03	0.002	0.022
GMAW filler wire (ER308L)	Supplier Test certificate	0.022	19.7	9.6	1.3	-	0.10	0.39	0.08	0.007	0.016
1.2mm Dia	*	0.020	19.6	10.3	2.2	-	0.30	0.39	0.08	0.007	0.016

* indicates testing by spark emission optical spectroscopy.

5.2. Welding Power Source

A, ESAB make Aristo 2000 – LUD 450 UW model, direct current (D.C) welding power source along with a MEK 44C wire feeder was employed in the present investigation. The power source was capable to operate for different welding processes such as SMAW, GTAW, GMAW and P-GMAW in both the synergic and non-synergic modes at a given command regarding the material and diameter of electrode/filler wire as well as shielding gas. During operation with the GMAW the welding current was regulated by changing the wire feed rate (V_w). During P-GMAW process in synergic mode operation at a given wire feed rate the power source was capable to self adjust the other parameters such as arc voltage (V), peak current (I_p), base current (I_b), pulse frequency (f) and peak current duration (t_p), whereas in non-synergic mode it was possible to operate the power source by manually setting all the parameters with maintainance of appropriate correlations among them. In the power source the peak current, and background current, was capable to operate in steps of 4 A, whereas the pulse frequency and pulse current and base current duration in steps of 2 Hz and 0.1 ms respectively.



Figure 5-1 Photograph of power source used in this investigation.

The power source was fitted with a control panel along with screen for displaying different set of parameters as well as soft push buttons to input different parameters of welding. The power source was fitted with a push type wire feed unit which consists of two sets of U-grooved wire drive rollers to accommodate required diameters of the filler wires. The pressure on the wire drive rollers was suitably adjusted to avoid slippage of the filler wire. The filler wire was fed to the arc through a water-cooled welding torch suitable to use up to 500A welding current

for different diameters of filler wire ranging from 0.8 to 2.0 mm. The power source was connected with 3-phase electrical supply for its operation as per requirement.

5.3. Fixture and Torch Manipulator

The fixture and torch manipulator are required to hold the base material properly and guide the welding torch during operations of welding.

5.3.1. Welding fixture

To fix the base plates rigidly in order to avoid distortion during welding, a fixture was used as shown in Fig.5.1. The fixture consists of a thick mild steel supporting plate of size $450 \times 350 \times 40$ mm and two clamping plates of dimension $300 \times 150 \times 40$ mm. A groove of dimension $200 \times 50 \times 5$ mm was made at center along the length of the supporting plate and a copper backing plate was fitted in the groove. The backing plate along its centre line of longitudinal surface was also having a groove to support root reinforcement of the weld as shown in Fig.5.1. During welding the base plates were rigidly fixed and clamped in the fixture. The clamping force was released after the plates naturally cool down to ambient temperature.

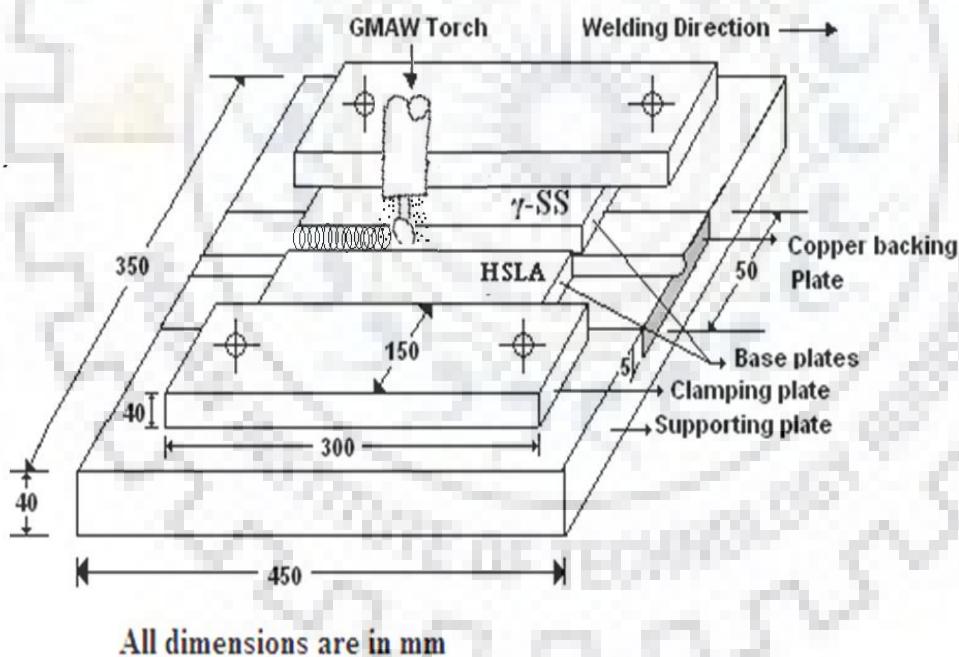


Figure 5-2 Schematic diagram of welding fixture.

5.3.2. Torch manipulator

A mechanized GMA welding torch manipulator, “Gulco make KAT” travel carriage has been used in this work. It was capable to hold the welding torch rigidly in the arms and clamping pivots to adjust it at any desired position with the help of rack and pinion arrangement as well as to vary the travel speed in the range of 2.6 – 83.8 cm/min with a digital display during deposition of weld bead on plate and preparation of weld joint. The reliability of the digital

reading of travel speed of the carriage was verified before use by measuring the length and time of travel with the help of a scale and a stopwatch of least count 0.01 second respectively at different speeds.

5.4. Instrumentation and Recording

Instrumentation and recording includes recording of parameters of welding as well as thermal behaviour of the weld pool.

5.4.1. Welding parameters

During P-GMA welding their respective mean current or welding current, along with arc voltage and wire feed speed was displayed on the LED screen fitted on the control panel of the power source. To verify the values displayed on the LED screen the power source was also connected to a personal computer equipped with WMS4000 software to record on line the variation in welding current and arc voltage during operation (Fig.5.3 (a,b)). A wire feed measuring instrument was also used to check the accuracy of setting of the wire feed speed in operation.

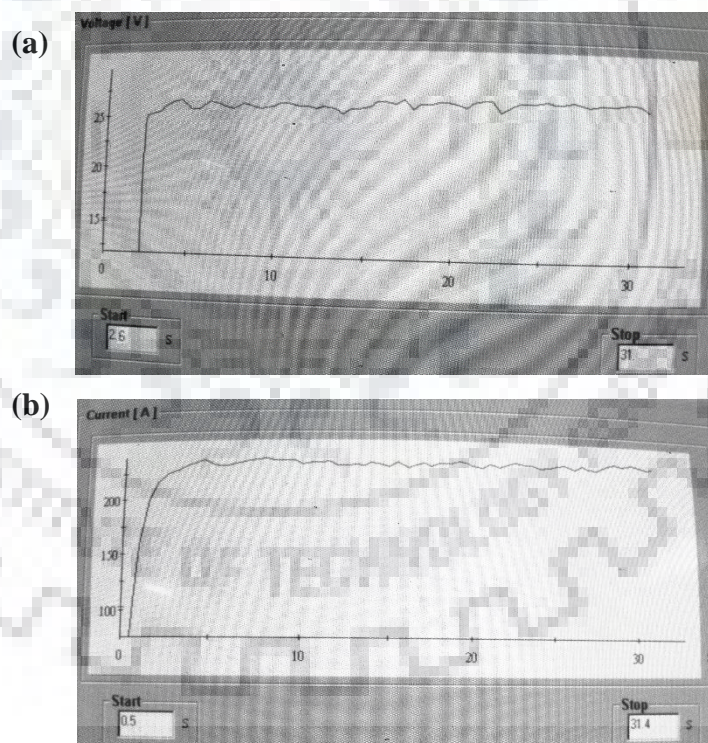


Figure 5-3 Typical behaviour of recording of WMS4000 software of (a) arc voltage, 25V (b) welding current, 240A.

The welding current and arc voltage was recorded by a transient recorder having a maximum resolution of 1 MHz suitably connected to the welding circuit for simultaneous recording of their behaviour during welding. The potential drop across a standard shunt (75 mV

= 600 A) connected in series with the welding circuit was fed to the transient recorder for estimation of the welding current. The transient arc voltage was measured by connecting the other channel of the transient recorder parallel to the welding circuit. The transient arc voltage and welding current were simultaneously recorded and displayed on the screen of the recorder having time (s) as ordinate and potential (V) as abscissa. During pulsed current welding the set values of the pulse parameters such as I_p , I_b , t_p and f were verified with their characteristics appeared in the transient recorder.

5.4.2. Thermal behaviour

5.4.2.1. Measurement of temperature of weld pool

The temperature of the weld pool was recorded during bead on plate deposition with the help of an R-Type thermocouple (Platinum-13 % Platinum Rhodium) of 0.25 mm diameter. The thermocouple was connected with computer through a “Strain Buster” (decentralized strain/temperature measuring module) for recording the output. The Strain buster was capable of recording the output of the thermocouple at a time interval of 10 ms in both of its two channels. The circuit diagram along with cooling system of welding torch head, strain buster and the photograph of complete welding and recording setup have been shown in Fig. 5.4, Fig. 5.5 (a) and (b) respectively.

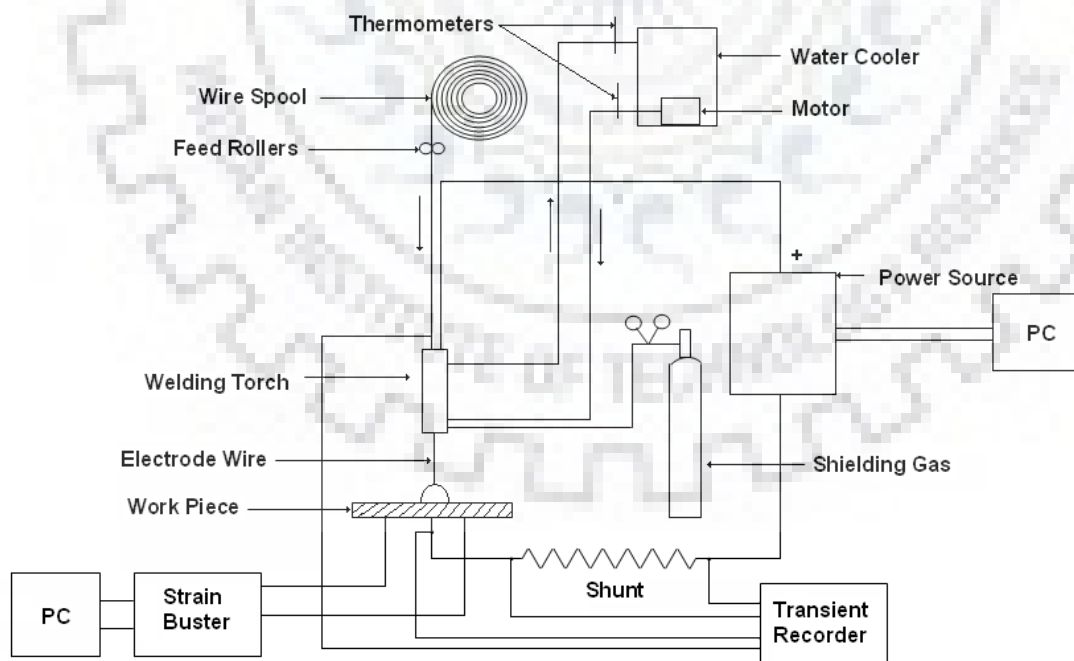


Figure 5-4 Schematic circuit diagram of welding and recording set up along with cooling system of torch head.



Figure 5-5 (a) Photograph of the strain buster (b) Photograph of the experimental set up used for welding.

5.4.2.2. Estimation of heat input (Ω)

The heat input (Ω) of P-GMAW process can be estimated as a function of welding or mean current (I or I_m), arc voltage (V), welding speed (S) and arc efficiency (η_a) as follows [Maruo H. et al 1984].

$$\Omega = \frac{\eta_a \times V \times [I(\text{or})I_m]}{S} \quad (5.1)$$

The mean current (I_m) of P-GMAW process as a function of base current (I_b), peak current (I_p), base current duration (t_b) and peak current duration (t_p) may be obtained as [Lancaster 1984] as

$$I_m = \frac{(I_b t_b + I_p t_p)}{(t_b + t_p)} \quad (5.2)$$

In case of ER308L grade electrode/filler metal under argon gas shielding the η_a of GMAW processes has been considered as 70% to 85% [Christensen et al 1965].

5.4.2.3. Estimation of average weld pool temperature

The average weld pool temperature (T_{WP}) of P-GMAW process has been estimated [Goyal et al 2008] by considering the heat transfer by superheated droplets of molten filler metal to the weld pool (Q_f) and temperature (T_d) of the point ($x(\xi)$, y , z) due to arc heating using double ellipsoidal heat source as follows (Fig.5.5).

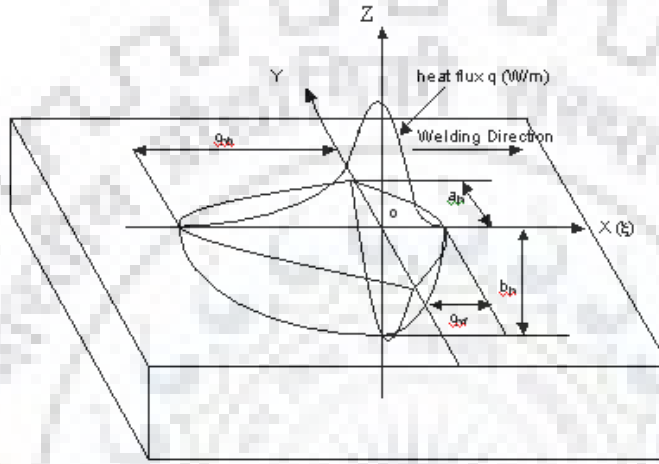


Figure 5-6 Schematic diagram of double ellipsoidal heat source (volumetric heat source).

$$T_{WP} = \frac{Q_f}{2.\pi.k} e^{-\lambda.S.\xi} \cdot \left[\frac{e^{-\lambda.S.R}}{R} + \sum_{n=1}^{\infty} \left(\frac{e^{-\lambda.S.R_n}}{R_n} + \frac{e^{-\lambda.S.R'_n}}{R'_n} \right) \right] + T_d \quad (5.3)$$

Where, λ and k are thermal diffusivity and thermal conductivity of base metal respectively. The R and ξ are distance (mm) of the point with respect to the central axis and along the x -axis of the welding arc respectively. R , R_n and R'_n are

$$R = \sqrt{\xi^2 + y^2 + (z - h)^2} \quad (5.4)$$

$$R_n = \sqrt{(2.n.d - (z - h))^2 + \xi^2 + y^2} \quad (5.5)$$

$$R'_n = \sqrt{(2.n.d + (z - h))^2 + \xi^2 + y^2} \quad (5.6)$$

Q_f is the heat transferred to the weld pool by the droplets of super heated filler metal and T_d is estimated as follows.

$$T_d = \frac{3\sqrt{3} \cdot Q_{AW}}{\rho \cdot c \cdot \pi \sqrt{\pi}} \int_0^t \left[\frac{dt'}{\left(\frac{A'}{\sqrt{(12a(t-t') + c_{hf}^2)}} + \frac{B'}{\sqrt{(12a(t-t') + c_{hb}^2)}} \right)} \right] + T_0 \quad (5.7)$$

The complete modeling detail for estimation of T_{WP} has been reported elsewhere [Goyal et al 2008].

5.4.2.4. Estimation of weld isotherm

The weld isotherm of dissimilar weld joint as a function of heat input (Ω), I_m and ϕ of different temperature for P-GMAW process has been estimated and plotted using the software origin 6.1 using Eq. 5.3. The weld isotherm dictates the geometrical and thermal aspects of weld pool ultimately governing the properties of the weld.

5.5. Weld Bead on Plate Experimentation

The studies on weld bead on plate experimentation give a through understanding of thermal and geometrical aspects of weld deposite through which it is possible to identify an optimised welding condition to apply in preparation of narrow gap dissimilar weld of thick section especially with ultra-narrow groove width having desired weld properties.

5.5.1. Welding

The welding was carried out by rigidly fixing the base plate in fixture to avoid any distortion during welding. The base plate was throughly cleaned before carrying out weld bead deposition to remove any dirt or grease adhering to the surface. The bead deposition was carried out in flat position by keeping the welding torch perpendicular to the base plate maintaining an electrode extension of 16-17 mm using the commercial (99.98%) argon gas as shielding at a flow rate of 18L/min. The flow rate of the gas was controlled through flow meter with a pressure regulator fitted to the gas cylinder. The bead on plate study was carried out at a constant arc voltage of $25 \pm 1V$ considering three levels of mean current (I_m) and 2 levels of heat input (Ω) of 200, 220 and 240A and 7.63 ± 0.4 , $9.81 \pm 0.5 kJ/cm$ respectively. The heat input was varied through a variation of welding speed.

In case of P-GMAW process at a given value of mean current, I_m , the pulse parameters I_p , I_b , t_p and f were varied to get different values of summerised influence of pulse parameters defined by the factor ϕ [Ghosh et al 1994, Ghosh 1999, Ghosh et al 2000, Ghosh et al 2001 and Ghosh et al 2007] of 0.05 and 0.25 respectively. For every set of parameters three weld beads, each of 100mm in length, were deposited and properties were studied to ensure reproducibility

of the process. The combinations of parameters facilitate to study and correlate the influence of pulse parameters and heat input on various characteristics of weld bead. The welding parameters used during bead on plate experimentation using P-GMAW process are shown in Table - 5.2 respectively.

Table 5-2 Pulse parameters and corresponding thermal behaviour used in weld bead on plate deposition by P-GMAW process.

Arc Voltage (V)	Heat Input (kJ/cm)	Welding Speed (S) (cm/min)	Mean Current (I_m) (A)	ϕ	Pulse Parameters					Thermal Behaviour	
					I_p	I_b	f (Hz)	t_b (sec)	t_p (sec)	Q_{AW} (J/s)	Q_r (J/s)
25±1	7.63±0.4	26.4	200±3	0.15	289	123	90	4.12	3.51	3614	4697
	9.81±0.5	21.4		0.25	246	164	95	4.07	3.49	3445	5204
	7.63±0.4	29.1	220±2	0.15	332	125	107	3.97	3.66	4136	4725
	9.80±0.5	23.4		0.25	295	164	106	4.09	3.51	2771	3925
	7.63±0.4	31.8	240±4	0.15	350	121	124	3.47	3.17	2812	4304
	9.81±0.5	25.7		0.25	316	164	126	3.84	3.01	1111	4070

5.5.2. Measurement of thermal behaviour of weld

At a given set of pulse parameters, the temperature of molten weld pool was measured during bead on plate weld deposition in order to verify validity of the analytical expression of eq. 5.3. To get weld pool temperature after achieving its stability two thermocouples were inserted from the bottom of the base plate in two different locations at distances of about 40 and 80 mm from the run on position of welding as schematically shown in Fig. 5.7(a). The two wires of the thermocouple are kept separate with the help of sleeve and beads. The beads were push fitted in the hole prepared by drilling process. Thermocouples were placed at different depths from the surface of weld as shown in Fig. 5.7(a). The depth of placement, D_T , of thermocouple as schematically shown in Fig. 5.7(b) was decided based on the estimation of weld isotherm matching with melting point of the austenitic stainless (γ -SS) steel as base plate using the analytical model proposed earlier [Goyal et al 2008], so that the tip of the thermocouple comes under fused weld pool without having a direct contact with the welding arc. In this regard the limitation of proposed model as it is unable to estimate the temperature of the weld pool within a radius of 2mm from arc center was duly considered. The weld isotherm was estimated by considering the temperature dependent thermo-physical properties of materials [Tamura et al 1988] as shown in Fig. 5.8 for austenitic stainless steel which are assumed to be in close approximation to those of the HSLA used in this work. The weld thermal

cycle was measured by using computerized data recorded as output of the thermocouples through “Strain Buster” as explained in section 5.4.2.1.

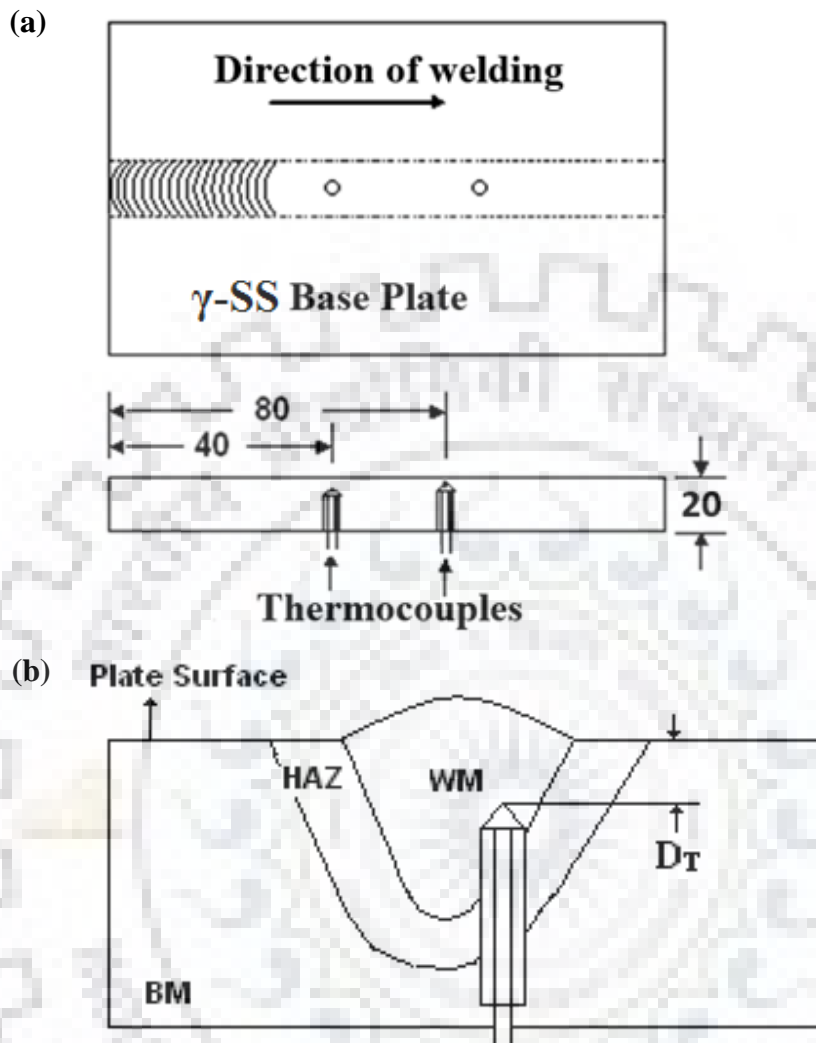


Figure 5-7 (a) Schematic diagram showing location of thermocouples in bead on plate deposition (b) Schematic diagram showing the depth of placement of thermocouple (D_T) and typical macrograph showing placement of thermocouple in weld pool.

The characteristics of weld bead observed at various welding parameters of different welding processes were analyzed with respect to geometrical aspects of weld bead as well as microstructure of weld and HAZ. The different aspects of the studies on weld bead characteristics have been detailed out as below.

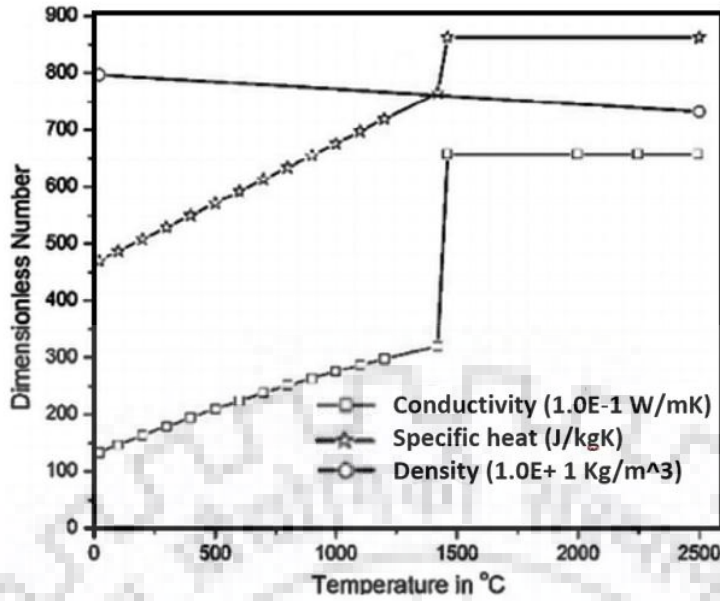


Figure 5-8 Temperature dependent thermo-physical properties of commercial mild steel.

5.5.2.1. Geometrical aspects of weld pool

The transverse section of weld bead collected from its central part of weld deposition assuring a stable welding was polished by standard metallographic procedure and etched by using electrolytic etching in 10% oxalic acid solution to reveal the weld geometry and its microstructure. The schematic diagram of geometrical aspects of weld bead has been shown in Fig. 5.9. The characteristics of different aspects of weld bead were studied by measuring the bead width (W_b), depth of penetration (P_d), height of reinforcement (H_r), area of fusion (A_F) and area of weld deposit (A_w) as well as deposition characteristics of weld bead such as deposition form factor (FF), fraction of base metal fusion per unit mass of bead deposition (F_{BMF}), dilution % (D_L) and bead toe angle (B_{TA}) by graphical method with the help of image analyzer software installed in a computer. The deposition form factor (FF), dilution of weld deposit (D_L) and fraction of base metal fusion per unit mass of bead deposition (F_{BMF}) were estimated in terms of geometric solution as follows.

$$FF = \frac{W_b}{H_r} \quad (5.8)$$

$$\%Dilution = \frac{A_F}{A_F + A_w} \times 100 \quad (5.9)$$

$$F_{BMF} = \frac{A_F}{A_w} \quad (5.10)$$

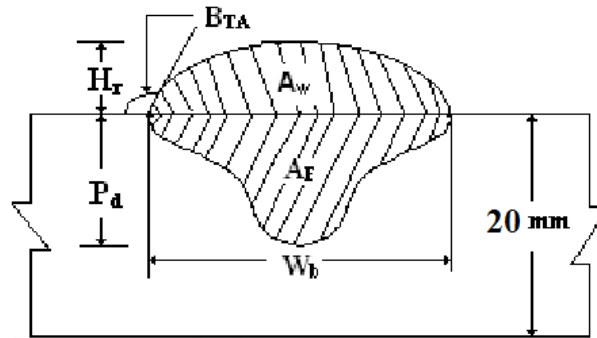


Figure 5-9 Schematic diagram showing geometrical aspects of weld bead.

5.6. Preparation of Single Seam Multi Pass Ultra-narrow Gap Weld Joints

P-GMA welding process is used for good arc stability by using commercial argon of 99.98% purity as shielding gas at a gas flow rate of 10-12 l/min, where contact tip to work piece distance was kept constant at about 16-17mm in order to facilitate proper torch manipulation in ultra-narrow groove.

5.6.1. Preparation of weld groove

The austenitic stainless steel (γ -SS 304LN) and controlled rolled high strength low alloy (HSLA) steel plates of 25mm thick of size 250 x 100mm has been used in preparation of weld joint. The conventional V-groove as per AWS specification [AWS hand book, 1994] and suitably designed ultra-narrow groove as schematically shown in Figs. 5.10(a-b) respectively were prepared by proper machining of the plates. The groove surface was checked visually followed by dye penetrant test to ensure the defect free groove wall.

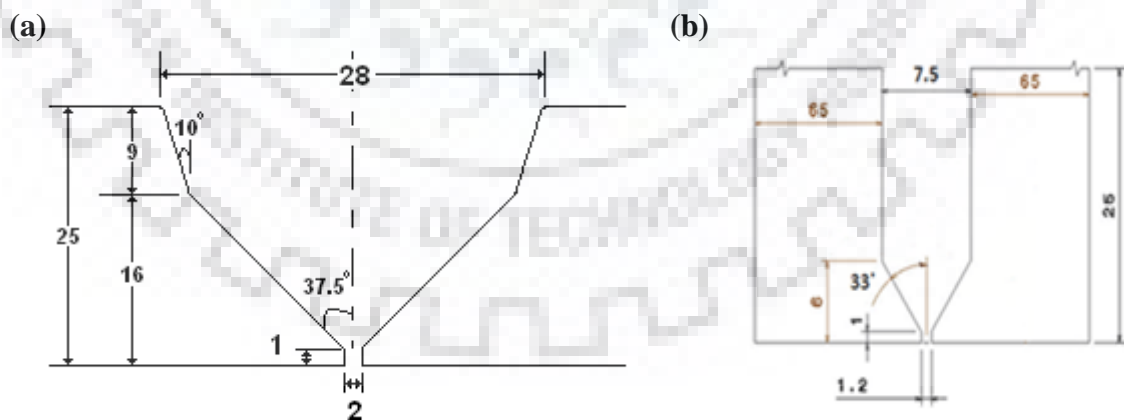


Figure 5-10 Schematic diagram of (a) conventional V-groove (CG) and (b) Ultra-narrow groove (UNG).

5.6.2. Preparation of weld joints

The welding was carried out by multi pass multi seam per layer deposition in case of conventional V-groove (CG) while for Ultra-narrow groove (UNG) the welding was carried out by multi pass single seam per layer deposition technique having the electrode placed at the groove centre with no angle of attack to the groove wall. The schematic diagram showing the weld deposit under these two techniques has been shown in Fig. 5.11(a-b). The dissimilar weld joints were prepared by using direct current electrode positive polarity as stated earlier. The root was supported by a copper backing plate fitted in a thick mild steel supporting plate of the fixture as stated in section 5.3.1. Prior to weld deposition, the both (γ -SS and HSLA Steel) base plates were thoroughly cleaned to remove the excess oxide layer and any dirt or grease adhering to the faying surface. The welding parameters used during preparation of weld joints under different welding process and procedures are shown in Table – 5.3.

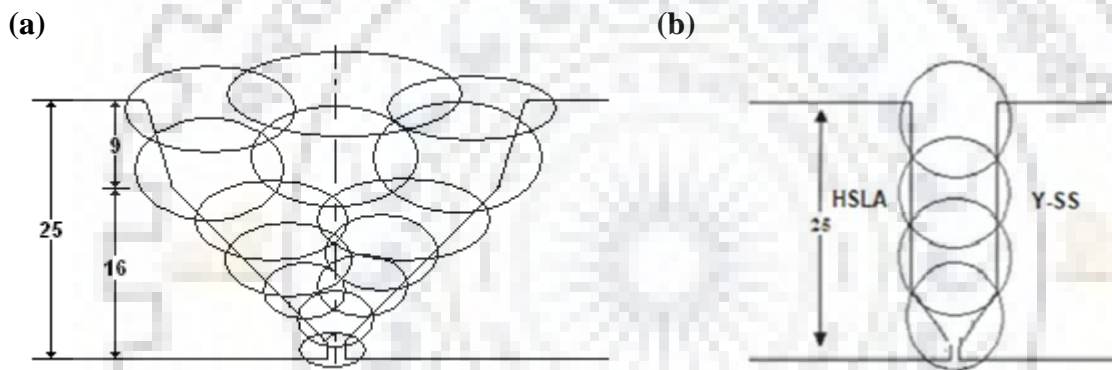


Figure 5-11 Schematic diagram of (a) multi pass multi seam per layer deposition and (b) multi pass single seam per layer deposition technique.

Table 5-3 Welding parameters used in weld joint studies under P-GMA welding process.

Arc Voltage, V	Heat Input, Welding Speed, Mean Current, Ω , kJ/cm S, cm/min I_m , A			ϕ	Pulse Parameters				
					I_p	I_b	f (Hz)	t_b (sec)	t_p (sec)
25 \pm 1	7.63 \pm 0.4	26.4	200 \pm 3	0.15	289	123	90	4.12	3.51
	9.81 \pm 0.5	21.4		0.25	246	164	95	4.07	3.49
	7.63 \pm 0.4	29.1	220 \pm 2	0.15	332	125	107	3.97	3.66
	9.80 \pm 0.5	23.4		0.25	295	164	106	4.09	3.51
	7.63 \pm 0.4	31.8	240 \pm 4	0.15	350	121	124	3.47	3.17
	9.81 \pm 0.5	25.7		0.25	316	164	126	3.84	3.01

5.6.3. Planning for collection of Specimen for different studies

Sectioning of the dissimilar weld joints of γ -SS and HSLA steel for fabrication of various test specimens was made with the help of power hacksaw. The collection of specimens for mechanical testing and metallography from different locations of the weld joint has been schematically shown in Fig. 5.12.

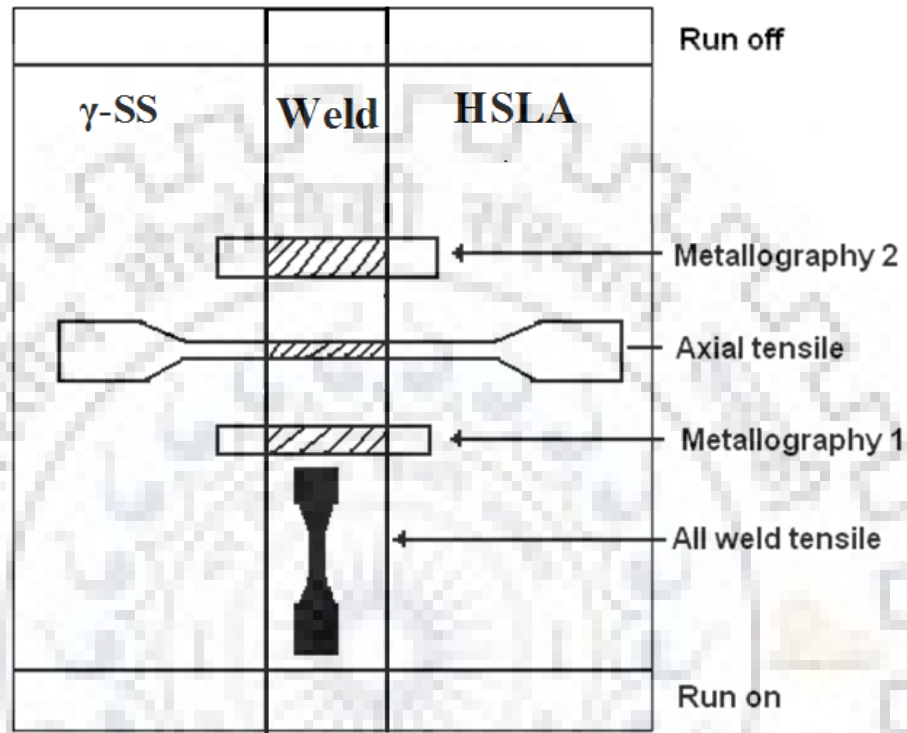


Figure 5-12 Schematic diagram of collection of test specimens from the dissimilar weld joint.

5.6.4. Non-destructive testing of weld joints

NDT of welds was carried out in two steps, first by carrying out dye penetrant test intermittently between the passes and secondly after the completion of weld joint by ultrasonic test. The methodology followed for carrying out these tests is explained in the following sections.

5.6.4.1. Dye penetrant test

The specifications for the dye penetrant test were prepared as per ASME section V. The test was conducted to detect and rectify the presence of any flaws at the weld groove surface after its machining and the filler passes carried out by P-GMA welding process.

5.6.4.2. Ultrasonic test

The specifications for ultrasonic test of weld joint were prepared as per ASME section V. The weld joints were fully tested by ultrasonic examination.



Figure 5-13 Photograph of Ultrasonic test on ultra-narrow gap weld joints.

5.6.5. Characterization of weld joint

5.6.5.1. Geometrical characteristics of weld joint

Geometrical characteristics of dissimilar weld joint of γ -SS and HSLA steel have been studied with respect to its weld appearance and size. The size of weld as revealed on the metallographically polished and electro etched transverse section of all the dissimilar weld joints has been graphically measured on the macro photographs of the joints captured by using automatic digital camera. The measurement was carried out in a computer with the help of an image analyzer software.

5.6.5.2. Thermal analysis of weld joint

A thermal model based on geometrical and thermal aspects of weld pool has been developed (chap.4) for producing a sound dissimilar weld joint using multi pass single seam per layer deposition technique in ultra-narrow groove by P-GMAW process. The model has been analysed considering different expressions in the light of production of a weld joint having no lack of fusion with the groove wall by comparing the result of it by experimental one.

5.6.5.3. Estimation of transverse shrinkage stress

During P-GMA welding at a given heat input per weld pass in both the multi pass multi layer weld deposition in conventional groove (CG) and multi pass single seam per layer deposition in ultra-narrow groove (UNG), the transverse shrinkage was measured using Vernier caliper having least count of 0.01 mm. The shrinkage was measured at a given straining length of 80 mm [Radaij 1992] from weld center line as shown in Fig. 5.14 (a). The measurement was carried out at each weld pass with respect to shrinkage of the plate from its initial position. After completion of welding the deflection of the plate from its initial position was measured using a

dial gauge placed at a given distance of 100 mm from weld center line (L_c) as shown in Fig. 5.14 (b).

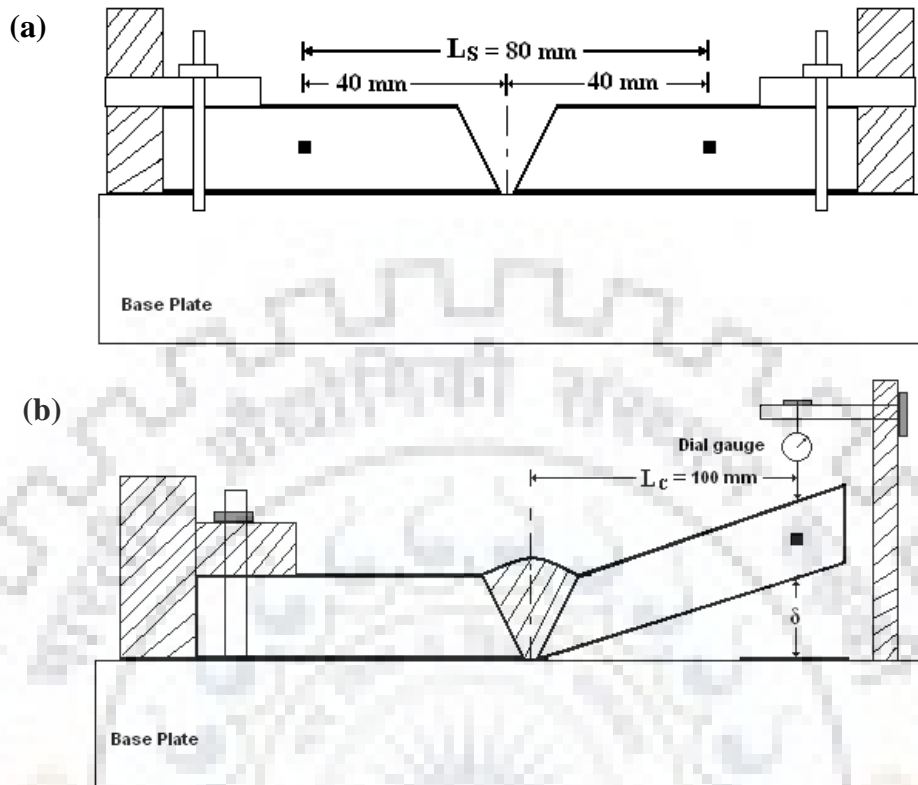


Figure 5-14 (a) Schematic diagram showing the technique of measurement of transverse shrinkage (b) Schematic diagram showing the technique of measurement of deflection.

The transverse shrinkage stress (σ_{tr}) developed in the weld joints under different welding processes, groove size and parameters was estimated through measurement of transverse shrinkage (Δ_{tr}) and restraint intensity (R) acting on the weld as follows.

$$\sigma_{tr} = \frac{\Delta_{tr}}{d} \times R \quad (5.11)$$

$$R = \frac{\eta^* \times E \times d}{L_w} \quad (5.12)$$

Where, d is the plate thickness (25mm), E is the Young's modulus of base material (210×10^3 MPa), L_w is the weld length (250 mm) and η^* is shape factor (0.15) [Radaij 1992 and Koichi Masubuchi 1980].

5.6.5.4. Estimation of bending stress

The bending stress (σ_b) developed due to distortion of weld joints during preparation under varied thermal behaviour of different welding processes and procedures was also estimated [Radaij 1992 and Koichi Masubuchi 1980] as follows.

$$\sigma_b = \frac{\eta^* \times M \times d}{2 \times I^m} \quad (5.13)$$

Where, M is the bending moment, I^m is the moment of inertia and d is plate thickness. The M and I^m are estimated [Khurmi 2002] as follows.

$$M = \frac{F \times L_c}{8} \quad (5.14)$$

$$I^m = \frac{b \times d^3}{12} \quad (5.15)$$

Where, L_c is the distance of measuring point (dial gauge tip, Fig. 5.13(b)) from the central axis of weld joint and b is plate width. The force (F) generated due to distortion of the plate was estimated as follows [Khurmi 2002] with the help of measured deflection (δ) by considering it as a case satisfying fixed beam theory in view of both end of the plate is fixed as explained earlier (Fig. 5.13(a)).

$$F = \frac{192 \times E \times I^m \times \delta}{L_c^3} \quad (5.16)$$

The F has been suitably estimated under different welding processes, procedures and parameters.

5.6.5.5. Metallographic studies

Studies on weld

The transverse sections of the base metal and the weld joints prepared by using the P-GMAW process were polished by standard metallographic procedure and etched by using electrolytic etching in 10% oxalic acid solution (Fig.5.15). Metallographic studies under optical microscope were carried out on the multi pass multi seam per layer (MPMSPL) weld deposit and multi pass single seam per layer (MPSSPL) weld deposit. The studies have been carried out largely at the central part of each weld deposit and reheat refined region of the weld passes. The microstructure of the weld has been analyzed by measuring its proportional content of columnar or coaxial dendrite and morphology of equi-axed grain region of the reheat refined. The dendrite fraction measurement was carried out, with the help of Axio vision software based image analyzer facility connected with the optical microscope. The image analysis was carried out on at least 21 randomly selected spots on weld joints.

Studies on HAZ

Studies on heat-affected zone (HAZ) of the base metal adjacent to fusion line were carried out on the transverse section of metallographically prepared and etched specimens of the weld

joints prepared by using different groove size and parameters as stated earlier. The studies were carried out under optical microscope (Leica make Fig.5.15) on the HAZ at both sides of the weld joint.

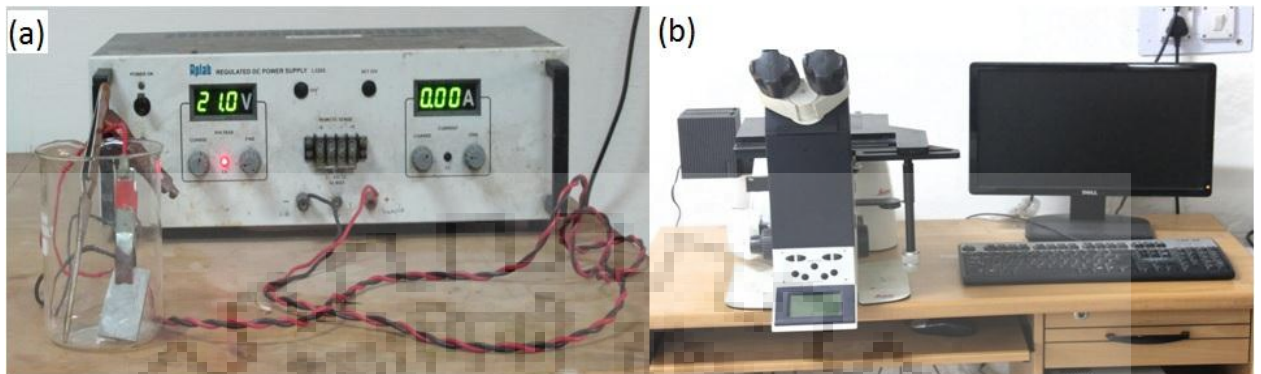


Figure 5-15 Photograph of Equipments used for microstructure recording (a) Electro-etching equipment (b) Leica Optical microscope

5.6.5.6. Porosity/Inclusion content

The porosity/inclusion content of base metal and weld deposit was measured with the help of image analyzer software used in optical microscopic studies on the metallographically polished un-etched transverse section of weld joint. The analysis was carried out on at least 21 randomly selected different locations of the matrix using point counting method. The analysis was made considering the area fraction of practically round shape black spots observed on matrix of weld deposit as porosity or a void containing inclusions in it. The volume fraction of the spots present in the matrix was estimated by assuming it as a linear function of their measured area fraction.

5.6.6. Studies on mechanical properties

The mechanical properties were studied by considering tensile properties as well as hardness across the weld.

5.6.6.1. Tensile testing

Tensile properties of the base metal and weld joint, such as the ultimate tensile strength (UTS), yield strength (YS) and percentage elongation were studied by using round tensile test specimens as per ASTM E8M standard. The tests were performed under uniaxial loading at a crosshead speed of 1mm/min using a tensile testing machine Instron Medium Capacity servohydraulic system includes 8802 systems accepting actuators upto 250kN capacity. The photograph of the Instron 8802 servohydraulic tensile testing machine used for testing has been shown in Fig.5.16. Tensile properties of weld joint were studied by using specimens from axial weld (weld at its centre) and all weld metal. The axial weld specimens were prepared by keeping

the weld at center of the gauge length whereas all weld specimens were prepared by machining out specimens from the all weld deposit. The dimensions of the base metal, axial weld and all weld specimens are schematically shown in Figs. 5.16 (a-c) respectively. The yield strength was estimated at 0.2% offset strain on stress-strain diagram of the uniaxial tensile test. Fracture surface of the base metal and all weld tensile specimens was examined in detail under scanning electron microscope as shown in Fig.5.18.



Figure 5-16 Photograph of the Instron 8802 servohydraulic tensile testing machine.

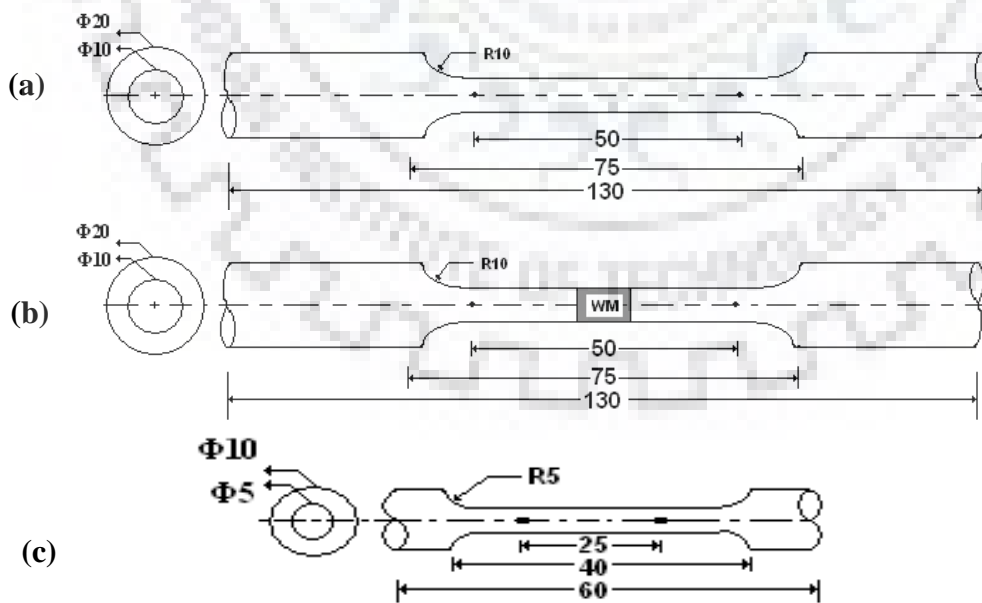


Figure 5-17 Schematic diagram of the tensile specimens (a) base metal (b) axial weld and (c) all weld metal (All dimensions are in ‘mm’)



Figure 5-18 Photograph of the Scanning Electron Microscope.

5.6.6.2. Hardness measurement

The hardness of the dissimilar weld joint across the weld and HAZ was measured by Vickers micro hardness testing of Leitz Wetzlar Germany at a load of 100 grams having provision of magnification of image upto X500. Prior to carrying out testing the machine was calibrated by measuring hardness of a standard sample at the same load. The photograph of the Vickers micro hardness tester used in the present study has been shown in the Fig. 5.19.



Figure 5-19 Photograph of the Vickers micro hardness tester.



This chapter presents analysis of the proposed thermal model and verification of it for preparation of sound ultra-narrow gap dissimilar weld joint of thick γ -SS and HSLA steel plates using MPSSPL narrow gap welding technique. The soundness of the ultra-narrow gap weld is primarily considered by its quality assuring the presence of no lack of groove wall fusion. The results of various experiments as entails in experimentation are presented and described. This chapter also describes the analysis of results in order to understand the influence of pulse current GMA welding processes and parameters on welding of 25 mm thick γ -SS and HSLA dissimilar steel plate. The characterization of weld joints has been made with respect to their shrinkage stress, mechanical and metallurgical properties resulting from different welding parameters producing sound weld joint. Necessary control of the welding parameters to improve weld quality has been analysed in the light of the prescribed model.

6.1. Characteristics of Base and Filler Materials

The base materials of 25 mm thick plates of γ -SS and HSLA steel has been characterised with respect to their microstructure, hardness, tensile properties and impact toughness which may be influenced by the thermal characteristics of arc welding. These observations have been used as a reference point to study the variation in characteristics of base metal of HAZ with a change in welding conditions.

6.1.1. Chemical Composition

Chemistry of the γ -SS (304LN) and HSLA (SAILMA-410HI/SA543 grade) base metal as well as the filler metals used in this work for producing dissimilar conventional and ultra-narrow gap welds is given in Table-6.1. The results primarily show that the chemical compositions of base metal and filler metals are in agreement to those prescribed in standard (ASTM) and the test certificate given by the supplier. It has been further observed that the GMAW filler wire is having relatively lower carbon and higher chromium content in comparison to that of SMAW electrode. It may have a beneficial effect in reducing or preventing micro fissuring in austenitic stainless steel weldments.

Table 6-1 Chemical compositions of γ -SS and HSLA steel base materials and welding filler metals.

Material	Testing method	Chemical analysis (Wt.%)										Equivalents	
		C	Cr	Ni	Mn	N	Mo	Si	Cu	S	P	Cr _{eq}	Ni _{eq}
Base metal γ -SS	ASTM	0.035	18-20	8-11	2.0	0.1- 0.16	-	0.75	-	0.03	0.04	-	-
	Test certificate	0.024	18.8	9.3	1.7	0.15	-	0.55	-	0.001	0.022	-	-
	*	0.022	19.0	9.1	1.8	0.16	0.19	0.57	0.30	0.002	0.021	19.21	13.22
Base metal (HSLA)	Test certificate	0.14	0.023	0.04 (v)	1.46	0.02 (Ti)	0.04 (Nb)	0.28	0.02	0.008	0.02	-	-
	SAILMA - 410HI/ SA543	*	0.154	0.014	0.08 (v)	1.50	0.02 (Ti)	0.04 (Nb)	0.31	0.03	0.02	0.022	-
GMAW filler wire (ER308L)	Test certificate	0.022	18.5	9.6	1.3	-	0.10	0.39	0.08	0.007	0.016	-	-
	*	0.020	18.6	10.3	2.2	-	0.30	0.39	0.08	0.007	0.016	19.27	11.05

* indicates testing by spark emission optical spectroscopy.

6.1.2. Microstructure

Typical microstructures of the γ -SS and HSLA steel base materials having homogeneously distributed grains in the matrix has been shown in Fig. 6.1(a-b) and Fig. 6.2(a-b) respectively. The average grain diameter of the γ -SS and HSLA steel materials lies in the range of 14 ± 3 and $12 \pm 4 \mu\text{m}$ respectively corresponding to ASTM number of 9.5 and 9 respectively. The γ -SS and HSLA base metal contains negligible inclusion and porosity content as shown in Table-6.2. The microstructures of the γ -SS consist of commonly known equiaxed grain twin structure and HSLA (SAILMA-410HI/SA543 grade) consist of ferrite and pearlite along the lamination of matrix of banded structure which has shown in Fig. 6.1(a-b) and Fig. 6.2(a-b).

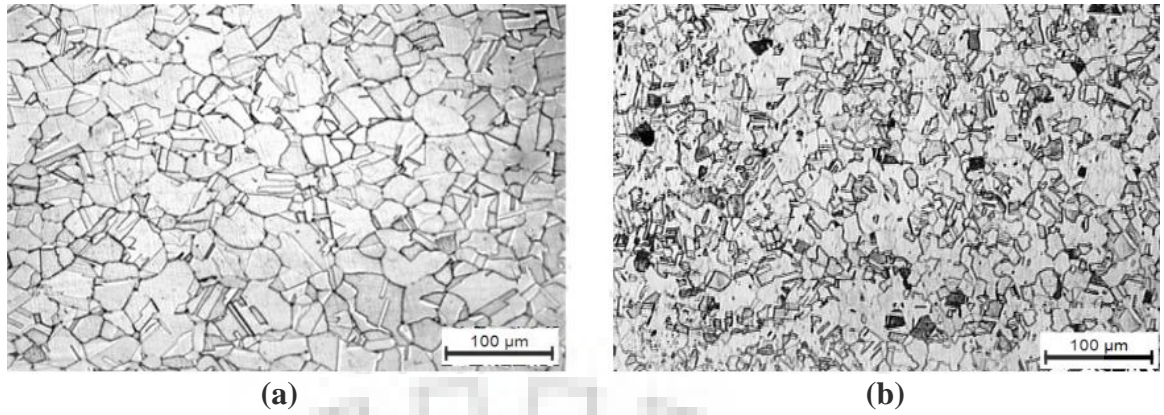


Figure 6-1 Typical microstructure of the γ -SS base metal (a) transverse direction and (b) longitudinal direction.

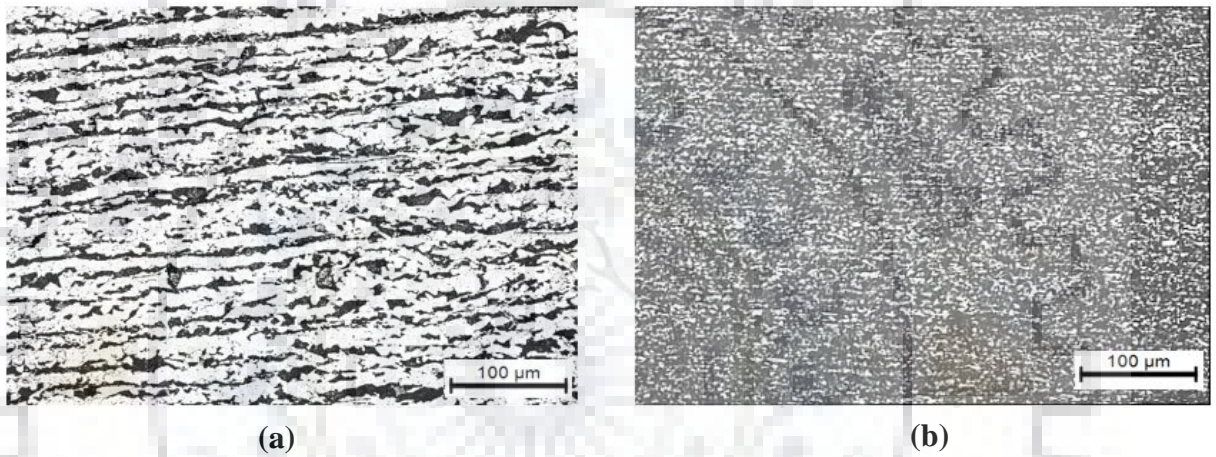


Figure 6-2 Typical microstructure of the HSLA steel base metal (a) transverse direction and (b) longitudinal direction.

Table 6-2 Inclusion content of dissimilar base Materials.

Process	Inclusions rating		Inclusion content, (Vol. %)
	Category	Severity level	
γ -SS Base Metal	B thin/B thick	0.7-1.5	0.20
	D thin/D thick	3.0-5.0	
HSLA Base Metal	B thin/B thick	0.43-1.8	0.17
	D thin/D thick	3.2-4.6	

6.1.3. Mechanical properties

6.1.3.1. Tensile properties

Tensile properties of the γ -SS and HSLA steel base materials in longitudinal and transverse directions of the plates with respect to direction of length of the component are shown in Table-6.3. The Table mainly shows that both the base metals are having comparatively higher yield

strength in longitudinal direction in comparison to that observed in transverse direction due to relatively smaller grain size Fig. 6.1(a-b) and Fig. 6.2(a-b). However, the ratio of yield strength (σ_y) to ultimate tensile strength (σ_u) of the base metals has not been found to vary significantly with the change in direction from the longitudinal to transverse one. Typical fractograph of the longitudinal tensile specimens of γ -SS and HSLA steel has been shown in Fig. 6.3. The wide spread fine dimples observed on the fractured surface (Fig. 6.3) indicates high ductility of the base metal.

Table 6-3 Tensile properties of base materials of different gauge length.

Material	Gauge length (mm)	Orientation	Tensile properties of base material						
			U.T.S. (MPa)		Y.S. (MPa)		YS/UTS Ratio	Elongation (%)	
γ -SS	25	Longitudinal direction	704	687	376	365	0.53	74.2	72.7
			686		362			72.5	
			669		357			69.7	
	50	Transverse direction	667	663	338	340	0.51	68.7	70.6
			664		340			70.8	
			658		342			72.5	
HSLA	25	Longitudinal direction	567	567	430	434	0.76	27	29
			565		432			29	
			570		441			33	
	50	Transverse direction	537	539	424	421	0.78	20	23
			539		421			26	
			543		419			25	

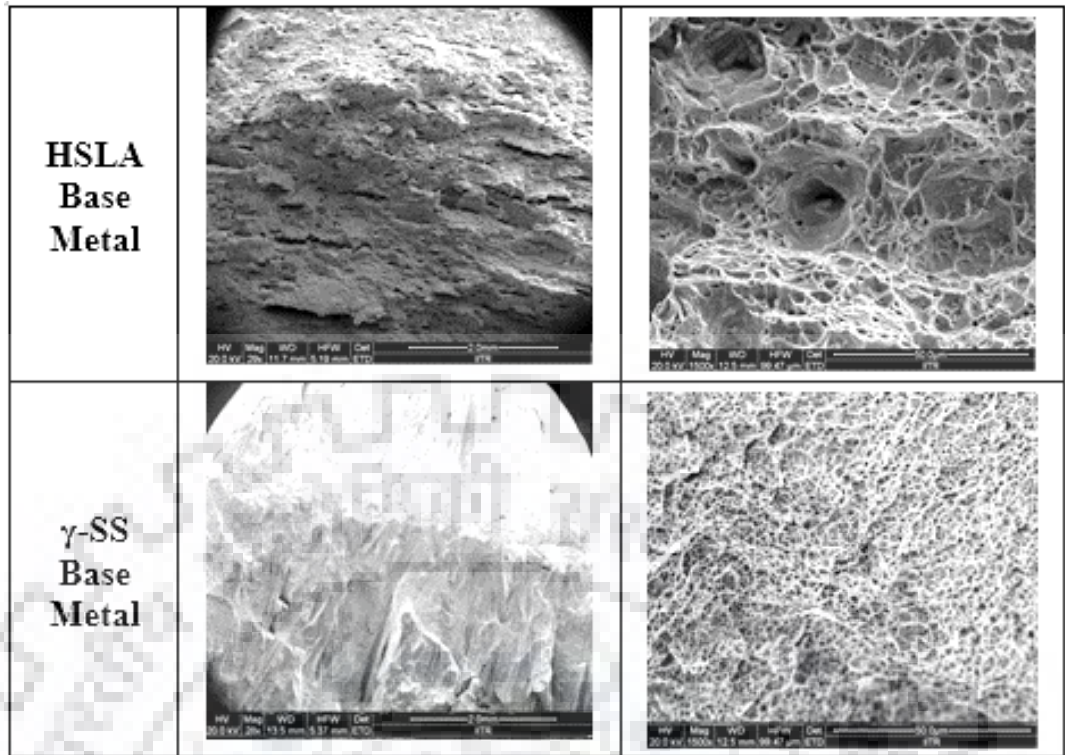


Figure 6-3 Typical fractograph of tensile sample at relatively low and high magnifications of HSLA steel base metal and γ -SS base metal.

6.1.3.2. Hardness

Typical indentation of Vickers's micro hardness test on the γ -SS and HSLA steel base material has been shown in Fig. 6.4(a-b). The indentation marks has not shown any pin cushioning effect resulting from sinking of the metal around the flat faces of the pyramid and hence depicts the true characteristics of the base materials. The observed hardness of the γ -SS and HSLA steel base metals has been found to lie in the range of 225-250 VHN and 176-184 VHN respectively.

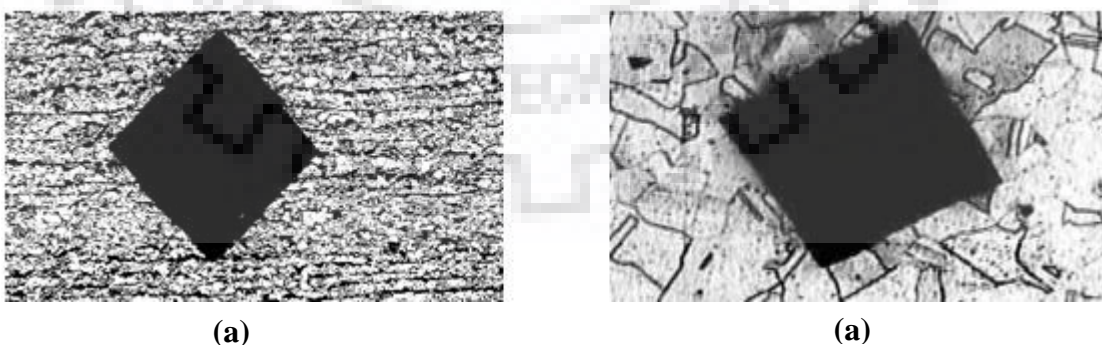


Figure 6-4 Typical indentation observed in (a) HSLA and (b) γ -SS steel base metal.

6.1.4. Summary

The γ -SS and HSLA steel base materials used for studies on bead on plate and weld joint are having homogeneously distributed equiaxed grains in the matrix along with negligible amount of inclusion/porosity. The base materials show comparatively finer grain size than that of commercially used austenitic stainless steel and structural steel resulting in to superior mechanical and fracture properties. Thus, thermal influence of welding process and procedure for joining of such steel must be criticality analyzed to impart comparable properties to the weld joint.

6.2. Studies on Newly Developed Nozzle Head Device

A narrow rectangular faced torch nozzle, suitable for appropriate manipulation inside a practically narrowest possible weld groove, has been designed by removing both of its lengthwise side walls as shown in Fig.3.3 (Chapter 3). This is done to avoid burning of the side wall of the nozzle being close to the electrode tip. As such the general approach of increase in wall thickness of the copper nozzle to avoid its burning could be ignored as it consequently enhances the nozzle width. Increase of nozzle width is not compatible to the objective of exploring GMAW with narrowest possible groove width in case of thick section butt welding. The use of such torch nozzle in narrow groove welding is considered by lengthwise placing of the rectangular faced nozzle in the direction of welding, where the walls of the narrow groove may virtually act as lengthwise side wall of the nozzle as schematically shown in Fig.3.5 (a) (Chapter 3). However, the success of such nozzle in producing sound weld having no discontinuity defect of lack of fusion primarily depends upon providing an appropriate oxidation protective inert gas shielding and enough thermal intensity to the weld pool required for necessary groove wall fusion and inter-pass fusion in single pas per layer of weld deposition. After each weld pass the deposited weld metal fill the weld groove and to maintain the contact tip to weld distance (15-17 mm) one has to uplift the welding nozzle. Such movement of welding torch or nozzle introduces an open exposure between the nozzle and groove wall of the plate. Thus, there is a requirement of shortening of the nozzle head as shown in Fig.3.5 (b) (Chapter 3) for effective shielding of arc zone by covering the opening between the nozzle and groove wall, which otherwise may introduce turbulence in shielding of the arc zone and degrade the weld quality.

6.2.1. Performance Analysis of Simulated Gas Shielding

The different in dynamics of shielding gas flow sets in during using the newly conceived narrow torch nozzle in narrow gap welding from that happens during using the conventional

nozzle of GMAW torch in conventional V-groove butt welding of 25mm thick plate (Fig.6.5) has been studied. In this study, 3-D model of using conventional nozzle with conventional groove has been developed for verifying the effect of inlet flow rate of shielding gas on its coverage area and velocity inside the conventional groove. The simulated results show (Fig.6.6) that the model developed for conventional nozzle with applied boundary condition gives adequate range of shielding gas velocity which is required (2-5 m/sec) [Dreher et.al.] to produce sound weld as shown in Fig. 6.7 (a-d).

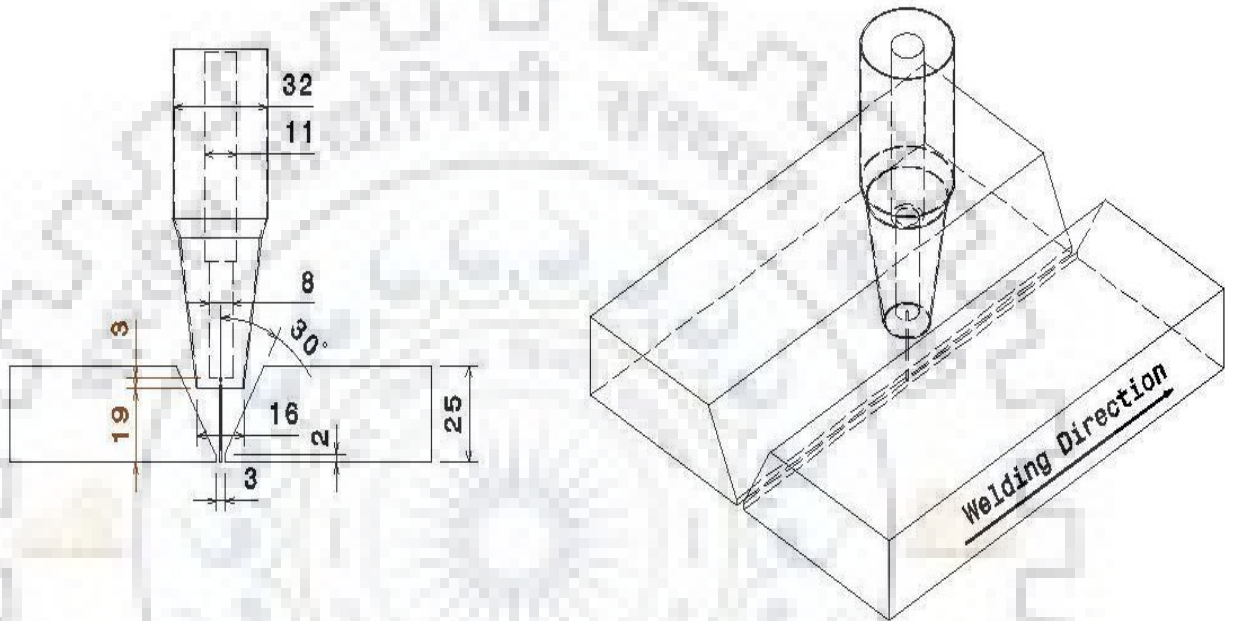


Figure 6-5 Schematic diagram of conventional GMAW welding torch with 28mm groove opening.

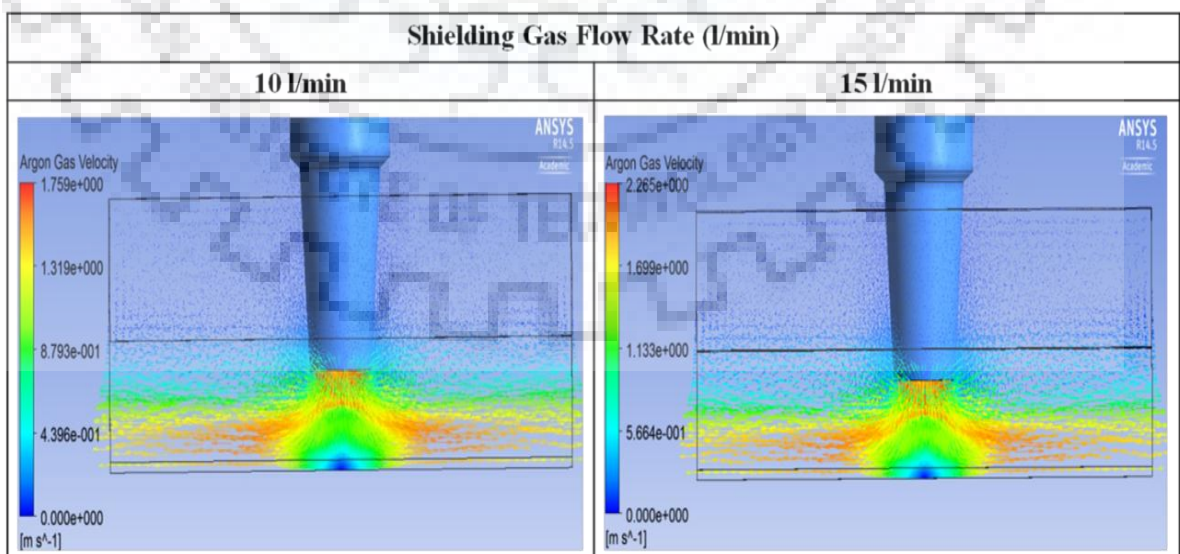


Figure 6-6 Simulation result of shielding gas flow in conventional groove opening of 28mm in 25mm thick plate.

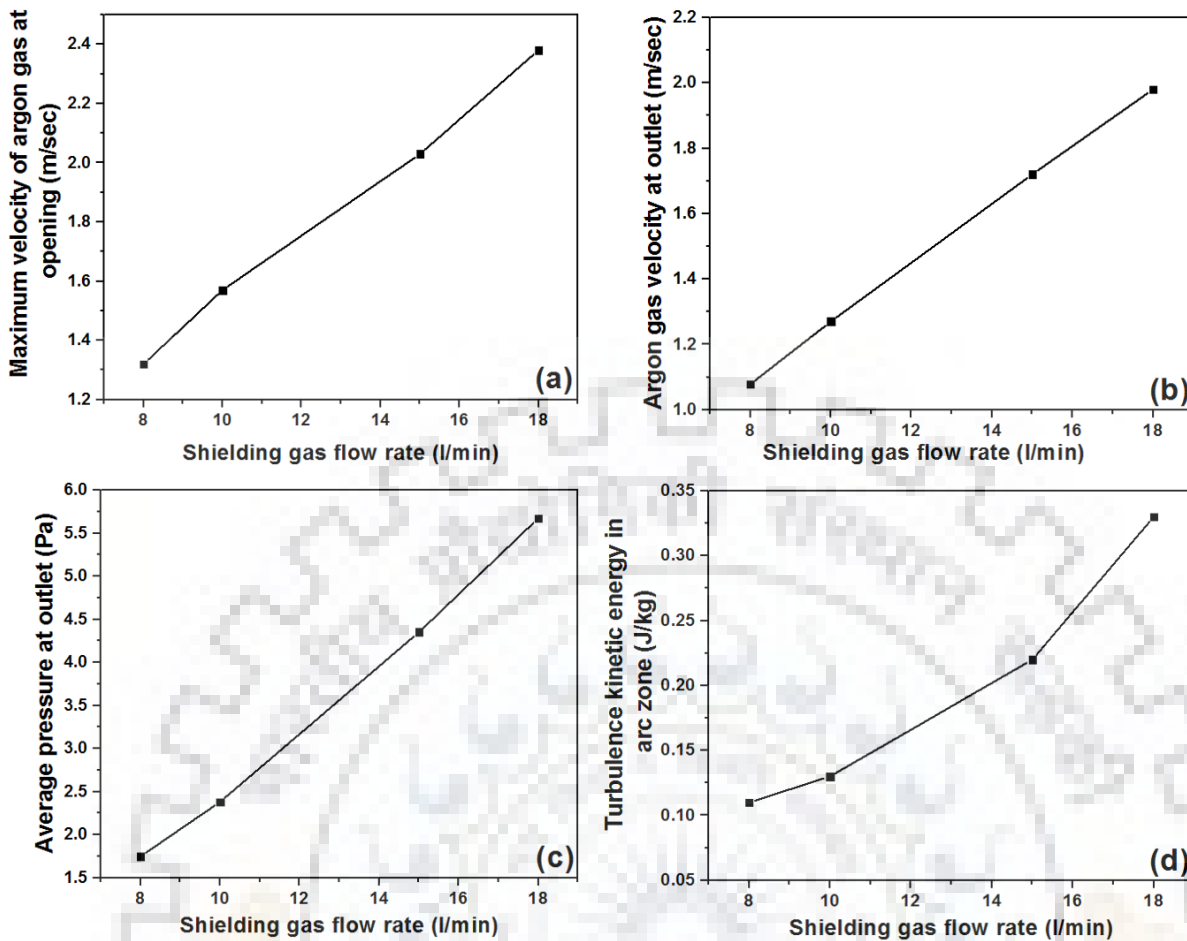


Figure 6-7 Influence of gas flow rate on different flow parameter.(a) Maximum velocity of argon gas at opening (m/sec), (b) Argon gas velocity at outlet (m/sec), (c) Average pressure at outlet (Pa) and Turbulence kinetic energy in arc zone (J/kg).

6.2.2. Shielding Gas Flow Characteristics

Primary objective of studying the results of simulated model analysis is to realize the possibility of manipulation of GMA welding torch in a narrowest possible groove of thick section welding and to produce a practically porosity and oxidation free sound weld with no lack of groove wall and inter pass fusion. Accordingly the attention is basically put forward to study the characteristics of shielding gas flow inside the narrow groove primarily to avoid turbulence and the arc characteristics promoting a weld pool efficient enough to give required groove wall fusion at different gas flow rate and nozzle tip angle as stated above. The arc characteristics are studied mainly with respect to its length and width (spread) especially to realize the thermal distribution in weld pool inside the narrow groove. The gas pressure at outlet of the welding torch as well as the velocity and turbulence kinetic energy of shielding gas flow at different zone was estimated.

At different projection angle of the nozzle tip varying from 0-60° the effect of flow rate at 5, 8, 10 and 12 l/min on flow characteristics of argon gas shielding inside the narrow groove has been shown in Fig.6.8. Similarly the influence of flow rate of the argon gas shielding and variation of projection angle of the nozzle tip on arc characteristics and thermal distribution inside the narrow groove has been shown in Fig. 6.9.

In Fig.6.8 and Fig.6.9 the results were evaluated using vector plots of shielding gas concentration at different zone of the nozzle inside the narrow groove. Fig.6.8 is a vector plot of shielding gas without MHD at different gas flow rate (5, 8, 10 and 12l/min) with 0° to 60° nozzle tip projection angle. It shows the streamline flow of shielding gas at different gas flow rate inside the narrow groove. The change in gas flow distribution with increasing nozzle tip angle is noticeable in Fig.6.8 which shows that the density of argon gas increases near the expected arc zone with increasing nozzle tip angle. This is due to the principle of the conservation of mass which states that the smaller the nozzle outlet area, the higher the velocity of the existing gas as simulated and demonstrated in Fig.6.9.

Fig.6.9 represents the temperature and the argon gas flow field in GMAW arc systems. When projection angle is increased the area of outlet is reduced, so the velocity, pressure and turbulence kinetic energy increases. To produce better shielding quality and arc stability turbulence kinetic energy should be minimum. It can be observed that as the outlet area of the nozzle decreases, the shielding gas columns to the adverse effects of the cross draft increases. All the characteristics may be understood by the principle of conservation of mass, which explains the resistant of shielding gas flowing through a narrower area, the velocity has to increase in order to maintain mass flow rate. It is also noticed that when the gas flow rate increases from 5 to 12l/min the visibility of arc is reduces. This may have happened due to the increase of outlet velocity of shielding gas which efficiently removes significant amount of the heat from the arc to its surrounding by absorption and convection. The effect of shielding gas flow rate and the nozzle tip angle of welding torch on the above mentioned characteristics of the arc zone have been shown in Table 6.4 and Table 6.5.

The observations of the simulation studies on different behaviors of gas flow inside the narrow groove have been plotted as a function of the projection angle of nozzle tip at different shielding gas flow rate as shown in Figs.6.8(a-b) and 6.9(a-b). The Fig.6.8 (a) and (b) shows that at a given gas flow rate the increase of projection angle of nozzle tip appreciably increases the maximum velocity of argon flow at the opening and outlet of the nozzle respectively that may create turbulence in gas flow. While at a given projection angle of nozzle tip the increase of gas flow rate also significantly enhances the same.

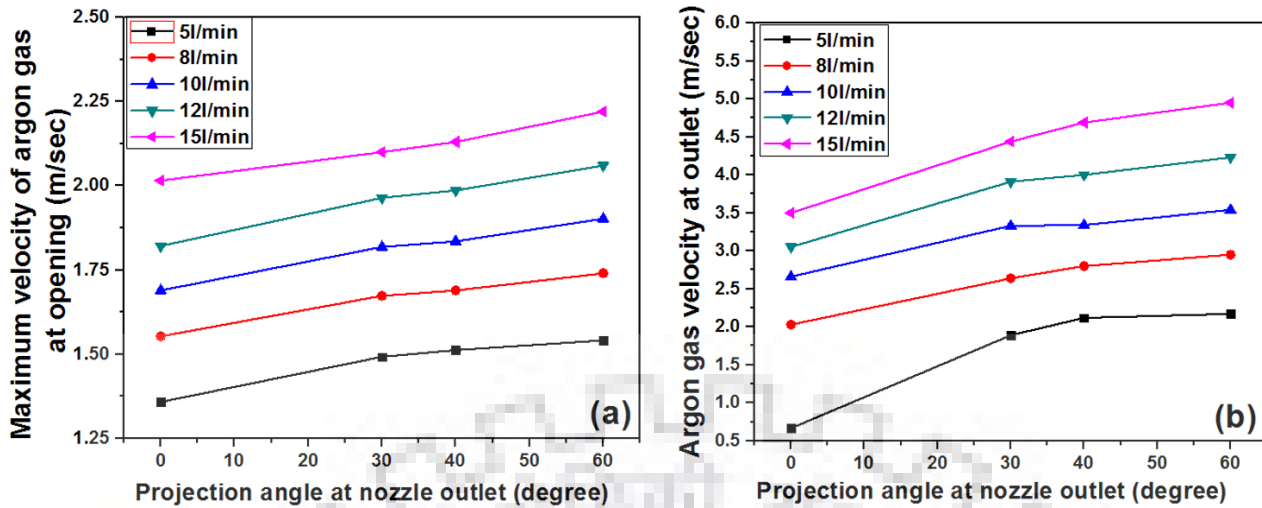


Figure 6-8 At a given gas flow rate effect of projection angle of nozzle tip on the argon shielding gas flow characteristics as (a) maximum velocity at opening and (b) velocity at outlet.

The primary design of the nozzle was to ensure narrowest possible sound weld joint of thick section by adequate flow of shielding gas with a stable arcing inside the narrow weld groove of plate wall supporting the shielding gas flow as stated above in order to produce. The performance of the newly designed nozzle in such condition of narrow groove welding studied at nozzle tip angle and gas flow rate varied from 0° to 60° and 5 to 12 l/min respectively shows that at a given flow rate of shielding gas its pressure outlet and turbulence in arc zone increases with the increase of nozzle tip projection angle (Figs. 6.9(a) and (b)). The figures also show that at a given nozzle tip angle the increase of gas flow rate creates more turbulence and eddies in arc zone inside the narrow groove.

Table 6-4 Flow characteristics of argon gas shielding inside narrow groove without MHD.

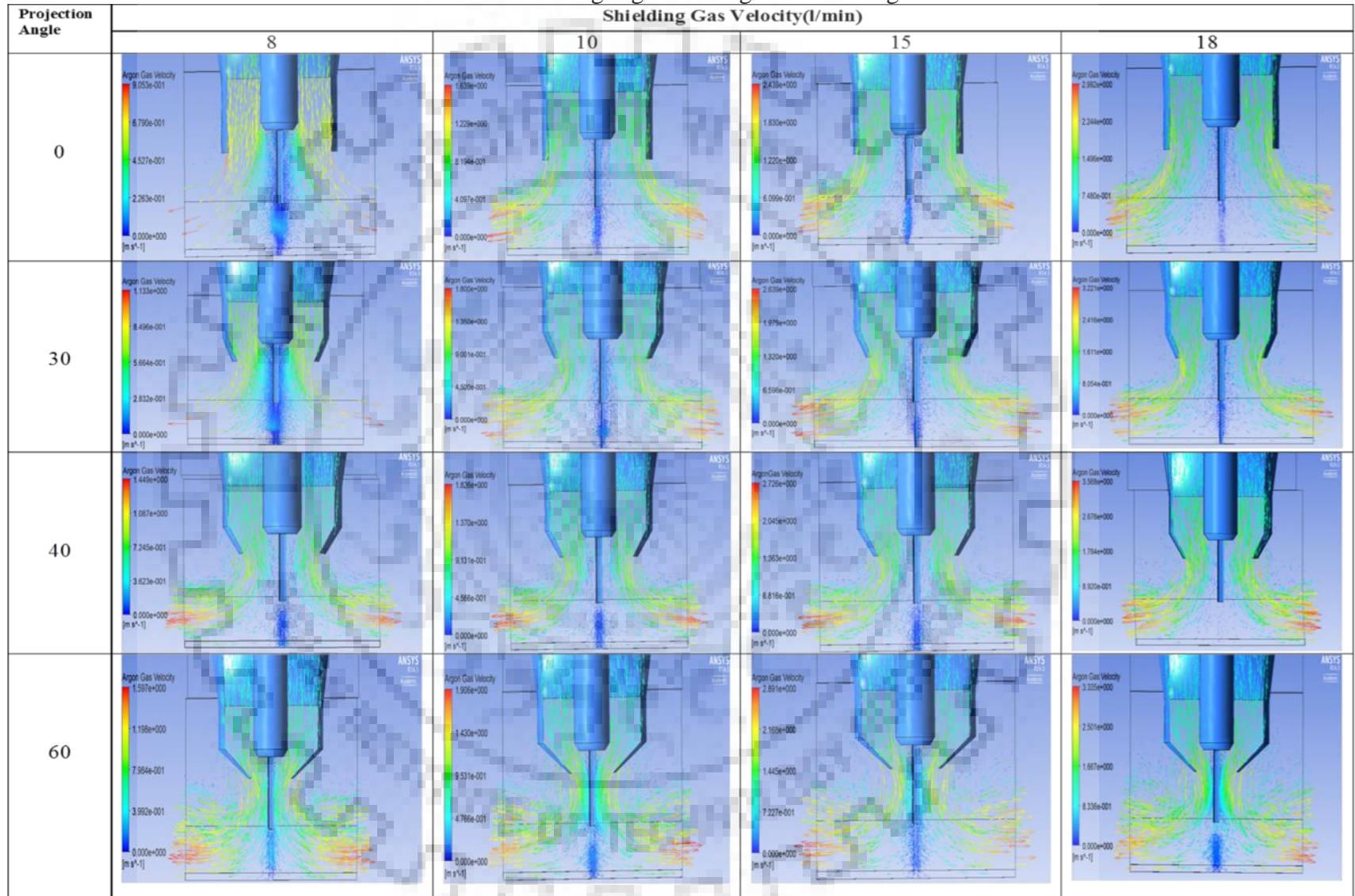
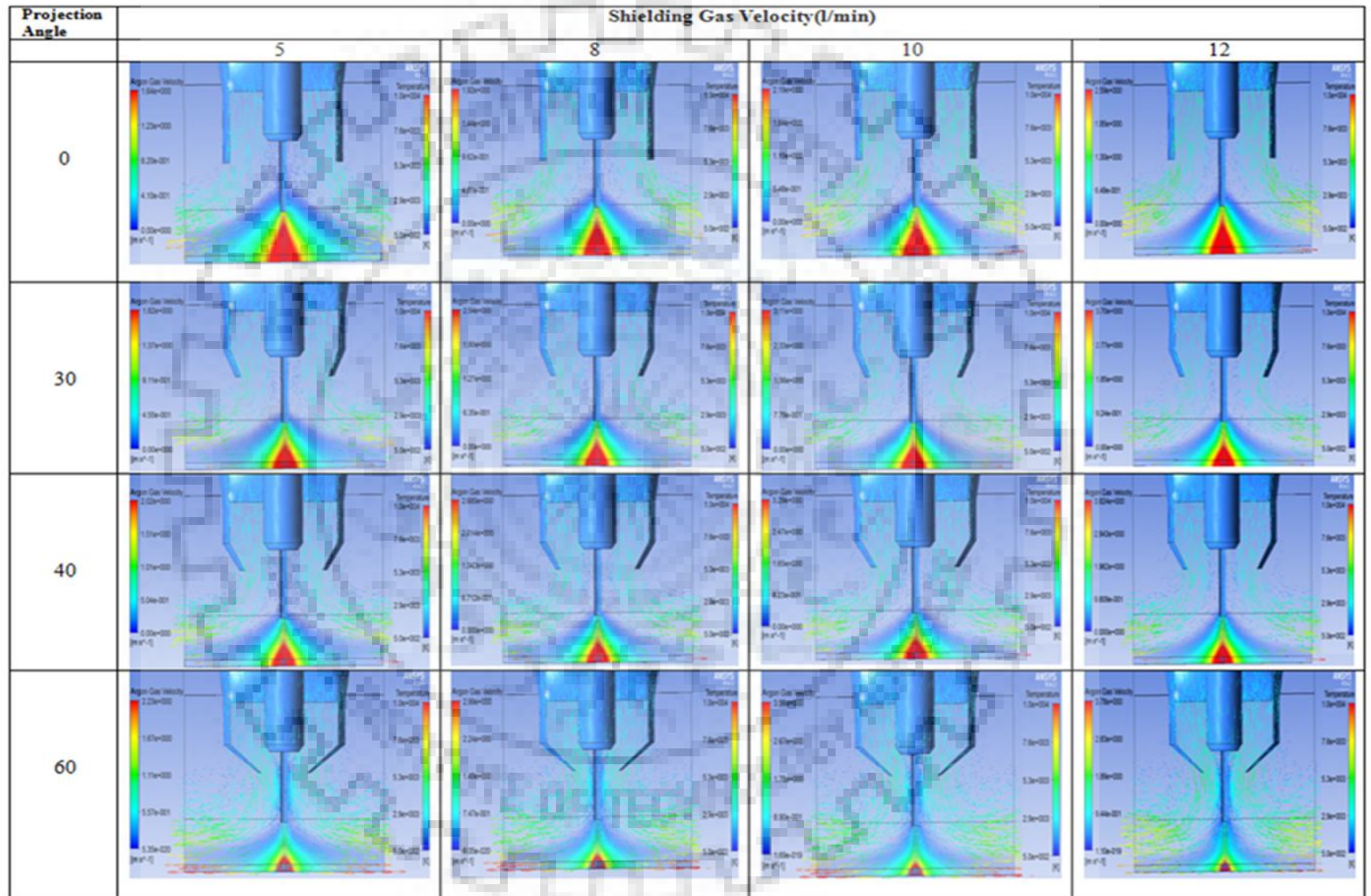


Table 6-5 Flow characteristics of argon gas shielding inside the narrow groove with MHD.



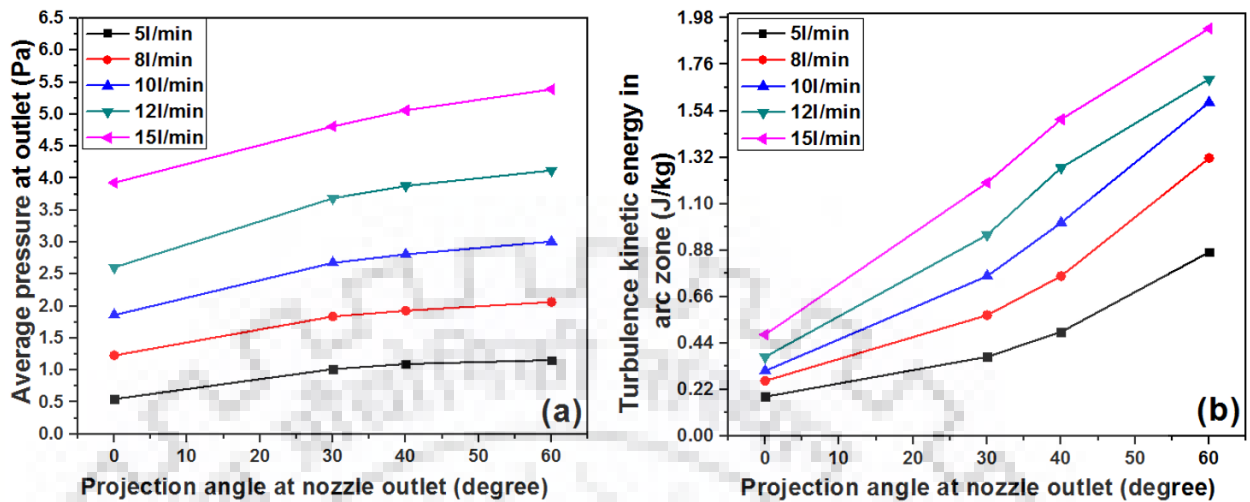


Figure 6-9 At a given gas flow rate the effect of projection angle of nozzle tip on the argon shielding gas flow characteristics as (a) average pressure at the outlet and (b) turbulence kinetic energy in arc zone.

The effect of gas flow rate on length and diameter of arc inside the narrow groove has been plotted as a function of projection angle of nozzle tip at different shielding gas flow rate as shown in Figs. 6.10(a) and (b) respectively. It shows that the length and diameter of arc inside the narrow groove decrease with the increase of nozzle tip angle and shielding gas flow rate. This has primarily happened due to appreciable removal of arc heat by shielding gas. The interaction of shielding gas and arc significantly increases with increasing gas flow rate as well as nozzle tip angle.

The above observations effectively give some directions to design and construct the torch nozzle. The newly developed nozzle is primarily aimed to protect the weld pool through shielding gas without any atmospheric contamination and turbulence in the arc zone. Based on the observations of Figs.6.10-6.12 it may be realized that in order to achieve this aim 0° projection angle of the nozzle head is useful which can provide the required arc length and diameter at 10-12 l/min shielding gas flow rate. This is because in this range of flow rate the required shielding gas velocity can be obtained to support a steady flow field inside narrow groove with negligible effect of turbulence. The understandings (Figs.6.10-6.12) about the influence of gas flow rate and projection angle of nozzle tip on gas flow behavior inside the narrow groove, arc diameter and arc length lead to some useful planning of nozzle designing and its use in narrow weld groove.

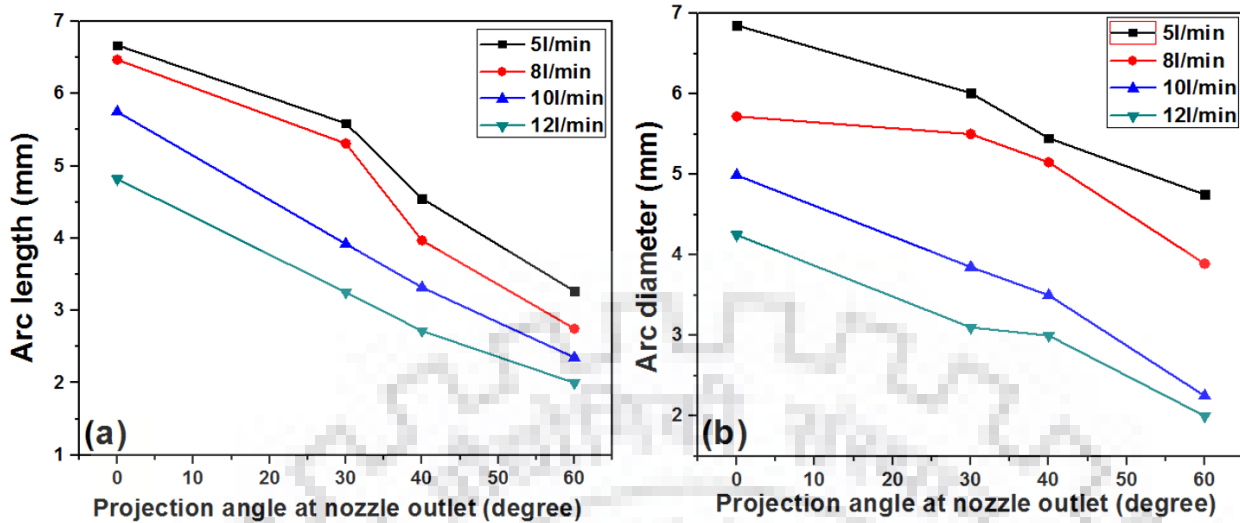


Figure 6-10 At a given argon shielding gas flow rate the effect of projection angle of nozzle tip on the arc characteristics as (a) arc length and (b) arc diameter.

The results are simulated using vector plots of mass concentration of argon gas flow at 12 l/min as typically shown in Fig.6.13 for the 0° and 60° nozzle tip projection angle respectively. The influence of flow rate of the argon gas shielding at 12 l/min on the arc characteristics and thermal distribution inside the narrow groove with MHD has been also shown in this figure. In this case the results were evaluated using vector plots of shielding gas concentration at different zone of the nozzle inside the narrow groove. It shows that there exists a streamline flow of shielding gas at different gas flow rate inside the narrow groove. The change in velocity distribution of gas flow with increasing nozzle tip angle is also noticeable, which indicates that the density of argon gas flow increases near the expected arc zone with increasing nozzle tip angle. This may be understood from the principle of the conservation of mass which states that a smaller nozzle outlet area enhances the velocity of shielding gas as simulated and demonstrated in Fig.6.13.

Fig.6.11 also depicts the temperature and argon gas flow field in the arc system of GMAW process. It shows that an increase of projection angle of the nozzle tip reduces the area of gas outlet which consequently enhances its velocity, pressure and turbulence kinetic energy as per conservation of mass principle. To produce better shielding quality and arc stability turbulence kinetic energy should be minimum. It is observed that as the outlet area of the nozzle decreases, the resistance of the shielding gas columns to the adverse effects of the cross draft increases. This is justified because the velocity of shielding gas has to be increased while flowing through a narrower area in order to maintain mass flow rate. Here also it is noticed that at a given gas flow rate the increase of projection angle of the nozzle tip from $0-60^{\circ}$ and at a given nozzle tip angle the

increase of gas flow rate from 5 to 12 l/min significantly reduces the visibility of arc due to efficiently removal of heat from the arc as discussed earlier.

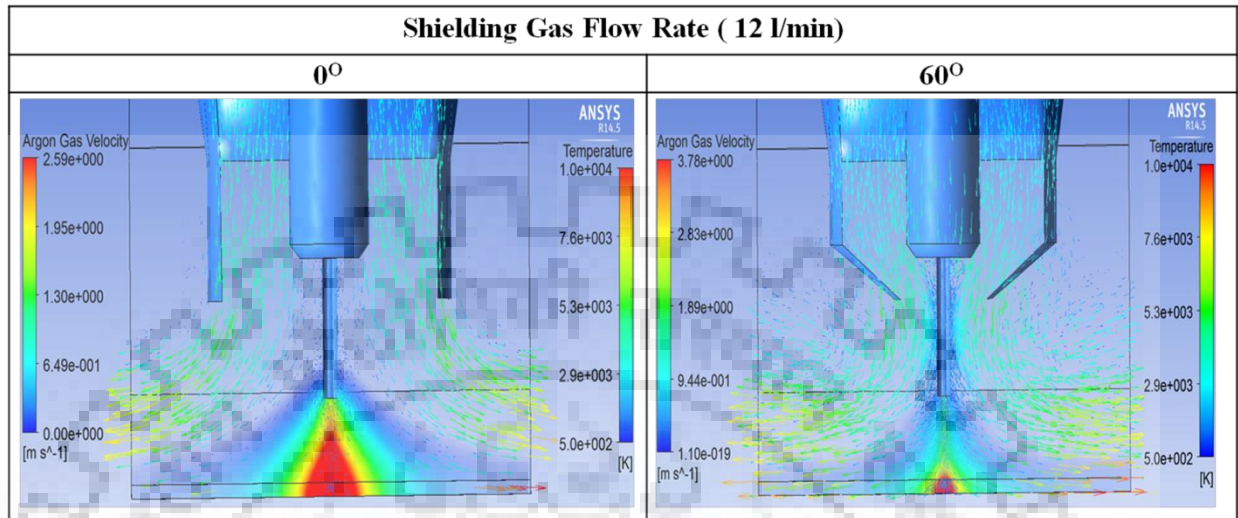


Figure 6-11 Typical flow characteristics of argon gas shielding inside the narrow groove with MHD.

After laying the first pass in single bead per layer in narrow groove of multi-pass welding, the deposition of second pass may require suitable lifting of the torch nozzle which necessitates shortening of the nozzle length in order to avoid the exposure of its side wall, which is no longer fully protected by the narrow weld groove wall. Thus the flow characteristics of argon gas shielding inside the narrow groove with MHD for the second pass has been simulated as shown in Fig.6.12. The figure and its observations plotted in (Figs.6.13-6.15) shows the influence of gas flow rate on the outlet velocity of the shielding gas and its pressure and turbulence level inside the narrow groove during second pass. During the second pass the shielding gas flow behavior is not changed significantly but the diameter and length of the arc reduces as compared to those measured during the first pass. The figure shows that at 12 l/min gas flow rates the reduced diameter and length of the arc is not very much suitable for preparation of sound weld joint. This may have primarily happened because at this gas flow rate the velocity of shielding gas considerably increases as observed in Fig.6.13 (a). Thus, it is realized that the 8-10 l/min gas flow rate supports the acceptable arc length and diameter. Further the comparative characteristics of gas flow behavior during first and second pass depicted in Figs.6.14 and 6.15 reveals that at this level of gas flow rate (8-10 l/min) the outlet velocity of shielding gas is lying well within the acceptable level of 2-5 m/sec as discussed above.

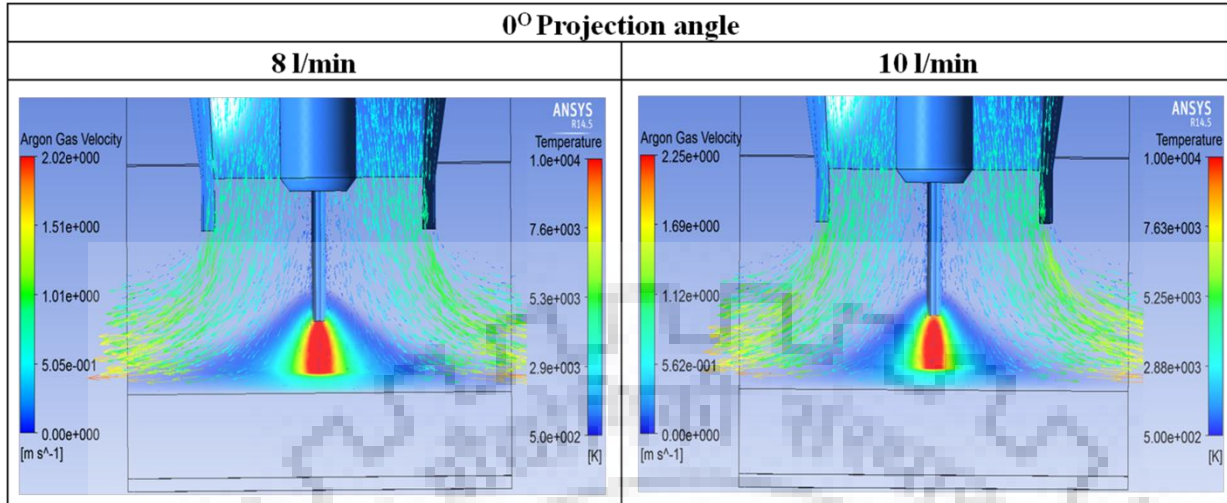


Figure 6-12 Flow characteristics of argon gas shielding inside the narrow groove with MHD for 2nd pass.

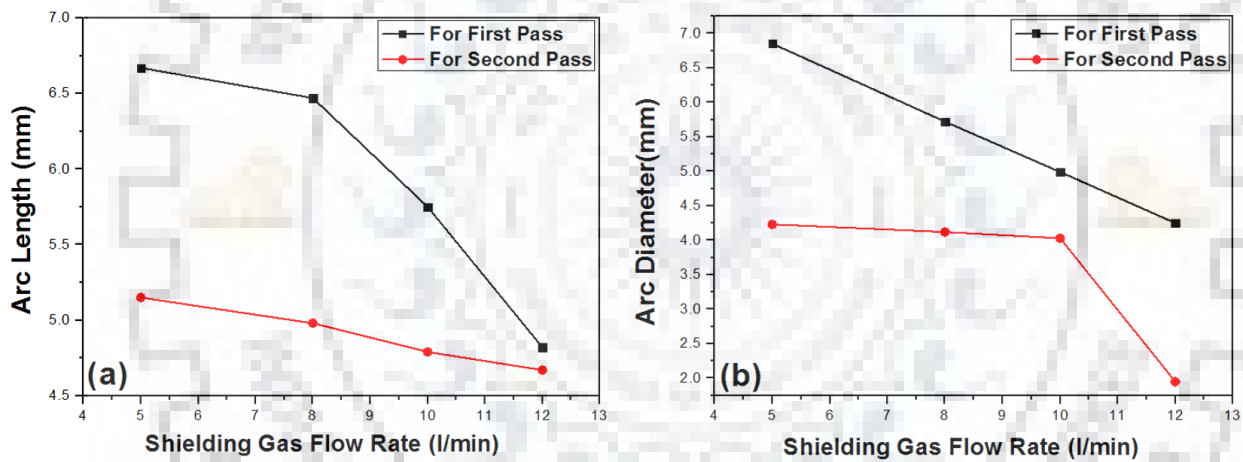


Figure 6-13 Difference in arc characteristics during first and second pass as (a) arc length and (b) arc diameter.

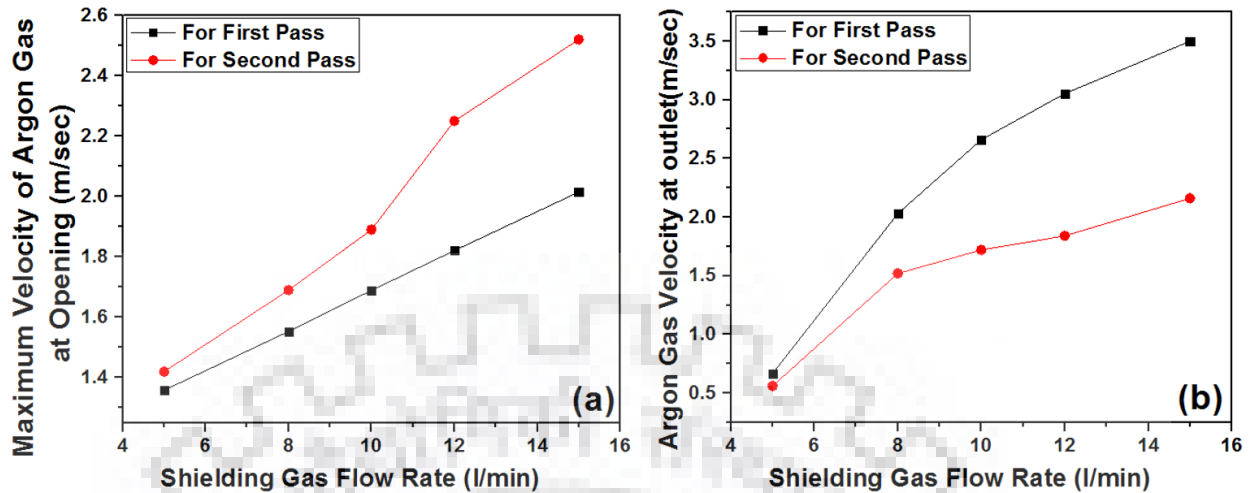


Figure 6-14 Difference in argon gas flow characteristics during first and second pass as (a) maximum velocity at opening and (b) velocity at outlet.

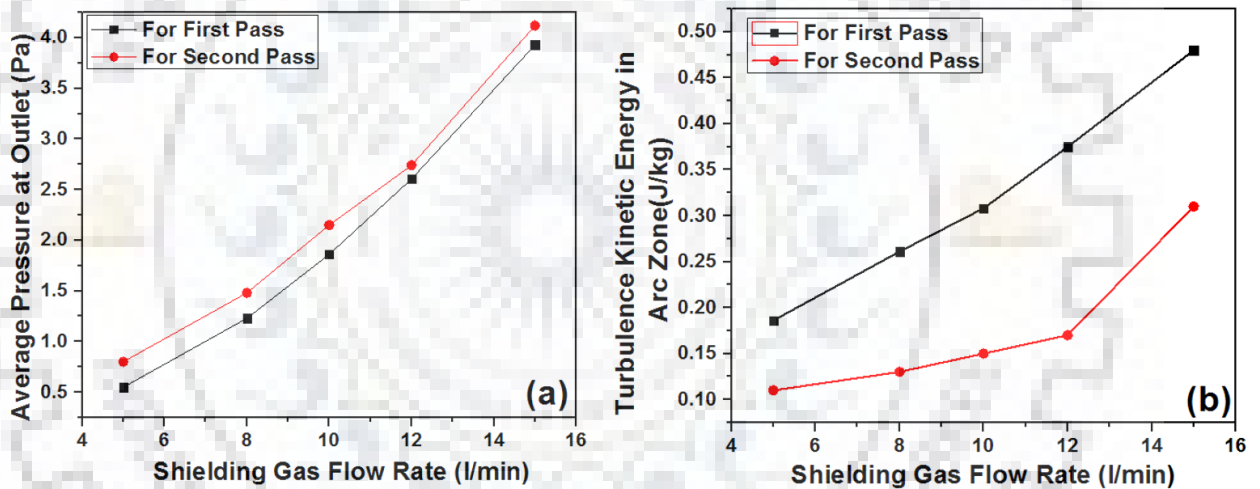


Figure 6-15 Difference in argon gas flow characteristics during first and second pass as (a) average pressure at the outlet and (b) turbulence kinetic energy in arc zone.

6.2.3. Summary

A rectangular faced narrow torch nozzle head designed by removing both of its lengthwise side walls along the direction of welding suits close fitting manipulation inside a practically narrowest possible weld groove to get support from the groove wall for creation of a protected zone of arc shielding with appropriate dynamics of argon gas flow during GMA welding of 25 mm thick plate. A simulated model analysis of shielding gas flow dynamics and its flow rate successfully establishes its optimization for employing P-GMAW process by vertically placed electrode depositing single bead per layer in narrow weld groove of 7.5 mm face opening.

6.3. Characteristics of P-GMAW Weld Bead on Plate

The acceptability of the weld joint in MPSSPL ultra-narrow gap dissimilar welding of γ -SS and HSLA steel is primarily governed by required fusion in both sides of dissimilar groove wall as well as in earlier deposited weld deposit at an optimum thermal exposure giving rise to a minimum heat affected zone (HAZ) of undesirable microstructure on both side of dissimilar base metal. The extent of fusion of the base metal largely depends upon nature of thermal behavior and metal transfer of the weld dictating shape and size of the weld pool and its temperature. The heat content of weld pool is largely governed by its mass per unit length and temperature. The shape and size of weld pool affects the properties of the weld and HAZ. Achieving all these aspects can be more precisely addressed by using P-GMAW process controlled by summarized influence of pulse parameters proposed earlier [Ghosh et al 2000] and defined by a hypothetical factor ϕ derived on the basis of energy balance concept of the system, because it more thoroughly facilitates governing the weld characteristics including its microstructure [Ghosh 1996, Ghosh et al 2006, Ghosh et al 2008, Goyal et al 2008 (b), Hussian et al 1996, Randhawa et al 1998, Randhawa et al 2000, Agrawal 2010]. In this respect the nature of variation in characteristics of weld bead and weld isotherm as a function of ϕ , Ω and I_m has been studied and its understanding may be beneficial in using P-GMAW to produce desired weld quality.

The thermal behaviour of weld has been studied considering heat transfer to the weld by the arc, superheated molten droplets [Goyal et al 2008 (b), Ghosh et al 2006, Agrawal 2010], heat input (Ω), temperature of weld pool (T_{WP}) and weld isotherm governing shape and size of weld pool. Therefore, to control the P-GMAW process in order to get desired weld quality in MPSSPL narrow gap welding, it is required to have an understanding of correlation among the Ω , T_{WP} , ϕ and I_m and weld characteristics. The P-GMA welding parameters used for bead on plate study has been shown in Table-5.2 (chap.5).

6.3.1. Thermal aspects of weld pool

At a given arc voltage of $25 \pm 1V$, the typical theoretically estimated thermal behavior of metal transfer as heat content per unit mass of droplet (Q_{de}) and temperature of droplet at the time of deposition (T_{de}) at different mean currents (I_m) of about 200 ± 3 , 220 ± 2 and $240 \pm 4A$ where the value of ϕ is 0.05 and 0.25 has been shown in Figs. 6.15(a) and (b) respectively. It has been observed that the Q_{de} and T_{de} reduces with the increase of ϕ at a given I_m and vice-versa. This is attributed to the heat gain by the droplet from energy input at the time of detachment from the electrode and

heat loss by convection and radiation during its flight from electrode tip to the weld pool. For a given shielding gas and specific distance between the electrode and the work piece, the heat loss during its flight from the electrode tip to the work piece primarily depends upon temperature of the droplet at the time of detachment from the electrode tip, surface area of the droplet and flight time. The diameter of droplets has been found to increase with increase of ϕ at a given I_m and at a given ϕ it reduces with increase of I_m whereas, the number of droplets transferred per pulse reduces with increase of ϕ at a given I_m or with the reduction of I_m at a given ϕ as shown in Fig.6.16 (a) and (b). Therefore the surface area of droplets is governed by relative enhancement of the diameter of droplets and decrement of number of droplets transferred per pulse. It has been found that total heat loss decreases with increase of ϕ at a given mean current and at a given ϕ it increases with an increase of mean current [Goyal et al 2008 (b), Ghosh et al 2006, Agrawal et al 2010]. The heat content of the droplet at the time of detachment has been found to reduce with an increase of ϕ at a given I_m and at a given ϕ with enhancement of I_m [Goyal et al 2008 (b), Ghosh et al 2006]. Considering all these facets, the Q_{de} and T_{de} will depend upon the comparative rate of the decrement of the heat content of droplet at the time of deposition and heat loss of the droplet during its flight from the electrode tip to the weld pool. Due to these reasons the trend of Q_{de} and T_{de} has been found as shown in Figs. 6.16(a) and (b) respectively. This is in agreement to the earlier study [Goyal 2007, Agrawal 2010] on aluminium alloys and HSLA steel showing similar trend of variation as explained above. Hence, it can be concluded that the thermal behaviour of metal transfer can be controlled up to certain extent by varying ϕ and I_m . The empirical correlations have been found as given below.

$$Q_{de} = 229.134 - 0.199I_m - 117.658\phi + 0.285I_m \phi \quad (6.1)$$

$$T_{de} = 4037 - 5.15I_m - 2699\phi + 6.12I_m \phi \quad (6.2)$$

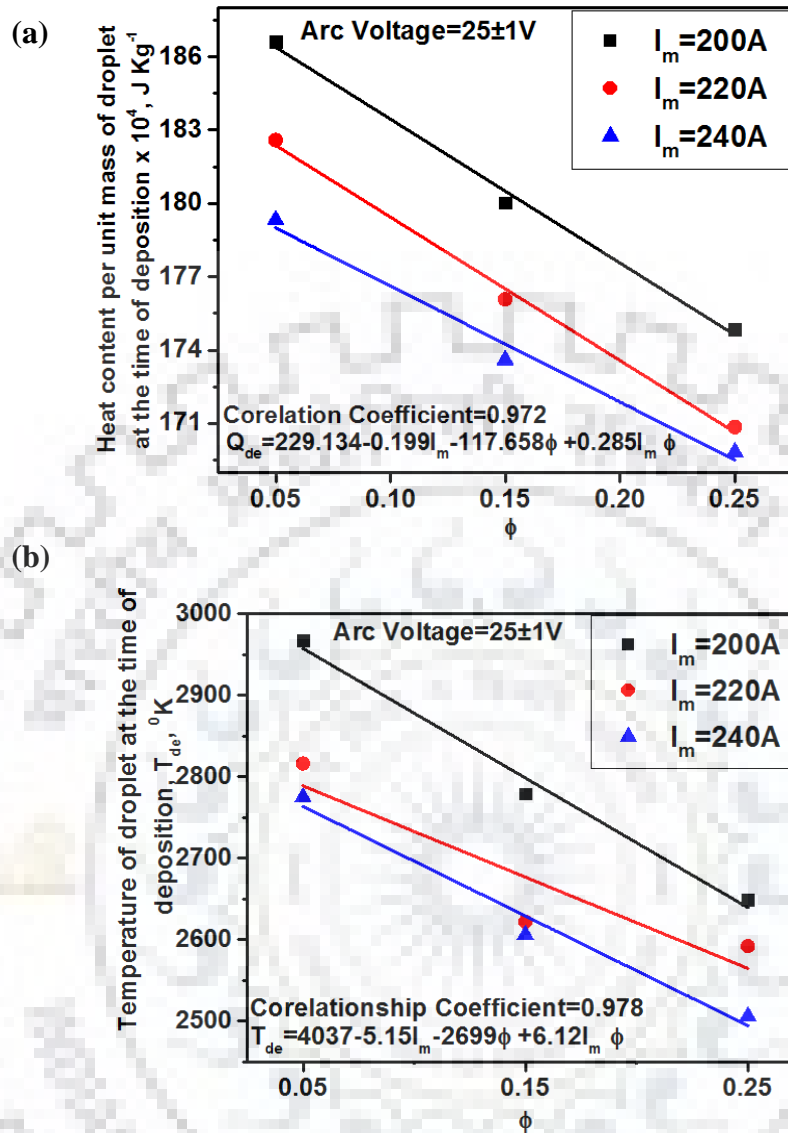


Figure 6-16 At a given arc voltage of 25±1V the effect of ϕ on (a) heat content per unit mass of droplet and (b) temperature of droplet at the time of deposition at different I_m of 200, 220 and 240A respectively.

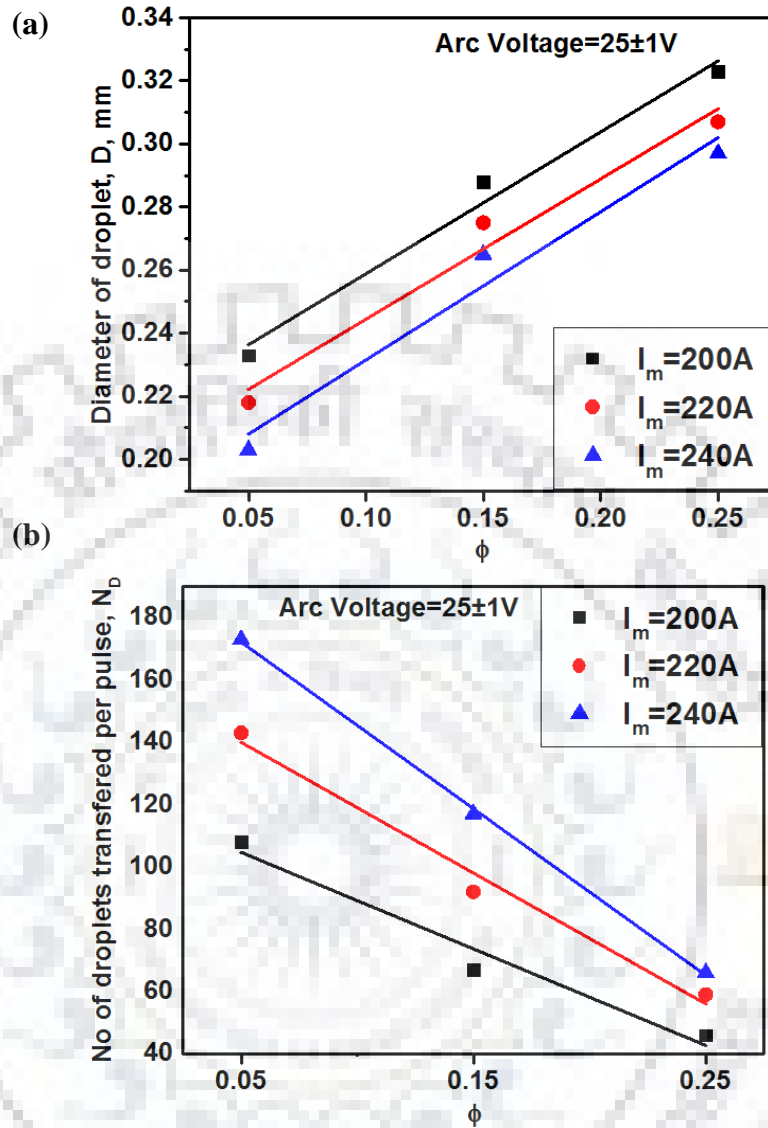


Figure 6-17 At a given arc voltage of $25 \pm 1V$ the effect of ϕ on (a) diameter of droplet and (b) number of droplet transferred per pulse at different I_m of 200, 220 and 240A respectively.

The thermal behavior of metal transfer being dictated by ϕ and I_m may affect the total heat transferred to the weld pool. The total heat transferred to the weld pool may govern the temperature (T_{WP}) and shape and size of weld pool consequently affecting the weld isotherm which ultimately influences thermal behavior of weld. Thus, the thermal behavior of weld pool has been studied considering total heat transfer to the weld pool, average weld pool temperature (T_{WP}) and weld isotherm under different pulse parameters (Table-6.4).

At a given arc voltage of $25 \pm 1V$ the influence of ϕ on theoretically estimated Q_T at different mean currents (I_m) of about 200 ± 2 , 220 ± 2 and $240 \pm 3A$ has been depicted in Fig. 6.17. The total

heat transferred to weld pool reduces with increment of ϕ at a given I_m and enhances with I_m at a given ϕ . The total heat transferred to weld pool Q_T is primarily dictated by the arc heat, largely depending upon the effective mean current and heat of filler metal transferred per unit time, which are having similar trend of variation with ϕ at a given I_m and with I_m at a given ϕ (Table-6.4). The empirical correlation of Q_T with ϕ and I_m at a given arc voltage have been worked out as follows.

$$Q_T = 29.08I_m - 3773.45\phi + 0.04I_m\phi + 1237 \quad (6.3)$$

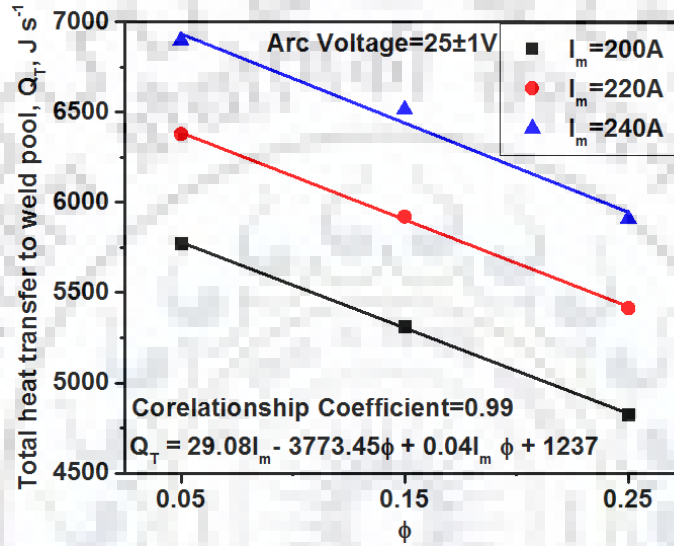


Figure 6-18 At a given arc voltage of $25\pm 1V$ the effect of ϕ on total heat transfer to weld pool at different I_m of 200, 220 and 240A respectively.

At a given arc voltage of $25\pm 1V$ the effect of ϕ on theoretically estimated weld pool temperature, T_{WP} at a depth of about 2.1 – 3.5mm from its surface and about 3.5mm from arc center under different Ω has been shown in Fig. 6.19(a) to (c). It has been observed that at a given Ω and I_m the T_{WP} reduces significantly with increase of ϕ , the T_{WP} enhances with increase of Ω at a given I_m and ϕ and it also increases appreciably with enhancement of I_m at a given Ω and ϕ . At a given Ω and I_m , the reduction of T_{WP} with the increase of ϕ may have primarily happened due to decrease of Q_{de} and T_{de} as explained earlier. While, the enhancement of T_{WP} with increase of Ω at a given I_m and ϕ is accredited to increase of total heat transferred to the weld pool (Q_T) per unit length. However the appreciable increment of T_{WP} with enhancement of I_m at a given Ω and ϕ has primarily happened due to increase of number of droplets transferred per pulse with the increase of I_m . This is because the molten metal droplets carry appreciable amount of heat while getting transferred to

weld pool. The empirical correlation of T_{WP} with respect to Ω and ϕ have been worked out as follows.

$$(T_{WP})_{200A} = 39.17 \Omega - 1202.23 \phi + 46.08 \Omega \phi + 1780.23 \quad (6.4)$$

$$(T_{WP})_{220A} = 50.69 \Omega - 760 \phi + 12.86 \Omega \phi + 1829.71 \quad (6.5)$$

$$(T_{WP})_{240A} = 8.448 \Omega - 1513.74 \phi + 82.43 \Omega \phi + 2375.78 \quad (6.6)$$

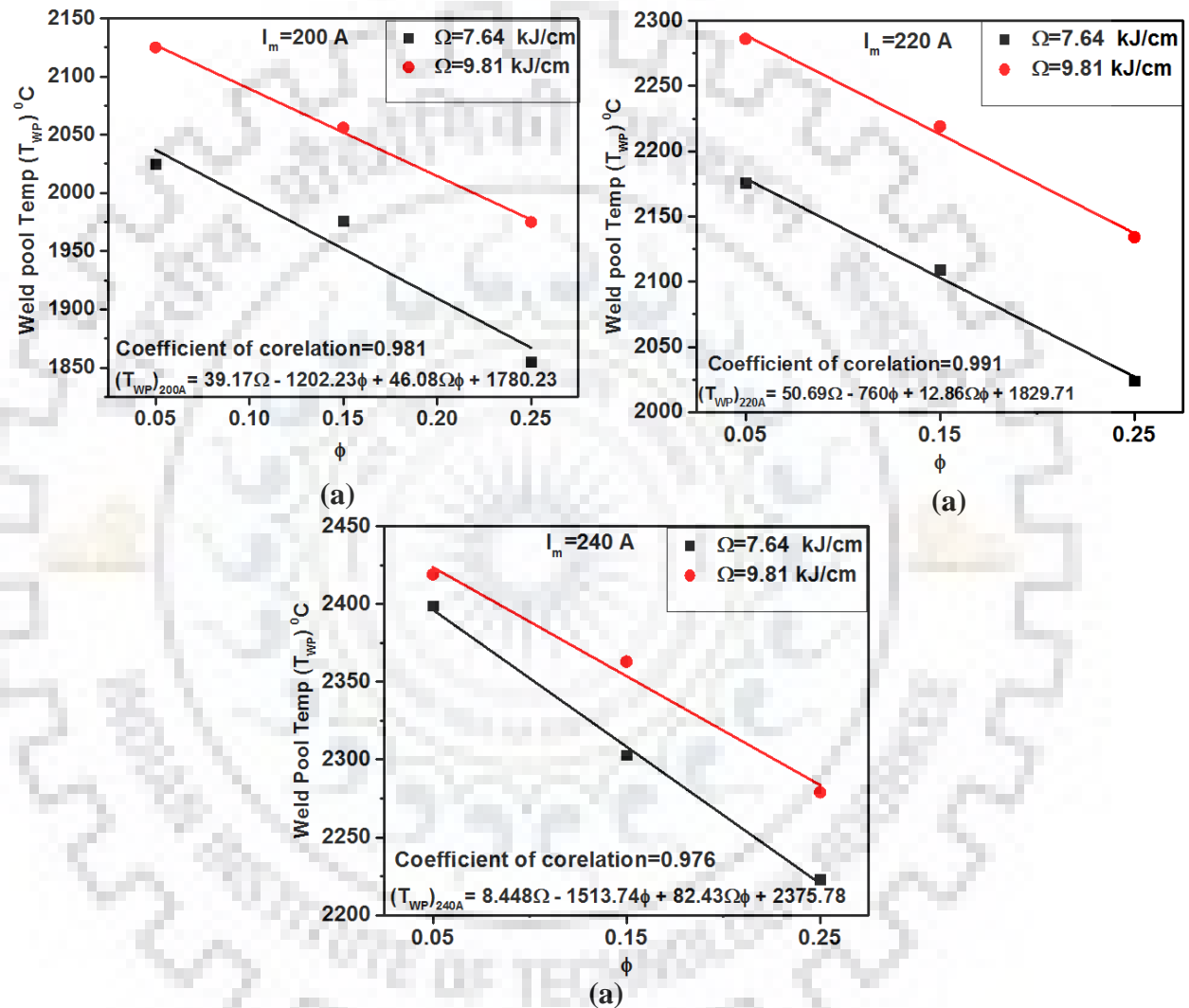


Figure 6-19 At a given arc voltage of $25 \pm 1 \text{ V}$, the effect of ϕ and Ω on weld pool temperature under different mean current of 200, 220 and 240 A respectively.

The mathematical expression (chap-5, eq.5.3) used for estimation of weld pool temperature has been verified for certain cases by comparing the theoretically estimated values with experimental measured values. At a given arc voltage of $25 \pm 1 \text{ V}$ a comparison of the theoretically estimated and measured values of T_{WP} at depths of about 2.5 – 3.0mm from molten pool surface at

different pulse parameters has been shown in Fig. 6.19. It has been observed that theoretically estimated values of T_{WP} are in good agreement with their corresponding measured values with a maximum deviation of about $\pm 8\%$. The limitation of the expression is that it is unable to estimate weld pool temperature correctly close to arc center within radius of 2 mm to avoid significant influence of arc heating [Goyal et al 2008 (b)].

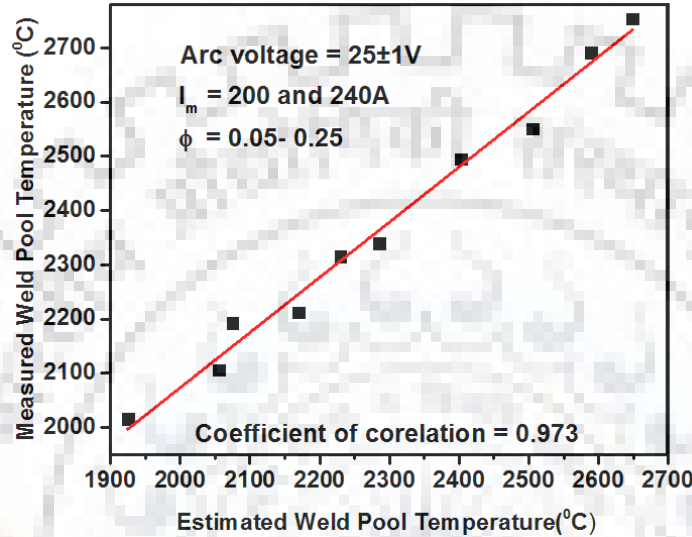


Figure 6-20 At a given arc voltage of $25\pm 1V$, comparison of measured and estimated weld pool temperature at depths of about 2.5 - 3mm from its weld pool surface at different I_m and ϕ .

The size and shape of the weld pool in welding process affects the mechanics and kinetics of solidification and thus, the microstructure and properties of the weld. The size and shape of weld pool along with the size and shape of heat affected zone also affects the thermally induced stresses that act on the weld leading to formation of residual stresses and distortion. The size of weld pool is dictated by the heat input, mean current and pulse current parameters of pulsed current gas metal arc welding and is governed by the isotherms predicted out of solutions of the heat flow equations. Thus, it is very much necessary to study the effect of these parameters on weld isotherm in order to critically understand, predict and ultimately control the final weld upto a maximum extent for desired performance of weld joint.

At a given arc voltage of $25\pm 1V$ the effect of ϕ on weld isotherm at different I_m and Ω lying in the range of 200A-240A and 7.64 ± 0.4 to 9.81 ± 0.5 kJ/cm respectively have been shown in Table 6.6 and 6.7. It is observed that the width and length of isotherm decreases with the increase of ϕ at a given I_m and Ω . This is attributed to the reduction in heat transferred to the weld pool with the increase of ϕ . It has been also observed that the increase of Ω at a given I_m and ϕ and the increase

of I_m at a given Ω and ϕ enhances the width of the isotherm. This is attributed to the enhancement of the heat transferred to the weld pool with the increment of Ω and I_m . It is further observed that increase of Ω at a given I_m and ϕ , which is achieved through the reduction of welding speed, decreases the length of the weld pool. This may have primarily happened because of its ability to cool the molten weld pool to relatively higher extent due to availability of comparatively more time at lower welding speed and higher Ω .



Table 6-6 At a given Ω (7.64 ± 0.4 kJ/cm) and arc voltage (25 ± 1 V) the effect of ϕ and I_m on weld isotherm at γ -SS plate.

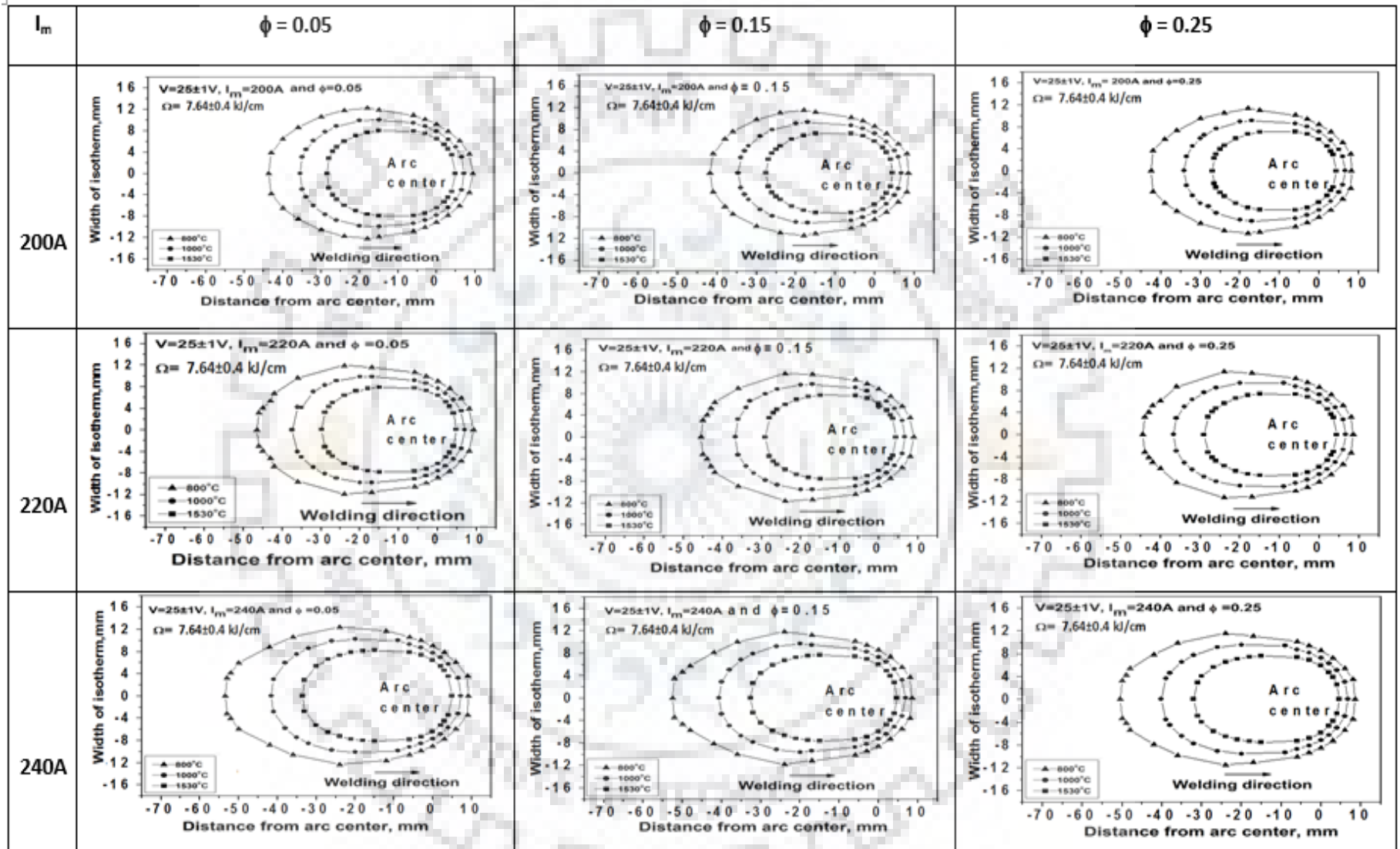
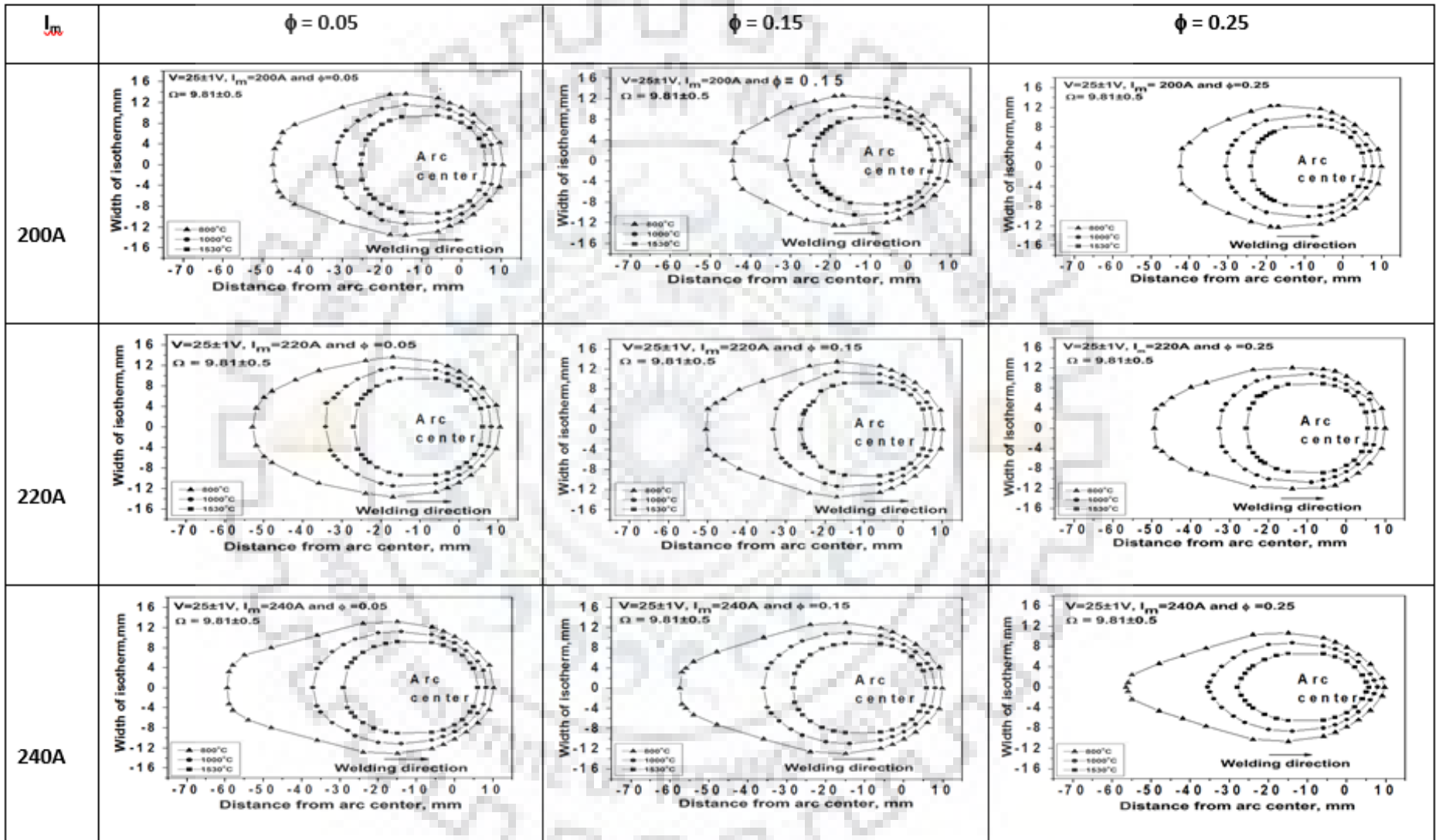


Table 6-7 At a given Ω (9.81 ± 0.5 kJ/cm) and arc voltage (25 ± 1 V) the effect of ϕ and I_m on weld isotherm at γ -SS plate.



6.3.1.1. Summary

Thermal aspects of weld pool of weld can be varied significantly with respect to heat input Ω and pulse parameters of welding of ϕ and I_m . The characteristics of variation of these have been obtained and empirical correlations have been found. The isotherm of the weld can be regulated appropriately by variation of Ω and pulse parameters in order to achieve the optimised conditions of welding.

6.4. Analysis and Validity of Proposed Thermal Model for MPSSPL Narrow Gap Weld

6.4.1. Analyses of the proposed model

The major aspects relevant to perform MPSSPL ultra-narrow groove dissimilar welding of Austenitic stainless steel to HSLA steel has been analyzed with the help of various expressions of the spatial model as stated above in order to support a proper selection of pulse parameters prior to carrying out dissimilar metal welding with appropriate groove wall fusion. A systematic approach in this regard with respect to the analyses of the geometry and thermal behavior of weld pool are stated below.

6.4.1.1. Geometry of molten pool inside weld groove

The geometry of molten weld pool inside a weld groove is primarily dictated by the geometry of the groove space available at each weld pass and the amount of weld deposit filling a specific depth of the weld groove. The amount of weld deposit per pass is primarily governed by the mean current and the welding speed, which consequently also affect the heat input.

In case of a given design of weld groove, the amount of weld deposit filling a specific depth of groove by each weld pass is dictated by the length of filler wire of a given diameter consumed per pass of weld deposition which is primarily a function of mean current, I_m and welding speed dictating the heat input. At a given arc voltage the effect of I_m on length of filler wire consumed per pass of weld deposition at different heat inputs of about 7.63 and 9.81 kJ/cm (Table-6.4), as estimated by using the eq. 4.3 (Chapter 4), has been typically shown in Fig. 6.21. The figure shows that at any weld pass, the length of filler wire consumed per pass of weld deposition increases with the enhancement of both the I_m and Ω . This has happened because the increase of I_m at a given Ω increases the wire feed rate resulting in more deposition of weld metal. Similarly at a given I_m the consumption of filler wire per pass of deposition increases with the increase of Ω through lowering of welding speed. In a weld pass under the heat input of 7.63 ± 0.4 and 9.81 ± 0.5 kJ/cm, the effect of I_m on volume of weld metal deposits per pass (V_m) of weld, as estimated by using eq. 4.2 (chap.4), has been shown in Fig. 6.22. The figure shows that the volume of weld deposit per pass also increases with the increase of both the I_m and Ω

because of its dependency primarily on the length of filler wire consumed per pass of deposition.

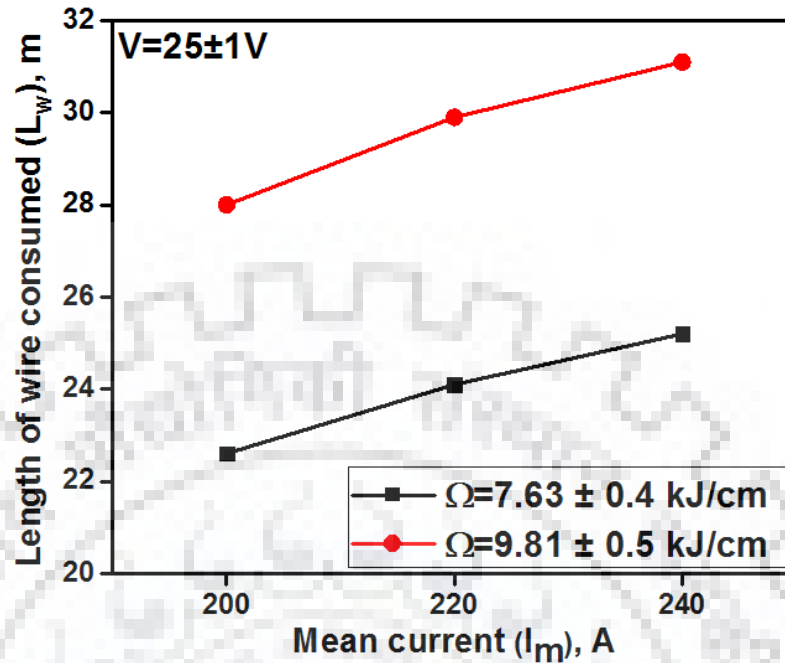


Figure 6-21 Effect of mean current on length of filler wire consumed per unit length of weld deposition at different heat input.

During filling of a ultra-narrow weld groove, the height of groove wall covered by the amount of metal deposition in each weld pass primarily depends upon I_m affecting the melting of filler wire and S which is controlling the amount of metal deposition per unit length and the groove space available at each pass. Thus, at a given I_m , the weld deposition per unit length can be broadly taken into account as a function of Ω . At different mean currents of 200, 220 and 240A, the effect of number of weld pass on height of the groove wall covered by weld pool at varied Ω of 7.63 ± 0.4 and 9.81 ± 0.5 kJ/cm, estimated by using the eq. 4.5 (chap.4), has been shown in Fig. 6.23 (a) and (b) respectively. The figure reveals that at a given Ω and I_m , the higher sequence of weld pass relatively reduces the height of groove wall covered by the weld pool whereas, at any weld pass it increases with the increase of I_m at a given Ω or with the increase of Ω at a given I_m . At a given Ω and I_m that gives rise to a constant mass of weld deposition for filling the weld groove, the reduction in height of the groove wall covered by the weld pool of higher number of weld pass of single seam deposition at each layer has happened due to in case of root pass there is a less area of weld groove and for the second and third pass (capping) which is larger groove opening. This phenomenon largely depends upon groove design with respect to the parallel groove wall governing the width of groove openings at different layers of weld pass as shown in Fig. 4.1 & 4.2 (Chapter 4).

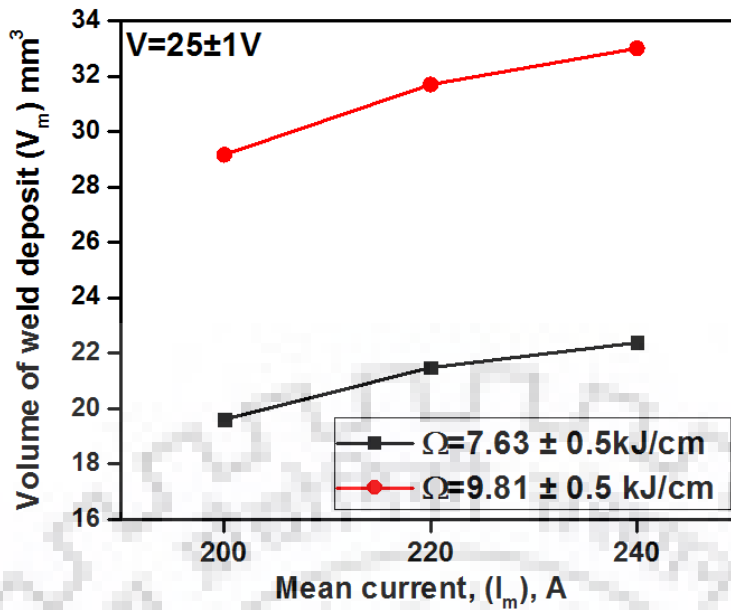


Figure 6-22 Effect of mean current on volume of metal deposited per unit length of weld at different heat input.

Table 6-8 Pulse parameters with corresponding thermal behaviour used in preparation of weld joint using P-GMAW process

Arc Voltage (V)	Heat Input (Ω) (kJ/cm)	Welding Speed (S) (cm/min)	Mean Current (I _m) (A)	φ	Pulse Parameters					Thermal Behaviour	
					I _p	I _b	f (Hz)	t _b (sec)	t _p (sec)	Q _{AW} (J/s)	Q _f (J/s)
25±1	7.63±0.4	26.4	200±3	0.05	289	123	90	4.12	3.51	3614	4697
	9.81±0.5	21.4		0.25	246	164	95	4.07	3.49	3445	5204
	7.63±0.4	29.1	220±2	0.05	332	125	107	3.97	3.66	4136	4725
	9.80±0.5	23.4		0.25	295	164	106	4.09	3.51	2771	3925
	7.63±0.4	31.8	240±4	0.05	350	121	124	3.47	3.17	2812	4304
	9.81±0.5	25.7		0.25	316	164	126	3.84	3.01	1111	4070

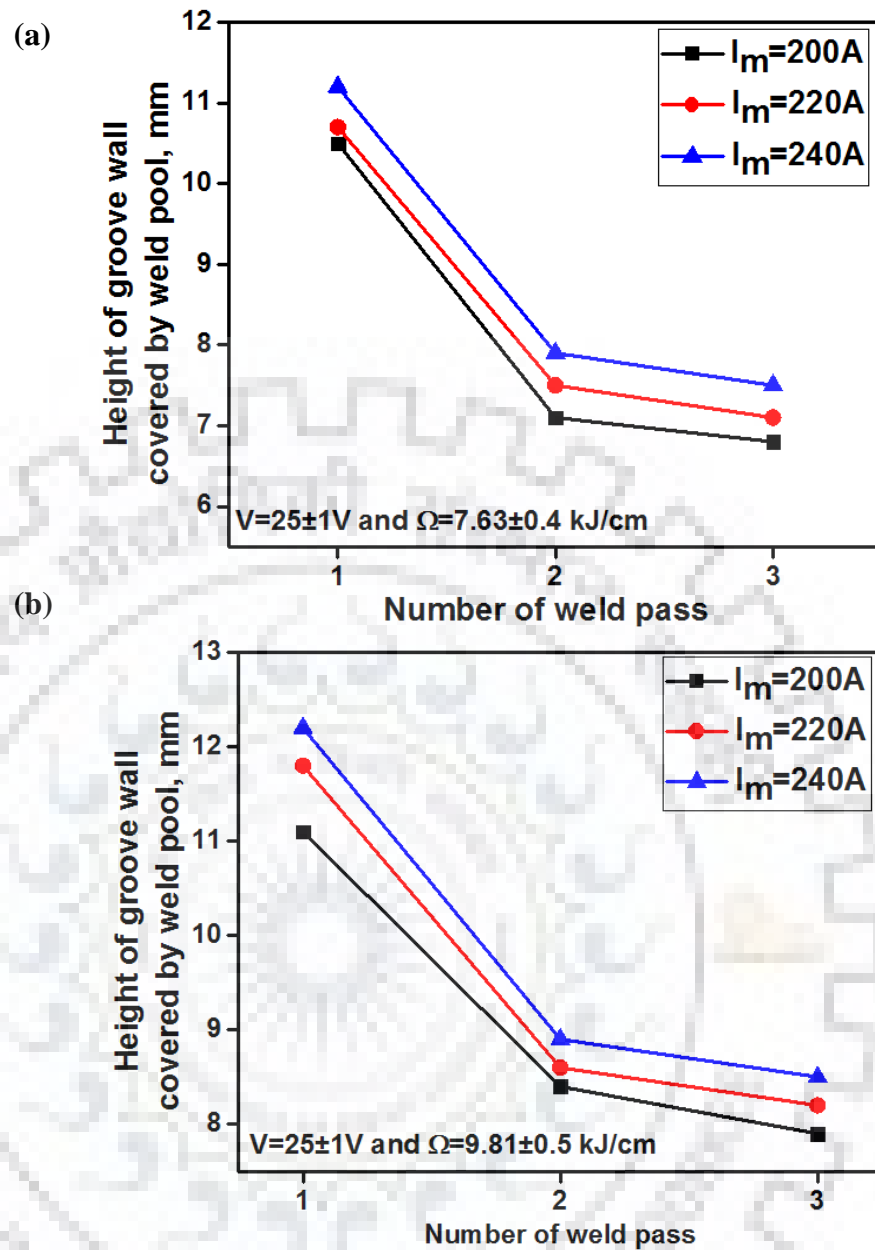


Figure 6-23 At different mean currents effect of number of weld pass on height of the groove wall covered by weld pool at varied Ω of (a) 7.63 ± 0.4 and (b) 9.81 ± 0.5 kJ/cm.

6.4.1.2. Thermal behaviour of molten pool inside weld groove

In order to produce a dissimilar weld joint free from lack of fusion the weld pool inside the ultra-narrow groove must have enough heat required to fuse both sides of the dissimilar groove wall as well as a part of earlier deposited weld. The heat content of the weld pool is primarily dictated by the amount of weld deposit and the temperature of the weld pool. In view of this an

analysis of the model has been carried out for estimation of heat required to produce a sound dissimilar ultra-narrow gap weld joint on the basis of total mass of metal to be fused from the each side of dissimilar groove wall and earlier deposited weld as well as thermal behaviour of weld pool in each weld pass.

The total mass of fusion (m_t) inclusive of the fusion of dissimilar base metal at γ -SS groove wall (m_{bSS}) and HSLA steel groove wall (m_{bHS}) as well as weld metal of earlier deposit (m_w) required to prepare a sound joint at a given pass has been estimated using the eqs. 4.6 to 4.10 (chap.4) while, the minimum depth of fusion necessary to produce a sound weld joint has been considered as 1mm [Radaij D., 1992] for the estimation of m_{bHS} , m_{bSS} and m_w . At different mean currents, the effect of number of weld pass on the required m_{bHS} , m_{bSS} and m_t at each weld pass of Ω of 9.81 ± 0.5 kJ/cm has been shown in Figs. 6.24 (a,b) and Fig.6.25 respectively. The figures show that at a given Ω and I_m the required m_{bHS} and m_{bSS} reduces due to reduction in height of groove wall in contact with the weld pool (Fig. 6.49). However, the figures also show that with the enhancement of I_m at a given Ω and weld pass both, the m_{bHS} , m_{bSS} and m_t decreases due to introduction of significant lower heat.

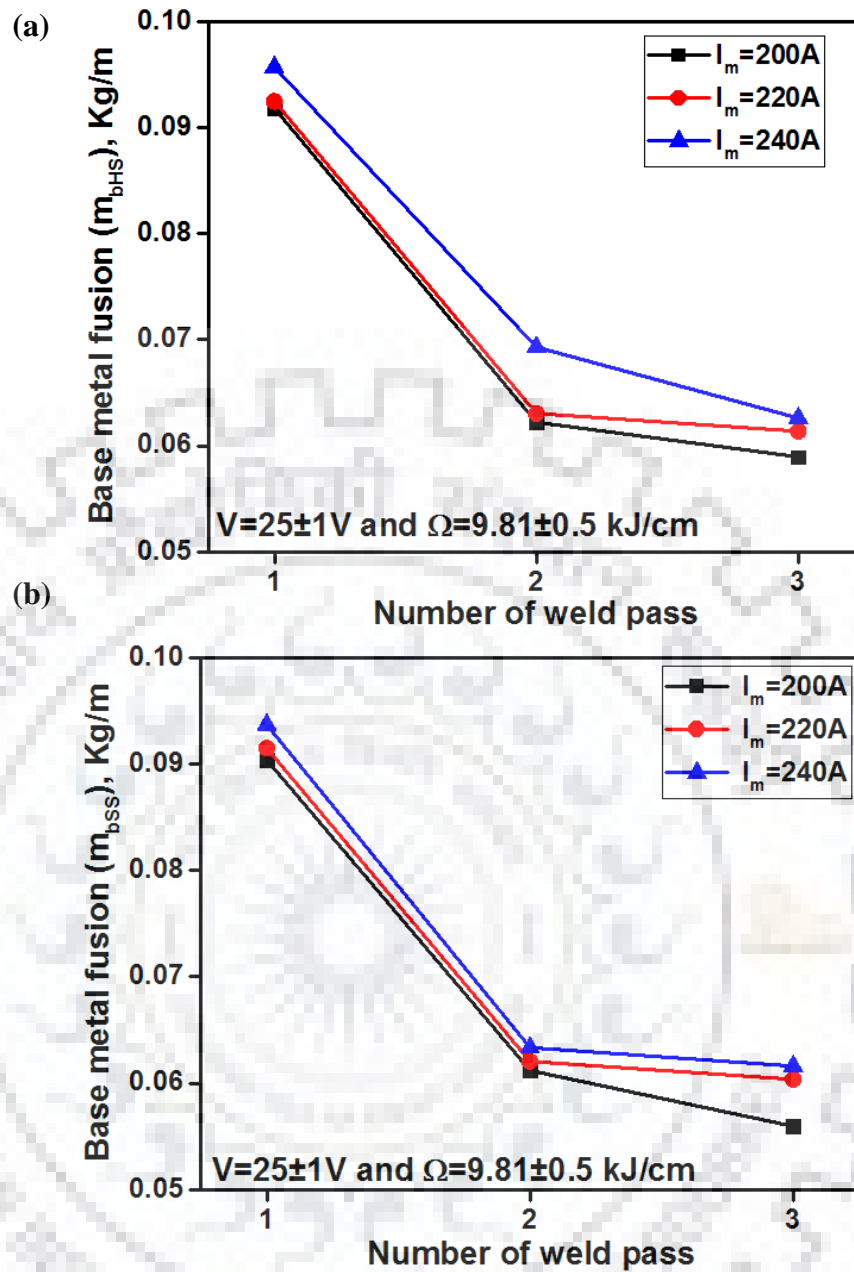


Figure 6-24 At different mean currents, the base metal fusion in dissimilar groove wall at different weld passes of (a) m_{bHS} and (b) m_{bSS}

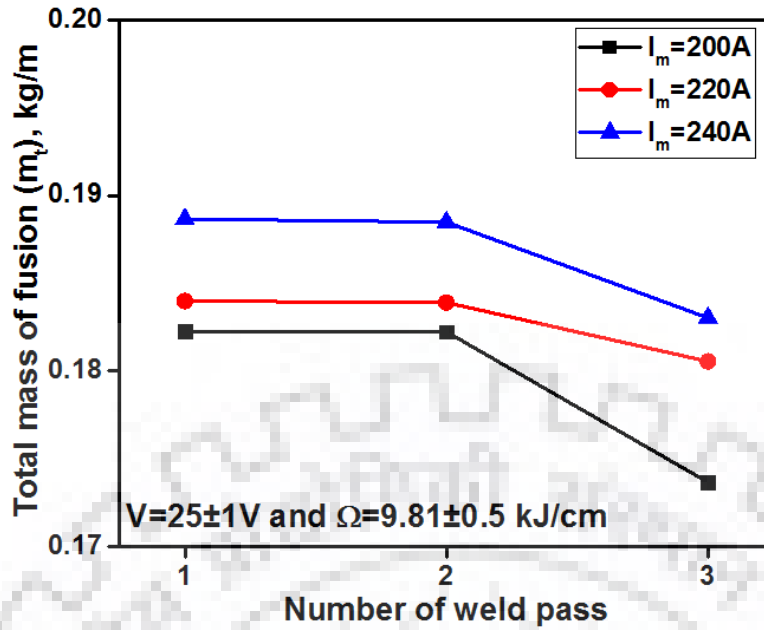


Figure 6-25 At different mean currents, the total necessary mass of fusion at each weld pass at Ω of 9.81 ± 0.5 .

In case of MPSSPL welding with no angle of attack of electrode to groove wall, a minimum amount of heat has to be primarily supplied by the molten weld pool for fusion of m_t . In this regard the requirement of heat to fuse m_{bHS} , m_{bSS} and m_W amount of metal for weld preparation can be estimated by eq.4.11, eq.4.13 and eq.4.14 (chap.4) respectively. Total heat (H_t) and the temperature of the weld pool (T_{rwp}) can be estimated using the eqs.4.14 and 4.18 (chap.4) respectively. It is observed (Fig. 6.26) that the requirement of total heat decreases with the increase of number of weld pass and I_m . It is also noticed that the required weld pool temperature decreases with the increase of weld pass at a given Ω and I_m and also reduces with the enhancement of I_m at a given Ω and weld pass respectively as shown in Fig. 6.27. It's because of the m_{bHS} , m_{bSS} reduces with the increase of weld pass at a given Ω and I_m . The reduction of total heat required with the increase of I_m at a given Ω and other two components of the three including weld pass respectively may have primarily happened due to a similar trend of reduction of m_t (Total mass of fusion) observed in this context and due to shrinkage which is discussed in the earlier chapter 5. A similar trend of decrease in T_{rwp} with the increase of weld pass beyond the first pass (root pass) to that of the H_t required for desired fusion to produce weld without lack of fusion because both of them are the function of m_t involved in each weld pass.

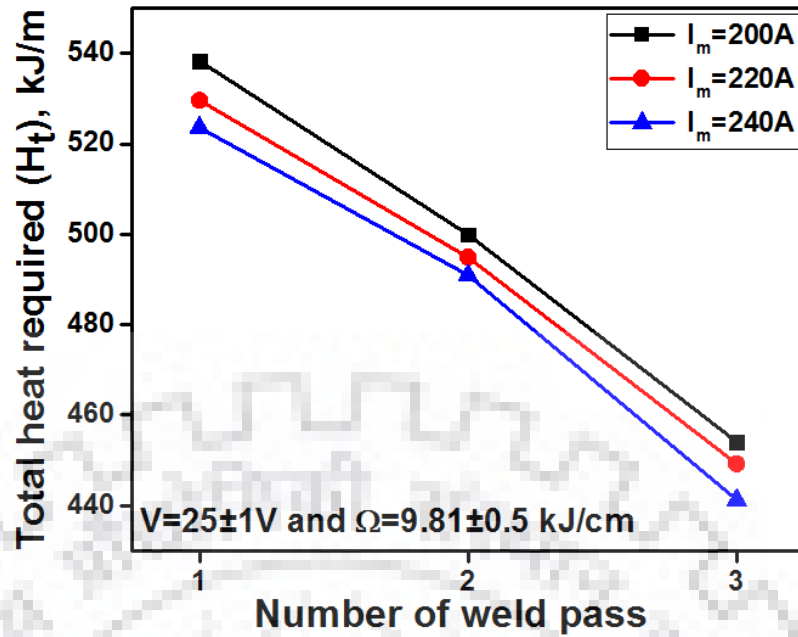


Figure 6-26 At different mean currents, the total heat required for desired melting of dissimilar groove wall at each weld pass at Ω of 9.81 ± 0.5 kJ/cm.

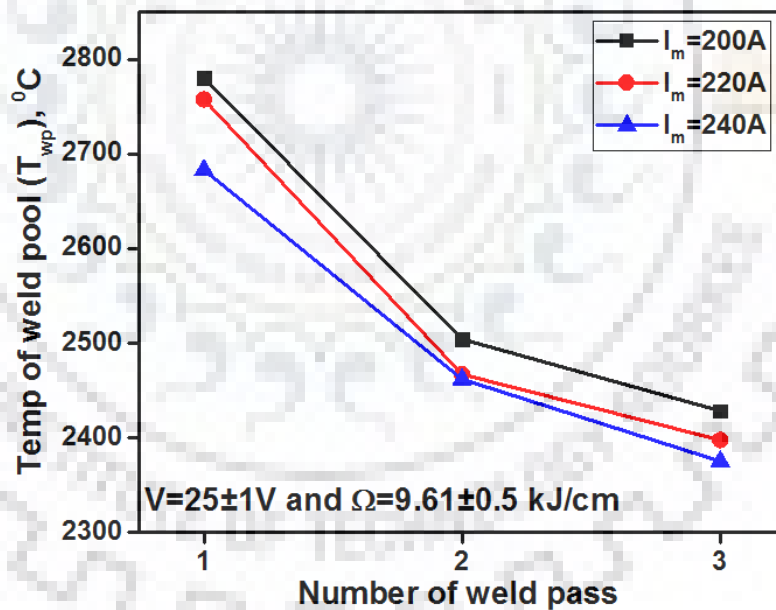


Figure 6-27 At different mean currents, the average weld pool temperature required at each weld pass for producing dissimilar sound weld joint at Ω of 9.81 ± 0.5 kJ/cm.

6.4.1.3. Heat transfer in molten pool and critical point of fusion in weld groove

During P-GMA welding the fusion of dissimilar groove wall and the part of earlier weld deposit finally depends upon distribution of a minimum required temperature. This is important in case of dissimilar weld joint where the melting temperature of opposite groove walls is different in a superheated weld pool with respect to the point of heat transfer from superheated

droplet inside a cavity formed on the weld pool. During variation in pulse parameters at a given arc voltage the depth of cavity (d) formed (Fig. 4.3, chap.4) by impingement of metal droplets to the weld pool at different mean currents of 200, 220 and 240A, as estimated by the eq. 4.39, has been typically shown in Fig. 6.28(a,b).

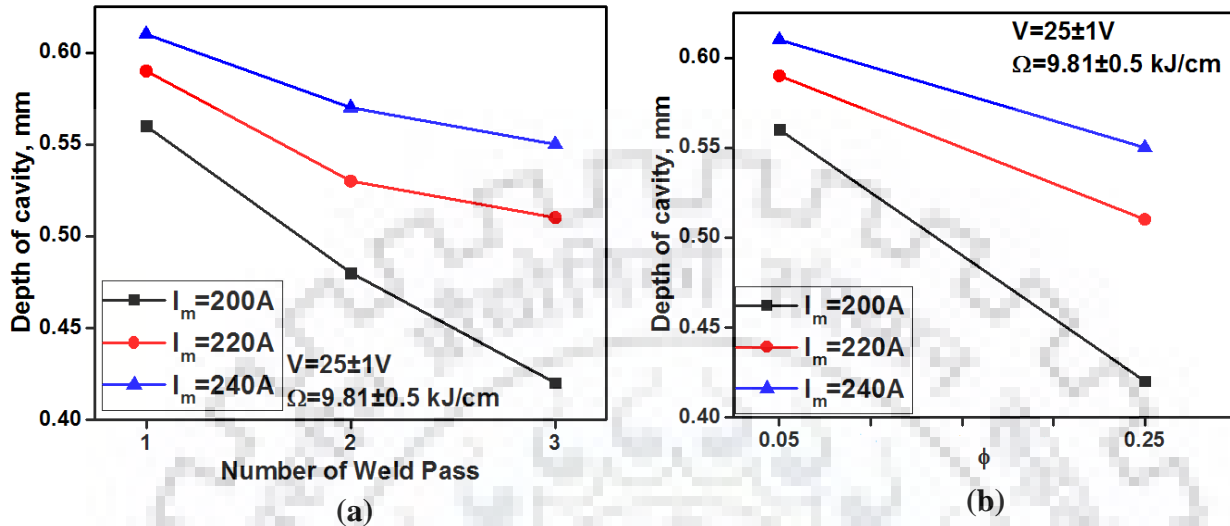


Figure 6-28 Effect of number of pass and ϕ on estimated depth of cavity formed by impingement of metal droplets at different mean currents.

The figure shows that the d decreases with the increase of weld pass number at a given I_m and Ω . At the same time, the d also enhances with the increase of I_m at a given Ω . The reduction of d with the increase of weld pass number at a given I_m and Ω has been attributed to decrease of kinetic energy of the droplet transferred to weld pool dictating the cavity formation [Goyal V. K. et. al., 2008(a)]. In spite of reduction in I_p with the increase of ϕ at a given I_m and Ω (Table-6.3), which reduces the velocity of droplet [Ghosh P. K. et. al. 2006], the enhancement of its kinetic energy is predominantly governed by the increase of mass of droplet (droplet size) [Ghosh P. K. et. al. 2006]. However, at a given ϕ the kinetic energy of the droplet increases with the enhancement of I_m , boosting the peak current, predominantly by an increase of droplet velocity in spite of its relatively reduced mass, while an increase in fluidity of the weld pool also acts favourably due to increase of its temperature [Devkumaran K. et. al., 2009] resulting a higher depth of cavity.

To control thermal distribution in super-heated weld pool surrounding the point of heat transfer by droplet inside the cavity, it is necessary to identify the critical points where the desired temperature of weld isotherm should exist for fusion of groove wall. In case of dissimilar groove wall in a MPSSPL ultra-narrow gap welding, the weld isotherm is not similar

in all the directions in reference to focal point of the cavity formed in weld pool as the primary point of heat transfer.

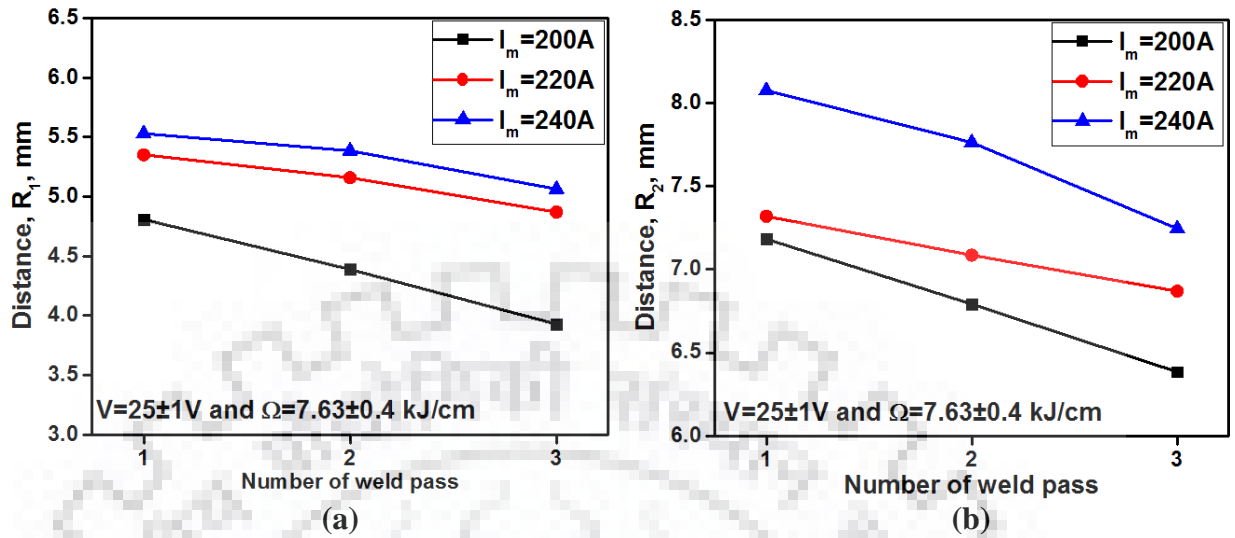


Figure 6-29 Variation of the distance R_1 and R_2 at each weld pass of a given Ω of 7.63 ± 0.4 kJ/cm under different I_m .

The points which primarily guide the soundness of weld joint with respect to lack of fusion may be considered as the touching points of the upper and lower layers of weld pool with the both side of dissimilar groove wall marked as P_1 and P_2 respectively as typically shown in Fig. 4.3 (chap.4). The distance of these two points from the center of the arc, P , on both side of dissimilar groove wall where the molten droplets are deposited in the cavity has been marked as R_1 and R_2 . R_1 and R_2 are the distance of upper and lower point of touching by weld deposit to dissimilar groove wall from the center of arc P to P_1, P_1' as well as P_2, P_2' respectively. The distances R_1 and R_2 with the change in number of weld pass, as estimated by the eqs. 4.20 and 4.21 (Chapter 4), under varying I_m of 200, 220 and 240A at the variation of Ω of 7.64 ± 0.4 kJ/cm and 9.81 ± 0.5 kJ/cm has been typically shown in Figs. 6.29 and 6.30 respectively. The figures show that both the distances R_1 and R_2 increase with the increase of Ω but decrease with the number of weld pass, however, both the distances R_1 and R_2 increase with the increase of I_m , while the other two respective parameters remain constant. Whereas, the enhancement of R_1 and R_2 with the increase of I_m or Ω at a given other parameters may have primarily happened due to increase of weld metal deposition per unit length. But, the R_2 always becomes higher than R_1 irrespective of any change in number of weld pass, Ω and I_m . Thus, maintaining a desired temperature of weld isotherm for groove wall fusion at the farthest point R_2 from the point P may be considered as the critical predominating factor to avoid lack of fusion in centrally laid MPSSPL ultra-narrow gap welding.

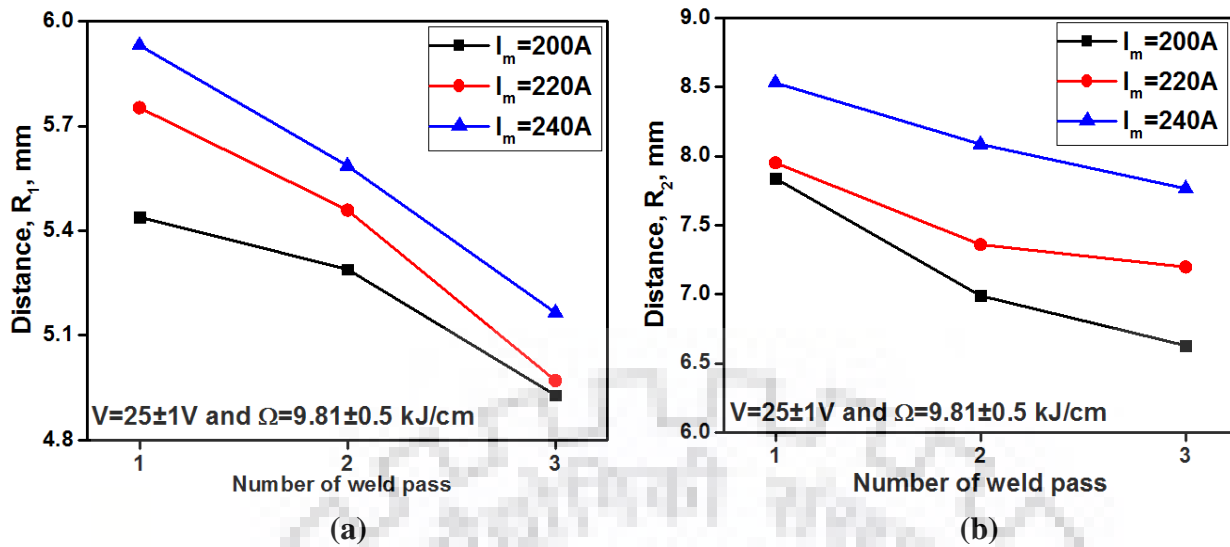


Figure 6-30 Variation of the distance R_1 and R_2 at each weld pass of a given Ω of 9.81 ± 0.5 kJ/cm under different I_m .

6.4.1.4. Weld isotherm in molten pool

At two values of ϕ , the weld isotherms of the weld pool at different pulse parameters and same heat input, as estimated by using the eqs. 4.24 and 4.33 (chap.4), which gives rise to MPSSPL ultra-narrow gap weld joint without lack of fusion are typically discussed below where, the arc voltage has been kept constant as $25\pm 1V$. The weld isotherms are determined in reference to the arc centre assumed as coinciding with the point P. At a given Ω and ϕ of 9.81 ± 0.5 kJ/cm, and 0.5 respectively, the typical weld isotherms at different I_m 200, 220 and 240A are shown in fig.6.31 (a-c) respectively. Similarly for another ϕ of 0.25 under the same Ω the weld isothermal at different I_m value 200, 220 and 240A are shown in Fig.6.32 (a-c) respectively. The figures reveal that the length and width of the weld isotherm relatively reduces with the increase of ϕ at a given Ω and I_m . It is further observed that the length and width of isotherm also increases with the increase of I_m at a given Ω and ϕ . In consideration of significant influence of welding speed on the shape of weld isotherm, the above observations are made with appropriate care of welding speed as per the parameters shown in Table-6.3. The reduction in length and width of the weld isotherm with the increase of ϕ at a given Ω and I_m may have primarily happened due to significant reduction in heat transfer by the arc and filler metal to the weld pool with the increase of ϕ [Kulkarni S. G.,2008, Devakumaran K., 2009]. The reduction in heat transfer by the filler metal happens primarily due to convection, conduction and radiation heat losses during transfer of droplets from the electrode tip to the weld pool. However, the increase of width and length of the weld isotherm with the increase of I_m at a given Ω and ϕ are primarily governed by the increase in amount of metal deposition enhancing

the heat transfer to the weld pool. The width of weld isotherm at a given set of Ω , I_m and ϕ provides an idea regarding its possibility to touch the dissimilar groove wall and fuse appreciably by a given set of pulse parameters. The weld isotherm shown in Fig.6.31 and Fig. 6.32 may give rise to appropriate fusion with the both side of dissimilar groove wall because the weld pool associated with these isotherms may touch and fuse the dissimilar groove wall leading to production of a weld joint without any lack of fusion.



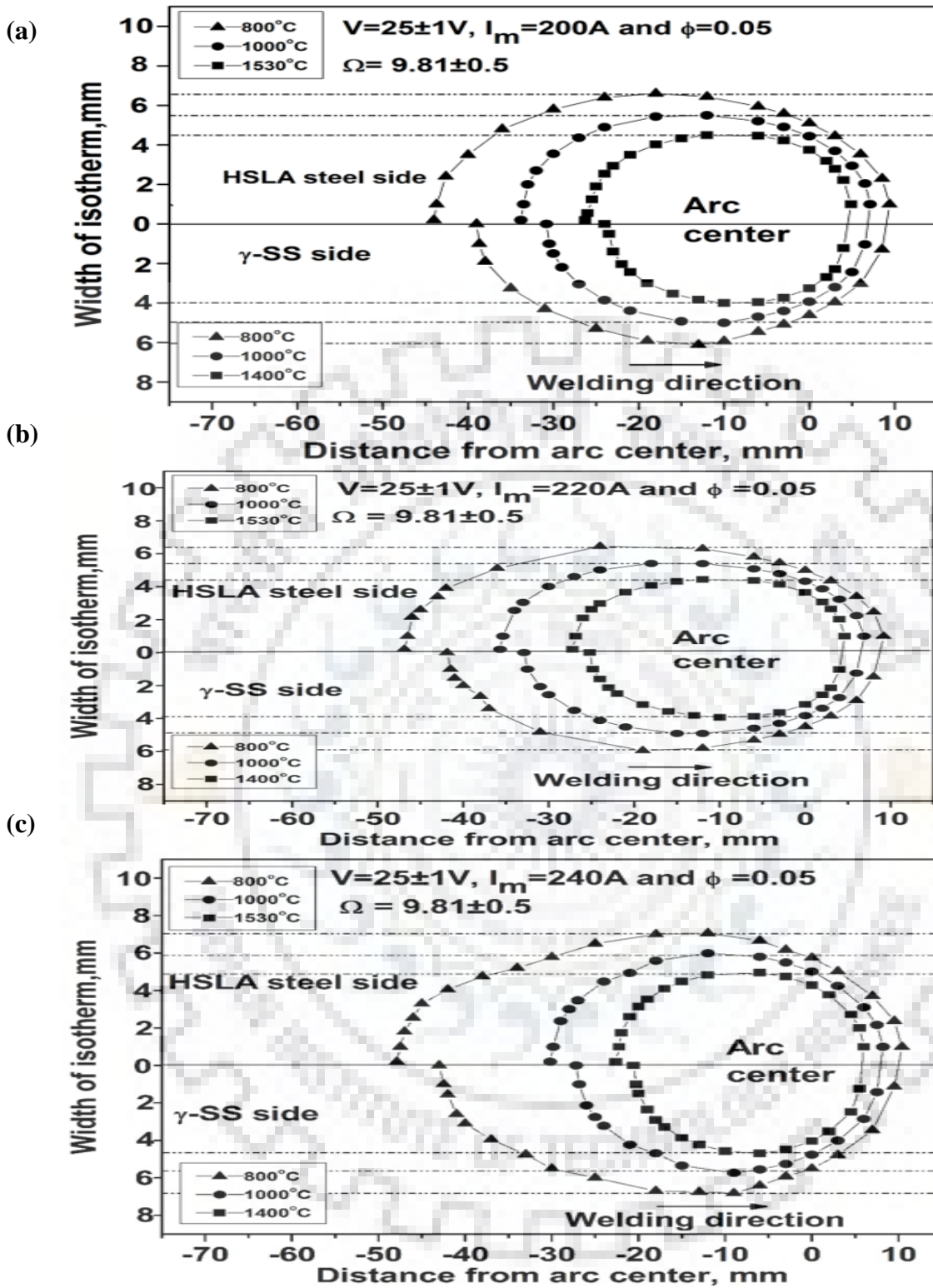


Figure 6-31 At a given arc voltage the typical isotherm of weld pool at different I_m and same ϕ value respectively of (a) 200A and 0.05, (b) 220A and 0.05 and (c) 240A and 0.05 at Ω of 9.81 ± 0.5 .

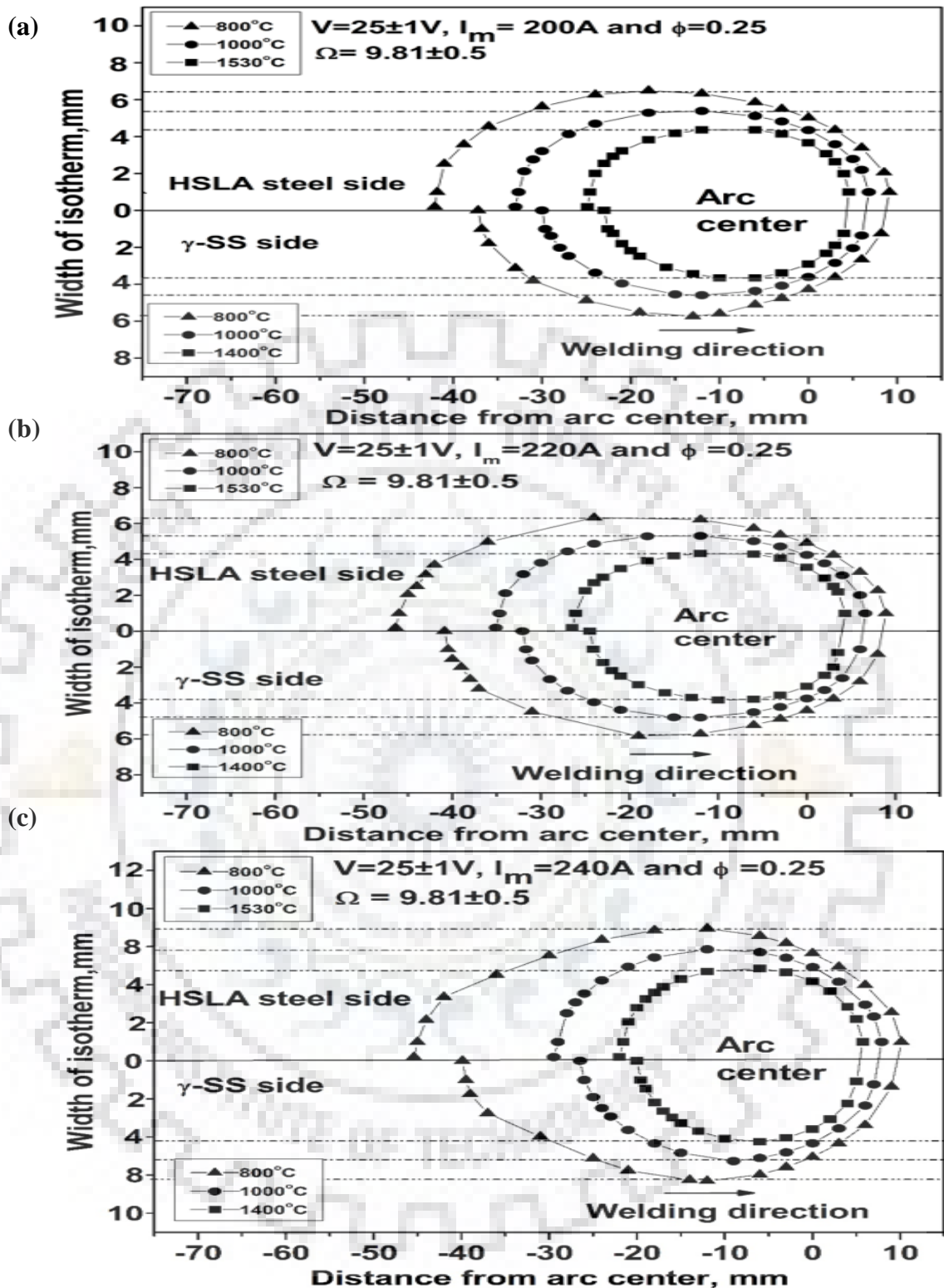


Figure 6-32 At a given arc voltage typical isotherm of weld pool at different I_m and ϕ respectively of (a) 200A and 0.25, (b) 220A and 0.25, (c) 240A and 0.25 and at Ω of 9.81 ± 0.5 .

6.4.2. Validity of model analysis

In order to justify the validity of the model analysis as stated above the condition of weld pool in centrally laid MPSSPL ultra-narrow groove dissimilar weld with respect to its ability to

fuse the both side of dissimilar groove wall has been analyzed at various pulse parameters. Out of them two typical theoretical conditions of analyses representing the situation of welding without and with groove wall fusion are presented here followed by their experimental verification.

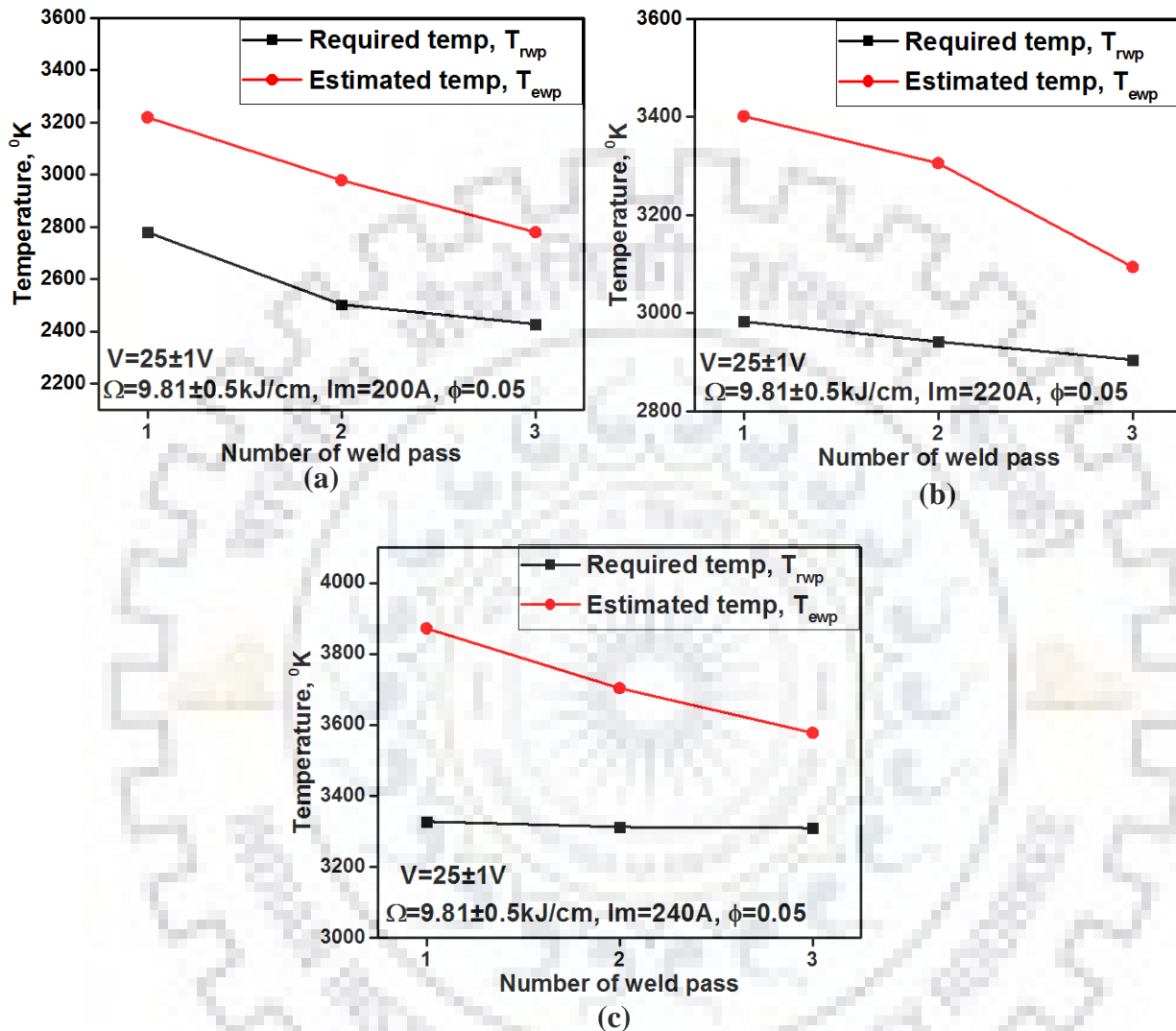


Figure 6-33 Comparison of the estimated and required temperature of the weld pool at different I_m and ϕ respectively of (a) 200A and 0.05, (b) 220A and 0.05 and (c) 240A and 0.05 at Ω of 9.81 ± 0.5 kJ/cm.

At a given Ω of 9.81 ± 0.5 kJ/cm, the estimated temperature (T_{ewp}) of the weld pool and the required temperature (T_{rwp}) of an weld pool (Fig. 6.33 (a-c), Fig. 6.34 (a-c)) for desired fusion of metal as estimated on the basis of m_t (Total base metal fusion) at a given Ω of 9.81 ± 0.5 kJ/cm, a comparison of the T_{ewp} and T_{rwp} of an weld pool at different I_m and ϕ respectively of (a) 200A and 0.05, (b) 220A and 0.05 and (d) 240A and 0.05, which may give rise to sound weld without lack of fusion in both side of dissimilar groove wall according to their weld isotherm has been shown in Fig. 6.31 (a-c), Fig. 6.32 (a-c).

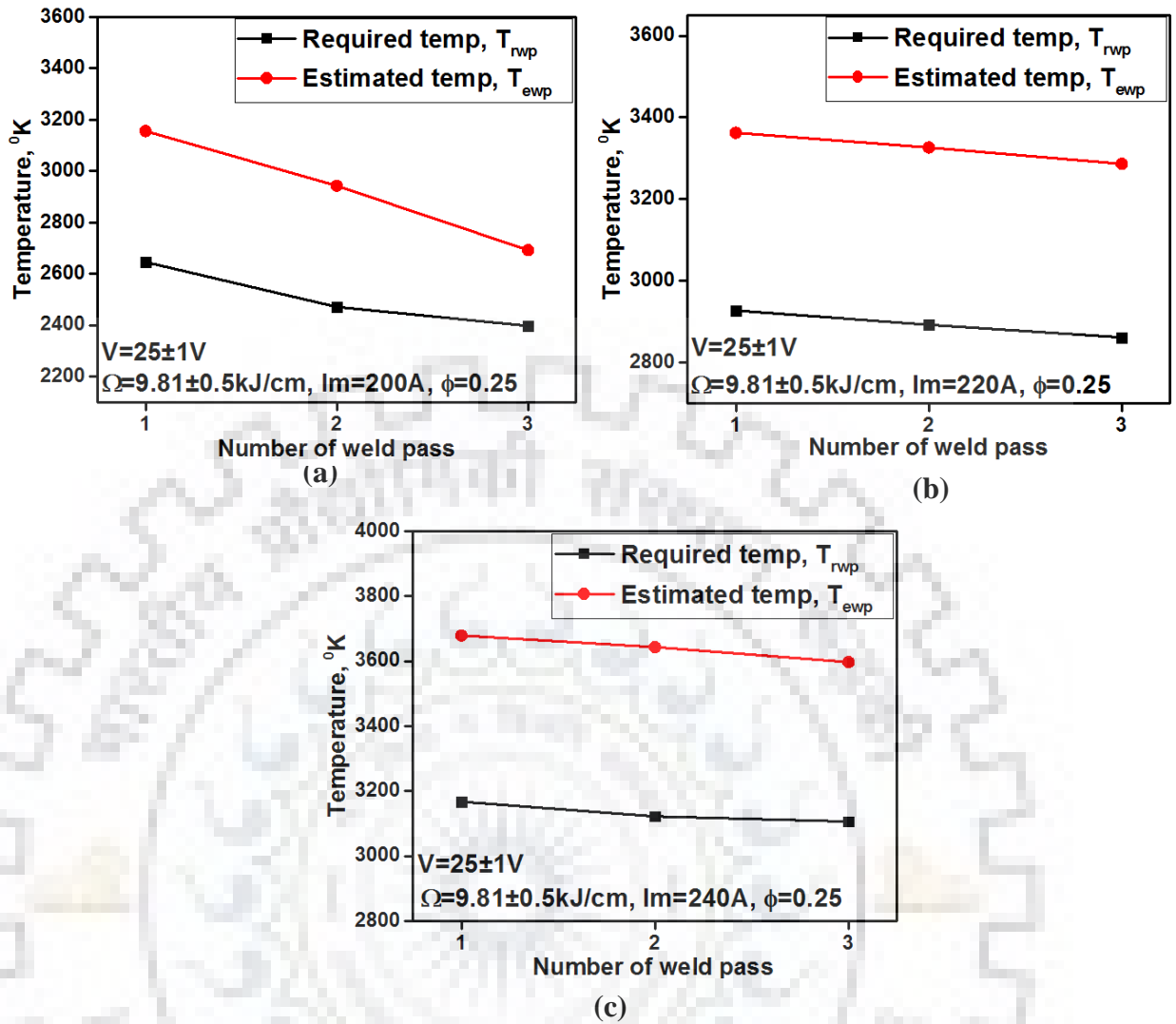


Figure 6-34 Comparison of the estimated and required temperature of the weld pool at different I_m and ϕ respectively of (a) 200A and 0.25, (b) 220A and 0.25, (c) 240A and 0.25 at Ω of 9.81 ± 0.5 kJ/cm.

6.4.3. Analyses of weld performance

Typical appearance of the centrally laid MPSSPL ultra-narrow groove P-GMA dissimilar weld joints prepared by weld deposition at a constant arc voltage ($25\pm 1V$) and Ω of 7.64 ± 0.4 kJ/cm using the I_m and ϕ respectively of (a) 200A and 0.05, (b) 220A and 0.05 and (c) 240A and 0.05 has been shown in Fig. 6.35(a-c). Similarly the appearance of ultra-narrow groove P-GMA dissimilar weld joints prepared by weld deposition at the same arc voltage but relatively higher Ω of 9.81 ± 0.5 kJ/cm using different I_m and ϕ respectively of (a) 200A and 0.05, (b) 220A and 0.05, (c) 240A and 0.05 has been typically shown in Fig. 6.36 (a-c). Similarly the appearance of similar ultra-narrow groove P-GMA dissimilar weld joints prepared by weld deposition at the same arc voltage and same Ω of 9.81 ± 0.5 kJ/cm using different I_m and ϕ

respectively of (a) 200A and 0.25, (b) 220A and 0.25, (c) 240A and 0.25 has been typically shown in Fig. 6.37 (a-c). In agreement to the weld isotherms presented in Fig. 6.31 and Fig. 6.32 according to the model prediction, it appears that in all the cases of Fig. 6.35(a-c) the weld pool is unable to touch the both side of groove wall showing lack of fusion to it weld passes of filling the weld groove. Whereas, the Fig. 6.36 (a-c) shows that at relatively higher Ω of 9.81 ± 0.5 kJ/cm the weld pool is well in contact with the groove wall which may give rise to appropriate fusion in it which is also predicted from weld isotherms. However, the features of weld deposit revealed in the photographs presented in Fig. 6.36 and Fig 3.37 further confirms that at a given Ω of 9.81 ± 0.5 kJ/cm the pulse parameters I_m and ϕ have significant influence on uniform spreading and intimate contact of weld pool in the weld groove. It is observed that at a given ϕ of 0.05 and 0.25, increase of I_m from 200 to 240A relatively improves the contact of weld pool to the both side of groove wall, whereas at a given I_m of 200 to 240A a low value of ϕ i.e. 0.05 further improves it to reduce lack of dissimilar groove wall fusion during multi pass weld deposit. The said improvement in groove wall fusion with the increase of I_m and decrease of ϕ primarily happens due to increase of droplet temperature at the time of deposition [Ghosh P. K. et. al. 2006] enhancing the heat transfer to the weld pool [Devakumaran K., 2009] resulting higher weld pool temperature [Devakumaran K. et. al., 2009, Goyal V. K. et. al., 2008(a)] with wider bead width and large external weld toe angle. Thus, it may be assumed that in spite of getting better groove wall fusion at higher Ω , keeping pulse parameters having lower ϕ and higher I_m may further assure preparation of a sound weld joint avoiding lack of fusion in it.

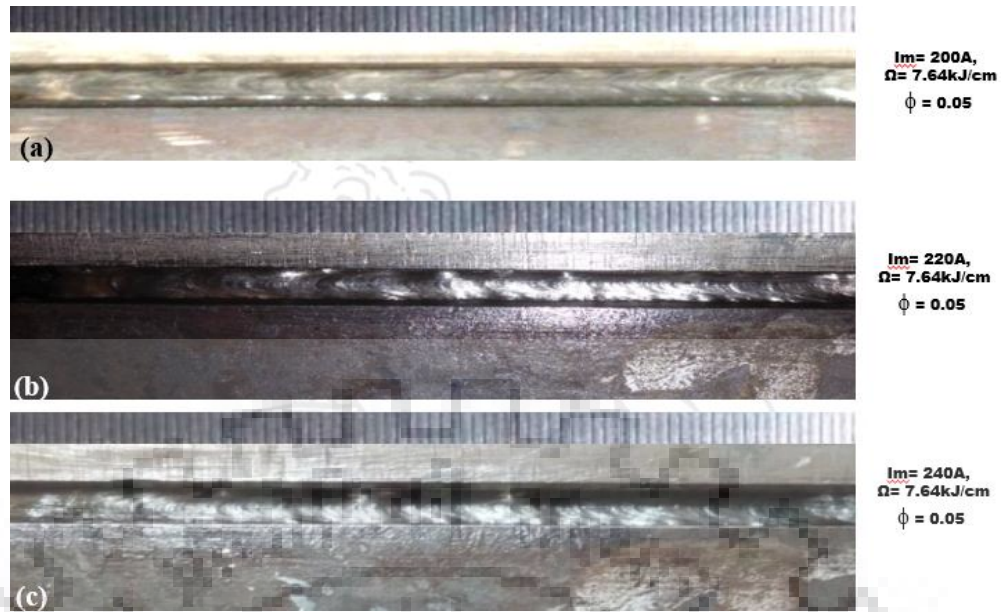


Figure 6-35 Typical appearance of interrupted intimate contact of single seam per layer weld deposit with the dissimilar groove wall in ultra-narrow gap welding at (a) 200A and 0.05, (b) 220A and 0.05, (c) 240A and 0.05 at Ω of 7.64 ± 0.5 kJ/cm.

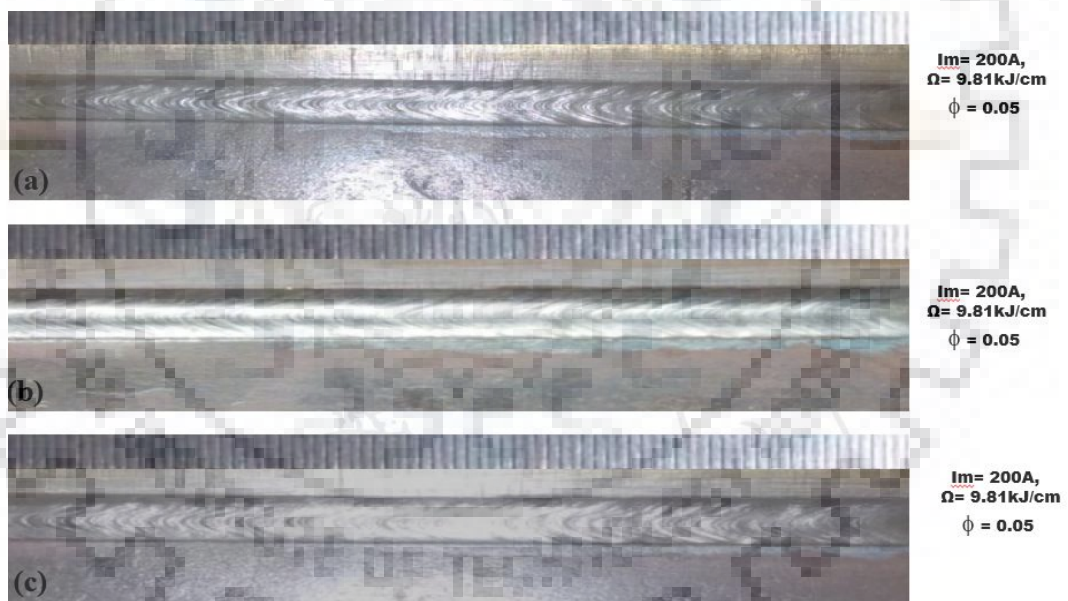


Figure 6-36 Typical appearance of uninterrupted intimate contact of single seam per layer weld deposit with the dissimilar groove wall in ultra-narrow gap welding at (a) 200A and 0.05, (b) 220A and 0.05, (c) 240A and 0.05 at Ω of 9.81 ± 0.5 kJ/cm.

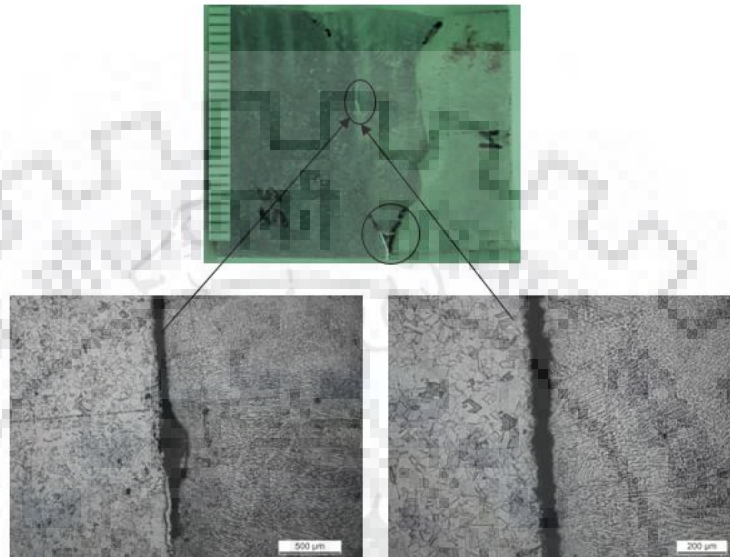


Figure 6-37 Typical appearance of uninterrupted intimate contact of single seam per layer weld deposit with the dissimilar groove wall in ultra-narrow gap welding at (a) 200A and 0.25, (b) 220A and 0.25, (c) 240A and 0.25 at Ω of 9.81 ± 0.5 kJ/cm.

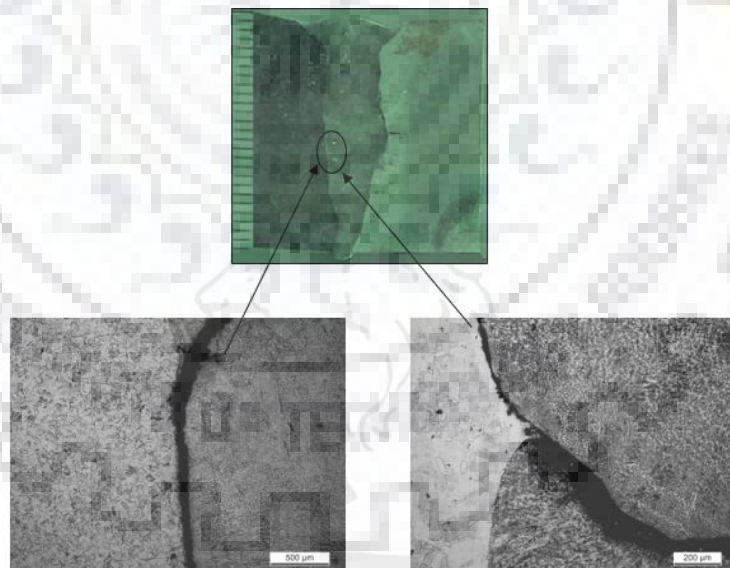
Transverse section of the multi pass dissimilar welds revealing their soundness of it with respect to lack of fusion in dissimilar groove wall has been shown in the macrographs presented in Figs. 6.38 (a-c) and Figs. 6.39 (a-c) where the Ω has been kept at 7.63 ± 0.4 and 9.81 ± 0.5 kJ/cm respectively at a given arc voltage of $25 \pm 1V$. The Fig. 6.38 shows that at the low Ω of 7.63 ± 0.4 kJ/cm using a relatively low I_m and high ϕ of 200A and 0.05 respectively, starts resulting a lack fusion in groove wall from about second layer of weld pass in γ -SS side from the root of the weld groove, which is broadly in agreement to the model analyses shown in Fig. 6.38 (a). However, at the same Ω an increase of I_m to 220A and 240A with ϕ of 0.05 (Fig. 6.38 (b,c)), resulting a lack fusion in groove wall from about second layer of weld pass in γ -SS side from the root of the weld groove, which is also broadly in agreement to the model analyses shown in Fig. 6.38(a). The use of relatively higher Ω of 9.81 ± 0.5 kJ/cm has been grossly found to improve the situation with respect to the groove wall fusion in case of using any I_m and ϕ where, in contrast to the observations of Fig. 6.39(a-c) no lack of both side of dissimilar groove wall fusion has been practically marked in the region of weld passes from the root as shown in Fig. 6.39(a-c). It might have resulted because of application of relatively stronger weld isotherm giving rise to wider weld pool with comparatively higher temperature of it. This is also very much in the line of model analyses shown in Fig. 6.39 (a-c) showing that the temperature of weld pool estimated from the welding parameters is always significantly higher than the required temperature for fusion at the groove wall giving rise to required fusion to it producing

a sound ultra-narrow groove weld joint. The temperature of weld pool estimated from the welding parameters is forced towards higher side resulting in production of weld joint without any lack of fusion for relatively higher Ω of 9.81 ± 0.5 kJ/cm due to application of relatively stronger weld isotherm and larger amount of weld deposition per unit length of the weld.

(a)



(b)



(c)

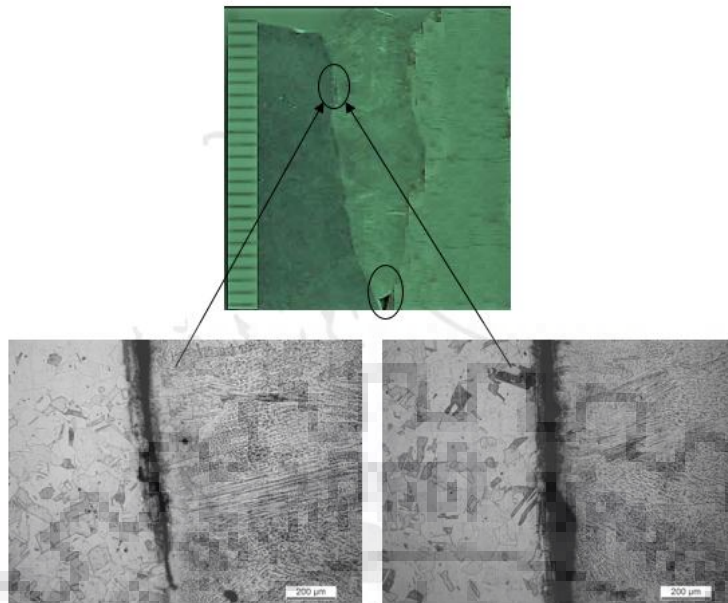
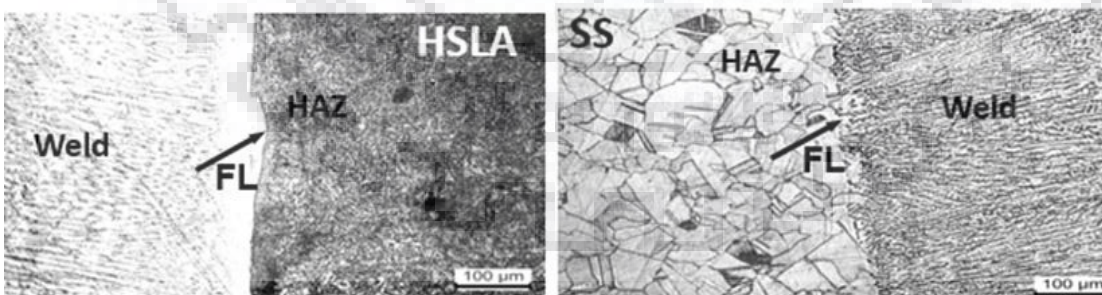
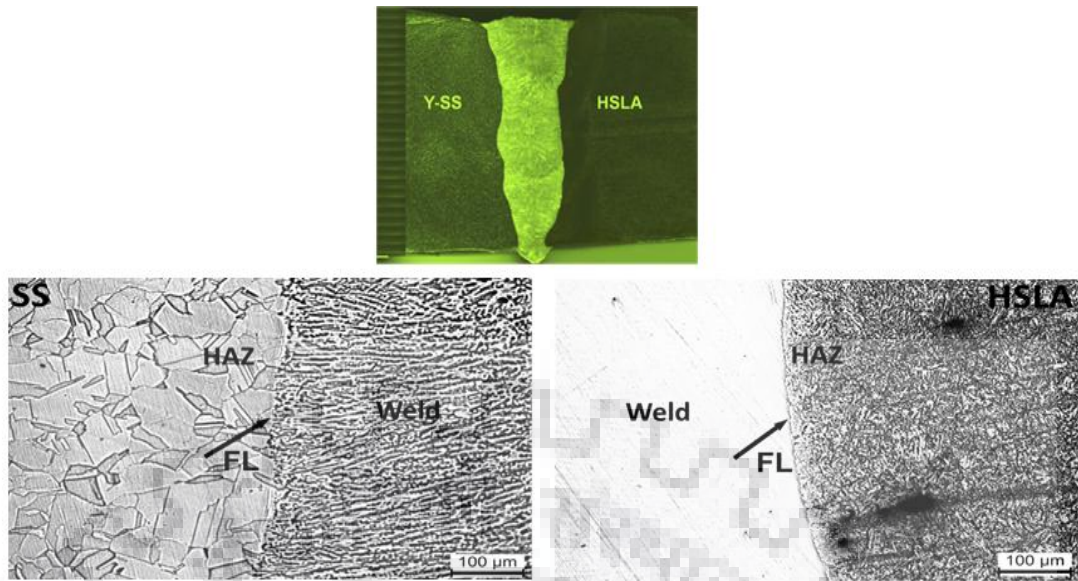


Figure 6-38 Lack of fusion at groove wall typically observed in transverse section of dissimilar weld joint prepared at a given arc voltage and Ω of 25 ± 1 V and 7.63 ± 0.4 kJ/cm respectively under different I_m and ϕ respectively of (a) 200A and 0.05, (b) 220A and 0.05 and (c) 240A and 0.05.

(a)



(b)



(c)

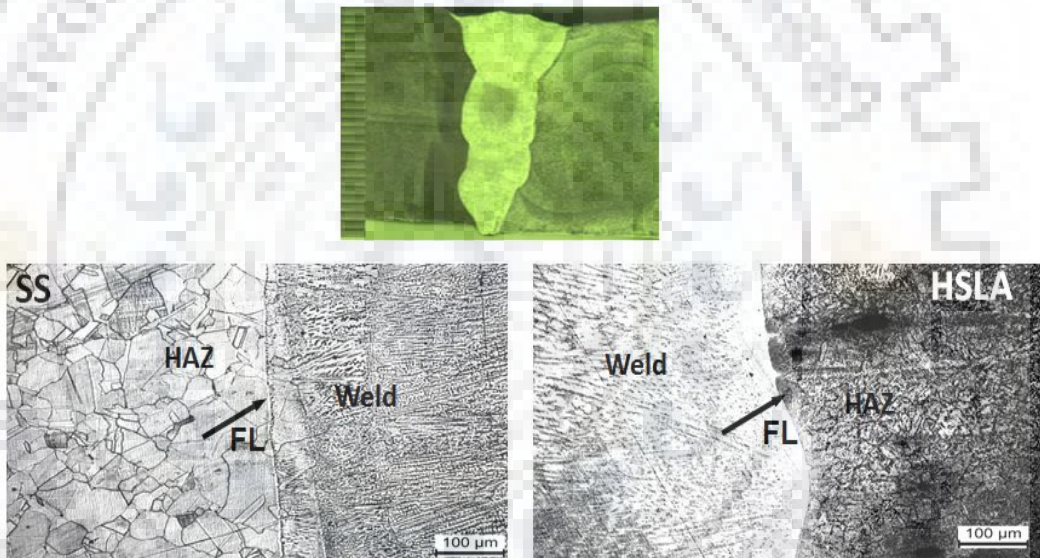


Figure 6-39 Without lack of fusion at groove wall typically observed in transverse section of weld joint prepared at a given arc voltage and Ω of $25 \pm 1V$ and 9.81 ± 0.5 kJ/cm respectively under different I_m and ϕ respectively of (a) 200A and 0.05, (b) 220A and 0.05 and (c) 240A and 0.05

6.5. Characteristics of Multi Pass Single Seam per Layer Centrally Laid Ultra-narrow Gap P-GMA Dissimilar Weld

The appropriate use of pulse parameters allows the production of ultra-narrow gap weld joint free from lack of dissimilar groove wall fusion by MPSSPL centrally laid weld deposition

in ultra-narrow weld groove of thick dissimilar sections using P-GMAW process. The right selection of pulse parameters with the help of model developed (Chap.4) on the basis of thermal and geometrical aspects of weld pool has facilitated to carry out the P-GMAW for producing sound dissimilar weld of γ -SS and HSLA steel. The primary advantage of pulse current gas metal arc welding (P-GMAW) arises from its ability to more precisely control the thermal and geometrical aspects of weld pool specially in the case of dissimilar weld joint. It dictates soundness of weld joint through comparatively more accurate manipulation of energy input as well as energy distribution within the process of welding by appropriate selection of pulse parameters. Thus, the pulse parameters of ϕ , I_m and Ω also affect the metallurgical characteristics and mechanical properties of the weld [Goyal et al 2008, Ghosh et al 2000, Ghosh et al 2007]. The P-GMAW process also gives rise to development of comparatively low heat buildup in weld pool largely arising out of unique control over the characteristics of arc and metal transfer along with interruption in weld metal deposition under the pulse current [Waszink et al 1982, Wang F et al 2003, Wang G et al 2004, Agrawal et al 2010].

The model explained in Chapter 4 along with the knowledge gained out of bead on plate studies can significantly help to decide the pulse parameters which may be used for production of a weld joint free from lack of fusion in MPSSPL centrally laid narrow gap welding of thick dissimilar sections using P-GMAW process. The effect of ϕ at various pulse parameters on shrinkage stress, mechanical and metallurgical properties of the weld have been studied. The properties of dissimilar weld joint as per the parameters selected using P-GMAW process in MPSSPL centrally laid ultra-narrow gap welding has been compared with those of conventional groove multi pass multi seam per layer (MPMSPL) dissimilar weld joint prepared using same process of P-GMAW under similar range of heat input.

6.5.1 Weld appearance and size

6.5.1.1 Multi-pass multi seam per layer conventional V-groove P-GMA dissimilar weld joint

At a given arc voltage (V), ϕ , I_m and Ω of $25\pm 1V$, 0.05, $220\pm 3A$ and $9.81\pm 0.5kJ/cm$ respectively, the typical macrograph of the dissimilar weld as revealed in transverse section of the conventional V-groove (CG) weld joint prepared using MPMSPL welding has been shown in Fig. 6.40. The figure shows the soundness of weld joint with respect to lack of fusion between the inter bead deposit and the dissimilar groove wall to weld deposit.

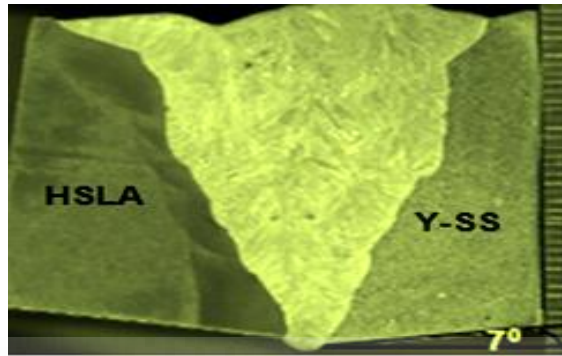


Figure 6-40 Typical macrograph of conventional V-groove P-GMA dissimilar weld joint at a given arc voltage and Ω of $25\pm 1V$ and $9.81\pm 0.5kJ/cm$ and ϕ , I_m of 0.05, 220A.

6.5.1.2 Multi-pass single seam per layer centrally laid narrow gap P-GMA weld joints

At a given close range of arc voltage (V) and Ω of $25\pm 1V$ and $9.81\pm 0.5kJ/cm$ respectively, the typical macrographs of the weld as revealed in transverse section of the MPSSPL centrally laid ultra-narrow gap dissimilar weld joints prepared at different mean currents (I_m) of about 200 ± 2 , 220 ± 3 and $240\pm 4A$ under different ϕ of 0.05 and 0.25 have been shown in Fig. 6.41. The dissimilar welds are prepared by using the pulse parameter in conformation to the model analysis for producing the weld joint free from lack of fusion. The figure typically reveals the uniformity of weld joints as well as their soundness in reference to the presence of discontinuity defect in them.

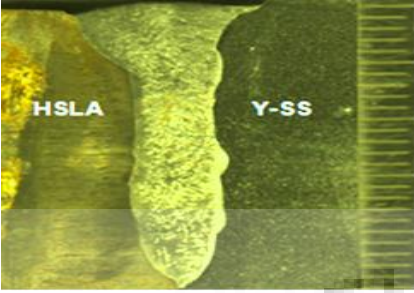
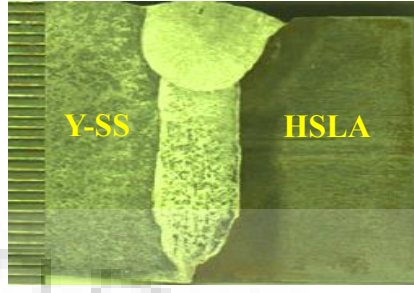




I_m (A)	Different ϕ	
	$\phi = 0.15$	$\phi = 0.25$
200		
220		
240		

Figure 6-41 Typical macrographs of ultra-narrow groove P-GMA dissimilar weld joints at a given arc voltage and Ω of $25 \pm 1V$ and $9.81 \pm 0.5kJ/cm$ respectively under different ϕ and I_m .

Area of weld (A_w) at a given arc voltage (V) and Ω of $25 \pm 1V$ and $9.81 \pm 0.5kJ/cm$ respectively under different ϕ and I_m for MPSSPL centrally laid ultra-narrow gap weld joint has been compared with that of MPMSPL conventional groove weld joint in Fig. 6.42. It is revealed that MPSSPL centrally laid ultra-narrow groove dissimilar weld joints are having considerably lower A_w than that of the MPMSPL conventional V-groove weld joint by about 50-65%.

The area of weld observed in case of commonly used narrow gap P-GMA weld joint has been reported of the order of $304-315 \text{ mm}^2$ [Devkumar, 2009], which is 47-50% higher than that observed in present investigation on MPSSPL narrow gap weld. Thus, the narrow groove used in the present investigation of narrow groove P-GMA weld prepared by using MPSSPL process has been defined as ultra-narrow groove. The observed less area in case of ultra-narrow gap weld may be due to narrow groove weld joint requires comparatively less number of passes to fill the gap and less amount of weld deposition as compared to commonly used narrow groove and conventional V-groove P-GMA weld joint respectively. This has primarily happened

because of MPSSPL narrow gap welding gives an opportunity to use further narrow groove in comparison to that for preparation of narrow groove P-GMA weld in earlier cases.

It is further observed that at a given Ω and I_m , the A_w of MPSSPL centrally laid ultra-narrow groove weld relatively decreases with the increase of ϕ . This is accredited to reduction in melting rate of filler wire and dilution of the base metal with the increase of ϕ due to decrease in total heat content per unit mass of filler metal at the time of deposition (Q_{dc}) [Figs. 6.17(a)] [Goyal et al 2008]. However, it is also revealed that at a given ϕ and Ω , the A_w of ultra-narrow groove weld marginally increases with the enhancement of I_m which may be accredited to enhancement of total heat transferred to the weld pool leading to more dilution.

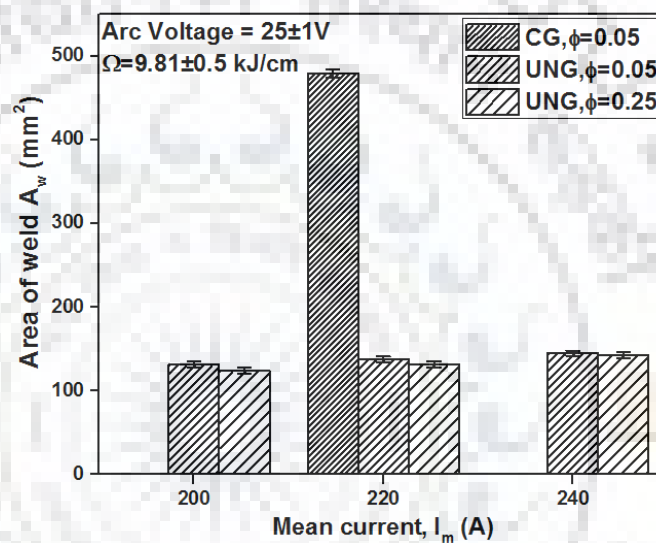


Figure 6-42 Effect of weld groove size and I_m and ϕ on weld area of P-GMA dissimilar weld joints prepared at a given arc voltage and Ω of $25\pm 1V$ and $9.81\pm 0.5kJ/cm$ respectively.

6.5.2 Transverse shrinkage stress and bending stress

The cumulative shrinkage at a given arc voltage (V) and Ω of $25\pm 1V$ and $9.81\pm 0.5kJ/cm$ respectively under different ϕ and I_m for MPSSPL centrally laid ultra-narrow gap dissimilar weld joint of γ -SS and HSLA steel has been compared with that of MPMSPL conventional V-groove dissimilar weld joint in Fig. 6.43. It is found that the cumulative shrinkage marginally increases with the enhancement of number of weld pass irrespective of the variation in either ϕ and I_m or size of weld groove. It is further observed that cumulative shrinkage under similar range of Ω in case of MPMSPL conventional groove weld joint is appreciably higher as compared to MPSSPL centrally laid ultra-narrow gap dissimilar weld joint. This has primarily happened due to comparatively higher amount of weld deposition per unit length in conventional weld groove.

At a given arc voltage (V) and Ω of $25 \pm 1V$ and $9.81 \pm 0.5 kJ/cm$ respectively at different ϕ of 0.05 and 0.25, the effect of I_m on measured transverse shrinkage (Δ_{tr}) during MPSSPL centrally laid narrow gap P-GMA weld joint and MPMSPL conventional groove P-GMA weld joint has been shown in Fig. 6.44. It is observed that the use of MPSSPL centrally laid ultra-narrow groove dissimilar weld significantly reduces the transverse shrinkage by about 67-72% than that of the MPMSPL CG dissimilar weld. It is further observed that at a given I_m and Ω , the increase of ϕ reduces the transverse shrinkage of the weld. This may have primarily happened because of decrease in temperature of weld pool and size of the weld isotherm with the increase of ϕ as explained earlier (section-6.2.2.1). However, it has been found that at a given ϕ and Ω , the increase of I_m enhances the estimated transverse shrinkage. This might have primarily happened because of increment of Q_{dc} with I_m (Fig.6.16(a)).

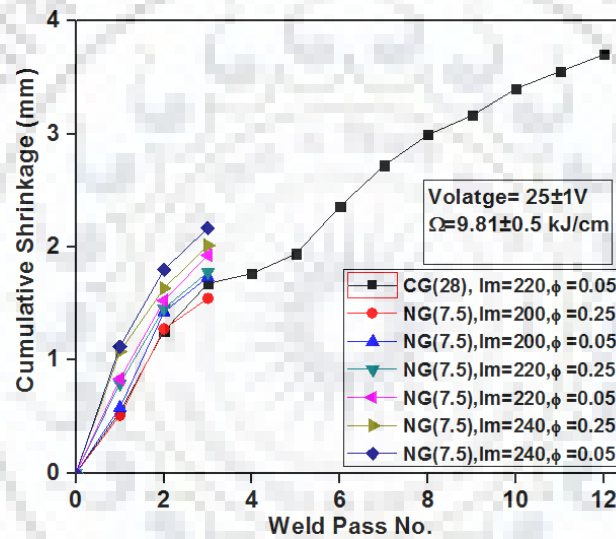


Figure 6-43 Effect of weld groove size and I_m and ϕ on cumulative shrinkage of P-GMA dissimilar weld joints prepared at a given arc voltage and Ω of $25 \pm 1V$ and $9.81 \pm 0.5 kJ/cm$ respectively.

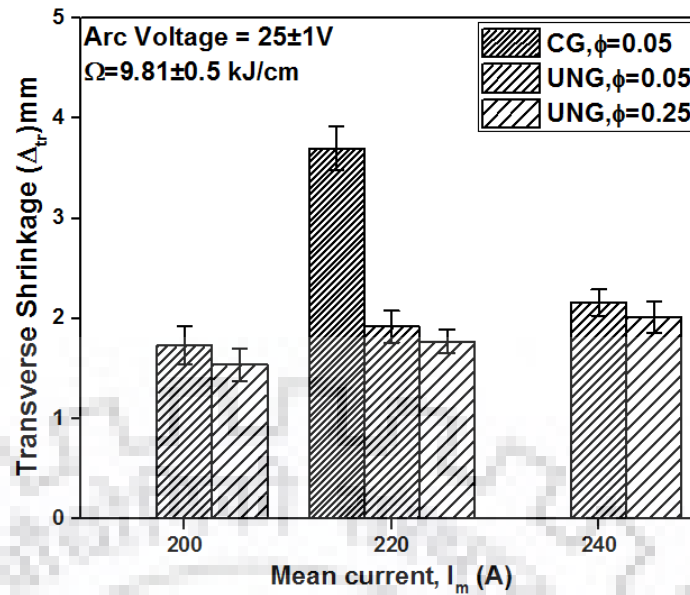


Figure 6-44 Effect of weld groove size and I_m and ϕ on transverse shrinkage of P-GMA dissimilar weld joints prepared at a given arc voltage and Ω of $25\pm 1V$ and $9.81\pm 0.5kJ/cm$ respectively.

The variation in transverse shrinkage as a function of I_m and ϕ , also results into changes in transverse shrinkage stress of the weld. The effect of I_m and ϕ at a given Ω on estimated transverse shrinkage stress of MPSSPL centrally laid ultra-narrow groove P-GMA dissimilar weld joints and MPMSPL conventional groove P-GMA dissimilar weld joint has been shown in Fig. 6.45. It is revealed that at a given Ω , the transverse shrinkage stress developed in the weld joint prepared in case of MPSSPL centrally laid ultra-narrow groove dissimilar weld is 45-60% lower than that observed in case of MPMSPL conventional groove dissimilar weld joint. It is also observed that at a given Ω and I_m increase of ϕ reduces the transverse shrinkage stress while at a given ϕ and Ω increase of I_m enhances the transverse shrinkage stress due similar nature of variation of measured transverse shrinkage with ϕ and I_m as explained earlier.

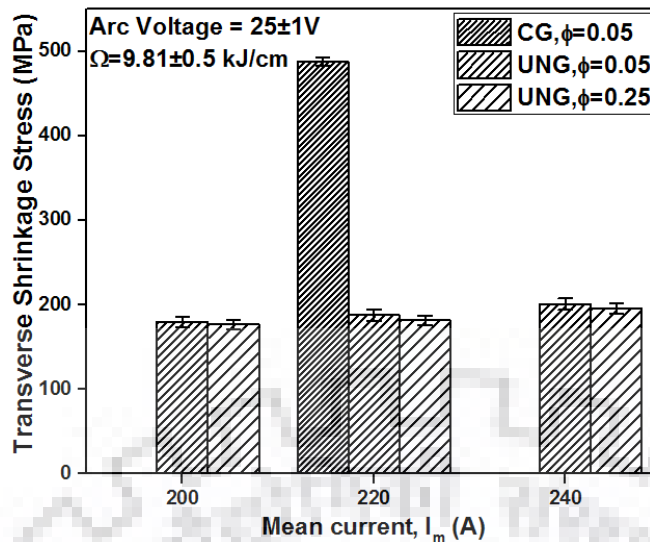
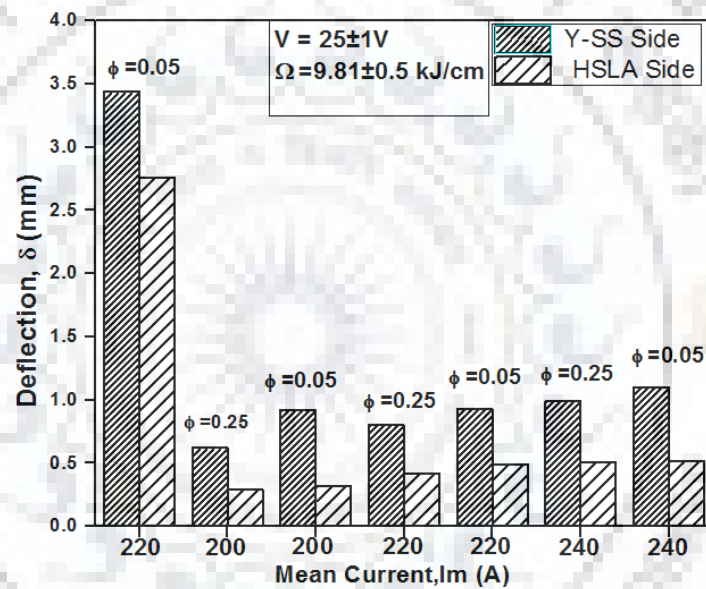


Figure 6-45 At a given arc voltage and Ω of $25\pm 1V$ and $9.81\pm 0.5kJ/cm$ effect of weld groove size and I_m and ϕ of P-GMA weld joints on transverse shrinkage stress.

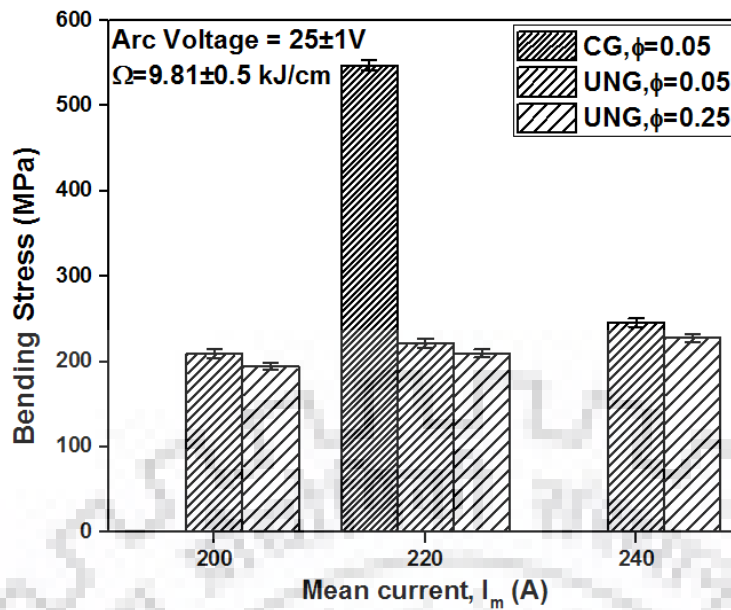
At a given similar range of arc voltage (V) and Ω of $25\pm 1V$ and $9.81\pm 0.5kJ/cm$ respectively at different ϕ of 0.05 and 0.25, the effect of I_m on measured deflection (δ) and estimated bending stress (σ_b) during MPSSPL centrally laid ultra-narrow gap P-GMA dissimilar weld joint and MPMSPL conventional V-groove P-GMA dissimilar weld joint has been shown in Fig. 6.46 (a) and (b). It is observed that the deflection in MPSSPL centrally laid ultra-narrow gap dissimilar weld joint is 71-85% on HSLA steel side and 77-90% on γ -SS side lower than MPMSPL conventional groove dissimilar weld joint. However bending stress of MPSSPL centrally laid ultra-narrow gap dissimilar weld joint is 45-64% lower than MPMSPL conventional groove dissimilar weld joint. The figure further show that both the deflection and bending stress reduces with the increment of ϕ at a given Ω and I_m whereas, these has been found to increase with the enhancement of I_m at a given Ω and ϕ . The nature of variation of deflection with respect to ϕ and I_m is in agreement to the nature of variation of the shrinkage (Fig.6.44) generating bending force in weld joint. The bending stress is primarily governed by deflection. Therefore the variation of bending stress with ϕ and I_m at a given Ω and arc voltage is of similar trend as deflection. In this context here it further confirms that the estimated transverse shrinkage in case of dissimilar weld joint is well in agreement to the bending stress estimated on the basis of distortion generated in weld joints.

One of the major causes of development of residual stresses in the weld joint is shrinkage of the weld on solidification. The shrinkage of weld on solidification is primarily attributed to amount of weld deposition in the weld groove which can be considerably reduced

by using centrally laid ultra-narrow gap MPSSPL welding technique. Thus it can be inferred that the weld joint with higher shrinkage are associated with comparatively higher residual stresses specially in dissimilar weld joint where the thermal properties of metals are different. Thus, MPSSPL centrally laid ultra-narrow groove P-GMA weld joint are having relatively lower residual stresses as compared to MPMSPL conventional groove weld joint. The residual stresses developed in MPMSPL commonly used narrow gap P-GMA weld has been observed to be of the order of 300 Mpa [Kulkarni, 2008] which is comparatively higher than shrinkage stress in the weld prepared by using ultra-narrow gap MPSSPL deposition technique under relatively lower I_m . However, to have clearer comparison of the development of residual stress, it should be measured experimentally for centrally laid ultra-narrow gap MPSSPL weld joint and studied further in detail in section 6.5.7



(a)



(b)

Figure 6-46 At a given arc voltage and Ω of $25\pm 1V$ and $9.81\pm 0.5kJ/cm$ effect of weld groove size and I_m and ϕ of P-GMA weld joints on (a) deflection and (b) bending stress respectively.

6.5.3 Microstructure of weld

The properties of dissimilar weld joint of γ -SS and HSLA steel often become quite sensitive to the microstructure of weld deposit. Earlier observation [Goyal et al, 2007] shows that the presence of coarse dendrites in weld metal can be considered as one of the primary cause of failure of weld joint. Therefore, to achieve desired properties of weld joint specially in case of dissimilar weld joints, a control over the coarsening of microstructure of weld metal is very important. The microstructure of weld is being governed by its chemical composition, temperature and cooling rate. The chemical compositions of the weld is primarily dictated by the compositions of filler metal as well as base metal which is ultimately controlled by degree of dilution and design of groove while the temperature is governed by the heat input, Ω and heat transferred to the weld pool controlling the cooling rate under the given heat sink. The cooling of weld primarily takes place by transfer of heat to the base metal through conduction while other heat transfer may be effective due to convection and radiation from molten weld pool to the surrounding. The use of P-GMAW process has been found to provide improvement in mechanical properties of weld primarily by refining of microstructure of weld metal, which may have caused by the interruption in metal deposition under the pulsed current (Agrawal et al 2010). The interruption in metal deposition affecting the solidification of weld pool to refine its microstructure largely depends upon the pulse parameters affecting the heat input and heat built up in it (Agrawal et al 2010, Ghosh et al 2017). Hence micro structural studies have been

carried out in order to analyze the influence of thermal aspects prevailing in MPSSPL centrally laid P-GMA dissimilar weld deposition and compared with MPMSPL conventional groove P-GMA dissimilar weld joint.

6.5.3.1 Conventional V-groove

At a given arc voltage (V), mean current (I_m), ϕ and heat input (Ω) of $25\pm 1V$, $220\pm 3A$, 0.05 and $9.81\pm 0.5kJ/cm$ respectively, the typical microstructure of different zone of MPMSPL P-GMA weld deposit revealing its scarcely distributed coaxial dendrite and reheat refined (RR) morphology under optical microscope has been shown in Figs. 6.47. The microstructure of the two distinctly different regions has been found to consist of both coaxial dendrite and reheat refined fine grain morphology. This may have primarily happened due to partial melting and heat treatment of earlier weld bead by subsequent weld deposition in multi pass welding process.

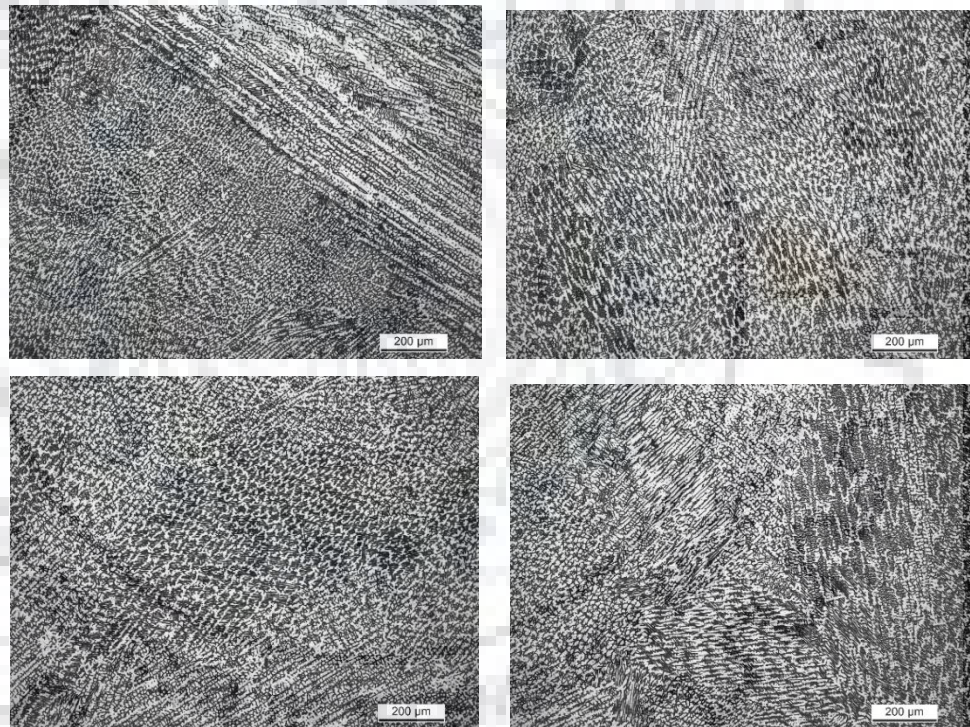


Figure 6-47 Typical microstructures of CG P-GMA weld deposit from its different portion of the weld joint at a given arc voltage, ϕ , I_m and Ω of $25\pm 1V$, 0.05 and $240A$ and Ω of $9.81\pm 0.4kJ/cm$.

6.5.3.2 MPSSPL Narrow Gap P-GMA Weld Joints

At a given arc voltage (V) and Ω of $25\pm 1V$ and $9.81\pm 0.5kJ/cm$ respectively, effect of ϕ and I_m on microstructure of MPSSPL centrally laid ultra-narrow gap P-GMA weld deposit has been shown in the micrographs presented in Fig. 6.48. Similar to MPMSPL conventional groove P-GMA weld joint, the microstructure here too consists of a mixture of scarcely distributed coaxial dendrite and reheat refined (RR) region in the multi pass welds. However, their amount and distribution in the multi pass welds have been found to vary with a change in parameters of welding of I_m and ϕ as discussed below. In MPSSPL centrally laid ultra-narrow gap welding, the variations in these aspects of weld deposits are primarily governed by the extent of partial remelting and reheat refinement of dendritic microstructure of an earlier deposited weld bead by a later one.

The variation in fraction of coaxial dendritic region and reheat refined region of weld deposit with the change in I_m and ϕ at a given Ω of $9.81\pm 0.5kJ/cm$ has been shown in Fig. 6.49, Fig. 6.50 and 6.51, Fig. 6.52 respectively. It has been observed that fraction of dendritic region of weld deposit is comparatively higher and consequently the reheat refined region are relatively lower in case of MPMSPL conventional groove P-GMA weld joint than that of MPSSPL centrally laid ultra-narrow groove P-GMA weld joint. This may have primarily attributed to application of milder weld isotherm largely due to relatively lower amount of weld deposition in MPSSPL centrally laid ultra-narrow groove P-GMA weld joint. It is further understood that at a given Ω and I_m the increase of ϕ enhances the dendrite fraction and consequently reduces the fraction of reheat refined region in the MPSSPL centrally laid ultra-narrow gap P-GMA weld while at a given Ω and ϕ the increase of I_m decreases the dendrite fraction and increases the reheat refinement fraction in the MPSSPL centrally laid ultra-narrow gap P-GMA weld. At a given Ω and I_m the enhancement of dendritic fraction and consequent reduction in reheat refinement fraction in the MPSSPL centrally laid ultra-narrow gap P-GMA weld with the increase of ϕ may have primarily attributed to relatively lower weld pool temperature [Goyal et al 2009, Agrawal et al 2010, Ghosh 2017] and amount of metal deposition per unit length. It is further observed that the fraction of dendritic region of weld deposit is comparatively lower and consequently the reheat refined region are relatively higher in case of MPSSPL centrally laid ultra-narrow groove than that of commonly used conventional MPMSPL narrow groove P-GMA weld joint [Devkumar, 2009]. This may have primarily attributed to application of milder weld isotherm largely due to relatively lower amount of weld deposition in MPSSPL centrally laid narrow groove P-GMA weld joint.

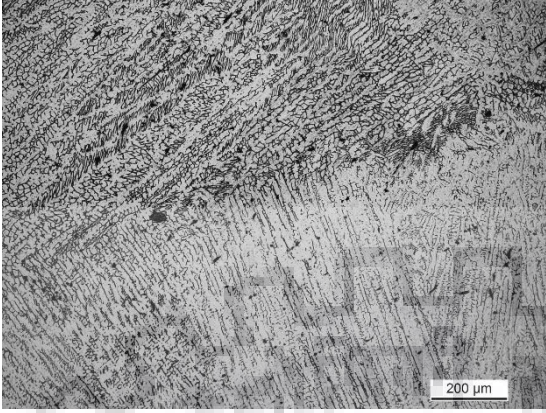
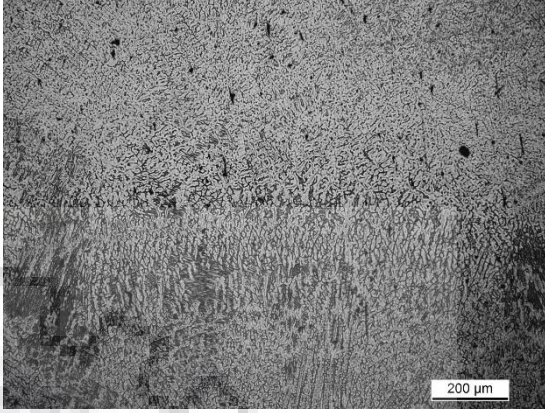
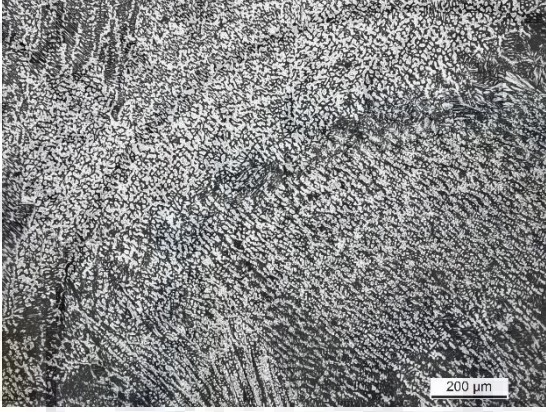
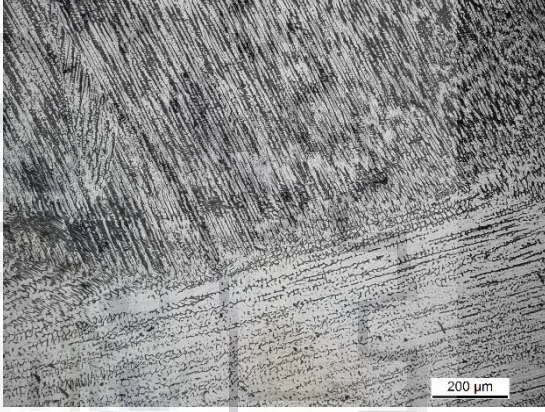
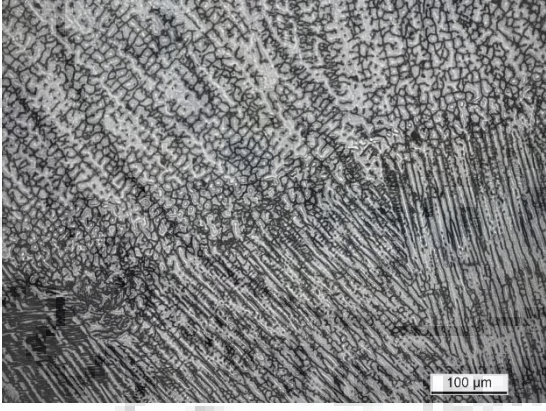
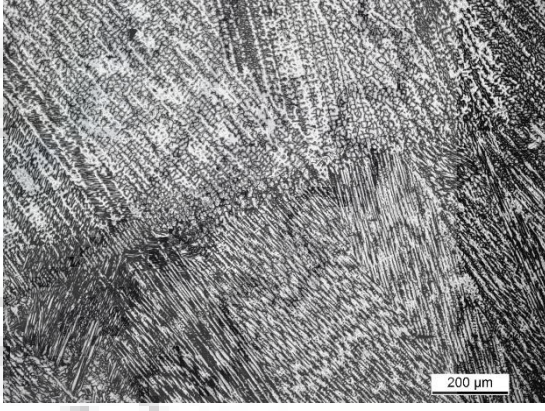
I_m (A)	Different ϕ	
	$\phi = 0.05$	$\phi = 0.25$
200		
220		
240		

Figure 6-48 At a given arc voltage and Ω of $25 \pm 1V$ and $9.81 \pm 0.5kJ/cm$ typical microstructures of intersection part of MPSSPL ultra-narrow gap P-GMA weld joint prepared at different I_m and ϕ .

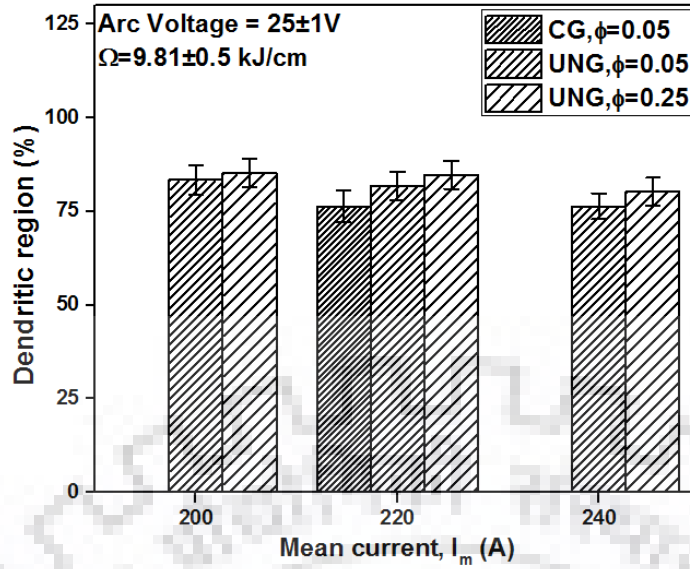


Figure 6-49 Effect of weld groove size, I_m and ϕ on percentage of dendritic region of P-GMA weld joints prepared at a given arc voltage and Ω of $25 \pm 1V$ and $9.81 \pm 0.5 \text{ kJ/cm}$ respectively.

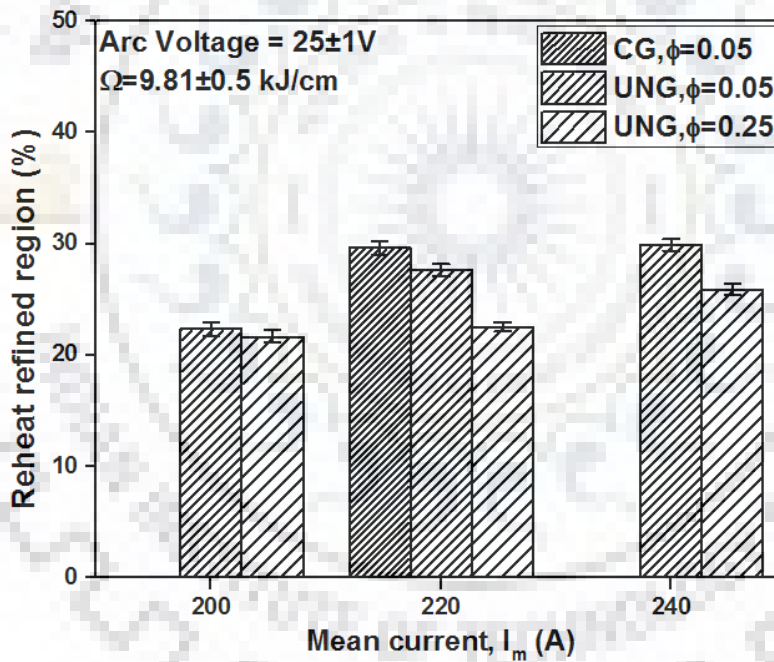


Figure 6-50 Effect of weld groove size, I_m and ϕ on percentage of reheat refined region of P-GMA weld joints prepared at a given arc voltage and Ω of $25 \pm 1V$ and $9.81 \pm 0.5 \text{ kJ/cm}$ respectively.

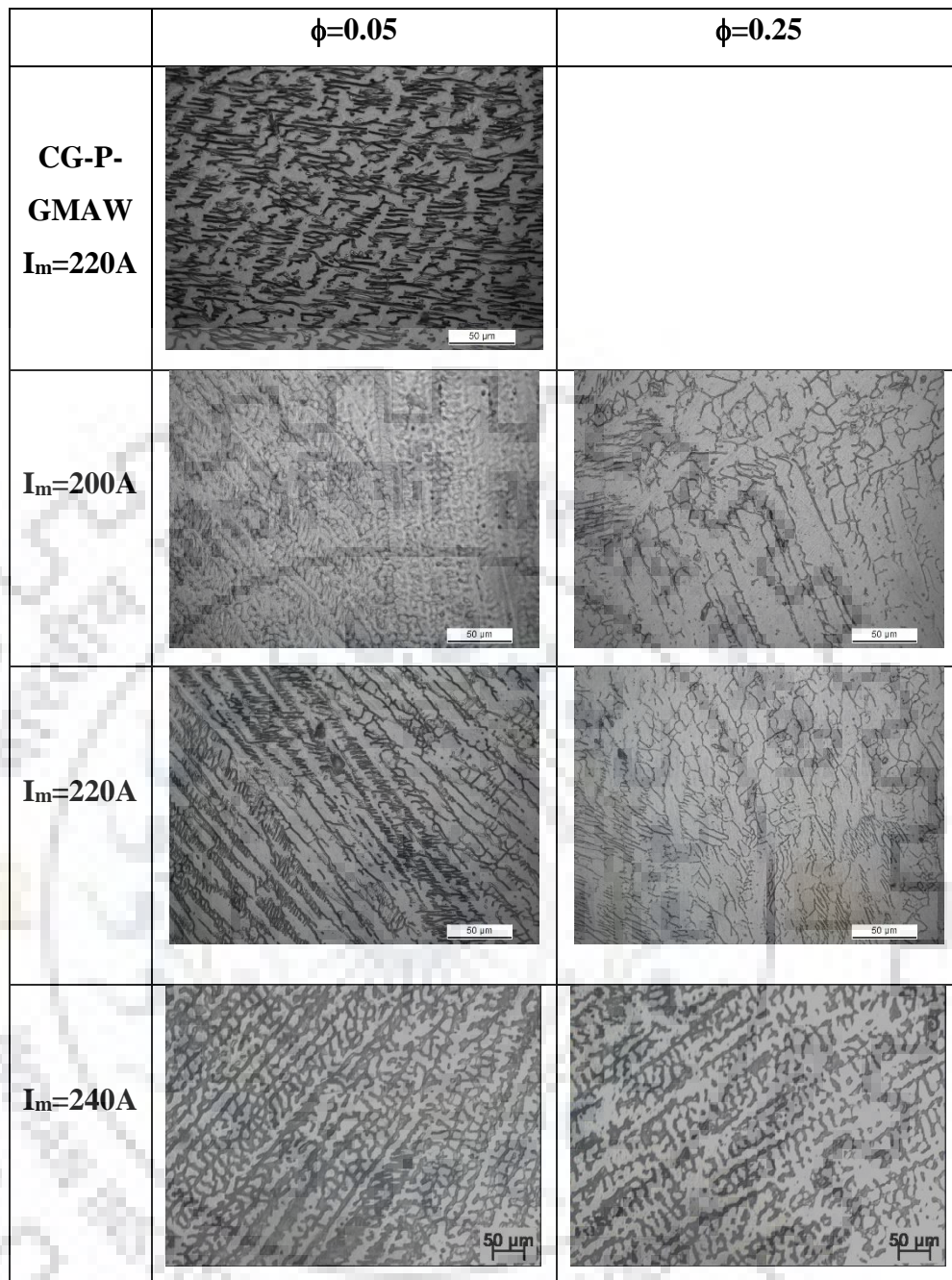


Figure 6-51 Typical dendritic microstructures of MPMSPL conventional groove P-GMA weld joint and MPSSPL ultra-narrow gap P-GMA weld joint at comparatively higher magnification prepared at diverse I_m and ϕ .

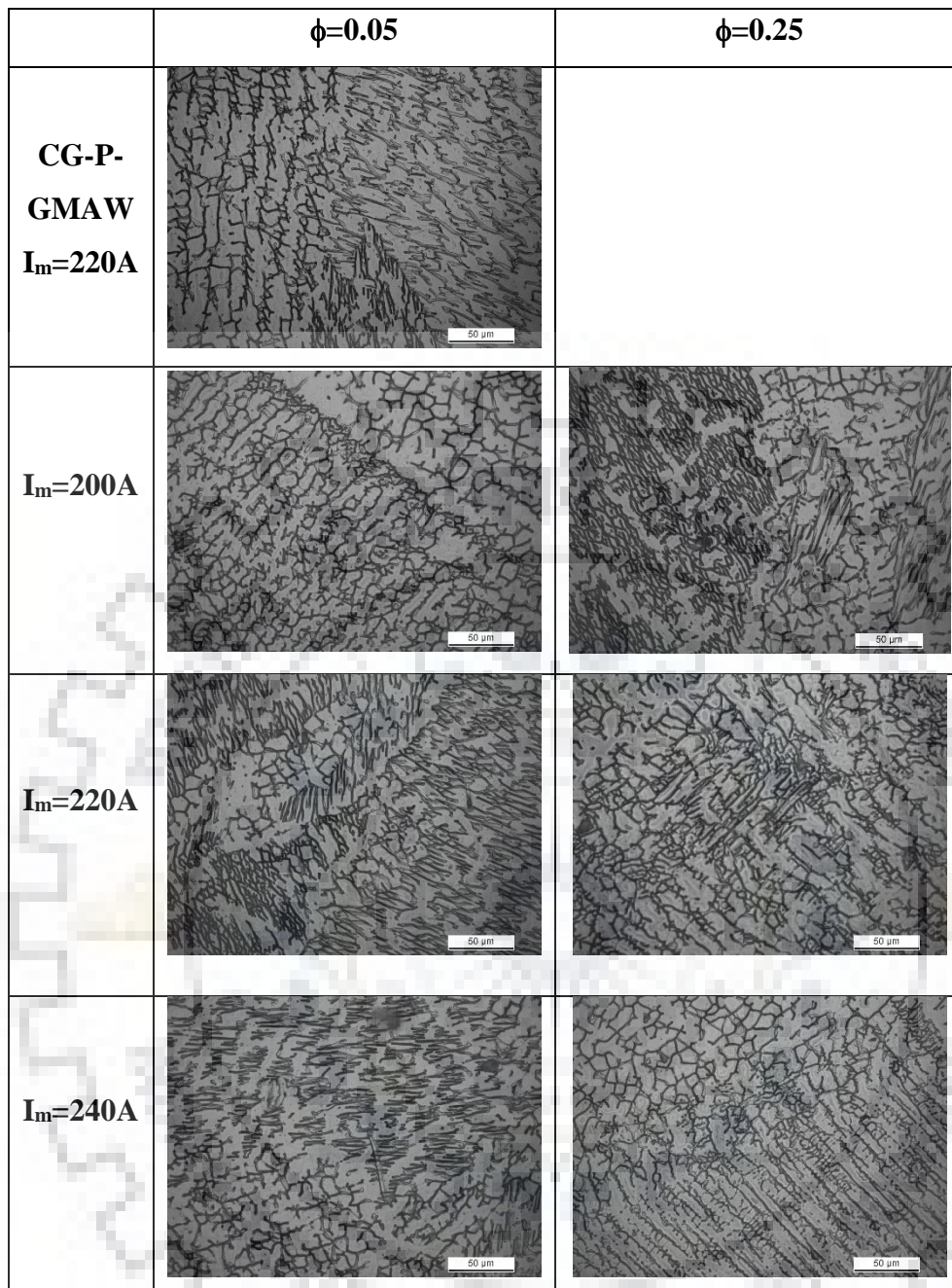


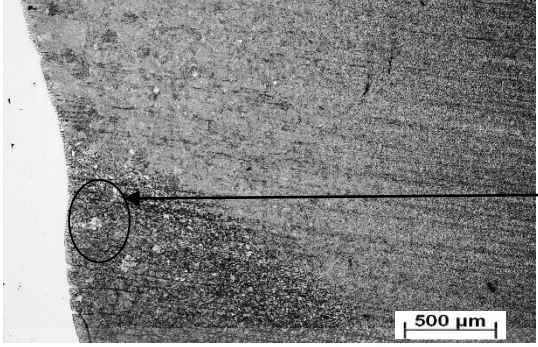
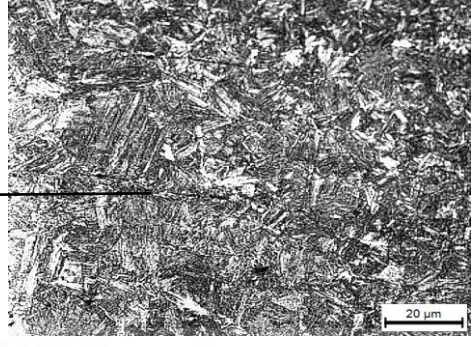
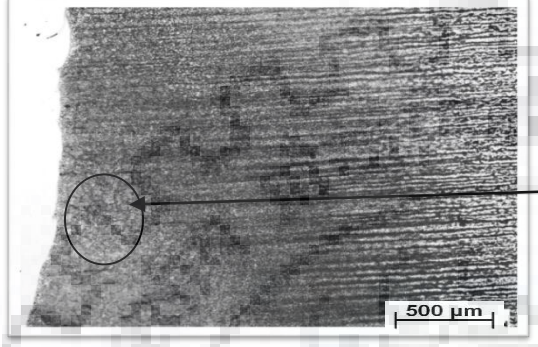
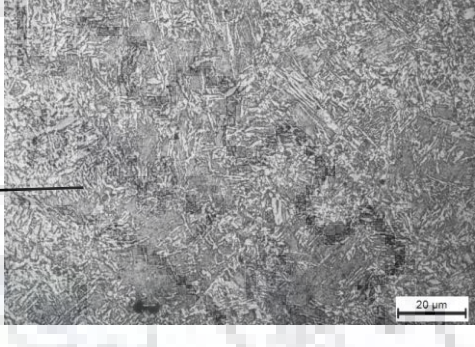
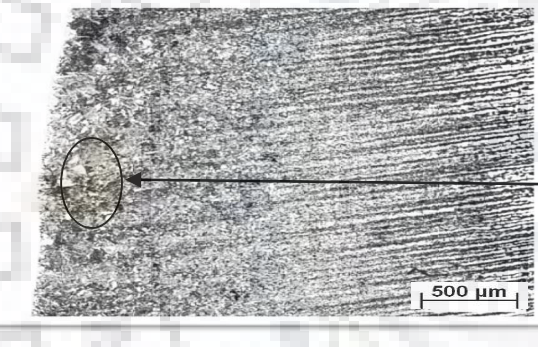
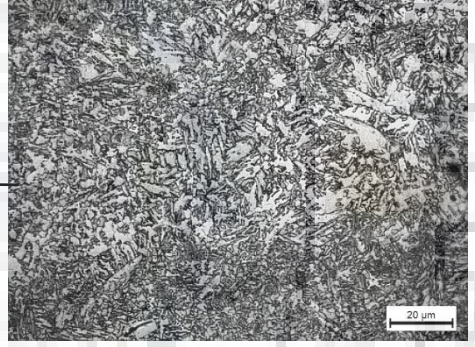
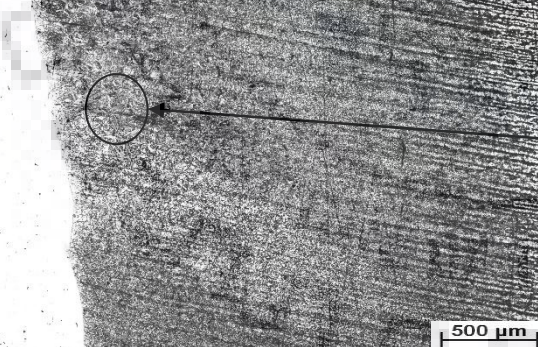
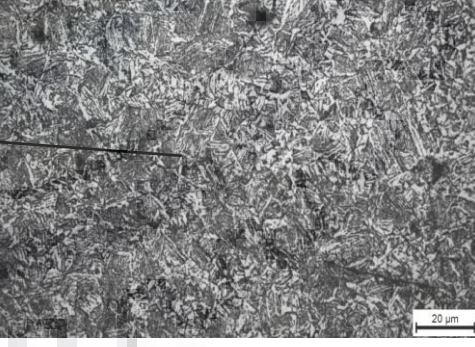
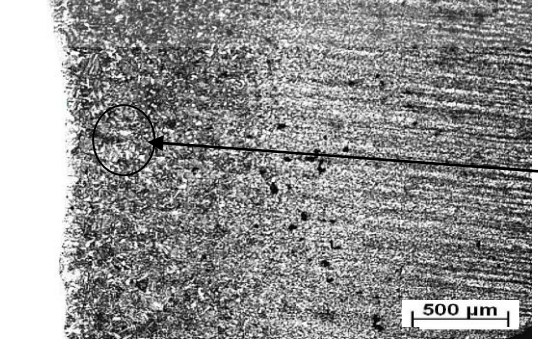
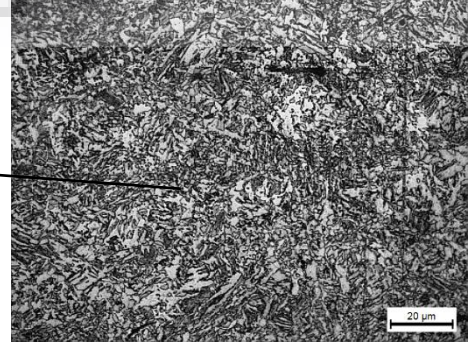
Figure 6-52 Typical reheat refined microstructure of MPMSPL conventional groove P-GMA weld joint and MPSSPL ultra-narrow gap P-GMA weld joint prepared at diverse I_m and ϕ .

6.5.4 Studies on HAZ

At a given arc voltage (V) $25 \pm 1V$, mean current (I_m) of 200A, 220A, 240A heat input (Ω) at $9.81 \pm 0.5 kJ/cm$ and ϕ value of 0.05, 0.25 the typical microstructures of the heat affected zone close to fusion line of the MPMSPL conventional groove P-GMA dissimilar weld joint of γ -SS and HSLA steel, as revealed at comparatively lower and higher magnification, has been shown in Fig. 6.52, Fig. 6.65. Similarly, the variation of typical microstructures of the heat affected zone close to fusion line of MPSSPL centrally laid ultra-narrow gap P-GMA dissimilar weld joint of γ -SS and HSLA steel, as revealed at

relatively low and high magnifications has also been shown in same Fig. 6.52 and Fig. 6.55, where the I_m and ϕ has been varied at a given Ω of $9.81 \pm 0.5 \text{ kJ/cm}$. The figures show that the microstructure of HAZ mostly it consists of bainite and acicular ferrite in HSLA side and the microstructure show that the γ -SS consists of commonly known equiaxed grains of austenite with twin structure. It has been observed that the microstructure of HAZ of both side of dissimilar metal becomes relatively coarser as one goes closer to fusion line in conventional and ultra-narrow gap weld joint. In γ -SS steel side in ultra-narrow groove dissimilar weld joints have comparatively very less grain coarsening than those observed in conventional groove weld joints. It is also observed that at a given Ω and I_m the increase of ϕ and at a given Ω and ϕ the decrease of I_m relatively reduces the width of the region of grain coarsening. This may have primarily happened because the increase of ϕ and decrease of I_m reduces the heat transferred to the weld pool. In view of this, the changes in microstructure of HAZ have been characterized by measuring the width of HAZ, defined by coarse grain region adjacent to fusion line, and the size of coarse grain of this region. At a given arc voltage (V) and Ω of $25 \pm 1 \text{ V}$ and $9.81 \pm 0.5 \text{ kJ/cm}$ respectively the effect of I_m and ϕ on width of HAZ has been shown in Figs. 6.58. The results show that at a given Ω and I_m the width of HAZ adjacent to fusion line on both side decreases with the increase of ϕ . The variation in width of HAZ with the change in I_m and ϕ may have happened primarily because of the variation in heat transferred to the weld pool as well as width and length of weld isotherm as it has been found in the bead on plate studies (section-6.2.2.5).

At a given arc voltage (V) and Ω of $25 \pm 1 \text{ V}$ and $9.81 \pm 0.5 \text{ kJ/cm}$ respectively effect of I_m and ϕ on coarse grain size adjacent to fusion line on both dissimilar side of the MPMSPL conventional groove P-GMA weld and MPSSPL centrally laid ultra-narrow gap P-GMA weld has been shown in Fig. 6.54 and Fig. 6.56. It is observed that the grain size in case of MPMSPL conventional groove P-GMA weld is comparatively much higher than that of MPSSPL centrally laid ultra-narrow gap P-GMA weld due to comparatively lower amount of metal deposition per unit length in the later one resulting in relatively lower thermal sock. The change in grain size as a function of I_m and ϕ is attributed to changes in severity of weld thermal cycle because of changes in weld pool temperatures as discussed in earlier section.

<p>CG-P- GMAW $I_m=220A$</p>		
<p>$I_m=200A$ $\phi=0.05$</p>		
<p>$I_m=220A$ $\phi=0.05$</p>		
<p>$I_m=240A$ $\phi=0.05$</p>		
<p>$I_m=200A$ $\phi=0.25$</p>		

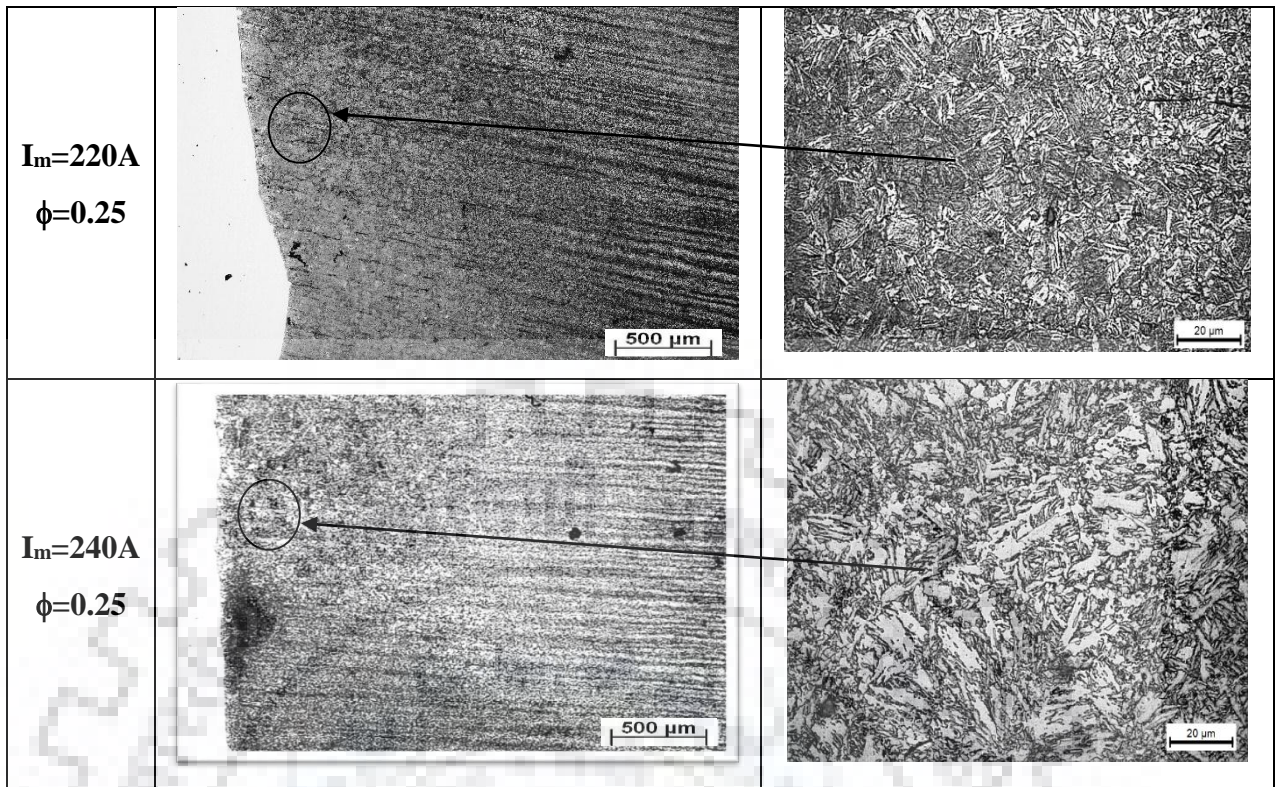


Figure 6-53 Typical microstructures of HAZ (HSLA side) at relatively low and high magnifications of conventional groove and narrow groove weld joints at a given arc voltage Ω of $25 \pm 1V$ and $9.81 \pm 0.5kJ/cm$ of varied I_m and ϕ .

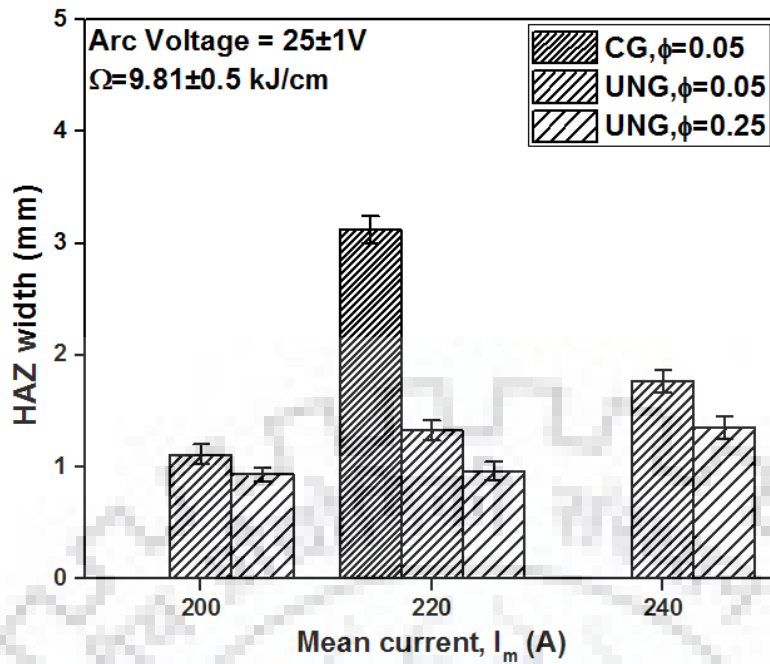


Figure 6-54 Effect of weld groove size, I_m and ϕ on HAZ width of P-GMA dissimilar weld joints (HSLA side) prepared at a given arc voltage and Ω of $25\pm 1V$ and $9.81\pm 0.5kJ/cm$ respectively

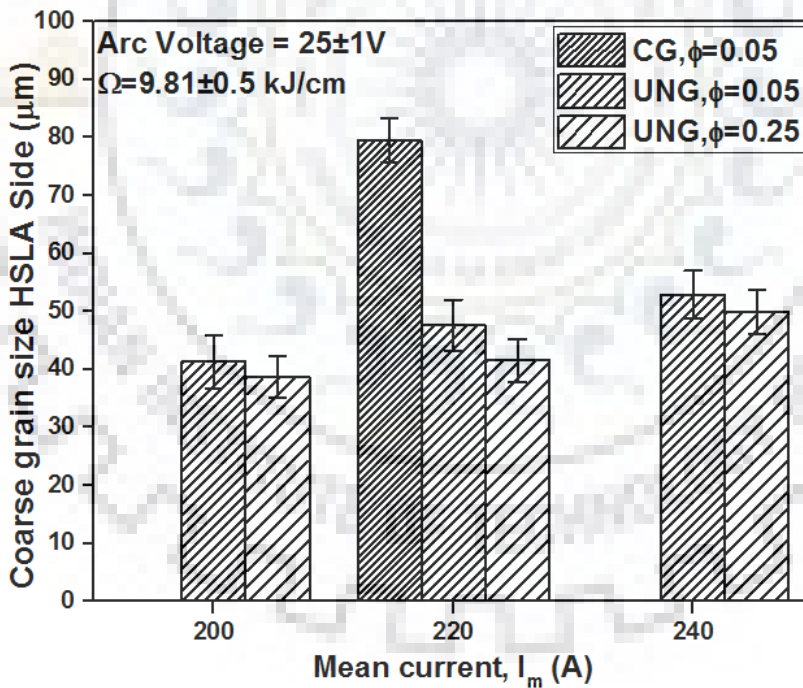


Figure 6-55 Effect of weld groove size, I_m and ϕ on coarse grain size adjacent to fusion line of P-GMA dissimilar weld joints (HSLA side) prepared at a given arc voltage and Ω of $25\pm 1V$ and $9.81\pm 0.5kJ/cm$ respectively.

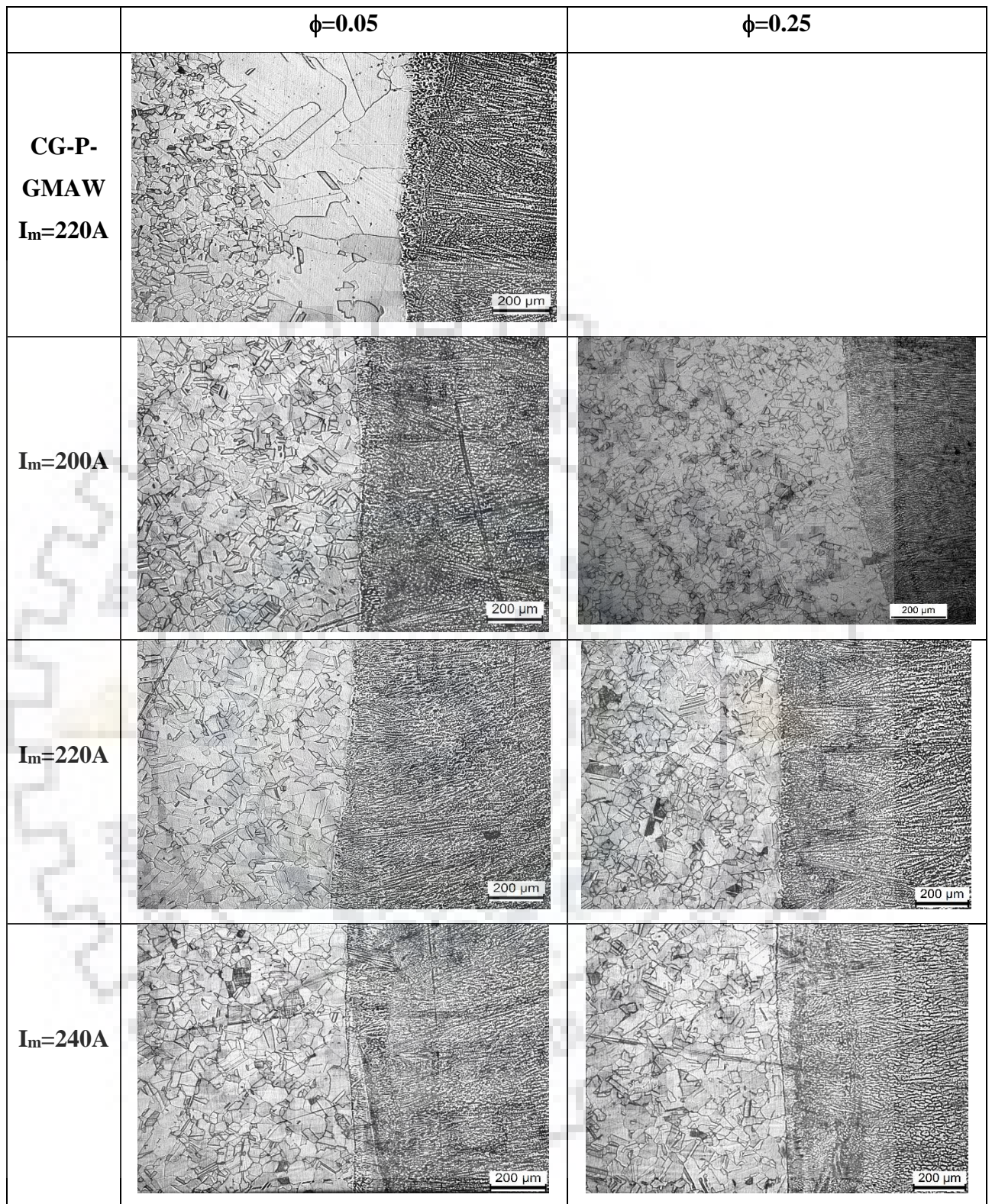


Figure 6-56 Typical microstructures of HAZ (γ -SS side) of conventional groove and ultra-narrow groove weld joints at a given arc voltage Ω of $25\pm 1V$ and $9.81\pm 0.5kJ/cm$ of varied I_m and ϕ .

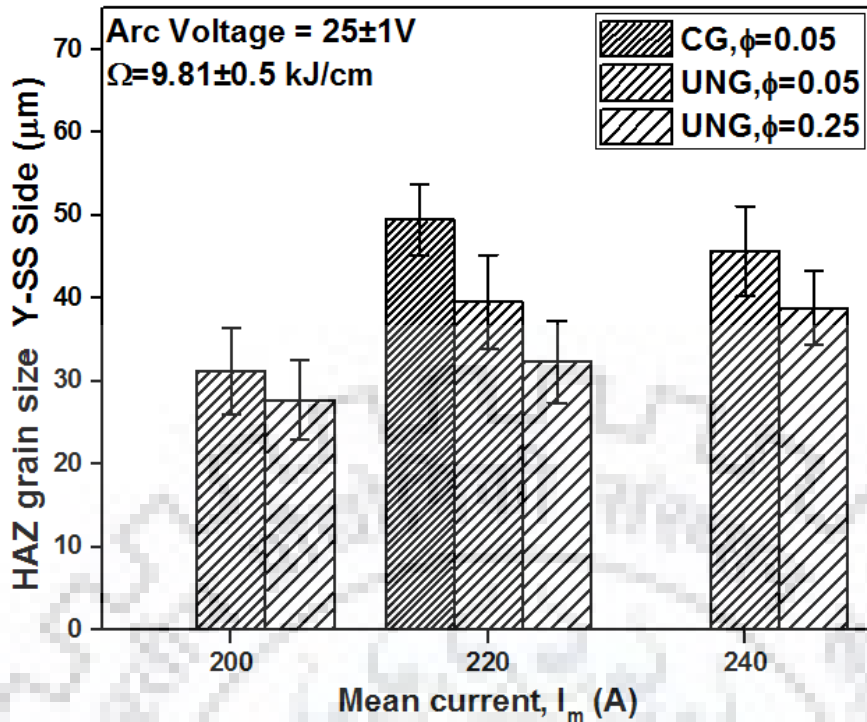


Figure 6-57 Effect of weld groove size, I_m and ϕ on coarse grain size adjacent to fusion line of P-GMA dissimilar weld joints (γ -SS side) prepared at a given arc voltage and Ω of $25\pm 1V$ and $9.81\pm 0.5kJ/cm$ respectively.

6.5.5 Tensile properties

Tensile properties of the dissimilar weld joint of γ -SS and HSLA steel have been studied for both axial and all weld specimens in order to compare it from that of the base material.

6.5.5.1 Axial weld

The location of fracture in the axial tensile specimens of the MPMSPL conventional groove P-GMA dissimilar weld joint and MPSSPL centrally laid ultra-narrow gap P-GMA dissimilar weld joint of γ -SS and HSLA steel has been typically shown in Fig. 6.58. The figure depicts that the fracture occurs always away from the weld on HSLA side and it is mostly from the HSLA base metal irrespective of the type of weld joint and welding parameters. It may be understood that tensile strength of weld joint is always higher than base metal in P-GMA welding process.

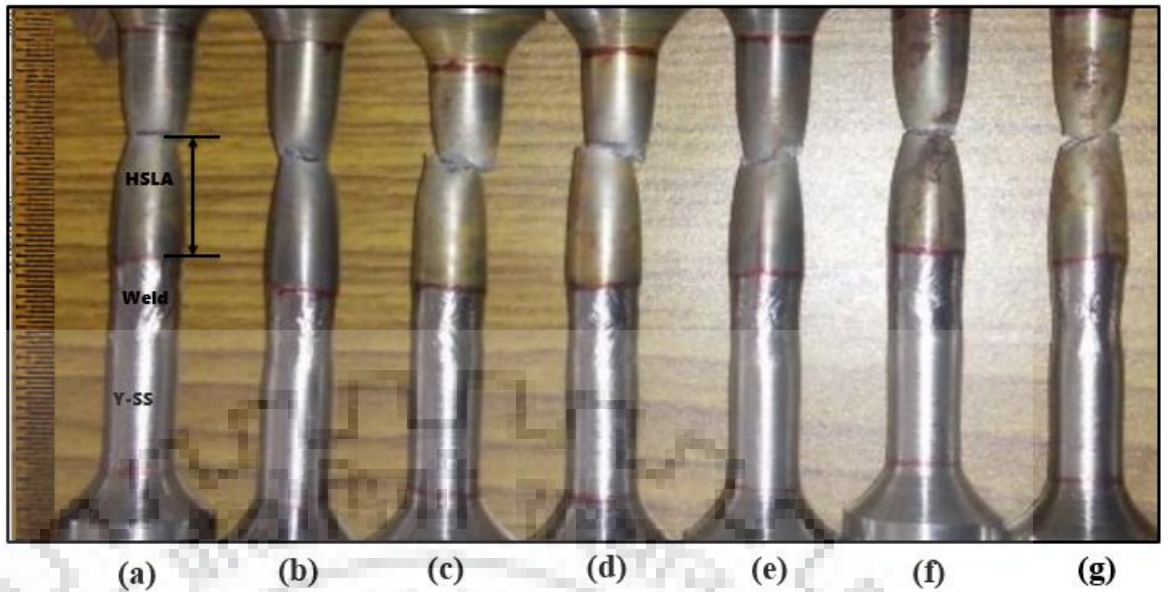


Figure 6-58 Typical location of fracture under tensile loading on axial weld test of MPMSPL conventional groove weld joint and MPSSPL narrow gap P-GMA weld joint at different ϕ and I_m of (a) UNG, 0.05 and 200A (b) UNG, 0.25 and 200A, (c) UNG, 0.05 and 220A, (d) UNG, 0.25 and 220A, (e) UNG, 0.05 and 240A (f) UNG, 0.25 and 240A and (g) CG, 0.05 and 220.

6.5.5.2 All weld

At a given arc voltage (V) and Ω of $25 \pm 1V$ and $9.81 \pm 0.5kJ/cm$ respectively, the effect of I_m and ϕ on tensile properties of all weld specimen machined out from center locations of MPMSPL conventional groove P-GMA weld joint and MPSSPL centrally laid ultra-narrow gap P-GMA weld joint have been shown in Figs. 6.59-6.62 respectively. Higher tensile properties by about 12-25% have been observed in case of MPSSPL centrally laid narrow gap P-GMA dissimilar weld in comparison to that at the MPMSPL conventional groove P-GMA dissimilar weld. Such a variation in tensile properties of weld is primarily attributed to changes in microstructure as well as chemical composition. It is observed that at a given Ω and I_m the yield strength (YS) and ultimate tensile strength (UTS) increases but the percentage elongation decreases with the increase of ϕ . It is also observed that at a given Ω and ϕ the increase in I_m appreciably reduces the yield strength (YS) and ultimate tensile strength (UTS) but enhances the percentage elongation. Such a variation of tensile properties with respect to I_m and ϕ may have happened due changes in fraction of dendritic and reheat refined (RR) region in the matrix. The fractured surface as revealed at relatively low and high magnifications of the all weld tensile specimens of the MPMSPL conventional groove P-GMA weld and MPSSPL centrally laid ultra-narrow gap P-GMA weld prepared by using different pulse parameters at a given Ω

has been shown in Fig. 6.94. The figure shows that the mode of fracture of the weld is ductile in nature with formation of dimples.

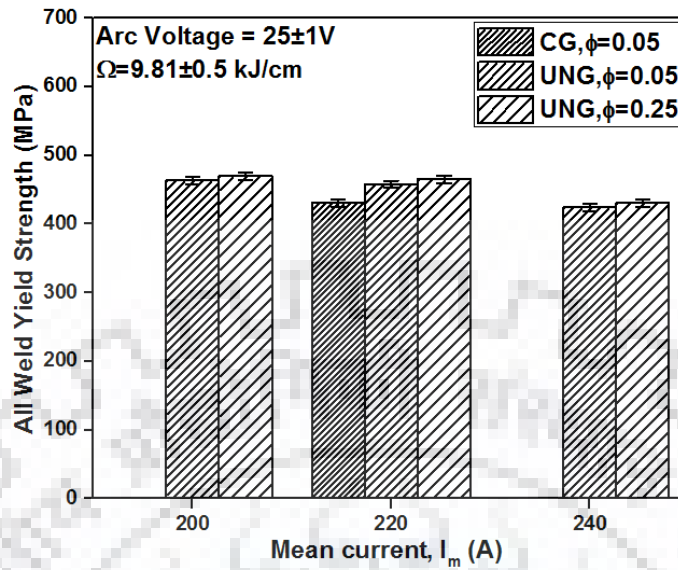


Figure 6-59 Effect of I_m and ϕ on yield strength of MPMSPL conventional groove weld joint and MPSSPL ultra-narrow gap P-GMA weld joint prepared at a given Ω of 9.81 ± 0.5 kJ/cm.

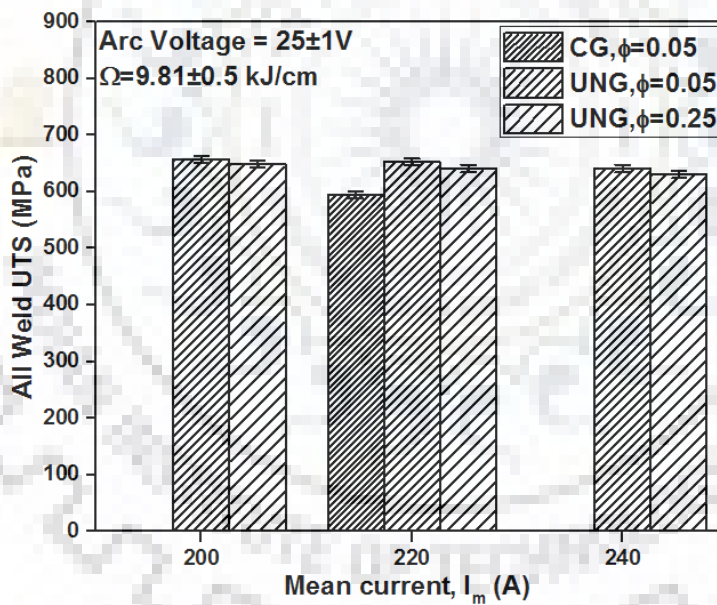


Figure 6-60 Effect of I_m and ϕ on ultimate tensile strength of MPMSPL conventional groove weld joint and MPSSPL ultra-narrow gap P-GMA weld joint prepared at a given Ω of 9.81 ± 0.5 kJ/cm.

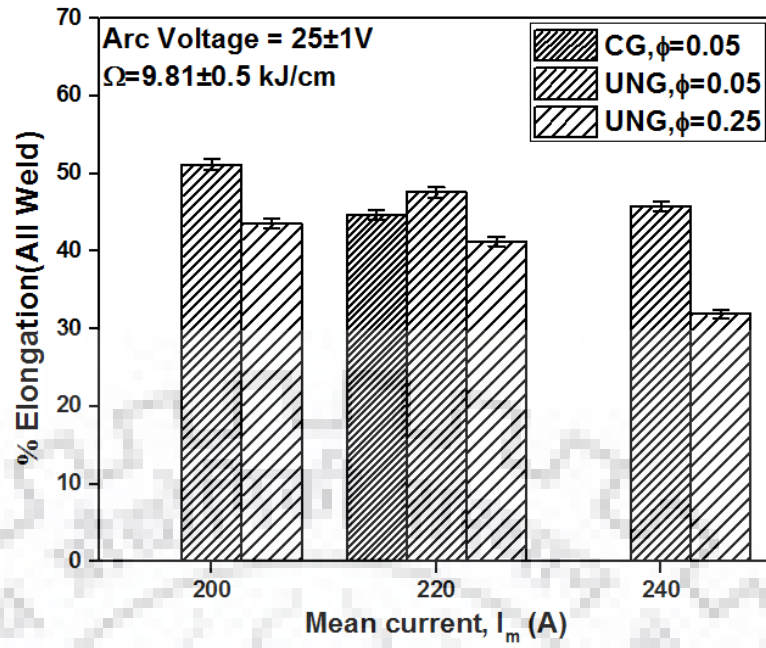


Figure 6-61 Effect of I_m and ϕ on % elongation of MPMSPL conventional groove weld joint and MPSSPL ultra-narrow gap P-GMA weld joint prepared at a given Ω of $9.81 \pm 0.5 \text{ kJ/cm}$.

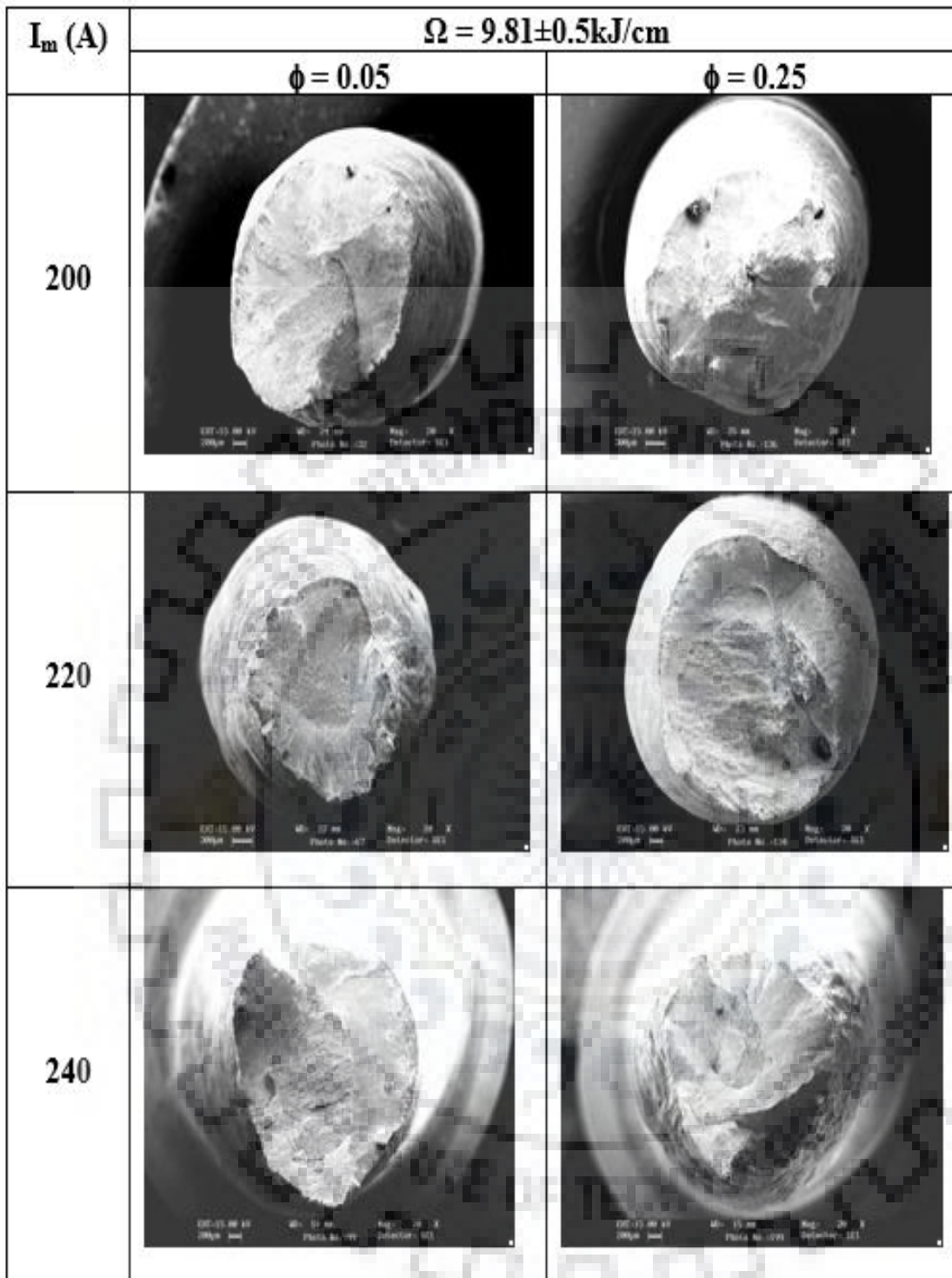


Figure 6-62 Typical fractured specimen of all weld tensile specimen of MPMSPL conventional groove weld joint and MPSSPL ultra-narrow gap P-GMA weld joint prepared at a given Ω of $9.81 \pm 0.5 \text{kJ/cm}$

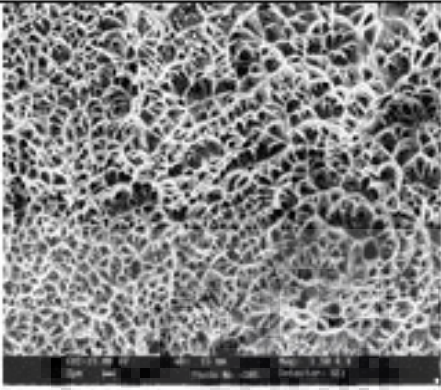
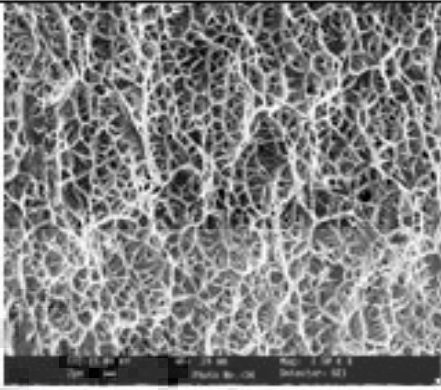
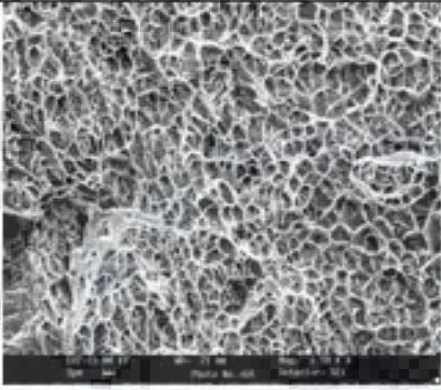
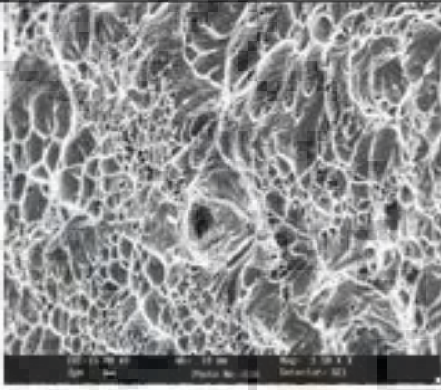
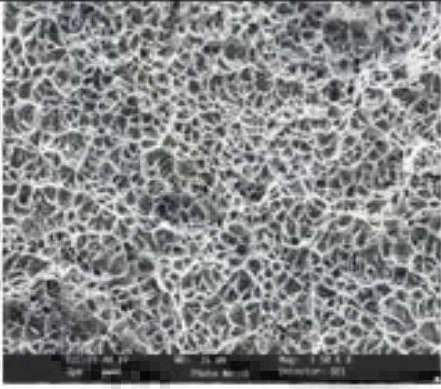
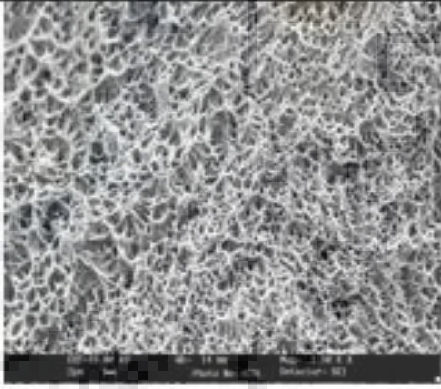
I_m (A)	$\Omega = 9.81 \pm 0.5 \text{kJ/cm}$	
	$\phi = 0.05$	$\phi = 0.25$
200		
220		
240		

Figure 6-63 Typical fractographs of all weld tensile specimen of MPMSPL conventional groove weld joint and MPSSPL ultra-narrow gap P-GMA weld joint prepared at a given Ω of $9.81 \pm 0.5 \text{kJ/cm}$.

6.5.6 Hardness measurement

The hardness distribution across the dissimilar weld joint of γ -SS and HSLA steel prepared at a given arc voltage (V) and Ω of $25 \pm 1 \text{V}$ and $9.81 \pm 0.5 \text{kJ/cm}$ respectively has been compared for MPMSPL conventional groove P-GMA weld joint and MPSSPL centrally laid ultra-narrow gap P-GMA weld joint in Fig. 6.68. The hardness distribution in γ -SS weld deposit and HAZ of γ -SS side in MPMSPL conventional groove P-GMA dissimilar weld joint is relatively lower

than MPSSPL centrally laid ultra-narrow gap P-GMA dissimilar weld joint because of comparatively coarser grain. It is further observed that influence of ϕ on hardness distribution appears to be practically negligible in weld and HAZ of γ -SS side in MPSSPL centrally laid ultra-narrow gap P-GMA weld joint. A considerable scattering of hardness across the weld and HAZ region are observed. The considerable amount of scatter in hardness may have occurred due to presence of comparatively larger number of different kinds of zones of microstructure having dendrite and reheat refined region. A slight reduction in the hardness has been observed near the fusion boundary. It may be attributed to coarse grain structure on both the sides of fusion boundary (weld metal and HAZ). Peak hardness was found in the HAZ of HSLA side in all the weld joints. As the distance increases from fusion boundary toward base metal, hardness decreases rapidly from the peak hardness on HSLA side. The peak hardness might have occurred in grain refined zone of HAZ.

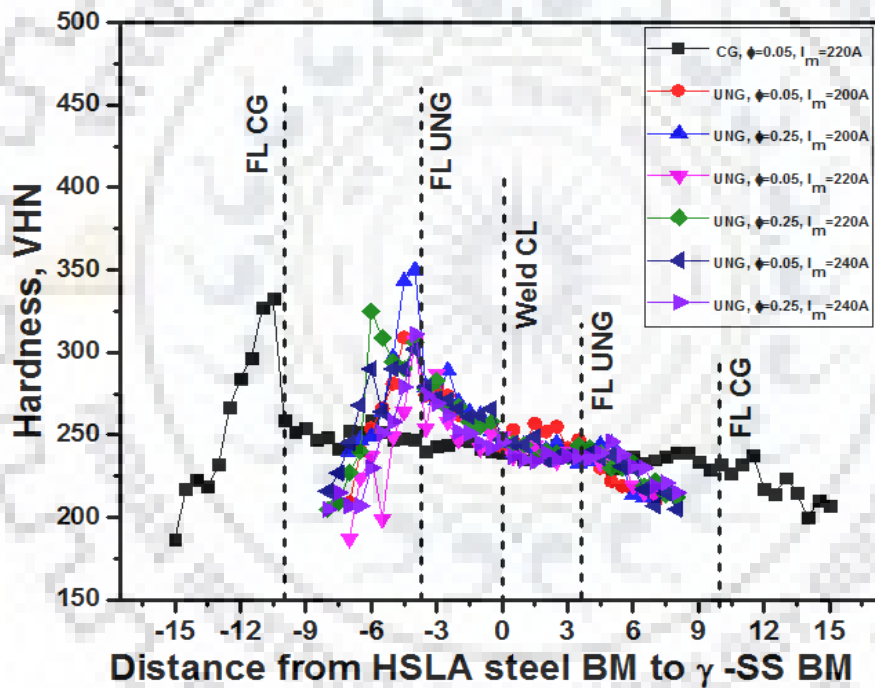


Figure 6-64 Typical variation in hardness observed across the MPMSPL conventional groove and MPSSPL ultra-narrow gap P-GMA dissimilar weld joints prepared at a given Ω of $9.81 \pm 0.5 \text{ kJ/cm}$ at different I_m and ϕ .

6.5.7 Residual Stresses

The longitudinal and transverse residual stresses present at different locations on top of the weld in reference to the centre and fusion lines the MPMSPL conventional groove and MPSSPL ultra-narrow gap P-GMA dissimilar weld joint of γ -SS and HSLA steel at a given weld width of 28mm and 7.5mm are shown in Fig. 6.69 (a) and (b) respectively. The figures

show that for MPSSPL ultra-narrow gap dissimilar weld joint at the top of the weld, longitudinal residual stress reduces by 24-31% at weld center, 57-64% at fusion line on γ -SS side, 40-43% at fusion line of HSLA steel side, 67-74% at γ -SS HAZ and 62-68% at HSLA HAZ area with the use of P-GMAW process in comparison to that obtained using MPMSPL conventional groove.

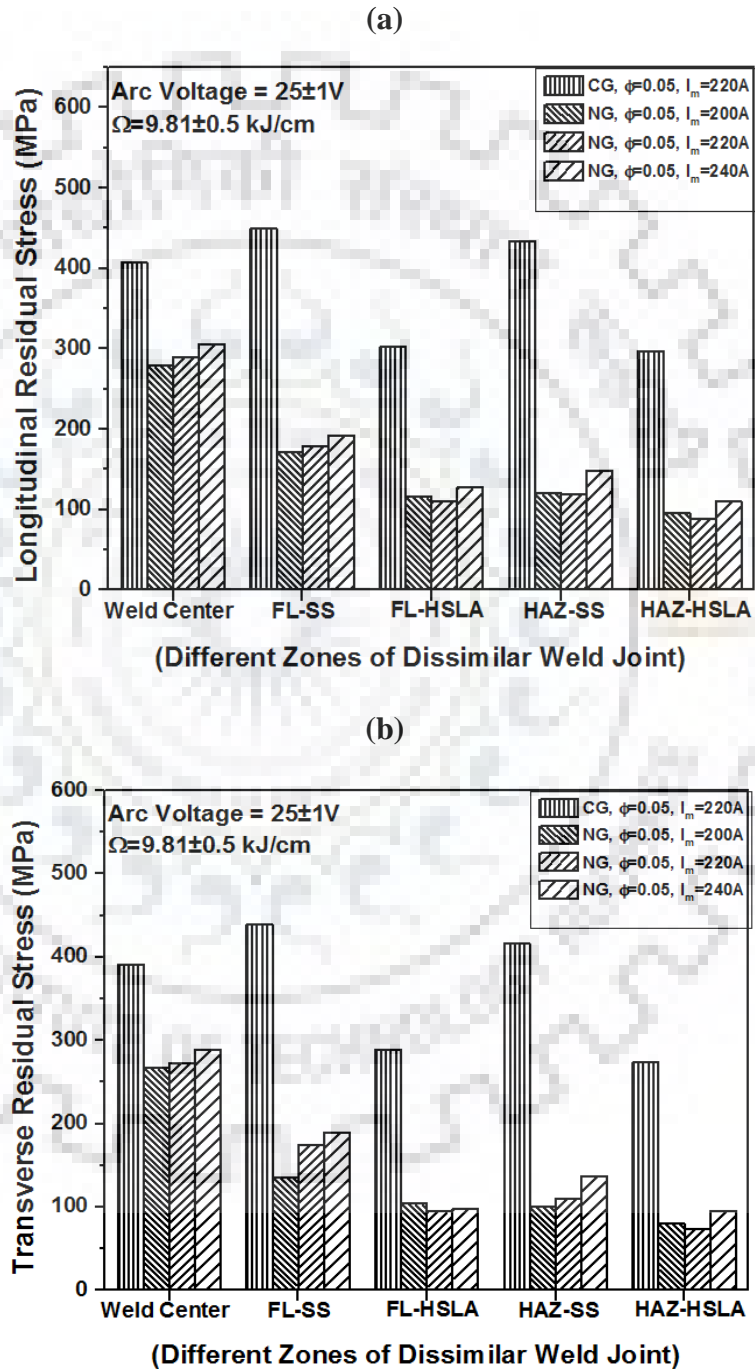


Figure 6-65 Typical variation in residual stresses at the top in the weld joint observed across the MPMSPL conventional groove and MPSSPL ultra-narrow gap P-GMA dissimilar weld joints prepared at a given Ω of $9.81 \pm 0.5 \text{ kJ/cm}$ at different I_m and ϕ .

Ultra-narrow gap welding technique further reduces harmful tensile longitudinal residual stresses with respect to those observed in case of the conventional V-groove weld joint specially in case of dissimilar weld joint. The transverse residual stress has also been found to follow a similar trend but having a magnitude comparatively higher than the longitudinal residual stress of the weld joint as it is commonly observed [Murugan et al 2001, Webster et al 2002, Fricke et al 2001, Deng et al 2008, Kulkarni et al 2008].

P-GMAW ultra-narrow gap technique is found to be advantageous in respect of reduction in residual stress distribution in dissimilar weld joint of γ -SS to HSLA steel. primarily due to the use of relatively less severe weld thermal cycle along with reduction in number of weld passes in comparison to those for conventional groove weld joint. Whereas a considerable difference in the development of residual stresses in the conventional and ultra-narrow gap welds may be attributed primarily to the severity of thermo mechanical characteristics arising out of differential expansion and contraction stresses resulting from multipass deposition, which becomes comparatively milder in case of the ultra-narrow gap weld holding appreciably lower amount of weld deposit [Radaij 1992, Anant et al 2017]. However, in P-GMA ultra-narrow gap dissimilar welds at different ϕ of 0.05 and 0.25, the residual stress distribution in both longitudinal and transverse direction varies negligibly at the top of weld. The significance of this nature of distribution of residual stresses in P-GMA ultra-narrow groove dissimilar weld of γ -SS and HSLA steel may be carefully considered in the context of the influence of residual stresses on kinetics of sensitization in weld and heat affected zone near to the fusion line.

6.5.1. Commercial benefits

6.5.1.1. Material consumption

At a given arc voltage (V) and Ω of $25\pm 1V$ and $9.81\pm 0.5kJ/cm$ the effect of I_m and ϕ on filler material consumption per meter length of weld of MPMSPL conventional groove and MPSSPL centrally laid ultra-narrow gap P-GMA dissimilar weld of γ -SS and HSLA steel has been shown in Fig. 6.70. The filler material consumption per meter length of weld for MPSSPL centrally laid ultra-narrow gap P-GMA weld has been found to be lower by about 40-54% and 79-83% as compared to commonly used narrow groove and conventional V-groove P-GMA weld joint respectively. This may be due to comparatively lower area of ultra-narrow groove weld as compared to commonly used narrow groove and conventional V-groove P-GMA weld joint which requires relatively less number of passes to fill the gap and less amount of weld deposition (section-6.5.2).

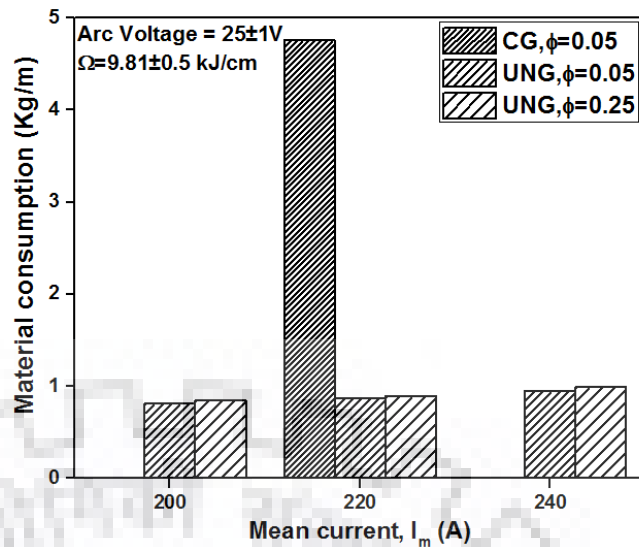


Figure 6-66 Effect of weld groove size, I_m and ϕ of P-GMA weld joints prepared at a given arc voltage and Ω of $25 \pm 1V$ and $9.81 \pm 0.5 \text{ kJ/cm}$ respectively on filler material consumption per meter length of weld.

6.5.9 Summary

The use of MPSSPL centrally laid ultra-narrow gap P-GMA welding technique improves the mechanical and metallurgical properties in comparison to those of MPMSPL conventional groove P-GMA welding processes due to relatively less amount of weld deposit in ultra-narrow gap. MPSSPL centrally laid narrow gap P-GMA weld also minimize the shrinkage stress and bending stress generated in weld joint. It is also found that the summarized influence of pulse parameter defined by the factor ϕ play important role in controlling the properties of P-GMA weld joint thick section steel. The improvement in mechanical and metallurgical properties of the weld joint is achieved at comparatively higher ϕ , I_m and lower Ω . The filler material consumption per meter length of weld for MPSSPL centrally laid ultra-narrow gap P-GMA weld has been found to be significantly lower than weld joints prepared by MPMSPL commonly used narrow gap and conventional groove P-GMA welding.



The specific conclusions drawn from different facets of the present work have already been given in the corresponding chapters. However, finally the generic conclusions drawn from the present work can be summarized as follows.

Design and Fabrication of Narrow GMAW Torch Nozzle Head Device

1. A rectangular faced narrow torch nozzle head designed by removing both of its lengthwise side walls along the direction of welding suits close fitting manipulation inside a practically narrowest possible weld groove to get support from the groove wall for creation of a protected zone of arc shielding with appropriate dynamics of argon gas flow during GMA welding of 25 mm thick plate.

Bead on Plate Studies

2. The analytical expressions proposed earlier [Goyal V. K. et. al., 2008] for estimation of temperature and isotherm of P-GMA weld deposit is justified to use for γ -SS steel with a variation lying in the range of 10 to 12% of their measured values.
3. The Heat input (Ω), summarised influence of pulse parameter ϕ and mean current (I_m) significantly affect the geometry and isotherm of weld pool, maintain good correlations with them.
4. At a given Ω the appropriate control of geometry and isotherm of weld deposit with a variation in pulse parameters as Ω and I_m of P-GMAW process may facilitate its use for narrow groove wall fusion by centrally laid weld deposit.

Thermal modelling of MPSSPL narrow gap pulse current GMA welding technique

5. The analytical model, in consideration of geometrical and thermal aspects of weld pool, is capable to decide appropriate pulse parameters with suitable heat input to produce a centrally laid MPSSPL ultra-narrow gap dissimilar weld joint of thick plates of γ -SS and HSLA steel free from lack of groove wall fusion.
6. The use of MPSSPL ultra-narrow gap P-GMA welding, by selection of pulse parameters giving rise to relatively lower value of summarized influence of pulse parameters at a given heat input under comparatively higher mean current assures the preparation of sound weld by avoiding lack of groove wall fusion.
7. It is understood that a centrally laid MPSSPL ultra-narrow gap P-GMA welding can be favourably manipulated by changing the pulse parameters without varying the heat input to produce a sound weld.

Studies on MPSSPL narrow gap pulse current P-GMA Weld Joint

8. MPSSPL ultra-narrow gap P-GMA dissimilar weld joints of γ -SS to HSLA steel significantly reduce the transverse shrinkage and estimated transverse shrinkage stress by about 45-60% than that of the MPMSPL conventional groove P-GMA dissimilar weld joints of γ -SS to HSLA steel.
9. The deflection in MPSSPL centrally laid ultra-narrow gap dissimilar weld joint is 71-85% on HSLA steel side and 77-90% on γ -SS side lower than MPMSPL conventional groove dissimilar weld joint.
10. The estimated transverse shrinkage stress and measured residual stresses in different zone of the top of the weld joint for MPSSPL ultra-narrow gap P-GMA dissimilar weld joints are significantly lower than stresses developed in case of commonly used MPMSPL narrow groove P-GMA weld joint.
11. The MPSSPL ultra-narrow gap P-GMAW increases the tensile properties of weld metal by about 12-25% in comparison to those of MPMSPL conventional groove P-GMA weld.
12. The fraction of cast dendritic region of weld deposit is comparatively lower in the MPSSPL ultra-narrow gap P-GMA weld joint than that of the MPMSPL conventional groove P-GMA weld joint.
13. The MPSSPL ultra-narrow gap P-GMA weld produces comparatively finer microstructure and produces very less effect on heat affected zone (HAZ) microstructure on both side of dissimilar weld joint and also lowers the grain coarsening in HAZ with respect to that observed in conventional groove weld joints.
14. The filler material consumption per meter length of weld for MPSSPL centrally laid ultra-narrow gap P-GMA weld has been found to be lower by about 40-54% and 79-83% as compared to commonly used narrow groove and conventional V-groove P-GMA weld joint respectively.

1. **AISI Designers handbook**, [1988], “Welding of stainless steels and other joining methods”.
2. **Allabhakshi, S**, Madhusudhan Reddy, G, Ramarao, V V, Phani Babu, C, Ramachandran, C S, [2002], “Studies on weld overlaying of austenitic stainless steel (AISI 304) with ferritic stainless steel (AISI 430)”, *National Welding Conference*, Chennai, India, Indian Institute of Welding, Paper 8.
3. **Allum, C. J.** and Quintino, L., [1985(a)] “Control of fusion characteristics in pulsed current MIG welding – Part I. Dependence of fusion characteristics of process parameters”, *Metal Construction*, Vol. 17 (4), pp. 242R-245R.
4. **Allum, C. J.** and Quintino, L., [1985(b)], “Control of fusion characteristics in pulsed current MIG welding – Part II, Simple model of fusion characteristics”, *Metal construction*, Vol. 17, pp. 314R -317R.
5. **American Society for Metals**, [1984], “HSLA Steels Technology and Applications”.
6. **American Society for Metals**, [1986], “HSLA Steels Metallurgy and Applications”.
7. **American Welding Society**, [1972], “Metals and their weldability”, *Welding hand book*, Section IV, sixth edition, pp. 67.37-67.38.
8. **Amin, M.**, [1981], “Synergic pulsed MIG welding” *Metal Construction*, Vol. 13(6), pp.349-353.
9. **Amin, M.** and Ahmed, N., [1987], “Synergic control in MIG welding”, *Metal Construction*, Vol. 19(1), pp 22-28.
10. **Amin, M.**, [1983], “Pulse current parameters for arc stability and controlled metal transfer in arc welding”, *Metal Construction*, Vol. 15(5), pp.272-287.
11. **Amuda, M. O. H.**, and Mridha, S., [2011], An Overview of Sensitization Dynamics in Ferritic Stainless Steel Welds, *International Journal of Corrosion*, Volume 2011 Article ID 305793, 9 pages
12. **Anant, R.**, Ghosh, P.K., [2017],” Ultra-narrow Gap Dissimilar Welding of Thick Section of Austenitic Stainless Steel to HSLA Steel”, *International Journal of Material Processing Technology(JMPT)*, 239:210-221, Impact Factor-3.14
13. **An assessment of integrity of PWR pressure vessels**, [1982], “Second report by a study group under the chairmanship of Dr.W.Marshall”, *United Kingdom Atomic Energy Authority*, P-14 (Section-5).

14. **Arselsen, O. M.**, Grong, O., Ryum, N., Christensen, N., [1986], “HAZ grain growth mechanisms in welding of low carbon micro-alloyed steels”, *Acta Metall.*, Vol. 34, pp. 1807-1815.
15. **Arthur, H** and Tuthill, P.E, [2002], “Stainless steels and specialty alloys for pulp and paper”, *Nickel development institute reference book series no 11025*.
16. **Asami, K.**, and Sakai, T. Hydrogen induced cracking at interface between stainless steel overlay weld metal and base metal in pressure vessel. *Transactions of the Iron and Steel Institute of Japan* 21(6).
17. **ASM hand book**, [1988], “Micro alloyed HSLA Steels”, *ASM International*.
18. **ASM Handbook**, [1990], “High-Strength Structural and High-Strength Low-Alloy Steels, Properties and Selection: Irons, Steels, and High-Performance Alloys”, Vol 1, *ASM International*, pp. 389–423
19. **ASM Handbook**, [1992], “Phase Diagrams”, Vol. 3, *ASM International*, Materials Park, OH.
20. **ASM handbook**, [1994], “Welding, Brazing and Soldering”, Vol. 6, *ASM International*, Materials Park, OH.
21. **ASM handbook**, [2001], “High-strength low-alloy steels”, *ASM International*, Materials society, pp.193–209.
22. **Austin, J.B.**, [1956], “Electric Arc Welding”, *Am. Tech. Soc.*, Chicago, pp. 61–62.
23. **Babu, S.S.**, David, S. A., [2002], “Inclusion formation and microstructure evolution in low alloy steel welds”, *ISIJ International*, Vol. 42, pp. 1344–1353.
24. **Bag S.** and **De A.** [2009],” Development of efficient numerical heat transfer model coupled with genetic algorithm based optimization for prediction of process variables in GTA spot welding”, *Science and technology of welding and joining*, Vol 14 (4), pp. 333-345.
25. **Basak, A**, Roy,D.K. and Dutta, G.L., [1995], “Adhesive wear characteristics of cast nitrogenated stainless steel”, *Wear* , Vol.184, pp. 241-244.
26. **Basu, B** and Raman R, [2002], “Microstructural Variations in a High-Strength Structural Steel Weld under Isoheat Input Conditions”, *Welding journal*, pp. 239S-248S.
27. **Basavaraju, C.**, [2000], “Simplified analysis of shrinkage in pipe to pipe butt welds”, *Nuclear Engineering and Design*, Vol.197, pp.239-247.
28. **Begeman, M.L**, Amstead B.H, Mashruwala U.I, [1950], “Effects of reduced atmospheric pressure on arc-welding characteristics”, *Weld. J.* 29 (10) 433s–440s.
29. **Bhadeshia, H.K.D.H**, [1999], *ISIJ Int.*, 39, pp.966–979.

30. **Bhadeshia, H.K.D.H**, David SA, Vitek J M, [1991], “Solidification sequences in stainless steel dissimilar alloy welds”. *Mater. Sci. Technol.* 7: pp.50–61
31. **Bhadeshia H. K. D. H.**, Svensson L. E. and Gretoft B. [1985],”A model for the development of microstructure in low alloy steel (Fe-Mn-Si-C) weld deposit”, *Acta. Metall.* Vol.33 (7), pp.1271-1283.
32. **Bhadeshia H. K. D. H.**, Cerjack H. and Easterling K. E. [1993],”Mathematical modeling of weld phenomena,” Institute of materials , London, 109-180.
33. **Blondeau, R.**, and Pressouyre, G, [1982], Contribution to a solution to the disbanding.
34. **Boo K.S.**, and Cho H. S. [1990],”Transient temperature distribution in arc welding of finite thickness plates”, *Proc. Inst. Mech. Eng., part B*, 204, pp.175-183.
35. **Brickstad, B.** and Josefson, B.L., [1998], “A parametric study of residual stresses in multi-pass butt-welded stainless steel pipes”, *International Journal of Pressure Vessels and Piping*, Vol.75, pp.11-25.
36. **Brooks, J.A.**, Williams, J.C. and Thompson, A.W., [1983], “Microstructural origin of the skeletal ferrite morphology of austenitic stainless steel welds”, *Metallurgical and Materials transactions A*, 14A, pp.1271-1284.
37. **Çam, G.**, Erim, S., Yeni, Ç. and Koçak, M., [1999], “Determination of mechanical and fracture properties of laser beam welded steel joints”, *Welding Journal*, Vol.78 (6), pp.193s-201s.
38. **Castro, R.J.**, de J.J, Cadenet, [1974], “Welding Metallurgy of stainless steel and Heat-Resisting Steel”, *Cambridge University Press*, Cambridge, P. 158.
39. **Cerjak, H.**, Nagel. G. and Prader, R., [1999], “Quantification of the toughness distribution in a heavy section submerged arc multilayer reactor pressure vessel weldment”, *Nuclear Engineering and Design*, Vol.190, pp.29–39.
40. **Chang, P.H.**, Teng, T.L., [2004], “Numerical and experimental investigations on the residual stresses of the butt-welded joints”, *Computational Materials Science*, Vol. 29, pp.511-522.
41. **Chapman, T.**, Offer, H., Sanders, W., Rusack, G., [1997], “Reduced stress welding process for nuclear plant Piping”, *Nuclear Engineering and Design*, Vol. 170, pp. 81-88.
42. **Chen, Y.T.**, Guo, A.M., Wu, L.X., Zeng, J., Li, P.H., [2006], “Microstructure and mechanical property development in the simulated heat effected zone of V treated HSLA steels”, *ACTA Metallurgica Sinica (English Letters)*, pp. 57-67.

43. **Choi, S.K.**, Yoo, C.D and Kirn, Y.S, [1998], “The dynamic analysis of metal transfer in pulsed current gas metal arc welding “ *Journal of Physics D, Applied Physics*, Vol.31,pp.207-215.
44. **Choi, S.K.**, Yoo, C.D. and Kim, Y.S., [1998 a], “Dynamic simulation of metal transfer, part I: Globular and spray transfer modes”, *Welding journal*, Vol. 77(1), pp.38-s-44-s.
45. **Christensen, N.**, de L. Davis, V., Gjermundsen, K., [1965], “Distribution of temperature in arc welding”, *British Welding Journal*. Vol.12 (2), pp. 54-75.
46. **Christensen K. H.**, Sorensen T. and Al-Erhayem [2003], “A neural network approach for GMA butt joint welding”, in book: *Proced. 11th Int. conf. on joining of materials*, pages 8, JOM Institute for joining of materials, Gilleleje, Denmark.
47. **Clark, J.** and Goswami, T., [2002], “Life prediction of stainless steels used in nuclear reactors”, *Mechanical Behaviour of Materials*, Vol. 13(5-6), pp. 273-282.
48. **Collard, J.F.**, [1988], “Adaptive pulsed GMAW control: The digipulse system”, *Welding Journal*, pp.35-38.
49. **Colombieer, L.** and Hochmann, L., [1967], “Stainless heat resisting steels”, *Edward Arnold Publishers Ltd.*, pp. 68-69.
50. **Cornu Jean**, [1988], “Advanced welding system” Vol. 2, *IFS Publication Ltd. UK*, pp.127-165.
51. **Covert, R.A.** and Tuthill, A.H., [2000], “Stainless steels: An introduction to their metallurgy and corrosion resistance”, *Dairy, Food and Environmental Sanitation*, Vol. 20(7), pp.506-517.
52. **Cox, C.W** and Kiser, S.D, [1992], “Fusion welding of dissimilar metals for high temperature strength”, *Welding journal*, pp. 67.
53. **Craig, E.F.**, [1987a], “A unique mode of GMAW transfer”, *Welding Journal*, Vol. 66(9), pp51-55.
54. **Craig, E.F.**, [1987b], “Pulsed spray welding- A mode of weld metal transfer that should revolutionize the GMAW process”, *Welding Journal*, Vol. 66(9), pp79.
55. **Craven, A.J.**, HE, K., Garvie, L. A. J., Baker, T. N., [2000(a)], “Complex heterogeneous precipitation in titanium niobium micro-alloyed Al-killed HSLA steels—I. (Ti, Nb) (C, N) particles”, *Acta mater.*, Vol. 48, pp.3857–3868.
56. **Craven, A.J.**, HE, K., Garvie, L. A. J., Baker, T. N., [2000(b)], “Complex heterogeneous precipitation in titanium niobium micro-alloyed Al-killed HSLA steels—I. (Ti, Nb) (C, N) particles”, *Acta mater.*, Vol. 48, pp.3869–3878.

57. **Cullison, A.**, [1994], “Two paths, one goal: a consumable to weld HSLA100”. *Welding Journal* 73(1): pp.51.
58. **Czyryca, E.J.**, Link, R.E., Wong, R.J., Aylor, D.A., Montemarano, T.W., and Gudas, J.P., [1990], “Development and certification of HSLA-100 steel for naval ship construction”. *Naval Engineers Journal*, 102 (3): pp.63.
59. **Das, S.K.**, Sivaprasad, S., Das, S., Chatterjee, S., Tarafder, S., [2006], “The effect of variation of microstructure on fracture mechanics parameters of HSLA-100 steel”, *Materials Science and Engineering A*, Vol. 431, pp. 68–79
60. **Das, C.R.**, Bhaduri, A.K., Srinivasan, G., Shankar, V., Mathew, S., [2008 (a)], “Selection of filler wire for and effect of auto tempering on the mechanical properties of dissimilar metal joint between 403 and 304L(N) stainless steels”, *Journal of materials processing technology* , In press.
61. **Das, C.R.**, Albert, S.K., Bhaduri, A.K., Srinivasan, G., Murty, B.S., [2008 (b)], “Effect of prior microstructure on microstructure and mechanical properties of modified 9Cr–1Mo steel weld joints”, *Materials Science and Engineering A* Vol. 477, pp. 185–192.
62. **Davies, A.C.**, [1983] “The science and practice of welding- Volume 1 Welding science and technology, Ninth edition”, *Cambridge University Press*, pp. 36-37.
63. **Davis, S.R.** [1993], Hard facing, weld cladding and dissimilar metal joining, welding brazing and soldering. In: *ASM handbook*, vol. 6. Ohio: ASM International; pp. 789–829.
64. **De A, Jantre, J and Ghosh, P.K.** [2004], "Prediction of weld quality in pulsed current GMAW process using artificial neural network" *Science and technology of welding and joining*, Vol.9, pp.253-259.
65. **DeLoach, Jr., J. J.**, [1995], “An overview of the U.S. Navy filler metal development program. *Proceedings of a TMS Symposium on Welding and Weld” Automation in Shipbuilding*, edited by R. DeNale, Cleveland, Ohio, p. 85.
66. **Delong, W.T.**, [1974], “Ferrite in austenitic stainless steel weld metal”, *Welding Journal*, Vol. (7), pp. 273-S to 286-S.
67. **Deng, D.**, Murakawa, H. and Liang, W., [2008], “Numerical and experimental investigations on welding residual stress in multi-pass butt-welded austenitic stainless steel pipe”, *Computational Materials Science*, Vol. 42, pp. 234–244.
68. **Devakumaran, K.**, [2009] “Pulsed current narrow gap gas metal arc welding of thick HSLA steel plate”, *Ph.D. Thesis*, IIT Roorkee, India.

69. **Dhooge, A.**, Dolby, R.E., Steinmetz, R., Vinckier, A.G., [1978], “A review of work related to reheat cracking in nuclear reactor pressure vessel steels”, *Int. J., Pres. Vessel & Piping*, Vol.6, pp.329-409.
70. **Dhua**, Sanjay Kumar, Mukerjee, Debasis, Subrahmanya, Darbha, [2002], “Weldability and micro-structural aspects of shielded metal arc welded HSLA-100 steel plates”, *ISIJ International*, Vol. 42, pp. 290–298.
71. **Dieter, G.E.**, [1988], “Mechanical Metallurgy”, *McGraw-Hill book company*, UK.
72. **Dissimilar metals**, [1992], *Welding handbook*. 7th ed. vol. 4. Miami: American Welding Society, pp. 514–47.
73. **Dong, P.**, [2001], “Residual stress analyses of a multi-pass girth weld: 3-D special shell versus axisymmetric models”, *Journal of Pressure Vessel Technology*, Vol. 123, pp.207-213.
74. **Dreher, M.**, Fussel, U., Schnick, M., [2009], Simulation of the shielding gas flow inside the torch and in the process region of GMA welding. Technical University Dresden, Germany.
75. **Eager T. W.** and Tsai N. S. [1983], “Temperature field produced by travelling distributed heat sources”, *Welding Journal*, vol. 62(12), pp.346s-355s.
76. **Eckel, J.F.** [1964], “Diffusion across dissimilar metal joints”. *Weld J*, 43:170s-18.
77. **Elmer, J.W.**, Olson, D.L. and Matlock, D.K., [1982], “Thermal expansion characteristics of austenitic stainless steel filler metals”, *Welding Journal*, Vol. 61 (9), pp. 293s–301s.
78. **Emerson R.W**, Hutchinson WR., [1952], “Welded joints between dissimilar metals in high temperature service”. *Weld J*; 31, pp.126s–141.
79. **Erve M.**, Wesseling, U., Kilian, R., Hardt, R., Brtimmer, G., Maier, V. and Ilg, U., [1997], “Cracking in stabilized austenitic stainless steel piping of German boiling water reactors characteristic features and root cause”, *Nuclear Engineering and Design*, Vol. 171, pp. 113-123.
80. **Essers W G**, and Walter R [1981], *Welding journal*, Vol.60, pp.37s-42s.
81. **Faber, G.**, Gooch T., [1982], “*Welding in the World*”, 20 (5/6) pp.88.
82. **Fallick, J.C.**,and Szumachowski, “Shielded metal arc welding”, *Welding hand book*, pp.44-104.
83. **Fanous Ihab F. Z.**, Younan Mehar Y. A. and Wifi Abdalla S.[2003], “3D finite element modeling of welding process using element birth and element movement techniques”, *Transection of ASME*, vol.125, pp.144-150.

84. **Featherstone Rd** and Rockford IL, [1995], "The basic of gas metal arc welding", *Fabricator and manufacturer association.Intl.*pp.813-855.
85. **Fenggui Lu**, Shun Yao, Songnian Lou, and Yongbing Li [2004], "Modeling and finite element analysis on GTAW arc and weld pool", *Computational Material Science*, Vol.29, pp.371-378.
86. **Fernández, J.**, Illescas, S., Guilemany, J.M., [2007], "Effect of microalloying elements on the austenitic grain growth in a low carbon HSLA steel", *Materials letter*, Vol. 61, pp. 2389-2392.
87. **Ferraresi, V.A.**, Figueiredo K.M., Hiap T. Ong, J.Brazilian, [2003], "*Soc. Mech.Sci.Engg*". XXV pp.229-234.
88. **Fricke, S.**, Keim, E. and Schmidt, J., [2001], "Numerical weld modelling-a method for calculating weld-induced residual stresses", *Nuclear Engineering and Design*, Vol. 206, pp.139-150.
89. **Futamura, K.**, [1978], "Application of narrow gap automatic welding process to heavy steel structures of building", *Australian Welding Journal*, pp.37-40.
90. **Gao, H.**, Guo, J.M., Blackburn, Hendricks, R.W., [1997], "Determination of residual stress by X-ray diffraction in HSLA-100 steel weldments" *Navel surface welfare centre*, Bethesda, Maryland.
91. **Gery, D.**, Long, H. and Maropoulos, P., [2005], "Effect of welding speed, energy input and heat source distribution on temperature variations in butt joint welding", *Journal of Materials Processing Technology*, Vol. 167, pp. 393-401.
92. **Garcia C.I**, DeArdo AJ, Raykin E, Defilippi JD,[1995], "International Symposium on high performance steel for structural applications".Ohio, Cleveland,pp.155.
93. **Gauzzi F.**, Missori S., [1988], "*Journal of Materials Science*" 23 pp.782.
94. **Ghosh P.K**, Gupta P C, Gupta S R and Rathi R, [1991], *J. Mater. Sci.*, 26, pp.6161–6170.
95. **Ghosh, P.K**, and Dorn L,[1994], *Trans. Ind. Inst. Met.*, 47, pp.401–408.
96. **Ghosh, P.K**, and Rai, B.K., [1998], "Correlations of pulse parameters and bead characteristics in pulsed current flux cored GMAW process", *Indian Welding Journal*, Vol. 31(4), pp.30-39.
97. **Ghosh, P.K**, and Sharma, V., [1991], "Weld bead chemistry and its characteristics in pulsed MIG welded Al-Zn-Mg alloy", *Materials Transactions JIM*, Vol. 32(2), pp.145-150.
98. **Ghosh, P.K**, Dorn L and Goecke S F, [2001], *Joining Mater*, 13, pp.1–7.
99. **Ghosh, P.K**, Gupta P.C and Rathi R, [1990], *Met. Trans. JIM*, 31, pp.723–729.
100. **Ghosh, P.K**, Gupta P.C and Somani R: Z. [1991], *Metallkd.*, 82, pp.756–762.

101. **Ghosh, P.K.**, [1996], "An analysis of weld characteristics as a function of pulse current MIG welding parameters", *International Journal on Joining of Materials*, Vol. 8(4), pp. 157-161.
102. **Ghosh, P.K.**, [1999], "Decide pulse parameters for desired properties of pulsed current GMAW weld", *International Welding Conference (IWC-99) on Welding and Allied Technology" Challenges in 21st century*," New Delhi, Feb. 15-17, pp. 18-28.
103. **Ghosh, P.K.**, Dorn, L., Devakumaran, K., Hofmann, F., [2009 (a)] "Pulsed current gas metal arc welding under different shielding and pulse parameters; part-2: Behaviour of metal transfer" *ISIJ Int.*, Vol. 49(2), pp.261-269.
104. **Ghosh, P.K.**, Dorn, L., Hubner, M. and Goyal, V.K., [2007 (a)], "Arc characteristics and behaviour of metal transfer in pulsed current GMA welding of aluminium alloy", *Journal of Materials Processing Technology*, Vol. 194, pp. 163
105. **Ghosh, P.K.**, Kulkarni, S.G., Kumar, M. and Dhiman, H.K., [2007 (b)], "Pulsed current GMAW for superior weld quality of austenitic stainless steel sheet", *ISIJ International*, Vol. 47(1), pp. 138-45.-175.
106. **Ghosh, P.K., Dorn, L.**, Kulkarni, S. and Hoffmann, F., [2008], "Arc characteristics and behaviour of metal transfer in pulsed current GMA welding of stainless steel", *Journal of Material Processing Technology*, Vol. 209, pp. 1262-1274.
107. **Ghosh, P.K.**, Goyal, V. K., Dhiman, H.K., Kumar, M., [2006], "Thermal and metal transfer behaviour in pulsed current GMA weld deposition of Al-Mg alloy", *Sci. Technol. Weld. Joining*, Vol. 11(2), pp. 232-42.
108. **Ghosh, P.K.**, Gupta S.R., and Jain N.K., [1989], "Studies on the properties of weld metal deposited at various pulse frequencies in MIG-Welding of Al-Mg alloy", *Indian Welding Journal*, pp.550-558.
109. **Ghosh, P.K.**, Gupta, P.C. and Goyal, V.K., [1998], "Stainless steel cladding of structural steel plate using pulsed current GMAW process", *Welding Journal*, Vol.77(7), pp.307s-312s.
110. **Ghosh, P.K.**, Gupta, P.C. and Somani, R., [1991 (a)], "Influence of pulse parameters on bead geometry and HAZ during bead on plate deposition by MIG welding process", *J. Metallkde.*, Vol. 82(10), pp. 756-762.
111. **Ghosh, P.K.**, Gupta, P.C. and Somani, R., [1991 (b)], "Influence of pulse parameters on the porosity formation in pulsed MIG weld deposit of aluminium alloy", *International Journal of Joining of Materials*, Vol. 3(2), pp.49-54.
112. **Ghosh, P.K.**, Gupta, S.R. and Randhawa, H.S., [1999], "Characteristics and criticality of

- bead on plate deposition in pulsed current vertical-up GMAW of steel”, *International Journal for Joining of Materials*, Vol. 11(4), pp. 99-110.
113. **Ghosh, P.K.**, Gupta, S.R. and Randhawa, H.S., [2000], “Characteristics of a pulsed-current, vertical up gas metal arc weld in steel”, *Metallurgical Transactions A*, Vol. 31A, pp.2247-2259.
 114. **Ghosh, P.K.**, and Ghosh A.K., [2004], “Control of residual stresses affecting fatigue life of pulsed current GMA weld of high strength Al-alloy”, *Met. Mater. Trans.*, 35A, 8, pp. 2439-2444.
 115. **Ghosh, P.K.**, Gupta, S.R., Gupta, P.C. and Rathi, R., [1990 (a)], "Influence of pulsed MIG welding on the microstructure and porosity content of Al-Zn-Mg alloy weldment", *Practical Metallography*, Vol. 27, pp. 613-626.
 116. **Ghosh, P.K.**, Gupta, S.R., Gupta, P.C. and Rathi, R., [1990 (b)], “Pulsed MIG welding of Al-Zn-Mg alloy”, *Material Transactions of JIM*, Vol. 31 (8), pp. 723-729.
 117. **Ghosh, P.K.**, Rai B.K., [1996], “Characteristics of pulsed current bead on plate deposit in flux cored GMAW process”. *ISIJ Intet*. Vol.36, pp.1036-1045.
 118. **Ghosh, P.K.**, Dorn L, [1993], “*Inter.Journal.Joining Materials*”, pp.143.
 119. **Goldak J.**; A. Chakravarti and M. Bibby, [1984], “A New Finite Element Model for Welding Heat Sources” *Met. & Mat. Trans. B*, Vol.15B, 299-305.
 120. **Goyal, V.K.**, Ghosh, P.K., Saini, J.S., [2008 (a)] “ Influence of pulse parameters on characteristics of bead on plate weld deposits of aluminium and its alloy in the pulsed current gas metal arc welding process”, *Mater. Trans. A*, Vol. 39A, pp. 3260- 3275.
 121. **Goyal, V.K.**, Ghosh, P.K., Saini, J.S., [2008 (b)], “Analytical studies on thermal behaviour and geometry of weld pool in pulsed current gas metal arc welding”, *J. Met. Proc. Tech*, Vol. 209, pp.1318-1336.
 122. **Goyal, V.K.**, Ghosh, P.K. and Saini, J.S., [2007], “Process controlled microstructure and cast morphology of dendrite in pulsed current gas metal arc weld deposits of aluminium and Al-Mg Alloy”, *Metallurgical and Materials Transactions A*, Vol.38(8), pp. 1794-1805.
 123. **Goyal, V.K.**, Ghosh, P.K. and Saini, J.S., [2006], “Influence of pulse parameters on solidification behaviour of pulsed current GMA weld deposition on Al-Mg alloy”, *Procd. Int. Conf. Manufacturing Technology Design & Research Conference*, IIT Roorkee, December 2006.
 124. **Graham F.D**, [1966], “Audels Welder Guide”, *Taraporevala Sons and Co.*, Bombay.
 125. **Gunasegaram D.R**, Farnsworth D.J, and Nguyen T.T, [2009], "Identification of critical factors affecting shrinkage porosity in permanent mold casting using numerical simulations

- based on design of experiments", *Journal of material processing technology*, Vol.209, pp1209-1219.
126. **Gunduz, S.**, Cochrane, R.C., [2005], "Influence of cooling rate and tempering on precipitation and hardness of vanadium micro-alloyed steel", *Materials and Design*, Vol. 26, pp. 486–492.
 127. **Gupta P.C.**, Ghosh P.K. and Vissa S., [1998], "Influence of pulse frequency on the properties of HAZ in pulsed MIG-welded Al-Zn-Mg alloy", *Int.Conf.on welding technology*, UOR, pp.171-177.
 128. **Hafele,P.**, [1994], "A numerical calculation of the energy release rate for non-self-similar crack growth for mixed mode fracture", *International Journal of Fracture*, Vol. 66, pp. R25-R32.
 129. **Halmoy E.**, H. Olsen and S. Samuelsen [1983], "Adaptively controlled MIG narrow gap welding, Development and innovations for improved welding production, Proceedings first internal conference, England, 5(8), pp.13-15.
 130. **Hamad Mahal Hssain**, [1994], Influence of pulsed current MIG- Welding on the mechanical properties of Al-Zn-Mg alloy weldment, *Ph.D Thesis*, UOR.
 131. **Hearns W.H.** (Ed.), [1982], "Metals and their Weldability", vol.4, *Welding Handbook*, seventh ed., *American Welding Society*, pp. 514.
 132. **Heald, P.R.**, Maidigan, R.B., Siewert, T.A. and Lin, S., [1994], "Mapping the droplet transfer modes for an ER-1000 S-1 GMAW electrode", *Welding Journal*, Vol. 73(2), pp 38-s-43-s.
 133. **Henderson, I.D.**, Steffens, H.D., [1976], "Fracture toughness of narrow-gap welded joints in the nuclear pressure vessel steel 22NiMoCr37, *Nuclear Engineering and Design*, Vol. 36, pp. 273-285.
 134. **High-Strength Low-Alloy Steel**, [1979], "Status, Selection and Physical Metallurgy", *Battelle Press*,
 135. **Holsberg P.W.**, Guda, J. P., and Caplan, I. L., [1995], "Navy's welding research picks up steam". *Advanced Materials and Processes* 138(1): 45.
 136. **Hong, S.G.** Jun, H.J., Kang, K.B., Park, C.G., [2003], "Evolution of precipitates in the Nb–Ti–V micro-alloyed HSLA steels during reheating" *Scripta Materialia*, Vol. 48, pp. 1201–1206.
 137. **Houldcroft P.I**, [1967], "Welding Process", Cambridge University Press, Cambridge, pp. 43.

138. **Hou, Huoran.**, Chen, Qian., Liu, Qingyou., Dong, Han., [2003], “Grain refinement of a Nb–Ti microalloyed steel through heavy deformation controlled cooling”, *Journal of Materials Processing Technology*, Vol. 137, pp. 173–176.
139. **Hoyt, J.J.**, Asta, M., Karma, A., [2003], “Atomistic and continuum modeling of dendritic solidification”, *Materials Science and Engineering*, Vol. 41, pp.121–163.
140. **Huang M.L** and Wang L, [1998], “Carbon Migration in 5Cr-0.5Mo/21Cr-12Ni Dissimilar Metal Welds”, *Metallurgical and Material Transaction A*, Vol 29A, pp.3037.
141. **Hulka, K.**, F. Heisterkamp, [1998], *Mater. Sci. Forum* 284-286, pp. 343-350.
142. **Hussain, H.M.**, Ghosh, P.K., Gupta, P.C. and Potluri, N.B., [1996], “Properties of Pulsed Current multipass GMA welded Al-Zn-Mg alloy”, *Welding Journal*, Vol. 75(7), pp. 210-s-215-s.
143. **Hyde, T.H.**, Williams, J.A., and Sun, W., [2002], Factors, Defined from Analysis, Contributing to the Creep Performance of Weld Repairs, Creep Performance of Weld Repairs OMMI (Vol. 1, Issue 3)
144. **Imanaka, T.**, Nakano, S., Shimomura, J., and Yasuda, K. [1985], Hydrogen attack in Cr-Mo Steels and disbonding of austenitic stainless weld overlay. Kawasaki Steel Technical Report No. 13. September. (Translation of Kawasaki Steel Giho 17[1], pp 84-92.
145. **Innyi, T.**, [1975], “Narrow gap welding for corner joint in box grinder made of heavy high tensile strength (80 Kg/mm class) steel”, *Advanced Welding Technology*, Japan Welding Society, pp. 387-390.
146. **Internal Report** No. IGC/DPEND/NDTES/FA1/1998.[1998], “Failure Analysis of Thermowell Boss of Fast Breeder Test Reactor (FBTR) Steam Generator”; Unpublished.
147. **Ishizaki K.**, [1962], “Interfacial tension theory of the phenomenon of arc welding-mechanism of penetration”, Proceedings of Symposium on Physics of Arc Welding, *The Institute of Welding*, London, pp. 195–209.
148. **Jacobsen, N.**, [1992], “Monopulse investigation of drop detachment in pulsed gas metal arc welding”, *Phys. D, Appl. Phys.*, Vol. 25, pp. 783-797.
149. **Jang, G.B.**, Kim, H.K., Kang, S.S., [2001], “The effects of root opening on mechanical properties, deformation and residual stress of weldments” *Welding Journal*, Vol. (3), pp. 80s-88s.
150. **Jefferson T.B.**, [1951], “The Welding Encyclopedia”, 13th Edition, *McGraw- Hill*, New York, p. 491.
151. **Jilong, Ma** and Apps, R.L., [1982], “MIG transfer discovery of importance to industry”, *Welding & Metal Fabrication*, Vol. 14, No. 9, pp. 307-316.

152. **Johnson,P.G.**, Szekely, R.B., Madigan and Quinn, T.P., [1995], “Power characteristics in GMAW: experimental and numerical investigations”. *Welding Journal*, Vol. 74(3), pp 93-s-102-s.
153. **Jones D.F.**, U.S. Patent 6,744,013, “Welding Torch for Use in Gas Metal Arc Welding”, (Parweld Limited) 1 June 2004.
154. **Joseph A**, Ramesh AS, Jayakumar T, Murugan N.[2001], “Failure analysis of a dissimilar weld joint in steam generator”. *Pract Metallogr* , 38(12): pp.667–79.
155. **Joseph A.**, Harwig, D., Farson, D. F. and Richardson, R., [2003], “Measurement and calculation of arc power and heat transfer efficiency in pulsed gas metal arc welding”, *Science and Technology of Welding and Joining*, Vol. 8(6), pp. 400-406.
156. **Kanbe Y.** and K. Suda [1986],” Narrow gap welding process with oscillating arc, loopnap in narrow gap welding, The state of art in Japan, Japan welding society, Japan, pp.60-64.
157. **Kang, Y.H.** and Na, S.J., [2003], “Characteristics of welding and arc signal in narrow groove gas metal arc welding using electromagnetic arc oscillation”, *Welding Journal*, Vol. 82 (5), pp. 93s-99s.
158. **Kanjilal P.**, Pal T. K. and Majumadar S. K. [2007],”Prediction of mechanical properties in submerged arc weld metal of C-Mn steel”, *Materials and Manufacturing Process*, Vol.22, pp.114-127.
159. **Kanjilal P.**, Pal T. K. and Majumadar S. K. [2006],”Combined effect of flux and welding parameters on chemical composition and mechanical properties of submerged arc weld metal,” *Journal of Material Processing Technology*, Vol.171, 223-231.
160. **Kawahara M** and I Ashano, [1986], BHK type narrow gap GMA welding process in narrow gap welding”, *The state of art in Japan, Japan welding society*, pp. 39-45.
161. **Kearns, L.P.**, [1978], “Welding Handbook”, American welding society, Vol. II, pp.131 to 137.
162. **Kelly T.F**, Cohen M, Vandersande J B., [1984], “Rapid solidification of a droplet-processed stainless steel”. *Met. Trans.* A15, pp. 819–833.
163. **Khodabandeh, Ali Reza.**, Jahazi, Mohammad, Yue, Steve, Boucher, Philippe, [2005], “Impact toughness and tensile properties improvement through microstructure control in hot forged Nb–V micro-alloyed steel”, *ISIJ International*, Vol. 45, pp. 272–280.
164. **Khurmi, R.S.**, [2002] “Strength of materials”, 22nd Ed., *S. Chand & Company*, India.
165. **Kim, Y.S.** and Eagar, T.W., [1993a], “Analysis of metal transfer on gas metal arc welding”, *Welding Journal*, Vol. 72(6), pp. 269-s-278-s.

166. **Kim, Y.S.** and Eagar, T.W., [1993 b], “Metal transfer in pulsed current gas metal arc welding”, *Welding Journal*, Vol. 7, pp. 279s-287s.
167. **Kim, Y.S.**, D.M. and Eagar, T.W., [1991], “Analysis of electrode heat transfer in gas metal arc welding”, *welding Journal*, Vol. 70 (1), pp. 20s-31s.
168. **Kliber, J.**, Schindler, L., [1996], “Recrystallization/precipitation behaviour in microalloyed steels”, *Journal of Materials Processing Technology*, Vol. 60, pp. 597-602.
169. **Klueh R.L.**, and King JF. [1982], “Austenitic–ferritic weld joint failures”. *Weld J*, 61, pp.302s–311.
170. **Klueh R.L.** [1974], “The effect of carbon on 2.25Cr–1Mo steel (I) microstructure and tensile properties”. *J Nucl Mater*, 54, pp.41–54.
171. **Klueh R.L.** [1974], “The effect of carbon on 2.25Cr–1Mo steel (II) creep rupture properties”. *J Nucl Mater*, 54, pp.55–63.
172. **Kobayashi T**, Kuwana T, and Kikuchi Y,[1971], “Study on the effect of pulsed TIG welding parameters on delta-ferrite content, shape factor and bead quality in orbital welding of AISI 316L stainless steel plate”,*J Jpn. Weld. Soc.* Vol.40, pp.221-231.
173. **Kobelco**, Welding Today.
174. **Koichi Masubuchi**, [1980], “Analysis of welded structures”, 1st Ed., *Pergamon Press*, New York.
175. **Komanduri R.** and Hou Z. B. [2000], “Thermal analysis of the arc welding process: Part 1. General solutions”, *Met. Mat. Trans. B*, vol.31B, pp.1353-1370.
176. **Koseki T**, Matsumiya T, Yamada W, Ogawa T., [1994], “Numerical modeling of solidification and subsequent transformation of Fe–Cr–Ni alloys”. *Metall. Mater. Trans. A25*, pp. 1309–1321.
177. **Kulkarni, S.G.**, P.K. Ghosh, S. Ray, H.S. Kushwaha, K.K. Vaze, P.K. Singh and J. Krishnan., [2005], “Comparative studies on characteristics of conventional V-groove and narrow groove SMA welds of 304LN stainless steel pipes”, *Procd. Int. Weld. Congress, Ind. Inst. Weld*, Mumbai, 16-19 February IWA 021
178. **Kulkarni, S.G.**, [2008] “Narrow gap pulse current gas metal arc welding of thick wall 304LN stainless steel pipe”, *Ph.D. Thesis*, IIT Roorkee, India.
179. **Kumar Subodh** and Bhaduri S.C. [1994],” Three-Dimensional Finite Element Modeling of Gas Metal-Arc Welding”, *Met. & Mat. Trans. B*, Vol. 25B, 435–441.
180. **Kuziak R** , Botd T and Yi-Wen Cheng,[1995], “Microstructure Control of Ferrite-Pearlite High Strength Low Alloy Steels Utilizing Microalloying Additions”, *Journal of material processing technology* 53, Vol.53, pp.255-262

181. **Laing, B.**, Heid, R. and Pollack, A., [1985], "Narrow gap welding of HY-100 plate using close loop, adaptive feedback, through-the-arc tracking technology", *Welding Journal*, Vol.64 (11), pp. 38s.
182. **Lambert-Perlade, A.**, Gourgues, A.F., Pineau, A., [2004], "Austenite to bainite phase transformation in the heat-affected zone of a high strength low alloy steel", *Acta Materialia*, Vol. 52, pp. 2337-2348.
183. **Lambentt, J.A.**, [1989], "Assessment of the pulsed GMA technique for tube attachment welding" *Welding Journal*, Vol. 68(2), pp 35-43.
184. **Lancaster, J.F.**, [1984], "The Physics of welding", *Pergamon Press*, New York, USA.
185. **Lenivkin V.A.**, [1981], "The continuity of current in pulsed arc welding with pulses of varying shape" *Welding production*, pp.12 to 14.
186. **Lee, Y.**, Lee, T., Kim, B.H., and Lee, C.H., [2015]., Superior Bonding Properties of Dissimilar Steel Joint Produced by Electroslag Remelting, *Met. Mater. Int.*, Vol. 21, No. 6 pp. 1054-1060.
187. **Li G.F.**, Charles E.A., [2001], "Effect of post weld treatment on stress corrosion cracking of a low alloy steel to stainless steel transition weld", *Corrosion science.*, pp.1963-1983.
188. **Liew C**, Wahab M A, Painter M J, [1993], "The Prediction of Temperature Distribution in Gas Metal Arc Welds", *Proceedings Welding Technology Institute of Australia: Australian Institute of Non-destructive Technology, Fabcon: Fabfair Conference.*
189. **Linnert, G.**, [1994], "Welding Metallurgy" Vol. 1, 4th Ed., *American Welding Society*, Miami, Florida.
190. **Lin, Y.C.** and Chen, P.Y., [2001], "Effect of nitrogen content and retained ferrite on the residual stress in austenitic stainless steel weldments", *Materials Science and Engineering A*, Vol. 307, pp. 165-171.
191. **Liu, S.** and Siewert, T.A., [1989], "Metal transfer in gas metal arc welding: Droplet rate", *Welding Journal*, Vol. 68(2), pp. 52s-58s.
192. **Losz, I.M.B.**, and Challenger, K. D., [1989], "Microstructure and properties of a copper precipitation strengthened HSLA steel weldment". *Proceedings of the 2nd International Conference on Trends in Welding Research*, Gatlinburg, Tennessee, pp. 229.
193. **Lothongkum, G.**, Chaumbai P., Bhandhubanyong P., [1999], "TIG pulse welding of 304L austenitic stainless steel in flat, vertical and overhead positions", *Journal of material processing technology*, Vol. 89-90, pp. 410-414.

194. **Lowke, J.J.**, Morrow, R., Haider, J. and Murphy, A.B., [1997], "Prediction of gas tungsten arc welding properties in mixtures of argon and hydrogen", *IEEE Transaction on Plasma Science*, Vol. 25, pp. 925-930.
195. **Lundin C.D.**, [1982], *Welding Research Supplement* 61 (2) p.58.
196. **Lucus, W.**, [1992], "Choosing a shielding gases -part II", *Welding and Metal Fabrication*, Vol. 60, pp. 269 to 276.
197. **Madhusudan Reddy G**, [2000], "Weldability of HSLA steel using austenitic Stainless Steel Filler Wires", *Journal of Materials Processing Technology*, pp.23-33.
198. **Madhusudhan Reddy G**, Mohandas T, Tagore G.R.N, [1995], "Weldability studies of high-strength low-alloy steel using austenitic fillers", *Journal of Materials Processing Technology*, Vol. 49, pp. 213-228.
199. **Mahapatra M. M.**, Dutta G. L., Pradhan B. and Mandal N. R. [2006], "Three dimensional finite element analysis to predict the effects of SAW process parameters on temperature distribution and angular distortions in single pass butt joints with top and bottom reinforcements", *International Journal of Pressure Vessel and Piping*, Vol.83, pp.721-729.
200. **Malin, V.Y.**, [1983a], "The state-of-the-art of narrow gap welding", Part I, *Welding Journal*, Vol.62(4), pp. 22-36.
201. **Malin, V.Y.**, [1983b], "The state-of-the-art of Narrow Gap welding", Part II, *Welding Journal*, Vol.62(6), pp.37-46.
202. **Manohar, P. A.**, Chandra, T., Killomore, C.R., [1996 (a)], "Continuous cooling transformation behavior of micro-alloyed steel containing Ti, Nb, Mn and Mo", *ISIJ International*. Vol. 36, pp. 1486-1493.
203. **Manohar, P. A.**, Dunne, D.P., Chandra, T., Killomore, C.R., [1996 (b)], "Grain growth predictions in micro-alloyed steels", *ISIJ International*, Vol. 36, pp. 194-200.
204. **Maruo, H.** and Hirata, Y., [1984], "Study of pulsed MIG welding", *IIW Doc. SG 212-258-84*, Welding Department, Osaka University, Japan.
205. **Matsuda, F.**, and Nakagawa, H. [1984], Simulation test of disbonding between 2.25%Cr-1%Mo steel and overlaid austenitic stainless steel by electrolytic hydrogen charging technique. *Transactions of JWRI* 13(1), pp.159-161.
206. **Matsuda, F.**, Nakagawa, H., and Tsuruta, S. [1986], Proposal of hydrogen blistering mechanism associated with disbonding between 2.25Cr-1Mo steel and Type 309 overlaid Metal. *Transactions of JWRI* 15(2), pp.207-208.

207. **Matthews, J.R.**, Lassaline, E.E., Porter, J.F. and Leewis, K.G., [1992], "Evaluating frequency modulated GMA welding of HY 80 steel", *Welding Journal*, Vol. 71(9), pp. 49-53.
208. **Megudeeswaran G.**, Balasubramanian V. and Reddy G. Madhusudhan. [2009], "Effect of welding consumables on fatigue performance of shielded metal welded high strength quenched and tempered steel joints", *Journal of material engineering and performance*, Vol. 18(1), pp.49-56.
209. **Metals Handbook**, [1979], "Properties and selection: Nonferrous alloys and pure metals", Vol. 2, 10th ed., *ASM International*, Metal Park, Ohio.
210. **Ming-Chun Zhao**, Ke Yang, Yi-Yin Shan, [2003], "Comparison on strength and toughness behaviors of micro-alloyed pipeline steels with acicular ferrite and ultrafine ferrite", *Materials Letters*, Vol. 57, pp. 1496–1500.
211. **Mohan S**, Ved Prakash, J.P. Pathak, [2002], "Wear characteristics of HSLA steel", *Wear*, Vol.252, pp.16-25.
212. **Mohandas T**, [1995], "Heat affected zone softening in high strength low alloy steel", *Science and technology of welding*, pp. 43-57.
213. **Mujahid M** et al., [1992], "Processing, microstructure and properties of microalloyed and other modern high strength low alloy steels", *Conference Proceedings, Pittsburgh, PA*, A. J. DeArdo, ed., *TMS-AIME*, Warrendale, PA, pp. 341.
214. **Murugan, N., Parmar, R.S.**, [1994], "Effect of MIG process parameters on the geometry of the bead in the automatic surfacing of stainless steel", *Journal of Material Processing Technology*, Vol. 41, pp. 381-398.
215. **Murugan, N., Parmar, R.S.**, [1995], "Mathematical models for bead geometry prediction in automatic stainless steel surfacing by MIG welding", *International Journal for Joining of Materials*, Vol. 7(2/3), pp.71-80.
216. **Murugan, S.**, Rai, S.K., Kumar, P.V., Jayakumar, J., Baldev Raj, and Bose, M.S.C., [2001], "Temperature distribution and residual stresses due to multi-pass welding in type 304 stainless steel and low carbon steel weld pads", *International Journal of Pressure Vessels and Piping*, Vol. 78, pp.307-317.
217. **Nagesh D.S.**, and Datta G.L, [2002], "Prediction of weld geometry and penetration in shielded metal-arc welding using artificial neural network", *Journal of material processing technology*, Vol.123. pp.303-312.

218. **Nagesh D.S.**, and Datta G.L, [2010], “Genetic algorithm for optimization of welding variables for height to width ratio and application of ANN for prediction of bead geometry for TIG welding process”, *Applied Soft Computing*, Vol.10. pp. 897-907.
219. **Nakayama H.** [1976], “Application of narrow gap automatic CO₂ arc weaving horizontal position welding process to heavy steel structures of building ”, *IIW Doc. XII-632-76, XII-B-193-76*, p34.
220. **Nakajima H.**, A. Nagai and S. Minehisa [1986],” Rotating arc narrow gap MIG welding process in narrow gap welding, The state of art in Japan, *Japan welding society, Japan*, pp.74-80.
221. **Na S. J.** and Lee S. Y. [1987], “A study of three dimensional analysis of the transient temperature distribution in gas tungsten arc welding”, *Proc. Inst. Mech. Engg. (London)*, part B, 201, pp.149-156.
222. **Narayanasamy, R.**, Parthasarathi, N. L., Sathiya Narayanan, C., Venugopal, T., Pradhan, H.T., [2007], “A study on fracture behaviour of three different high strength low alloy steel sheets during formation with different strain ratios” , *Materials and Design*, Vol.3, pp.320-338.
223. **Navneet gupta**, [2008], “Principle of materials science and engineering”, Dhanpat rai & co publisher, pp. 332-333.
224. **Nguyen N. T**; Ohta A.; Matsuoka K.; Suzuki N. and Maeda Y., [1999], “Analytical solution for transient temperature of semi-infinite body subjected to 3-D moving heat source”, *Welding Journal*, Vol. 78(8), 265-s –274-s.
225. **Nguyen N.T.**; Y. W. Mai; S. Simpson and A. Ohta, [2004],” Analytical approximate solution for the double ellipsoidal heat source in finite thick plate”, *Welding Journal*, Vol. 83(3), 82s-93s.
226. **Nomura, H.** and Sugitani, Y., [1984], “Further improvements of narrow gap welding techniques”, *Joining of Metals*, pp. 73-85.
227. **Nosse J.R.**, 3 April [2001], U.S. Patent 6,211,490, Nozzle for Shielded Arc Welding Gun, (to Lincoln Global, Inc.).
228. **Ohio**, [1997], “Hand book on materials for superconducting machinery”. *Battelle Columbas Laboratory*.
229. **Okuda N.**, T. Kashimura and H. Saita.,[1986],” Narrow gap GMA welding process , twisted arc welding process, in narrow gap welding, *The state of art in Japan, Japan welding society*, pp.46-55.
230. **Okada, H.**, and Naito, K. [1982], Hydrogen- induced disbonding of stainless weld

231. **Okagawa R.K**, Dixon R D, and Olson D L, [1983], *Welding Journal*.Vol.62, pp.204s-209s.
232. **Ollilainen V**, Kasprzak W and Holappa L, [2003], “The effect of silicon, vanadium and nitrogen on the microstructure and hardness of air cooled medium carbon low alloy steels”, *Journal of material processing technology*, Vol.134, pp. 405-412.
233. **Omar A**, [1998],”Effects of welding parameters on hard zone formation at dissimilar metal welds”, *Welding Journal*. 77 (2), pp.86s–93s.
234. **Onoro J**, and Ranninger C, [1997], “Fatigue behaviour of laser welds of high-strength low-alloy steels”, *Journal of Materials Processing Technology*, Vol.68, pp. 68-70.
235. **Onozuka.M.**, Alfile.J.P, Aubert.ph,[2001], "Manufacturing and maintenance technologies developed for a thick-wall structure of the ITER vacuum vessel, Fusion engineering and design", *Overlay in hydrodesulfurizing reactor. Proceedings of the First International Conference on Current Solutions to Hydrogen Problems in Steels. Washington, D.C*, pp 397-410.
236. **Padilha, A. F.** and Rios, P.R., [2002], “Decomposition of austenite in austenitic stainless steels”, *ISIJ International*, Vol. 42(4), pp. 325–337.
237. **Painter M.J**, Jarvis L,[1992], “Numerical Modelling the SAW process, Institute of Metals and Materials”, *Conference On Modelling and Control of Materials Processing*, Wollongong.
238. **Palani, P.K.** and Murugan, N., [2006], “Selection of parameters of pulsed current gas metal arc welding”, *Journal of Materials Processing Technology*, Vol. 172, pp. 1–10.
239. **Paley Z.** and Hibbert P. D. [1975],”Computation of temperature in actual weld design”, *Welding Journal*, Vol. 54, 385s-392s.
240. **Pavelic V**, Tanbakuchi R, Uyehara O. A. and Myers P. A. [1969],”Experimental and computed temperature histories in gas tungsten arc welding of thin plates”, *Welding Journal*, Vol.48, pp. 295s-305s.
241. **Parmar R.S**, [1997], “Welding engineering and technology”, *Khanna publishers*, pp.530-532.
242. **Parvathavarthini N**, and Dayal R.K.,[2002], “Influence of chemical composition, prior deformation and prolonged thermal aging on the sensitization characteristics of austenitic stainless steels”, *Journal of nuclear materials*, Vol.305, pp. 209-219.
243. **Pathak A. K.** and Dutta G. L. [2000], ”3D finite element analysis on heat flow in welding under varying arc length”, *Indian welding journal*, vol. 33, no.4, pp.24-29.

244. **Peng-Hsiang Chang**, Tso-Liang Teng, [2004], “Numerical and experimental investigations on the residual stresses of the butt-welded joints”, *Computational Material Science*, Vol. (29), pp.511-522.
245. **Philip C**, and Terry P.E, [1999], “Practice periodical on structural design and construction”, pp.13-16.
246. **Philip C.**, Member P.E., [1999], “ASCE.Analysis of thermal stresses at dissimilar metal pipe welds”. *Practice periodical on structural design and construction*. pp.13.
247. **Piatti, G.** and Vedani, M., [1990], “Relation between tensile properties and microstructure in type 316 stainless steel SA weld metal”, *Journal Of Materials Science*, Vol.25, pp. 4285-4297.
248. **Pickering, F.B.**, [1978] “Physical metallurgy and the design of steels” *Applied science publishers*, London.
249. **Powell, G.L.F.**, Herfurth, G., [1998], “Charpy V-notch properties and microstructures of narrow gap ferritic welds of a quenched and tempered steel plate”, *Metallurgical and Materials Transactions A*, Vol. 29 (A), pp.2775.
250. **Prasad N. Silva** and Sankara Narayan T. K., [1996], “Finite element analysis of temperature distribution during arc welding using adaptive grid techniques”, *Welding Journal*, vol. 75, pp.123s-128s.
251. **Prasad, S.N.**, [2003], “Influence of austenitisation temperature on the structure and properties of high strength low alloys”, *Materials science and Engineering*, pp.287-297.
252. **Praveen, P.**, Yarlagadda, P.K.D.V. and Kang, M.J., [2005], “Advancements in pulse gas metal arc welding”, *Journal of Materials Processing Technology*, Vol. 164–165, pp. 1113–1119.
253. **Pressouyre, G.**, Chaillet, J., and Vallette, G., [1982], “Parameters affecting the hydrogen disbonding of austenitic stainless clad steels”. *Proceedings of the First International Conference on Current Solutions to Hydrogen Problems in Steels*. Washington, D.C.
254. **Quinn, T.P.**, Maidgan, R.B. and Siewert, T.A., [1994], “An electrode extension model for gas metal arc welding”, *Welding Journal*, Vol. 73(10), pp. 241s-247s.
255. **Quintino, L.** and Allum, C.J., [1984], “Pulsed GMAW: Interactions between process parameters, Part I”, *Welding and Metal Fabrication*, Vol. 16(4), pp. 126-129
256. **Race, J.**, [1992]., Carbon Diffusion Across Dissimilar Steel Welds, Phd Thesis, 1992, Cambridge University, UK
257. **Radaij, D.**, [1992], “Heat effects on welding”, *Springer-Verlag*, USA.

258. **Rajashekhhar, K.**, Harendranath, C.S., Raman, R. and Kulkarni, S.D., [1997], “Microstructural evolution during solidification of austenitic stainless steel weld metals: A color metallographic and electron microprobe analysis study”, *Materials Characterization*, Vol. 38, pp. 53-65.
259. **Randhawa, H.S**, Ghosh P K and Gupta S R,[2000], *ISIJ Int.*, 40, pp.71–76.
260. **Randhawa, H.S**, Ghosh P K and Gupta S R, [1998],”Geometric characteristics of pulsed current positional GMA weld”, *Iron and steel Institution of japan International*, Vol.38, No-4, pp 276-284.
261. **Randy K**, Kent and Roy Baggerly, [2003], Intergranular corrosion, Corrosion hand book, pp.777-785.
262. **Redding, C.J.**, [2002], “Fume model for gas metal arc welding”, *Welding Journal*, Vol. (6), pp.95s-103s.
263. **Robert W. Messler, Jr.**, [1999], “Principles of welding” *John Wiley and sons*, New York.
264. **Ronay B**, [1960], “The importance of polarity in arc welding”, *Weld. Engineer* 45 (3), pp.32–33.
265. **Roos, Eberhard.**, Stumpfrock, Ludwig., Schuler, Xaver., Eisele, Ulrich., [2005], “Fracture mechanics safety analysis of components based on fracture mechanics characteristics combined with multiaxiality of the stress state”, *International Journal of Pressure Vessels and Piping*, Vol. 82, pp. 355–362.
266. **Roschin V.V.** [1969], “Residual stresses in pipe joints between dissimilar steels”. *Weld Prodn* 1969; 9, pp. 55–8.
267. **Rose S**, Schnick M, Hertel M, Zschetzsche J, and Füssel U,[2010], “Transient simulation of pulsed current gas metal arc welding processes and experimental validation”, *International Scientific Colloquium, Modelling for Material Processing*, pp. 16-17.
268. **Rosenthal D.** and Cambridge M. [1946],” The theory of moving sources of heat and its application to metal treatments”, *Transaction of the A.S.M.E.*, 68, 849-865.
269. **Rosenthal D**, [1941], “Mathematical theory of heat distribution during welding and cutting”, *Welding J. Res. Suppl.* 20 (5), pp. 2205– 2345.
270. **Rossi B.E**, [1941], “Welding and its Applications”, *McGraw-Hill*, New York, p. 127.
271. **Rothwell, A.B** and Malcolm Gray, [1976] “ Welding of HSLA [Micro-alloyed] structural steels”, *Proc. International Conference*, Rome, Italy.
272. **Rowe M.D.**, Nelson T.W. and Lippold J.C., [1999], “Hydrogen-Induced Cracking along the Fusion Boundary of Dissimilar Metal Welds”, pp.31-s to 37s.

273. **Rowley T**, Rowberry TR, Alldridge C.[1969], “Problems associated with the design, inspection and use of large diameter ferritic/austenitic joints in power plant”, proceedings of international conference welding dissimilar metals. *Met Constr Br Weld J*, 1(12s), pp.13–17.
274. **Sahay, S.S.**, Malhotra, C.P., Kolkhede, A.M., [2003]. “Accelerated grain behavior during cyclic annealing”. *Acta Mater.* 51, pp.339–346.
275. **Samanta S.K**, Mitra S.K, and Pal T.K, [2006], “Effect of rare earth elements on microstructure and oxidation behaviour in TIG weldments of AISI 316L stainless steel”, *Material science and Engineering A*, Vol.430, pp.242-247.
276. **S´anchez-Cabrera, V.M.**, Rubio-Gonz´alez, C., Ru´ız-Velab, J.I. and Ram´irez-Baltazar, C. , [2007], “Effect of preheating temperature and filler metal type on the microstructure, fracture toughness and fatigue crack growth of stainless steel welded joints”, *Materials Science and Engineering A*, Vol.452–453, pp. 235–243
277. **Sarafianos, N.**, [1992], “Structure morphology effect of Ti and Nb stabilized austenitic stainless steel welds on corrosion properties”, *Journal of Material Science*, Vol.27, pp. 226-232.
278. **Sarkani, S.**, Tritchkov, V. and Michaelov, G., [2001], “An efficient approach for computing residual stresses in welded joints”, *Finite Elements in Analysis and Design*, Vol.35, pp.247-268
279. **Sasmal, B.**, [1997], “Mechanism of the formation of $M_{23}C_6$ plates around undissolved NbC particles in a stabilized austenitic stainless steel”, *Journal of Material Science*, Vol.32, pp. 5439 – 5444.
280. **Swada, S.**, Hori, K., Kawahara, M., Takao, M. and Asano, I., [1979], “Application of narrow gap process” *Welding Journal*, Vol. 59(9), pp.17-25.
281. **Schnick M**, Fussel U, Hertel M, Spille-Kohoff, Murphy A B, [2010], “Metal vapour causes a central minimum in arc temperature in gas-metal arc welding through increased radiative emission”, *Journal of Physics*, Vol.43, pp.1-5.
282. **Shaikh, H.**, Khatak, H.S., Sahadri, S.K. and Gnanamoorthy, J.B., [1995], “ Effect of ferrite transformation on the tensile and stress corrosion properties of type 316 L stainless steel weld metal thermally aged at 873^0 K ”, *Metallurgical and Materials transactions A*, Vol.26A, pp. 1859- 1868
283. **Shankar V**, Gill T.P.S, Mannan S.L, and Sundaresan S, [2003a], “Effect of nitrogen addition on microstructure and fusion zone cracking in type 316L stainless steel weld metals”, *Material science and engineering*, Vol. A343, pp. 170-181.

284. **Shankar, V.**, Gill, T.P.S., Mannan, S.L. and Sundaresan, S., [2003b], “Solidification cracking in austenitic stainless steel welds”, *Sadhana*, Vol. 28(3/4), pp.359–382.
285. **Shome, M.**, [2007], “Effect of heat-input on austenite grain size in the heat-affected zone of HSLA-100 steel”, *Materials Science and Engineering*, pp. 454–460.
286. **Shome, M.**, Gupta, O.P., Mohanty, O.N., [2004], “A modified analytical approach for modelling grain growth in the coarse grain HAZ of HSLA steels”, *Scripta Materialia*, Vol.50, pp.1007–1010.
287. **Shanmugam, A.**, Raja, A., Santhakumari, A., Rohira, K.L. and Murti, K.G.K., [1997], “Process stability criterion for MIG welding”, *Indian Welding Journal*, Vol. (1), pp. 32 to 36.
288. **Shtrikman, M.M.** and Grinin, V.V., [1977], “The automatic narrow gap welding of high strength steels and titanium alloys”, *Welding Production*, Vol.24(1), pp.19-23.
289. **Shtrikman, M.M.** and Grinin, V.V., [1979], “On stability of the gap width in the argon shielded narrow-gap welding of short workpieces”, *Welding Production*, Vol. 26(3), pp.19-23.
290. **Shvachko, V.I.**, [2000], “Cold cracking of structural steel weldments as reversible hydrogen embrittlement affect”, *Int. J. Hydrogen Energy*, Vol. (25), pp. 473-480.
291. **Sierdzinski, M.S.** and Ferree, S.E., [1999], “New low hydrogen flux cored wires for welding high strength steels”, *Proceedings of International welding conference*, New Delhi, 15-17 Feb., Vol. 1, pp.381.
292. **Siewert, T.A.**, McCowan, C.N. and Olson, D.L., [1988], “Ferrite number prediction to 100 FN in stainless steel weld metal”, *Welding Journal*, Vol.67(), pp.289s–298s.
293. **Sindo Kou**, [1987], “Welding Metallurgy” John Wiley and sons, New York.
294. **Smati, Z.**, [1986], “Automatic pulsed MIG welding”, *Welding Journal*, Vol. 65(1), pp.38s-44s.
295. **Sobolev V.V**, Guilemany J.M, and Calero J.A, [1995], "*Material science technology technology*, 11(8), pp.810.
296. **Sobolev**, [1987], *Comm.Acad.sci.USSR.Metals*, Vol.3, pp.76.
297. **Stasko, Renata.**, Adrian, Henryk., Adrian, Anna., [2006] , “Effect of nitrogen and vanadium on austenite grain growth kinetics of a low alloy steel”, *Materials Characterization*, vol. 56, pp. 340–347.
298. **Stenbacka, N.** and Person, K.A.,[1989], “ Shielding gases for gas metal arc welding”, *Welding Journal*, Vol. 68, No. 11, pp 41-47.

299. **Subramaniam S**, White D R, Jones J E and Lyons D W, [1999], *Weld.J.*, 68, pp.166s-172s.
300. **Subramaniam, S.**, White, D.R., Jones, J.E. and Lyons, D.W., [1998], “Droplet transfer in pulsed gas metal arc welding of aluminium”, *Welding Journal*, Vol. (11), pp.458s-464s.
301. **Suban, M.** and Tusek, J., [2001], “Dependence of melting rate in MIG/MAG welding on the type of shielding gas used”, *Journal of Material Processing Technology*, Vol.119, pp. 185 to 192.
302. **Sundaram, P.**, Pandey, R. K., Kumar, A. N., [1987] “Effect of the welding process and heat input on the fracture toughness of welded joints in high strength low alloy steel”, *Materials Science and Engineering*, Vol. 91, pp. 29-38.
303. **Sun.Z**, and Karppi R, [1996], “The application of electron beam welding for the joining of dissimilar metals an overview”, *Journal of Materials Processing Technology*.Vol. 59, pp.257 -267.
304. **Suzuki K**, Fukakura J,Kashiwaya H.J, [1987], “*Japan Society Material Science*”, 36, 1090±6
305. **Swift R.A**, Gulya JA, [1973], “Temper embrittlement of pressure vessel steels”.*Weld J*, 52, pp.57s–668.
306. **Swift R.A**, Rogers HC. [1973], “Embrittlement of 2.25Cr–1Mo steel weld metal by post weld heat treatment”. *Weld J*, 52, pp.145s–153.
307. **Tamura, I.**, Hiroshi Sekine, Tomo Tanaka, Chiaki Ouchi, [1988], “Thermo-mechanical processing of high strength low alloy steels” *Butterworth & Co.*
308. **Tanaka, O.**, Takeba, K., and Matsushita, NY. [1984], "High speed overlay welding with strip electrodes",*Welding Review*, pp. 58–62.
309. **Tavassoli, A.A.**, [1995], “Assessment of austenitic stainless steels”, *Fusion Engineering and Design*, Vol.29, pp. 371-390.
310. **Tekriwal, P.** and Mazmuder, J., [1988], “Finite element analysis of 3-dimensional transient heat transfer in GMA welding”, *Welding Journal*, Vol. 67, pp.150s-156s.
311. **Teng, T.L.**, Chang, P.H. and Tseng, W.C., [2003], “Effect of welding sequences on residual stresses”, *Computers and Structures*, Vol.81, pp.273-286.
312. **Teng, T.L.**, Fung, C.P. and Chang, P.H., [2002], “Effect of weld geometry and residual stresses on fatigue in butt-welded joints”, *International Journal of Pressure Vessels and Piping*, Vol. 79, pp. 467–482.

313. **Terumi, N.** and Kazuo, H., [2002], “Wire melting behaviour by non-steady heat conduction numerical analysis in gas metal arc welding”, *Quarterly Journal of the Japan Welding Society*, Vol. 20(1), pp.53-62.
314. **Tgpro**, Thailand, unpublished.
315. **Thainox**, Thailand, unpublished.
316. **Thompson S.W.** and G. Krauss, [1989], *Metall. Trans. A*, 20, pp.2279-2288.
317. **Trindade, F.M.** and Allum, C.J., [1984], “Characteristics in steady and pulsed current GMAW”, *Welding and Metal Fabrication*, Vol. 16(9), pp 264-271.
318. **Tsai C. L.**, Lee S. G., Shim Y. L., Jaeger J. J. and Chasten C. P., [1992], “ASME heat transfer in material processing, (JHTD), vol. 224, pp.9-17.
319. **Tsegelsky V.**, [1976], “The Electric Welder”, *Foreign Language Publishing House*, Moscow.
320. **Tso-Liang, T.**, Chin-Ping, F., Peng-Hsiang, C., [2002], “Effect of weld geometry and residual stresses on fatigue in butt-welded joints”, *Pressure Vessels and Piping*, Vol. (25), pp. 473-480.
321. **Tujsek, J.**, [2000], “Experimental investigation of gas tungsten arc welding and comparison with theoretical predictions”, *IEEE Transactions on Plasma Science*, Vol. 28, pp. 1688 to 1693.
322. **Tusek, J.** and Suban, M., [2000], “Experimental research of the effect of hydrogen in argon as a shielding gas in arc welding of high-alloy stainless steel”, *International Journal of Hydrogen Energy*, Vol.25, pp. 369 to 376.
323. **Tyagi V.**, 9 May [2000], U.S. Patent 6,060,690, Welding Nozzle for Improved Gas Coverage, (to Caterpillar Inc.) 9 May 2000.
324. **Quintino, L.** and Allum, C.J., [1984], “Pulsed GMAW: Interactions between process parameters, Part I”, *Welding and Metal Fabrication*, Vol. 16(4), pp. 126-129.
325. **Varughese, R.**, Pense, A. W., [1993], “Microstructural development in the coarse-grained, heat affected zone in titanium vanadium micro-alloyed HSLA steels”, *Materials Characterization*, Vol. 30, pp. 35-43.
326. **Vishnu P. R.**, Li W. B. and Esterling K. E. [1991], “Heat flow model for pulsed welding”, *Journal of Mat. Sc. & Tech.*, vol. 7, pp.649-659.
327. **Viswanathan R.**, and Bakker W.T, [2000], “Materials for boilers in ultra supercritical power plants”, *proceeding of 2000 international joint power generation conference*, pp.1-22.

328. **Vornovitskii, L.V.**, Gelpern, S.A., Tureshskii, A.V., [1977], “The manual narrow gap arc welding of non-rotating joints in pipelines”, *Welding Production*, Vol. 24(6), pp.18-20.
329. **Wang, F.**, Hou, W.K., Hu, S.J., Asibu, S.K., Schultz, W.W. and Wang, P.C., [2003], “Modelling and analysis of metal transfer in gas metal arc welding”, *Journal of Physics D: Applied Physics*, Vol. 36, pp. 1143–1152.
330. **Wang, G.**, Huang, P.G. and Zhang, Y.M., [2004], “Numerical analysis of metal transfer in gas metal arc welding under modified pulsed current conditions”, *Metallurgical and Materials Transactions B*, Vol. 35B, pp.857-866.
331. **Waszink J H**, and Graat L H J [1983], *Welding journal*, Vol.62, pp.109s-116s.
332. **Waszink, J.H.** and Van, Den Heuvel G.J.P.M.,[1982], “Heat generation and heat flow in the filler wire in GMAW welding”, *Welding Journal*, Vol. 61(8). pp.269s-282s.
333. **Waszink, J.H.** and Piena, M.J., [1986], “Experimental Investigation of drop detachment and drop velocity in GMAW”, *Welding Journal*, Vol. 65(11), pp 289s-298s.
334. **Weber, J.**, [1982], “Pulsed GMAW- A pulse for mild western metalworker”, *Welding Journal*, Vol 61(11), pp 51-52.
335. **Webster, P.J.**, Ananthaviravakumar, N., Hughes, D.J., Mills, G., Preston, R.V., Shercliff, H.R. and Withers, P.J., [2002], “Measurement and modelling of residual stresses in a TIG weld”, *Applied Physics A Materials Science & Processing*, Vol. A74 [Suppl.], pp. S1421–S1423.
336. **Welding hand book**, Metals and their weldability section IV, *American Welding Society*.1972.
337. **Welding Hand Book**, [1984], 7th ed., vol. 4, *American Welding Society*, pp. 93–128.
338. **Wells A. A.** [1952], “Heat flow in welding”, *Welding Journal*, Vol.4, pp 263s-267s.
339. **Williams J.A.**, [1984], “Residual stresses in austenitic–ferritic transition joints fabricated with austenitic weld metal”. *High Temp Technol* 1984; 2, pp. 135–40.
340. **Wilson A.D**, et al, [1988], “Properties and microstructures of copper precipitation aged plate steels, micro alloyed HSLA steels”, in *Conference Proceedings*, ASM, Metals Park, OH, pp. 259-275.
341. **Wyatt L.M.** [1969], “Dissimilar metal joints used in the steam circuit of electrical generating plants”, proceedings of international conference welding dissimilar metals. *Met Constr Br Weld J*, 1(12s), pp.66–71.
342. **Xiaofei Yu**, Shenhao chen and Liang wang [2009],”Effect of solution treatment conditions on the sensitization of Austenitic stainless steel”, *Journal of the Serbian chemical society*, Vol 74(11) pp 1293-1302.

343. **Xiao, F.**, Liao, B., Ren, D., Shan, Y., Yang, K., [2005], “Acicular ferritic microstructure of a low-carbon Mn–Mo–Nb microalloyed pipeline steel”, *Materials Characterization*, Vol. 54, pp.305-314.
344. **Xue Q**, Benson D, Meyers M A, Nesterenko V.F, Olevsky E.A,[2003], “Constitutive response of welded HSLA 100 steel”, *Materials Science and Engineering*, Vol.A354, pp.166-179.
345. **Yaowu Shi** and Zhunxiang Han, [2008], “Effect of weld thermal cycle on microstructure and fracture toughness of simulated heat-affected zone for a 800Mpa grade high strength low alloy steel”, *Journal of material processing technology*, Vol.207.pp.30-39.
346. **Yaghi, A.H.**, Hyde, T.H., Becker, A.A., Williams, J.A. and Sun, W., [2005], “Residual stress simulation in welded sections of P91 pipes”, *Journal of Materials Processing Technology*, Vol.167, pp.480-487.
347. **Yongyuth, P.**, Ghosh, P.K., Gupta. P.C., Patwardhan, A. K., Prakash. Satya, [1992], “Influence of macro/microstructure multi-pass submerged arc welded on the toughness of 'All Weld' C-Mn steel deposits”, *ISIJ International*. Vol. 32, pp.771-778.
348. **Yue.X**, Lippold J.C,Alexandrov B.T, and Babu S.S,[2012],”Continuous cooling transformation behavior in CGHAZ of naval steels”,*Welding Journal*.pp 67s-75s.
349. **Zarandi, Faramarz.**, Yue, Steve., [2005], “Improvement of hot ductility in the Nb-microalloyed steel by high temperature deformation, *ISIJ International*, Vol. 45, pp. 686–693.
350. **Zhang Y.M.**, E. Liguó, R. Kovacevic, [1998], *Welding Journal*. pp. 458s-469s.
351. **Zhao, M.C.**, Yang, K., Shan, Y.Y., [2003], “Comparison on strength and toughness behaviors of microalloyed pipeline steels with acicular ferrite and ultrafine ferrite”, *Materials Letters*, Vol.57, pp.1496–1500.
352. **Zrilica, M.**, Grabulov, V., Burzic, Z., Arsic, M., Sedmak, S., [2007] “Static and impact crack properties of a high-strength steel welded joint”, *International Journal of Pressure Vessels and Piping*, Vol. 84, pp. 139–150.

Annexure A
SCOPE FOR FUTURE WORK

In light of the understanding on the work presented in this report it is realised that following aspects of studies have to be carried out further to improve the reliability of performance of MPSSPL ultra-narrow gap P-GMA welding of thick steel section.

1. The ceramic narrow gap torch nozzle head should be tried out for better life of torch nozzle as well as further narrowing down the groove size.
2. The argon-helium shielding gas mixture should be tried, in order to have superior bead characteristics especially with respect to its thermal behaviour, in MPSSPL ultra-narrow gap P-GMAW of thick similar or dissimilar steel section.
3. The narrow gap P-GMA welding technique with narrow torch nozzle should be tried in higher thick wall steel section.
4. The estimated transverse shrinkage stress and bending stress generated in weld joints as a function of ϕ , I_m and Ω should be compared with the measured residual stresses developed at different regions of extra narrow gap weld joint.



Patents

- 1) Gas metal arc welding torch head for ultra-narrow gap welding of thick section. (Application No. – 201611033570 dated 30:09:2016)

Publication (Journals Published)

- 1) **Ramkishor Anant, P.K. Ghosh**, Ultra-narrow Gap Dissimilar Welding of Thick Section of Austenitic Stainless Steel to HSLA Steel. International Journal of Material Processing Technology (JMPT), 239:210-221(2017).
- 2) **Ramkishor Anant, P.K.Ghosh**, Advancement in narrow gap GMA weld joint of thick section of austenitic stainless steel to HSLA steel, Materials Today: Proceedings, July (2017).
- 3) **Ramkishor Anant, P.K. Ghosh**, Thermal modeling of multipass ultra-narrow gap pulse current GMA welding of Austenitic Stainless Steel to HSLA Steel by single seam per layer deposition technique. International Journal of International Journal of Material Science Engineering-A (MSEA), Communicated.
- 4) **Ramkishor Anant, P.K. Ghosh**, Characteristics of Ultra-arrow Gap Weld of Austenitic Stainless Steel to HSLA Steel by Single-Seam per Layer Pulse Current GMA Weld Deposition. International Journal of Manufacturing Processes (JMP), Communicated.

Publication (International Conferences)

- 1) **Ramkishor Anant, P.K.Ghosh**, Advance technique to produce narrowest gap GMA weld joint of thick sections' 70th IIW Annual Assembly and International Conference (IIW-2017), Shanghai (China).
- 2) **Ramkishor Anant, P.K.Ghosh**, Advantage of narrow gap welding of dissimilar weld joint of thick section of austenitic stainless steel to HSLA steel. 10th Annual Assembly and International Conference on Trends in welding research (TWR-2016) - Tokyo (Japan).

- 3) **Ramkishor Anant**, P.K.Ghosh, Advance welding process and procedure for extra narrow gap dissimilar welding of thick section of austenitic stainless steel to HSLA steel. 68th IIW Annual Assembly and International Conference (IIW-2015) Helsinki (Finland).
- 4) **Ramkishor Anant**, P.K.Ghosh, Experimental Investigation On Transverse Shrinkage Stress And Distortion Of Extra Narrow And Conventional Gap Dissimilar Butt Joint Of Austenitic Stainless Steel To Low Alloy Steel. International Conference on Mining, Material and Metallurgical Engineering (MMME'2014)- Prague (Czech Republic).
- 5) **Ramkishor Anant**, P.K.Ghosh, Metallurgical and Thermal Analysis of Dissimilar Weld Joint of Austenitic Stainless steel to Low Alloy Steel. International Conference on Processing and Fabrication of Advanced Materials (PFAM-XXII' 2013) –Singapore.
- 6) **Ramkishor Anant**, P.K.Ghosh, Advancement in narrow gap GMA weld joint of thick section of austenitic stainless steel to HSLA steel, International Conference on Recent Trends in Engineering and Material Sciences (*ICEMS-2016*), JNU Jaipur, (India).

